Investigating a C1QTNF5 mutation associated with macular degeneration

Fern Slingsby

PhD

The University of Edinburgh

2009

Declaration

I declare that this thesis was composed by myself. The contributions of others to the work are clearly indicated. This work has not been submitted for any other degree or professional qualification.

Fern Slingsby
2009

Acknowledgements

I would like to thank Professor A. Wright and Dr X. Shu for giving me the opportunity to carry out this study. I would also like to thank all the members of the Wright Lab for their help and support over the last 3 years. In particular, I am grateful to Dr X. Shu for providing me with plasmids, cell lines and protocols, and Alan Lennon for his help with growing vast quantities of cell cultures. Thanks also to Kevin Chalmers, Brian Tulloch, Dafni Vlachantoni and Chloe Stanton, and HGU technical services whose technical support has been invaluable.

Thanks to Dr M. Wear (University of Edinburgh) for training me with regard to SPR and ITC, Dr P. Perry (MRC Human Genetics Unit) for training and assistance on various microscopy techniques, and Dr J. Creanor for carrying out the MALDI-TOF MS analysis.

I would like also to thank Prof. I Dransfield and Aisleen McColl (MRC Centre for Inflammation Research) to helping me with all aspects of the macrophage analysis, and to Shonna McCall for providing training on flow cytometry. Thanks to Dr A. Herbert, Prof. P. Barlow, Dr D.Uhrin and Henry Hocking (University of Edinburgh) for their discussion and advice. Particular thanks to Dr A. Herbert and Henry Hocking for allowing me to use their clones and purified proteins to investigate interactions with CFH.

Professor R. Sim (University of Oxford) has provided me with valuable advice, as well as CFH with which to carry out assays, and I am also grateful to Prof. S. Lea (University of Oxford) for giving up her time to discuss my results and allowing me to spend time in her lab. I would therefore also like to thank Joe Ceasar (University of Oxford) for his assistance, it is just unfortunate we didn't get the result we were hoping for!

Finally I would like to thank my family, who have supported me in every way possible throughout this whole experience.

Table of contents

Abstract

C1QTNF5 is a 25kDa short chain collagen of unknown function which is mutated in late-onset retinal macular degeneration (L-ORMD). L-ORMD is an autosomal dominant disease characterised by sub-retinal pigment epithelial deposits leading to photoreceptor death and visual loss and shows several similarities to age-related macular degeneration (AMD). A Tyr402His polymorphism in complement factor H (CFH), a regulatory protein in the innate immune system, has been associated with increased risk of AMD. C1QTNF5 and CFH are both expressed and secreted by the retinal pigment epithelium (RPE) which supports photoreceptors and is responsible for phagocytosis of shed rod photoreceptor outer segments (ROS). The properties of the normal C1QTNF5 and disease-associated Ser163Arg mutation were examined in detail, including protein characterisation, cellular processing and function. Recombinant wild type and mutant C1QTNF5 were produced and their multimerisation and solubility functions compared. Both proteins were found to be soluble and to form similar multimeric species which were resistant to reducing conditions, as seen in other short chain collagens. Due to the similarities between L-ORMD and AMD, a proposed interaction between C1QTNF5 and CFH was investigated. CFH is composed of 20 short consensus repeats (SCR) and interactions were confirmed between C1QTNF5 and both CFH and SCR modules 7-8 and 19-20. CFH showed a greater affinity for mutant C1QTNF5 compared with wild type on the basis of surface plasmon resonance assays. Stably transfected RPE-derived cell lines were created which expressed either wild type or mutant C1QTNF5. Both proteins were found to be secreted and showed similar cellular processing with no evidence of aggregation or retention of the mutant protein within the endoplasmic reticulum. In order to investigate C1QTNF5 function, phagocytosis of ROS by the stably transfected cell lines was carried out. Cells expressing wild type C1QTNF5 showed greater ROS phagocytosis compared with mutant C1QTNF5-expressing or untransfected cells. Addition of anti-C1QTNF5 antibody increased ROS phagocytosis further. In summary, it is proposed that wild type and mutant C1QTNF5 are secreted by the RPE where they interact with CFH. C1QTNF5 is also

shown to have a role in ROS phagocytosis, with mutation in C1QTNF5 affecting phagocytosis efficiency, which may contribute to sub-RPE deposit formation. The results suggest that CFH may also be involved in this process, suggesting a common pathogenic pathway between L-ORMD and AMD.

List of abbreviations

ABCA4…….….. ATP-binding cassette, sub-family A, member 4
aHUS……..…Atypical haemolytic-uraemic symdrome
AMD……..…Age-related macular degeneration
APOE……..Apolipoprotein E
ARM……...Age-related maculopathy
ARMS2…….Age-related maculopathy susceptibility 2
ATP……..….Adenosine-5'-triphosphate
BlamD…….…Basal laminar deposits
BlinD……..Basal linear deposits
BMC……...……...Basement membrane of the choriocapillaris
BMG……Basic minimal medium plus glycerol
BMM……..……Basic minimal medium plus methanol
BMR……....Basement membrane of the retinal pigment epithelium
BSA……Bovine serum albumin
C1QTNF5……..……C1q and tumour necrosis factor related protein 5
CCL-2…….Chemokine ligand-2
CCR-2…….....Chemokine receptor-2
cDNA……...Complementary DNA
CFH……..Complement factor H
CFHR……...……Complement factor H-related
CMV……Cytomegalovirus
CNV…….…Choroidal neovascularisation
CRBP……...…….Cellular retinol binding protein
CR…….……...Complement receptor
CRALBP……...Cellular retinaldehyde-binding protein
CRD……...…….Cystein-rich domain
CRIg…….……Macrophage complement receptor
CRP……C-reactive protein
CUB……...…….Cubilin

DAF……..…….Decay accelerating factor

DAPI……..4',6-diamidino-2-phenylindole

DMEM…….……Dulbecco's modified Eagle Medium

DMSO…….....…….Dimethyl sulfoxide

DNA……Deoxyribonucleic acid

DTT……...Dithiothreitol

ECM…….....Extracellular matrix

EBNA……...……Epstein Barr virus nuclear antigen

EBNA293... Epstein Barr virus nuclear antigen-transfected human embryonic kidney

EBP50……...……Ezrin-radixin-moesin binding phosphoprotein of 50 kDa

ECL…….....……Enhanced chemiluminescence

ECM……...Extracellular matrix

EDC……..1-ethyl-3-(3-dimethylaminopropyl) carbodiimide hydrochloride

EDTA…….....Ethylenediaminetetraacetic acid

EGFP…….……Enhanced green fluorescent protein

EL……....Elastin layer

ER……..Endoplasmic reticulum

ERG…….Electroretinography

FAK……...……..Focal adhesion kinase

FB……..Factor B

FCS……..…Foetal calf serum

FHL-1…….……Factor H-like protein 1

FI……Factor I

FITC…….....Fluorescein isothiocyanate

FITC-ROS…….……..FITC-labelled ROS

FOX03…….Forkhead box 03

GAG……..……...…Glycosaminoglycan

GCL……..…Ganglion cell layer

GFP……Green fluorescent protein

GMSA……..…….Gel mobility shift assay

GPI……..…….Glycosylphosphatidylinositol

GST……Glutathione *S*-transferase

HEK……...……Human embryonic kidney

HEPES…….4-(2-hydroxyethyl)-1-piperazineethanesulfonic acid

HGU……..……...……Human Genetics Unit

HI-PBS/BSA……..…..Heat-inactivated PBS plus 10mg/ml BSA

His-C1QTNF5……...……..C-terminal hexa-histidine-tagged C1QTNF5

His-gC1q……C-terminal hexa-histidine-tagged gC1q

HRP…….…….Horse radish peroxidise

HTRA1……..……High temperature requirement serine protease

ICL…….Inner collagenous layer

IEF…….……..Isoelectric focusing

IgG……..…..Immunoglobulin G

IL……...……....Interleukin

IMDM……...Iscove's modified Dulbecco's medium

INF-γ……Interferon-γ

IPM……...Inter photoreceptor matrix

IPTG…….Isopropyl β-D-1-thiogalactopyranoside

IRBP……..Interstitial retinal binding protein

ITC……..…….Isothermal titration calorimetry

LB……...Lauria broth

L-ORMD……...……..Late-onset retinal macular degeneration

LRAT……...…….Lecithin retinol acyltransferase

MAC……...……..Membrane attack complex

MALDI-TOF MS……

……Matrix-assisted laser desorption/ionisation time of flight mass spectrometry

MBL…….……Mannose-binding lectin

MASP…….…..Mannose-binding lectin-associated protease

MCP-1……..Monocyte chemoattractant protein-1

MDCK……...Madin-Derby canine kidney

MerTK……...C-mer proto-oncogene tyrosine kinase

MES…….2-(*N*-morpholino)ethanesulfonic acid

MFG-E8……...……Milk fat globule E8

MFRP……...……Membrane-type frizzled-related protein

MHC…….……Major histocompatibility complex

MMP……..Matrix metalloprotease

MOPS……...3-(N-morpholino)propanesulfonic acid

MPGNII…….…….Membranoproliferative glomerulanephritis type II

NHS……...*N*-Hydroxysuccinimide

OCL……..…Outer collagenous layer

ONL…….Outer nuclear layer

OPL……..……Outer plexiform layer

OR…….…….Odds ratio

ox-ROS…….…….Oxidised rod outer segments

PFA……Paraformaldehyde

PAGE……..Polyacrylamide gel electrophoresis

PBS……....Phosphate buffered saline

PCR…….…..Polymerase chain reaction

PEDF……Pigment epithelium-derived factor

PDI……...…….Protein disulphide isomerase

PI……Phosphatidylinositol

PS……..……Phosphatidylserine

qRT-PCR……..……. quantitative real time polymerase chain reaction

RCA……..…….……Regulators of Complement Activation

rd6……...……Retinal degeneration 6

RDH5……..Retinol dehydrogenase 5

ROS…….Rod outer segments

RPE…….Retinal pigment epithelium

RPE65…….….. Retinal pigment epithelium-specific protein 65kDa

RPM…….……..Revolutions per minute

SCR……...….Short consensus repeat

SDS…….……Sodium dodecyl sulphate

siRNA…….……..Small interfering ribonucleic acid

SNP…….……Single nucleotide polymorphism

SOC……..….Super optimal broth with catabolite repression

SPR……..Surface plasmon resonance

SSC……...Saline-sodium citrate

STAT1……...……Signal transducers and activators of transcription 1

TBE……...Tris/Borate/EDTA

TCA……..…..Trichloroacetic acid

TGF-β…….……Transforming growth factor β

TIMP……..…..Tissue inhibitor of metalloproteinase

TNF……...……Tumour necrosis factor

TLR4……....Toll-like receptor 4

TNF-α……..Tumour necrosis fator-α

TUNEL…….……Terminal deoxynucleotidyl transferase dUTP nick end labelling

VEGF…….……Vascular endothelial growth factor

X-gal…….5-bromo-4-chloro-3-indolyl-b-D-galactopyranoside

YPDS……..……Yeast extract peptone dextrose medium plus sorbitol

ZO-1……Zona occludens 1

List of figures

List of tables

1 CHAPTER 1

:

INTRODUCTION

1.1 The retina and retinal pigment epithelium

The retinal pigment epithelium (RPE) is a monolayer of pigmented cells forming the outer most layer of the retina. The RPE provides a supporting role for the retina, which contains the photoreceptor and nerve cells necessary for light processing, and acts as a barrier between the retina and the choroidal blood supply. Figure 1.1 shows a cross section of the vertebrate eye, with the RPE and retina covering almost the entire of the inside of the eye, up to the *ora serrata*. The only gap is where the optic nerve penetrates into the eye, creating the 'blind spot'. The *macula* is located directly posteriorly to the lens, in the central area of the retina. It is yellow in colour and represents an area of high photoreceptor density, with its central region, the *fovea*, having the highest photoreceptor density necessary for sharp image processing (Hildebrand & Goslow, 2001).

1.1.1 The structure of the retina

The retina processes light entering the eye, converting this into nerve impulses sent down the optic nerve and to the brain for processing, and is comprised of distinct layers, as can be seen from Figure 1.2. The most posterior layer is Bruch's membrane, joining the outermost layer of the retina to the innermost layer of the choroid. The RPE plasma membrane is continuous with Bruch's membrane at its basal side, and apically it forms microvilli which interdigitate with the photoreceptor outer segments. The RPE cells are pigmented, ensuring that no random reflection of light occurs within the eye. The photoreceptors consist of rods and cones and contain pigments, enabling light absorption to be converted into nerve impulses. Cones contain several different pigments, each susceptible to distinct wavelengths of light allowing for colour vision. The pigment present in rods is rhodopsin, with rods playing a role in night vision. Photoreceptor outer segments consist of folded stacks of hundreds of pigment-containing lamellae and have narrow connections to their inner segments and the main cell body containing the nucleus and mitochondria. The *macula* contains a higher density of cones than the more peripheral retina, with the *fovea* consisting of only cones. The anterior retina layers are also thinnest at the

fovea, ensuring maximum light reaches the photoreceptors. Photoreceptors synapse with bipolar cells, which in turn form synapses with the ganglion cells. Plexiform nerve cells form a mesh at each end of the bipolar cells. It is the ganglion cells which transmit the nerve impulses originating in the photoreceptors to the brain via their axons forming the optic fibre layer, which continues through the optic nerve to the lateral genticulate body in the brain (Hildebrand & Goslow, 2001).

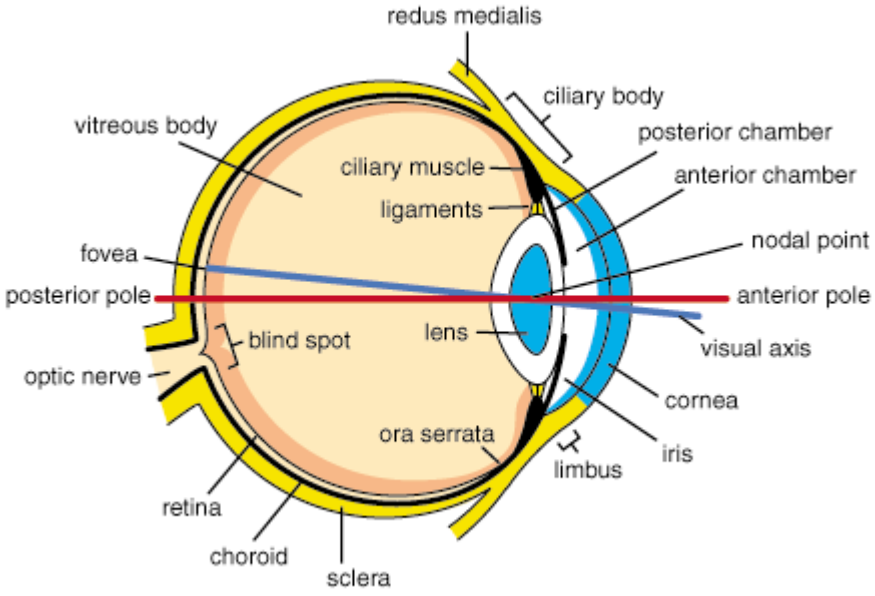

Figure 1.1: A cross section of the vertebrate eye.
(source: http://www.vision3k.com/images/struc_eye.gif)

The retina covers almost the entire inside of the eye, extending to the *ora serrata*. The RPE is located beneath the retina. The blind spot is created where the optic nerve pierces the retina. The macular is located directly posterior to the lens and contains the area of highest photoreceptor density.

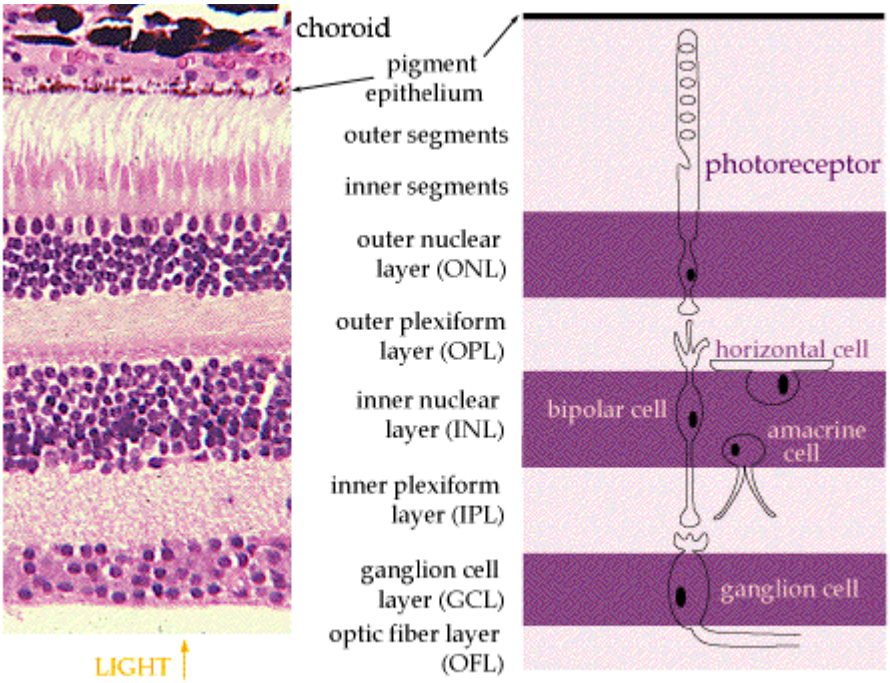

Figure 1.2: A cross section of the vertebrate retina.
(source: http://thalamus.wustl.edu/course/eye3.gif)

Light entering the eye through the lens then travels through several cell layers before it reaches the photoreceptors. Here it then activates rhodopsin and signal transduction from the photoreceptor, through the bipolar cells and ganglion cells. The impulse then travels down the ganglion cell axons which comprise the optic nerve and into the brain.

1.1.2 Bruch's membrane

Bruch's membrane is a pentalaminar structure. It is located beneath the retina, extending to the *ora serrata* and is pierced posteriorly by the optic nerve. The five layers it consists of are the basement membrane of the choriocapillaris (BMC), the outer collagenous layer (OCL), the elastin layer (EL), the inner collagenous layer (ICL) and the basement membrane of the RPE (BMR) (Marmor & Wolfensberger, 1998). Under electron microscopy, the BMC consists of two layers; a pale layer and a darker, electron dense layer. The dense layer is granular and contains collagens IV and VI, laminin and heparan sulphate, with collagen VI involved in basement membrane anchorage of the capillary epithelium (Marshall *et al.,* 1993). The OCL consists of collagens I, III and V, fibronectin, chondroitin sulphate, dermatan sulphate and proteoglycans. The collagen fibres are predominantly in the plane of the membrane, although some extend up through the EL into the ICL. The EL consists of an array of elastin fibres running parallel to Bruch's membrane, with dense areas forming nodes and less dense areas forming pores. The ICL is the same in composition as the OCL, although it is approximately twice the thickness. Finally, the BMR forms an uninterrupted layer similar in structure and chemical composition to the BMC but excluding collagen VI (Marmor & Wolfensberger, 1998)

Unlike the endothelial cells of the retinal blood vessels, the endothelial cells of the choriocapillaris are fenestrated, with the choroidal fenestrations permeable to proteins up to 70kDa (Pino *et al.,* 1981). The vessels of the choriocapillaris are approximately three times the width of the retinal blood vessels and have a two hundred-fold greater rate of blood flow (Alm *et al.,* 1973). This is to aid metabolite exchange by maintaining a high concentration gradient across the vessel walls. Metabolites and proteins can then pass through Bruch's membrane to the RPE. In addition to this inward flux there is also an outward flux of water and waste material from the RPE, with Bruch's membrane presenting a negligible barrier. However, as the eye ages the permeability of Bruch's membrane decreases with detrimental effects on the RPE and retina (Marmor & Wolfensberger, 1998).

1.1.3 The embryonic development of the RPE

Following invagination of the optic cup, the resulting two layers of neuroepithelium will flatten together and will become the RPE and retina. They are separated by a thin lumen filled with the inter photoreceptor matrix (IPM), providing the signalling control required for the different differentiation pathways of the two layers. Development of the two layers occurs in concert, with the RPE necessary for correct retinal development, secreting signalling factors required for photoreceptor differentiation (reviewed by Strauss, 2005).

Differentiation of the RPE is promoted by retinoic acid, secreted from the embryonic retinal anlage. The neuroectodermal cells differentiate into pigmented epithelium and then start to express retinoic acid themselves, as well as RPE65 (retinal pigment epithelium-specific protein 65kDa), which is involved in the recycling of components of the visual cycle. The RPE progenitor cells differentiate further to show apical to basolateral polarity, forming basal infoldings and apical microvilli. The basement membrane, in conjunction with the plasma membrane of the ajoining endothelium forms Bruch's membrane, with the RPE cells themselves secreting the required extracellular matrix components. Tight junctions form between the RPE cells and help to organise the cytoskeleton, further defining the apical to basolateral polarity. The formation of tight junctions signifies the formation of the blood-retina barrier, and coinsides with the onset of epithelial transport by the RPE (Strauss, 2005).

In the adult eye, the RPE apically forms microvilli which interdigitate with the photoreceptors. In the embryonic eye, this apical surface maturation is promoted by ezrin, causing the development of microvilli (Bonilha *et al.,* 1999), with ezrin knockout mice having substantially reduced apical microvilli and basal infoldings, as well as retarded photoreceptor development (Bonilha *et al.,* 2006). Under normal developmental conditions, as the RPE extends its apical microvilli, so the primordial photoreceptors extend their outer sements. When the process is complete the photoreceptor outer segments interdigitate with both long microvilli, which

maximise surface area for epithelial transport, and short microvilli, which are involved in phagocytosis of shed outer segments (Strauss, 2005).

1.1.4 Transport mechanisms and growth factor secretion in the RPE

The RPE plays a central role in supporting the retina and maintaining a constant microenvironment. Part of this role involves ensuring the correct volume and composition of fluid in the subretinal space. This is achieved through the transport of metabolites, fluid and ions. The RPE is comprised of polarised epithelium, and so has different transport mechanisms at the apical and basolateral membranes. Water transport occurs from the apical side to the basolateral side. Apically, there are membrane Na^+-K^+-ATPases and Na^+/K^+exchangers, and basolaterally there are membrane Cl^- channels and Cl^-/HCO_3^- exchangers, with the transport of water through aquaporins from the subretinal space into the RPE mainly driven by the transport of K^+ and Cl^-. In addition to fluid transport, the RPE is responsible for the removal of lactic acid, a major metabolic end product, from the subretinal space. This occurs via apical lac^--H^+ transporters, with lactic acid expelled basally from the RPE via different basolateral lac^--H^+ transporters. The pH balance within the RPE cells is maintained by Na^+/H^+ and Na^+/HCO_3^- exchangers in the apical membrane and Cl^-/HCO_3^- exchangers in the basolateral membrane (reviewed by Marmor & Wolfensberger, 1998, Strauss, 2005).

The RPE also secretes a number of growth factors, each with different roles in maintaining the structure and efficient function of the retina. Apically it secretes the neurotrophic factor pigment epithelium-derived factor (PEDF), and basally it secretes the vascular endothelial growth factor (VEGF). PEDF is an inhibitor of retinal angiogenesis, inhibits the migration of endothelial cells and has been shown to reduce photoreceptor apoptosis induced by hydrogen peroxide. VEGF promotes the growth of vascular endothelial cells and increases vascular permeability (reviewed by Tong *et al.,* 2006). VEGF and PEDF also have roles in retinal degeneration, discussed in Section 1.2.2.3.

Also secreted by the RPE are a number of proteins included in the family of matrix metalloproteases and their inhibitors. Matrix metalloproteinases (MMP) and their inhibitors are involved in maintenance of the extracellular matrix (ECM) and Bruch's membrane, with MMPs carrying out zinc-dependant ECM turnover. MMPs and their inhibitors secreted by the RPE include collagenases, gelatinases and tissue inhibitors of metalloproteases (TIMP) (Alexander *et al.,* 1990). Mutations in one such TIMP, TIMP3, have been associated with a form of retinal degeneration called Sorsby Fundus Dystrophy. This is an early-onset maculophathy with associated choroidal neovascularisation (CNV) and thickening of Bruch's membrane, similar to AMD (see Section 1.2), which is thought to be caused by both loss of function of TIMP3 and aggregation of the mutant protein (Arris *et al.,* 2003, Lin *et al.,* 2006).

1.1.5 The visual cycle

In addition to fluid and metabolite transport, the RPE is also responsible for the recycling of components involved in the visual cycle. This process is summarised in Figure 1.3. Signal transduction in the visual, or retinoid, cycle starts by rhodopsin light absorption in the photoreceptors. Rhodopsin consists of a seven transmembrane domain G-coupled receptor, opsin and the chromophore, 11-*cis*-retinal (Hargrave, 2001). Following light absorption, 11-*cis*-retinal undergoes a conformational change to become all-*trans*-retinal, changing rhodopsin to meta-rhodopsin and activating signal transduction (Okada *et al.,* 2001). Activated rhodopsin is then phosphorylated by rhodopsin receptor kinase and subsequent binding of arrestin. The now inactivated rhodopsin releases all-*trans*-retinal and binds 11-*cis*-retinal (Baylor, 1996, Baylor *et al.,* 1998).

All-*trans*-retinal can be regenerated back into 11-*cis*-retinal by the enzyme *cis-trans* isomerise. Photoreceptors lack this enzyme, so it is necessary for the all-*trans*-retinal to be transported to the RPE for this regeneration to occur. An adenosine triphosphate (ATP)-binding cassette protein, ABCA4, transports the accumulated all-*trans*-retinal from the interdiscal space into the photoreceptor cytosol. Here it is reduced to all-*trans*-retinol by all-*trans*-retinol dehydrogenase, and translocated to the RPE by the carrier protein, interstitial retinal binding protein (IRBP). Once

within the RPE, all-*trans*-retinol binds the cellular retinol binding protein, CRBP. Reisomerisation then occurs due to the binding of a protein complex consisting of lecithin retinol acyltransferase (LRAT), which transfers an acyl group to the all-*trans*-retinol forming all-*trans*-retinyl, RPE65, an isomerohydrolase, which converts the all-*trans*-retinyl ester to 11-*cis*-retinol, the retinol dehydrogenase RDH5, which converts the 11-*cis*-retinol to 11-*cis*-retinal, and cellular retinaldehyde binding protein (CRALBP), which accelerates the RDH5 enzymatic reaction. A supplementary pathway by which all-*trans*-retinal is converted back into 11-*cis*-retinal involves the RPE-retinal G protein receptor opsin, which uses light energy to drive the isomerisation reaction. It is suggested that this additional pathway helps to adapt the retinal turnover to changes in ambient light (reviewed by Strauss, 2005).

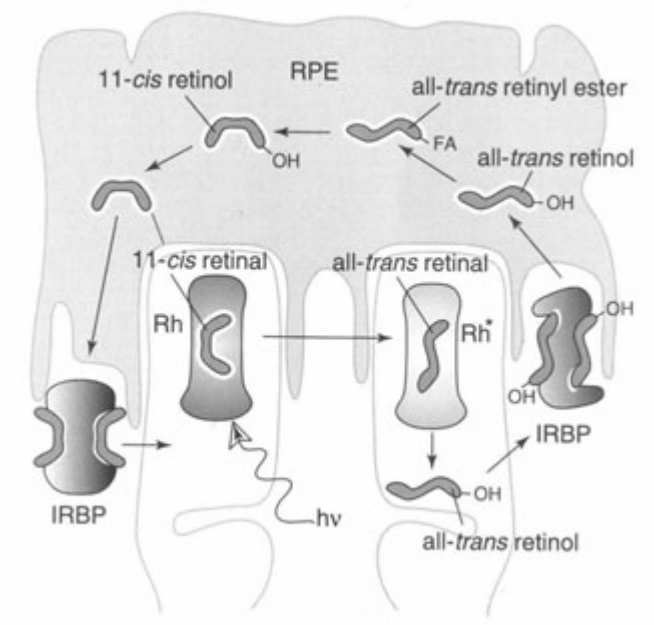

Figure 1.3: Retinoid processing in the visual cycle.
(source: biophysics.bumc.bu.edu/faculty/cornwall/)

Light entering the photorecetors activates rhodopsin, which contains the chormophore 11-*cis*-retinal. This undergoes a conformational change to become all-*trans*-retinal, activating signal transduction. All-*trans*-retinal is required to be transported to the RPE for recycling back into 11-*cis*-retinal. For this to occur, the all-*trans*-retinal is converted into all-*trans*-retinol, and transported by the carrier protein, IRBP, to the RPE. Here the all-*trans*-retinol is converted to all-*trans*-retinyl, before undergoing a further conversion into 11-*cis*-retinol. This can now be converted back into 11-*cis*-retinal and transported back to the photoreceptor to be activated by light once more.

1.1.6 RPE phagocytosis of rod outer segments

Within the photoreceptors, there is continuous replacement of disc membranes and intermittent shedding of rod outer segments (ROS). Shed ROS are phagocytosed by the RPE, forming phagosomes to be digested by RPE lysosomes (Young and Bok, 1969). This process follows a circadian rhythm with phagocytosis promoted by the onset of light (LaVail, 1976). RPE phagocytosis of ROS shows high selectivity, with cultured RPE shown to have preference for ROS over red blood cells, algae, bacteria and yeast, suggesting the involvement of specific receptors and ligands (Mayerson and Hall, 1986). In the macula, there is a higher ratio of photoreceptors to RPE cells requiring the RPE cells here to be adapted to cope with a higher turnover of ROS (Strauss, 2005).

1.1.6.1 Receptors and ligands involved in ROS phagocytosis

The presence of RPE/ROS-specific ligands and receptors involved in the RPE-ROS phagocytic cycle was confirmed by Gregory and Hall (1992) who raised an antiserum to an RPE plasma membrane-enriched fraction and showed this antiserum inhibited ROS binding to RPE. It was initially suggested that a mannose receptor on the RPE plasma membrane could be involved in ROS uptake, possibly by recognising a mannose residue on rhodopsin. However, this has not been confirmed, with conflicting studies either supporting (Boyle D *et al.,* 1991, Lutz D *et al.,* 1995) or dismissing (Hall *et al,.* 1990) this theory, and no conclusive evidence has as yet been presented. Figure 1.4 summarises the receptors and ligands currently known to be involved in ROS phagocytosis by the RPE.

Finnemann *et al.* (1997) have shown that the αvβ5 integrin is involved in RPE phagocytosis of ROS. They showed it is first detected in mice at P7, with adult levels reached at P11 (just prior to the start of phagocytosis at P12) and that blocking cultured cells with anti- αvβ5 antibodies reduces their phagocytosis levels by 85%. It was also shown that the αvβ5 receptor is necessary for ROS binding only, not internalisation, indicating another process is involved in internalisation of the αvβ5-

ROS complex. Nandrot *et al.* (2004) showed that in β5 knockout mice retinal photoresponses declined with age and autofluorescence increased. When cultured, $\beta5^{-/-}$ RPE showed no phagocytosis of ROS, and although *in vivo* basal levels of phagocytosis were maintained, the burst of phagocytic activity associated with the circadian shedding of ROS did not occur. It was subsequently shown by Nandrot *et al.* (2007) that the ligand for αvβ5 was the secreted glycoprotein milk fat globule E8 (MFG-E8), which has been shown to co-localise to the subretinal space. $MFG^{-/-}$ mice were found to lack the diurnal synchronisation of ROS phagocytosis, as was also observed in the $\beta5^{-/-}$ mice. MFG-E8 binds the αvβ5 integrin via its RGD motif, and also binds exposed phoshatidyl serine found on apoptotic cell surfaces. It was found to increase ROS binding to wild-type RPE primary cultures but did not affect levels in $\alpha v\beta5^{-/-}$ cells. In addition to its phagocytic role, αvβ5 also plays a role in apical retinal adhesion (Nandrot *et al.,* 2006). $\beta5^{-/-}$ mice showed weakened retinal adhesion independent of circadian rhythm, indicating that αvβ5 contributes to permanent retinal adhesion and stabilisation of the RPE/ROS interdigitation as well as binding ROS during phagocytosis.

ROS binding to the αvβ5 integrin has been shown to activate a signalling cascade involving focal adhesion kinase (FAK). This in turn phosphorylates C-mer proto-oncogene tyrosine kinase (MerTK), which activates the signalling cascade necessary for internalisation of the ROS (Finnemann *et al.,* 2003, Finnemann *et al.,* 2006). MerTK is a transmembrane protein with two fibronectin type-III domains, two immunoglobulin-like domains and one tyrosine kinase domain. It is mutated in the Royal College of Surgeons rat (D'Cruz *et al.,* 2000), which undergoes photoreceptor degeneration due to lack of ROS phagocytosis and accumulation of shed photoreceptors in the sub retinal space (Dowling *et al.,* 1962, Bok *et al.,* 1971), and has also been found to be mutated in autosomal recessive retinitis pigmentosa (Gal *et al.,* 2000).

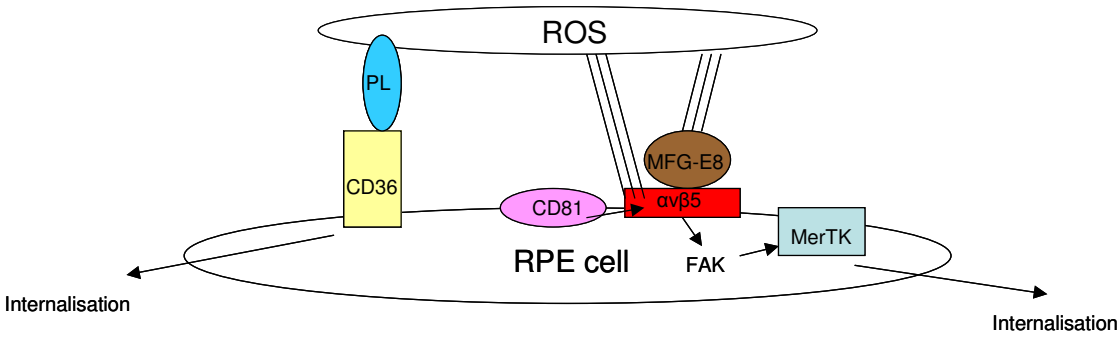

Figure 1.4: Receptors and ligands involved in ROS phagocytosis by the RPE.

CD36 recognises anionic phospholipids on the rod outer segment (ROS) surface, promoting phagocytosis. In a separate pathway, the αvβ5 integrin is responsible for ROS binding, with MFG-E8 acting as a ligand for both the integrin and the ROS. CD81 plays an indirect role involving integrin processing. ROS phagocytosis via this pathway activated FAK/MerTK signalling pathways resulting in ROS internalisation

The tetraspanin, CD81, has also been shown to interact with the αvβ5 integrin, although not in complex with FAK or MerTK (Chang *et al.,* 2007). Tetraspanins are four-transmembrane-domain proteins which act to regulate the function of integrins. They do this by regulating integrin trafficking and recycling, compartmentalization within the plasma membrane, facilitating lateral protein and lipid associations and recruiting intracellular signaling molecules to integrin tail domains (reviewed by Berditchevski *et al.,* 2001, Hemler *et al.,* 2005, Levy *et al.,* 2005). Co-immunoprecipitation experiments comfirmed the interaction, and over-expression of CD81 in cultured RPE cells increased ROS binding when compared with the wild-type. CD81 over expression did not increase ROS binding in αvβ5 integrin deficient cells, indicating that CD81 is not able to act independently of αvβ5. It was also shown that over-expression of CD81 increased apical surface levels of αvβ5 integrin (Chang *et al.,* 2007).

Another receptor identified as having involvement in ROS phagoyctosis by the RPE is CD36 (Ryeom *et al.,* 1996b). CD36 is a heavily glycosylated plasma membrane protein which has been shown to have roles in the uptake of apoptotic cells and modified lipids (Silverstein *et al.,* 2000). Apoptotic cells have exposed anionic phospholypids such as phosphatidylserine (PS) and phosphatidylinositol (PI) in their plasma membrane, with these phospholipids shown to be present on the surface of shed ROS too (Anderson *et al.,* 1970). It was shown by Ryeom *et al.* (1996a) that such phospholipids were likely receptors for CD36, as PS and PI vesicles were internalised by cultured RPE and such internalisation was blocked with anti-CD36 antibodies. Again using anti-CD36 antibodies, Finnemann *et al.* (2001) showed that CD36 regulated the rate of ROS internalisation but does not act during binding, and that such internalisation is independent of the αvβ5 integrin. The antibodies cross-linked CD36, up-regulating internalisation, probably due to CD36 dimerisation. This supported a signalling role for the protein. ROS are rich in unsaturated phospholipids such as docosahexaenoic acid (DHA) which is highly sensitive to oxidation. Conformation that oxidised phospholipids were ligands for CD36-

mediated phagocytosis of ROS came from analysis showing that light-induced oxidation of ROS phospholipids generated ligands for CD36-mediated phagocytosis by cultured RPE (Sun *et al.,* 2006).

1.2 Age-related macular degeneration

Age-related macular degeneration (AMD) is a late-onset disease of the central retina. Taking many decades to develop, the disease causes degeneration of the central retina resulting in loss of central vision. In some cases AMD can result in sudden loss of vision (Tezel *et al.,* 2004). It is the more severe form of the disease age-related maculopathy (ARM) and is the leading cause of blindness in developed countries where its incidence is increasing (Evans *et al.,* 1996). A study of the UK population over 75 years of age estimated that 3.7% were visually impaired as a result of AMD. For those over 90 years of age this rose to 14.4% (Evans *et al.,* 2004).

1.2.1 General disease symptoms

There are two forms of severe AMD, with geographic atrophy (GA, sometimes known as "dry AMD") and choroidal neovascularisation (CNV, or "wet AMD") respectively. GA is characterised by progressive atrophy of the RPE, subsequent loss of photoreceptors and a slow reduction in central vision. CNV includes abnormal blood vessel growth from the chriocapillaris, which can leak or haemorrhage into the retina and result in sudden loss of central vision. In both forms of the disease, sub-RPE deposits are observed, adjacent to and within Bruch's membrane. It is normal for some sub-RPE deposits to be present in the ageing eye, but in the case of AMD, extensive deposits can lead to disruption of RPE function, subsequent photoreceptor dysfunction and retinal atrophy (Tezel, 2004). Figure 1.5 shows normal and diseased retinas. In the early stages of the disease large, yellow drusen can be seen in the macula, although the patient has normal visual acuity. In the later stages, retinal atrophy is also observed and the patient will have resulting deficiencies in central vision (Fine *et al.,* 2000).

1.2.2 Deposits and changes in Bruch's membrane

Bruch's membrane thickens with age and sub-RPE deposits can be observed (Bird *et al.,* 2003). Thickening of Bruch's membrane is associated with increased lipid content and so decreased hydraulic conductivity and macromolecular permeability (Sheraidah *et al.,* 1993, Starita *et al.,* 1995, Moore *et al.,* 2001). One requirement of Bruch's membrane is to allow metabolic exchange between the RPE and the choroidal blood vessels, so if this is reduced then normal photoreceptor function is compromised (Bird *et al.,* 2003).

The sub-RPE deposits associated with AMD consists of three classes: basal laminar deposits (BlamD, diffuse deposits external to Bruch's membrane), basal linear deposits (BlinD, diffuse deposits internal to Bruch's membrane) and drusen (focal deposits). BlamD consist of fibrous long-spacing collagen and basement membrane materials, and are suggested to result from excess basement membrane secreted by a stressed RPE (van der Schaft *et al.,* 1992, van der Schaft *et al.,* 1993, Marshall *et al.,* 1992, Sarks *et al.,* 2007). BlinD consist of membranous material and are indicators of AMD disease progression. BlinD always appear after BlamD, and once RPE atrophy has occurred deposits become less membranous and BlamD increases (Curcio *et al.,* 1999, Sarks *et al.,* 2007).

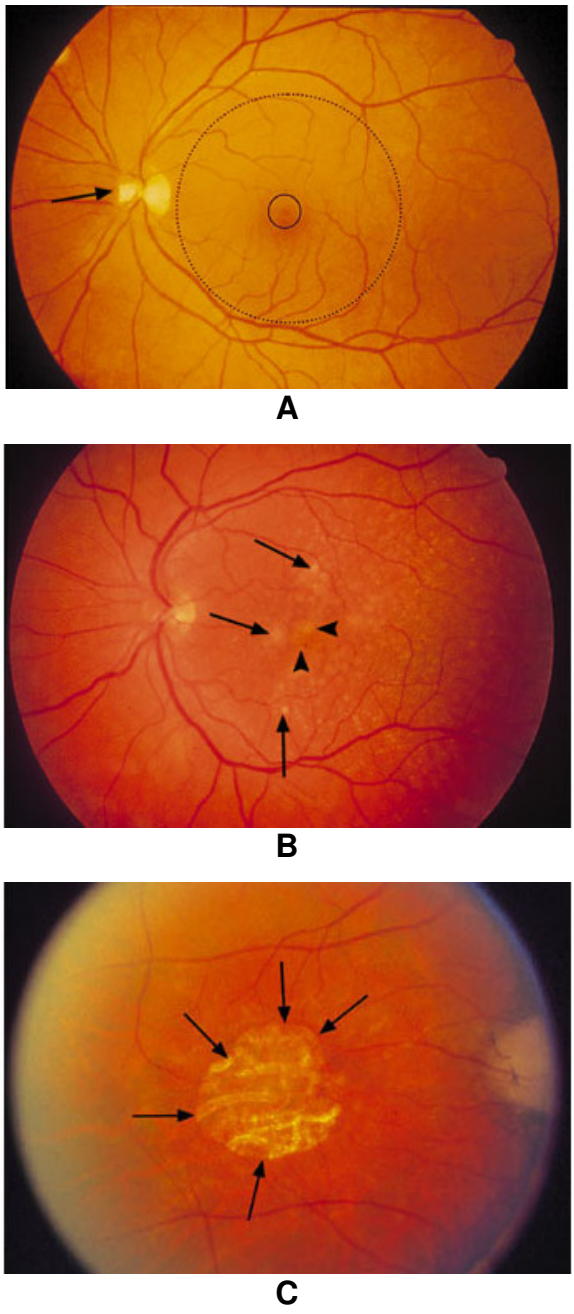

Figure 1.5: Diseased retina in AMD patients.
(source: Fine *et al.,* 2000)

Normal and AMD diseased retinas:
A – A healthy retina. The inner circle defines the fovea, the outer circle the macula. The arrow indicates the optic nerve.
B – The early stages of AMD. Arrows indicate large drusen, arrowheads indicate clumps of pigment. The patient still has normal vision.
C – The later stage of AMD. The arrows indicate central atrophy. The surrounding retina is normal. The patient will experience some loss of central vision.

Drusen are located between the RPE plasma membrane and the inner collagenous layer of Bruch membrane. Drusen morphology can vary and various classification systems have been proposed, but it is generally accepted that drusen will fall into one of two categories: soft or hard. Soft drusen have a diameter greater than 63µm with "visible thickness" whereas hard drusen are discrete and range in diameter from 1-63µm. It should be noted that BlinD are sometimes referred to as diffuse drusen (Hageman *et al.,* 1999).

Patients with large drusen have increased risk of developing CNV. Once CNV has developed, subsequent leakage of fluid or blood can result in distortion of vision, a blind spot or, in extreme cases, sudden loss of vision (Fine *et al.,* 2000).

1.2.2.1 The composition of drusen

Hageman *et al.,* (2001) summarise various studies into the classification and composition of drusen. Firstly, it is noted that although the role of drusen in AMD pathogenesis is not clear, their correlation with AMD is, so that the presence of drusen is considered a major risk factor for developing the disease. The composition of soft and hard drusen is actually very similar, so although they differ morphologically they can be considered to be otherwise the same. Drusen components identified include lipids, carbohydrates and protein. Lipid components include esterified and unesterified cholesterol, or lipoprotein such as apolipoprotein E (ApoE). The latter is probably produced locally within the retina whereas the other lipids would suggest vascular and hepatic origins respectively, pointing towards a heterogenous origin for drusen. Drusen-associated carbohydrates include sialic acids, glucoconjugates with terminal glucose/mannose, N-acetylglucosamine and O-glycosidically linked carbohydrates. Many protein components have been identified, including ubiquitin, integrins, beta-amyloid and fibronectin, as have proteins with an immunological function including immunoglobulin, C5b-9, C1q and MHC class II antigens. Crabb et al. (2002) carried out drusen proteome analysis by mass spectrometry and identified many proteins including TIMP-3, various crystallins and complement C9. Oxidative protein modifications were also observed, suggesting a role for oxidative injury in AMD. Complement factor H is also present in drusen

(Bok *et al.,* 2005), where immunohistology has revealed a drusen-wide localisation. The complement membrane attack complex (MAC) was shown to be associated with the drusen core. Cellular components have also been found associated with drusen. RPE basal blebs extend into drusen and RPE-derived basal laminae and organelles are also observed. Dentritic cell processes can be seen extending into the druse core (Hageman *et al.,* 2001).

It has been shown that zinc has a high concentration in macular and peripheral sub-RPE deposits, and is particular high within drusen themselves. Zinc is known to play a role in the accumulation of deposits and aggregates in neurodegenerative diseases such as Alzheimer's disease and Parkinson's disease, so it has been suggested that the high concentrations of zinc observed here may too play a role in deposit formation (Lengyel *et al.,* 2007).

1.2.2.2 Lipofuscin deposits

Lipofuscin deposits are fluorescent deposits associated with the ageing retina. Lipofuscin is thought to derive from lysosomal residual bodies arising from photoreceptor phagocytosis and digestion, and contain the end-products of oxidatively damaged lipids. Indeed, lipofuscin has been shown to contain the pyridinium bis-retinoid, A2-E, which has been shown to inhibit lysosomal degradation of proteins in cultured RPE cells, supporting lipofuscin being the product of incomplete ROS digestion (Reinboth *et al.,* 1997). Lipids can be oxidatively damaged by light entering the eye, with the RPE pigment melanin helping to reduce this damage. It therefore makes sense that there is a correlation between decreasing melanin levels and increasing lipofuscin levels (Weiter *et al.,* 1986). Indeed, accumulations of lipofuscin are associated with the ageing retina (Feeny-Burns *et al.,* 1984), and such deposits increase from the periphery to the posterior pole, with a drop in levels at the *fovea*, corresponding to levels of ROS phagocytosis (Weiter *et al.,* 1986).

1.2.2.3 Choroidal neovascularisation in AMD

It is thought that choroidal neovascularisation in AMD can arise due to unbalanced VEGF and PEDF expression. VEGF and PEDF are growth factors secreted by the RPE which promote and inhibit angiogenesis. VEGF levels are increased in the choroidal vascular membranes of patients with CNV, and animal models have shown VEGF can actually induce CNV. Also, laser induction of CNV increases local VEGF levels, and adenoviral transfection of the VEGF gene in rats causes the development of CNV. The specific role of PEDF in AMD is not clear. At low doses it inhibits the effects of VEGF and so CNV formation, and in animal models, adenoviral expression of PEDF can reduce laser-induced CNV. However, at high doses PEDF can induce endothelial proliferation (reviewed by Tong *et al.,* 2006).

1.2.3 Oxidative damage in the RPE and AMD

The RPE is exposed to high levels of oxidative stress. Some of this exposure is due to the phagocytosis of oxidised lipids contained in shed ROS, as discussed previously, whilst other exposures include short-wavelength radiation such as blue light (Algvere *et al.,* 2006), lipofuscin, high levels of oxygen from the choroidal blood supply and toxins such as cigarette smoke (Beatty *et al.,* 2000). The retina has developed defence mechanisms to protect against such oxidative damage. These include the antioxidant enzymes superoxide dismutase, catalase and glutathione peroxidise (Tate *et al.,* 1995, Frank *et al.,* 1999, Beatty *et al.,* 2000). It is thought that oxidative damage contributes to disease mechanisms in AMD.

1.2.4 Immune complexes and inflammation in the pathogenesis of AMD

The observation that proteins involved in immune responses, such as immunoglobulins, complement component C5 and the MAC, are associated with drusen led to the speculation that immune responses may contribute towards the pathogenesis of AMD. Due to the high levels of IgG detected by immunohistology in donated eyes of affected individuals, it was suggested that drusen formation occurs as a result of an immune response directed against RPE-derived antigens (Johnson *et al.,* 1999). Hageman *et al.* (2001) reviewed the current literature on drusen, covering

classification, structure and content, and put forward a hypothesis whereby drusen biogenesis is mediated by dendritic cells, recruited to the site of dysfunctional or sub-lethal RPE cells. Such cells, stressed and maybe undergoing necrosis due to influences such as injury, lipofuscin accumulation or oxidative damage, would release soluble cytokines to recruit dendritic cells from the choroidal blood vessels. Dendritic cell processes have been reported associated with small drusen, and in some regions protruding through Bruch's membrane. Once recruited and activated, dendritic cells could sustain or amplify the local inflammation and, in the case of AMD, chronic inflammation would persist with knock-on autoimmune responses. Therefore, it was proposed that drusen biogenesis occurs via two stages. The first stage involves a nucleation step, where RPE debris and dendritic cell-derived material accumulate, and the second stage involves deposition of drusen-associated constituents and a state of chronic inflammation leading to surrounding RPE cell dysfunction and subsequent retinal degeneration.

Anderson *et al.* (2002) carried out histological analysis of >400 donor AMD eyes using light, confocal and electron microscopy. They found lipofuscin-rich sub-RPE deposits containing recognisable organelles and melanin granules, suggesting an RPE origin for the debris. Analysis of drusen revealed the presence of inflammatory products including apolipoprotein E (ApoE), acute phase proteins such as C-reactive protein (CRP) and vitronectin, complement components including C5, C5b-9, C3b and C3d (see Section 1.4.1) and the complement regulators membrane co-factor (CD46) and complement receptor 1 (CR1) (see Section 1.4.2). Anderson *et al.* add to the hypothesis put forward by Hageman *et al.* to propose that primary RPE pathology (either genetic or environmental) compromises the RPE and causes the accumulation of debris between the basal lamina of the RPE and Bruch's membrane. Accumulation of debris acts as a "seeding" event resulting in a pro-inflammatory signal, involving up-regulation of local pro-inflammatory mediators, activation of the complement cascade and so deposition of associated proteins. Cellular blebs are proposed to act as nucleation sites for the formation of drusen, resulting in additional RPE cell degeneration of those cells in close proximity. It should be noted these are

hypotheses only, and although they appear to best describe the data at hand there is as yet no conclusive evidence for the biogenesis of drusen.

1.2.5 The role of phagocytes in AMD

Phagocytes present in the adult retina include dendritic cells, microglia and macrophages. Microglia can be found in the OPL, ONL and GCL, and originate from haemopoietic cells which enter via the blood vessels of the ciliary body and iris or the retinal vasculature, before differentiating into parenchymal microglia in the adult retina. In the healthy adult retina they provide roles in host defence against invading pathogens, immunoregulation and tissue repair. In the diseased eye they are involved in phagocytosis of sub-RPE debris (Chen *et al.,* 2002). Macrophages also play a role in sub-retinal debris clearance. Ineffective clearance of debris by resident retinal phagocytes such as microglia and dendritic cells leads to the recruitment of macrophages from the choroidal blood suppy (Forrester, 2003). Electron microscopy of donated eyes has shown macrophages to be associated with deposits in patients with AMD (Killingsworth *et al.,* 1990). Recruited macrophages are activated and therefore pro-angiogenic. It is therefore likely that their recruitment via chemoattractants such as immunoglobulins and complement components to the site of sub-retinal debris contributes towards disease progression (Forrester, 2003). Further evidence for the role of macrophages in AMD comes from the observation that systemic macrophages are recruited to sites where CNV is laser-induced in mice (Caicedo *et al.,* 2005).

1.2.5.1 Macrophage recruitment in AMD

Supporting evidence of a role for macrophages in the clearance of sub-RPE debris and the pathogenesis of AMD comes from analyses looking at mice deficient in the monocyte chemoattractant protein-1 (MCP-1 or CCL-2) or its cognate chemokine receptor (CCR-2). Mice deficient in either of these proteins developed lipofuscin deposits, drusen, photoreceptor atrophy and CNV, and had deposition of complement components and IgG in the RPE and choroid, as is seen in patients with AMD (Ambati *et al.,* 2003). It was therefore proposed that macrophage recruitment dysfunction may be involved in AMD pathogenesis. However, a comprehensive

genetic analysis was carried out in two independent case-control studies which found no evidence for an association between either CCL-2 or CCR-2 genetic variants and AMD. Levels of *CCL-2* and *CCR-2* mRNA were also examined in healthy and diseased RPE, with no differences in expression levels observed (Desprit *et al.,* 2008). Therefore, no evidence could be found to support a role for CCL-2 or CCR-2 polymorphisms in humans and risk of developing AMD.

1.3 Risk factors for AMD

Several risk factors have been identified for AMD. These can be environmental, and include cigarette smoking, light exposure and dietary polyunsaturated fatty acid content (Hawkins *et al.,* 1999, Mares-Perlman *et al.,* 1995, Smith *et al.,* 2001, Vojnikovic *et al.,* 2007). These environmental risk factors are all thought to contribute towards AMD disease progression by causing oxidative damage (Beatty *et al.,* 2000). Age is also a major risk factor for developing AMD. In one study, whilst there was an AMD prevalence of 0.2% in individuals aged 55-64 years, this increased to 13% in those over 85 (Smith *et al.,* 2001). In addition to environmental factors, it has been shown that there is a strong genetic influence in AMD. Analysis was carried out looking at AMD prevalence in monozygotic and dizygotic twins, with a concordance of 0.37 in the former compared with 0.19 in the latter. The heritability of AMD was estimated at 45% (Hammond *et al.,* 2002).

1.3.1 Genes showing association with AMD

Several genes have been associated with retinal degenerations, either mutated in diseases similar to AMD but showing Mendelian inheritance, or having polymorphisms which confer increased risk of developing AMD. For instance, sequence variation in *fibulin5*, a member of the fibulin gene family has been associated with increased risk of AMD (Stone *et al.,* 2004). Fibulin proteins interact with other extracellular matrix proteins such as collagens, elastins, fibronectins and elastins, and *fibulin3* was found to be mutated in a Malattia leventinese, a disease characterised by confluent sub-RPE drusen (Stone *et al.,* 1999). This would suggest extracellular matrix dysfunction can contribute towards AMD disease progression. It

has also been suggested that polymorphisms in the photoreceptor cell-specific ATP-binding cassette transporter gene (*ABCA4)* are associated with increased risk of AMD (Allikmets *et al.,* 1997, Allikmets *et al.,* 2000), although this has not been confirmed by others (Schmidt *et al.,* 2003). Other genes which have been implicated include *fibulin6, VEGF, APOE* and *TLR4* (*Toll-like receptor 4*) (Scholl *et al.,* 2007).

1.3.2 Identifying loci 1q25-q31 and 10q26 associated with risk of AMD

Whilst some models of AMD do show Mendelian inheritance, the vast majority of AMD risk appears to be complex, with disease susceptibility determined by a combination of environmental and genetic factors. Linkage analysis was carried out looking at a large family consisting of 20 affected and 10 unaffected individuals, with polymorphism in the *ARMD1* locus (1q25-q31) identified as being associated with increased risk (Klein, 1998). Further studies were carried out using linkage analysis and genomewide association studies which supported this result. Other regions were also identified, including a locus in chromosomal region 10q26 (Majewski *et al.,* 2003, Seddon *et al.,* 2003, Iyengar *et al.,* 2003, Schick *et al.,* 2003, Weeks *et al.,* 2004, Abecasis *et al.,* 2004). Fisher *et al.* (2005) carried out a genome-scan-meta-analysis (GSMA) of the combined data from these studies and highlighted the 10q26 locus as showing the greatest AMD susceptibility risk (p=0.00025), although 1q25-q31 was also highlighted. The 10q26 locus contains the genes for the high temperature requirement serine protease (HTRA1) and LOC387715 or ARMS2 (age-related maculopathy susceptibility 2), and 1q26-q31 contains the regulators of complement activation (*RCA*) gene cluster.

1.3.2.1 ARMS2/HTRA1 and risk of AMD

The single nucleotide polymorphism (SNP) identified in 10q26 lies in an intergenic region between the genes for *HTRA1* and *ARMS2*. There is currently a debate surrounding which polymorphism in the two genes is responsible for the increased risk of AMD, which is compounded by the two proteins being in strong linkage disequilibrium (Allikmets *et al.,* 2008). It has been reported that a polymorphism in the promoter region of *HTRA1* is responsible, with two studies in Chinese and Caucasian populations confirming this. HTRA1 is a protease chaperone activated in

response to cellular stress, and immunostaining has shown it to be localised within drusen of AMD individuals (DeWan *et al.,* 2006, Yan *et al.,* 2006). However, other studies have reported that the 10q26 locus risk is attributable to an allele arising from a deletion-insertion in *ARMS2*, removing the polyadenylation signal and resulting in unstable mRNA and a putative null allele (Kanda *et al.,* 2007, Fritsche *et al.,* 2008). The debate has yet to be resolved.

1.3.2.2 The *RCA* gene cluster

The "Regulators of Complement Activity" (RCA) gene cluster consists of a tandem array of >60 genes, 15 of which are complement-related. Within this region is a 355-kb segment encoding complement factor H (CFH) and the CFH-related proteins, CFHR3, CFHR1, CFHR4, CFHR2 and CFHR5. Complement factor H is a regulatory protein in the alternative activation pathway of the complement system involved in innate immunity, and consists of 20 short consensus repeats (SCR). *CFHR1-5* are thought to have arisen by partial gene duplication events of *CFH*, and contain homologues of CFH SCRs 6-9 and 19-20 (Zipfel *et al.,* 1994).

1.3.2.3 A complement factor H Y402H polymorphism and risk of AMD

Following on from the identification of 1q26-q31 being associated with increased risk of AMD, further investigations were carried out into this region to narrow down the specific loci responsible. Single nucleotide polymorphisms were analysed within this region, comparing case and control populations, with a Y402H polymorphism in *CFH* found to show significant association ($p=4.95x10^{-10}$ and $p<10^{-7}$). Odds ratios of 2.7/2.45 and 5.57 were given for heterozygosity and homozygosity of the high risk (402H) allele (Edwards *et al.,* 2005, Haines *et al.,* 2005). The Y402H polymorphism was again confirmed by a genomewide association study, with a SNP identified that was in linkage disequilibrium with Y402H. The homozygous risk was reported as a 7.4-fold increase (Klein *et al.,* 2005).

1.3.2.4 Risk associated with other *CFH* SNPs and haplotypes

Further investigation of *CFH* revealed additional SNPs associated with increased risk of AMD. Maller *et al.* (2006) identified an intronic non-coding SNP showing strong

association, and Hageman *et al.* (2005) showed risk association of I62V, a missense variant present in a predicted exon splice enhancer. Li *et al.* (2006) identified 20 variants within *CFH* which showed strong association with disease susceptibility greater than that reported for Y402H, with the SNPs showing the strongest association occurring in non-coding regions suggesting regulation of *CFH* expression may be important for disease progression. They found 4 major *CFH* haplotypes, 2 protective and 2 risk, and numerous rare haplotypes. From this it was concluded there are multiple disease-predisposing variants, and multiple *CFH* haplotypes modulate AMD risk. Hageman *et al.* (2005) also identified *CFH* haplotypes associated with risk of AMD. They identified an at-risk haplotype present in 50% of cases and 26% of controls, with homozygotes for the haplotype comprising 24% of cases and only 8% of controls. Protective haplotypes were also identified (OR = 0.44 – 0.55).

1.3.2.5 CFH-like proteins and AMD risk

An AMD protective haplotype was identified which contains an 83kb deletion of *CFHR1* and *CFHR3* (Hughes *et al.,* 2006). Looking at 173 cases and 170 controls, the deletion was found to be present in 20% of control chromosomes and 8% of cases. The deletion occurs 6.4kb downstream of *CFH* and *CFHL1* between two 29kb duplicated segments of DNA. This result was confirmed by Hageman *et al.* (2006), with Spencer *et al.* (2007) also confirming the protective effect of this *delCFHR1/CFHR3* haplotype.

1.3.2.6 Variants in Factor B and C2 are associated with risk of AMD

Factor B and C2 are proteins involved in the same complement pathway as CFH. The genes *BF* and *C2* are located in the Major Histcompatibility Complex III (MHCIII) region at chromosomal region 6p21. Haplotypes were identified in two studies associated with reduced risk of AMD. Gold *et al.* (2006) identified haplotypes of L9H in *BF* and E318D in *C2* (haplotype A), and R32Q in *BF* with a variant in intron 10 of *C2* (haplotype B) as conferring significantly reduced risks with odds rations of 0.45 and 0.36 respectively. Maller *et al.* (2006) confirmed the

association of these alleles with AMD, with $P<10^{-5}$ for haplotype A and $P<10^{-11}$ for haplotype B.

1.3.2.7 Variant in C3 is also associated with risk of AMD

C3 and C5 are major components of the complement cascade of which CFH plays a part. Yates *et al*. (2007) looked at 13 SNPs in C3 and C5 using English and Scottish cohorts to see if there was any association with AMD. An R102G polymorphism was found to be significantly associated in both groups (English $P= 5.9x10^{-5}$, Scottish $P=5.0x10^{-5}$). The C3 polymorphism L314P was also identified as showing association with risk of AMD. R102G and L314P are in strong linkage disequilibrium, however it was shown by Spencer *et al.* (2008) that the R102G polymorphism acting alone best explains the effect on disease risk.

1.4 The Complement System

The complement system is part of the innate immune system. It comprises >30 plasma and cell surface proteins, and provides host protection against invading pathogens and altered host cells. Complement activation can result in cell lysis, activation of inflammatory processes and phagocytosis (Walport *et al.,* 2001, Gros *et al.* 2008).

1.4.1 Complement activation

Complement activation occurs via the classical, alternative or mannose-binding lectin (MBL) pathways, initiating enzymatic cascades which result in the formation of inflammatory mediators and the membrane attack complex (MAC). This is a lipophilic protein complex which forms in the plasma membrane of targeted cells causing their lysis. Figure 1.6 summarises the pathways involved in complement activation. Following complement activation, C3 is cleaved to form C3b. C3b binds to the C3 convertases C4bC2a and C3bBb, formed by the classical, MBL or alternative pathways, to form the C5 convertases. These cleave C5 to C5a and C5b. C5b can then interact with C6, C7 and C8 at the target plasma membrane. This complex then combines with several molecules of C9 which form the MAC, a ring

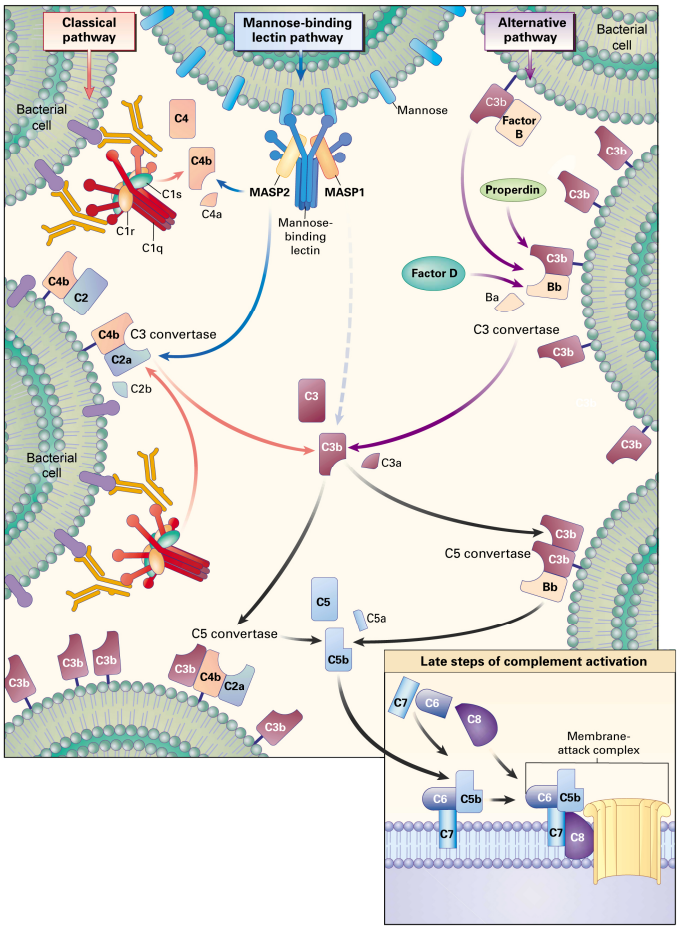

Figure 1.6: The complement pathway.
(source: Walport, 2001)

The three pathways involved in complement activation:
During classical activation, the C1q complex binds to antibodies bound to a target surface. C1q then cleaves C4 to C4a and C4b. C4b then cleaves C2, enabling the formation of the C4bC2a C3 convertase. During mannose-binding lectin (MBL) activation, MBL, in comlex with MASP1 and MASP2 (mannose-binding lectin-associates proteases 1 and 2), binds to mannose residues on bacterial cell surfaces. This then initiates formation of the C4bC2a C3 convertase in the same manner as C1q. During alternative pathway activation, low levels of C3 cleavage occur in the plasma. The resulting C3b can bind to cell surfaces, bind factor B and form the C3bB complex. Factor D then cleaves Factor B, resulting in the C3bBb C3 convertase. Both forms of the C3 convertase cleave C3 into C3b, which can then bnd to C4b and form the C5 convertase, and initiate formation of the membrane attack complex (MAC).

structure traversing the plasma membrane and causing cell lysis (Walport *et al.* 2001, Gros *et al.* 2008).

The classical activation pathway involves antibodies bound to target surfaces, which the C1 complex, comprising C1q, two molecules of C1r and two molecules of C1s, attaches to. This allows C1s to cleave C4 into C4a and C4b. C4b attaches to the target membrane and cleaves C2 into C2a and C2b. C4b combines with C2a to form the C3 convertase of the classical pathway, C4bC2a. This then cleaves C3 to form C3b (Walport *et al.,* 2001).

During MBL activation mannose-binding lectin (MBL) in complex with mannose-binding lectin-associated proteases 1 and 2 (MASP1 and MASP2) binds to mannose groups on the surface of bacterial cells. MASP2 cleaves C4 and, following the same mechanism as for the classical activation pathway, the C4bC2a convertase is formed. MASP1 is thought to cleave C3 directly to form C3b (Walport *et al.,* 2001).

At low levels, C3 spontaneously cleaves to form C3b in plasma. This can then bind to target surfaces where it combines with Factor B. Factor D then cleaves bound Factor B to form the C3 convertase of the alternative pathway, C3bBb. Properdin then binds to stabilise the structure (Walport *et al.,* 2001).

As well as forming the C3 convertases, cleavage of C3 is also required for opsonization of target surfaces for phagocytosis, for instance by macrophages. Following initial cleavage of C3, C3b is further degraded to iC3b, C3c and C3dg. These proteins bind to target surfaces and act as ligands for phagocyte complement receptors (see Section 1.4.2) (van Lookeren Campagne *et al.,* 2007).

1.4.2 Regulation of complement activation

Regulation of complement activation is required to prevent attack of host tissues. C3b is unable to discriminate against host or invading surfaces so mechanisms have evolved either to prevent C3b attachment to host surfaces or to deactivate it when it does. Complement regulators are either soluble or surface bound. Such surface-

bound receptors are the complement receptors, membrane co-factor (CD46) and decay accelerating factor (CD55). The main soluble regulator is CFH, which acts as a co-factor with Factor I (FI).

The coating of particles with C3b opsinizes them for recognition and phagocytosis by phagocytes expressing the complement receptors. These include CR1 (CD35), CR2 (CD21), CR3 (CD11b/CD18), CR4 (CD11c/CD18) (Pangburn *et al.,* 1980, Holers *et al.,* 1992) and the macrophage complement receptor CRIg. The CRIg receptor consists of membrane-attached IgV domains (Helmy *et al.,* 2006). It not only acts as a receptor of C3b-opsonized particles, but also inhibits the C3bBb convertase by attachment and steric hindrance of substrate binding (Wiesmann *et al.,* 2006).

CD46 is a type I transmembrane glycoprotein consisting of four short consensus repeats, followed by a serine, threonine and proline-rich region, a 12 amino acid region of unknown function, a transmembrane domain and a cytoplasmic anchor. CD46 is a cofactor for Factor I cleavage of C3b and C4b. C3b is cleaved to form C3bi and soluble C3f, whereas C4b is cleaved to form C4d and soluble C4c (Riley-Vargas *et al.,* 2004).

CD55 consists of four SCRs attached to the plasma membrane via a glycosylphosphatidylinositol (GPI)-anchor. It prevents the assembly or promotes the disassembly of C3bBb (Kim *et al.,* 2005).

1.5 Complement Factor H

Complement factor H (CFH) is a 155 kDa plasma glycoprotein consisting of 1213 amino acids. It is secreted mainly by the liver and into the circulation, and comprises 20 SCRs, each of approximately 60 amino acids, and an 18 amino acid leader sequence (Whaley *et al.*, 1976, Ripoche *et al.*, 1988).

1.5.1 CFH co-factor activity with Factor I

CFH was first shown to be a co-factor for Factor I-mediated degradation of C3b by Whaley *et al* (1976). This was later confirmed by Pangburn *et al* (1977). Factor H binds to C3b and prevents it from interacting with Factor B and acts as a co-factor in the cleavage of C3b to iC3b by Factor I, with which it also shows an interaction possibly to stabilise the complex (Pangburn *et al.,* 1978, Nagaki *et al.,* 1978, Conrad *et al.,* 1978, Pangburn *et al.,* 1977, Soames *et al.,* 1997). The domains within CFH capable of C3b binding have been identified to be within the N-terminal SCRs 1-4 (Kuhn *et al.,* 1995), the C-terminal SCR20, and a potential third site contained within the central SCRs of the molecule (Oppermann *et al.,* 2006, Jokiranta *et al.,* 2000, Sharma *et al.,* 2003). Further analysis of these sites revealed that each has a distinct C3b binding site. SCR1-4 will only bind to uncleaved C3b, SCR12-14 will interact with C3b, C3c and C3d, and SCR20 will only interact with the C3d component of C3b (Jokiranta *et al.,* 2000). Binding to cell-surface-bound C3b has been shown to occur via SRCs 19-20 (Ferreira *et al.,* 2006).

1.5.2 DAF activity of CFH

As well as showing co-factor activity for FI-mediated degradation of C3b, CFH shows decay accelerating activity, causing the dissociation of the C3 convertases bound to non-activator surfaces (Whaley *et al.,* 1976). This activity was confirmed by Kuhn *et al.* (1996) using alternative pathway convertases bound to the surface of sheep red blood cells. Recombinant fragments of CFH showed this activity mapped to SCR1-4, and that this activity was shared with the alternatively-spliced form of CFH, FHL-1 (see Section 1.5.6).

1.5.3 CFH binding polyanions and host cells

Following on from the initial observation that certain micro-organism-derived polysaccharides could bind C3b and that this complex was then resistant to CFH/Factor I inactivation (Fearon *et al.,* 1977), and from a further study showing host polyanions could enhance CFH affinity for C3b and so inhibit complement activation (Meri *et al.,* 1990), it was found that CFH recognises and binds to certain polyanions on host surfaces, providing host protection from complement activation.

Various polyanions have been identified as showing interactions with CFH, with the polyanion interaction sites within CFH mapped to SCR7 and SCR20 (Blackmore *et al.,* 1996, Blackmore *et al.,* 1998). Subsequently it has been shown that the initial binding of CFH to host endothelial cells occurs via the C-terminal SCR20 polyanion binding site (Jokiranta *et al.,* 2005, Ferreira *et al.,* 2006).

1.5.4 CFH interacts with CRP

C-reactive protein (CRP) is a 120kDa acute phase protein which causes amplification of the complement classical activation pathway (Volanakis *et al.,* 1974). It is a member of the pentraxin family of proteins, containing cyclic pentameric proteins. Synthesised in the liver, normal circulating plasma concentrations are less than 1μg/ml. However, following stimulation of expression, for instance by interleukins 1 (IL-1) and 6 (IL-6), plasma levels can increase up to 500μg/ml (Baumann *et al.,* 1994). It has been shown that CRP binds the surface of apoptotic cells, recruiting CFH and preventing assembly of the MAC. CRP then activates the classical pathway and so C3 opsinisation, facilitating removal of the apoptotic cell by phagocytes such as macrophages. CRP was also shown to up-regulate macrophage expression of the transforming growth factor β (TGF-β), thus reducing inflammation (Gershov *et al.,* 2000). CRP binding sites within CFH have been mapped to SCR7 and SCR8-11 (Jarva *et al.,* 1999, Giannakis *et al.,* 2003). There is some debate over the physiological relevance of the published data regarding CRP interactions with CFH and its subsequent influence on the phagocytosis of apoptotic cells, with other published studies challenging these findings. Hart *et al.* (2005) found no evidence that CRP facilitated uptake of apoptotic cells by macrophages, and Biro *et al.* (2007) suggest that in its native pentameric state CRP does not bind CFH. Previous studies have used CRP coated directly onto surfaces, however Biro *et al.* showed that unless CRP is attached to its ligand, phosphatidyl choline, it looses its pentameric structure. Native CRP is unable to activate the classical pathway unless bound to phosphacholine, whereas denatured CRP can. Also, when bound to phosphocholine, native CRP shows no interaction with CFH, suggesting that this interaction does not occur *in vivo*.

1.5.5 CFH secondary structure and regulation of activity

It has been suggested that CFH in plasma exists as a coiled, omega structure, reducing the exposure of several SCR residues, and that upon binding to glycosaminoglycans (GAG) or host cells the protein undergoes a conformational change. This then exposes residues and helps regulate when and where CFH activity can occur (Oppermann *et al.,* 2006). This model predicts that SCR20 is responsible for initial CFH ligand binding. Observations that 1) binding of CFH to endothelial cells occurs via the carboxy-terminal of the protein (Jokiranta *et al.,* 2005), 2) CFH interactions with cell-bound C3b can be inhibited by isolated recombinant SCR19-20 (Ferreira *et al.,* 2006), 3) the RGD domain in SCR4 is inaccessible in CFH but exposed in it's alternatively spliced form Factor H-like protein 1 (FHL-1) (which lacks SCRs 8-20) (Hellwage *et al.,* 1997), and 4) antibodies have been identified which interact with conformational epitopes of CFH but not the linear protein (Oppermann *et al.,* 2006) all support this model. Prosser *et al.* (2007) propose a model where CFH binds surface polyanions via SCR20 facilitating the subsequent binding of SCR6-8 (see Section 1.6.4, and Figure 1.8).

1.5.6 CFH-like proteins FHL-1 and CFHR-1-5

CFH, its alternatively spliced form FHL-1 and the CFH-like proteins, CFHR1-5, are all plasma glycoproteins predominantly produced and secreted by the liver. FHL-1 comprises CFH SCRs 1-7 plus 4 additional C-terminal amino acids. CFHR1-5 comprise SCRs which share homology with CFH SCRs 6-9 and 18-20 (Jozi *et al.,* 2008).

1.5.6.1 CFHR1-5 functions

The CFH-related proteins show similar ligand binding properties and functions to CFH (Jozsi & Zipfel, 2008). CFHR1 is thought to compete for surface ligand binding with CFH, and so the protective effect of a CFHR1 and CFHR3 deletion with regards to developing AMD may be due to increased CFH protection in the retina. CFHR3 and CFHR4 have been shown to bind the C3d region of C3b. Whilst neither protein shows DAF activity or independent co-factor activity with Factor I, when a small amount of CFH or FHL-1 is present then they enhance Factor I

mediated C3b inactivation (Hellwage *et al.,* 1999). CFHR5 has been shown to bind C3b, heparin and CRP, and displays co-factor activity with Factor I for the degradation of C3bBb, although to a lesser degree than CFH (McRae *et al.,* 2005). The proteins CFHR1-5 are therefore predicted to have roles in regulation of complement, either independently or possibly in cooperation or competition with CFH (Jozsi & Zipfel, 2008).

1.5.6.2 FHL-1 function

FHL-1, like CFH, displays decay accelerating factor (DAF) and factor I co-factor activity. SCR1-4 have been shown to be necessary for co-factor activity with Factor I, as is observed with CFH, and, again as observed with CFH, DAF activity has also been mapped to this region, although FHL-1 shows reduced DAF activity when compared with CFH, and contains an exposed RGD motif on SCR4 which is not exposed on CFH. This enables cell adhesion via integrin receptors, and FHL-1 is thought to play a role in the spreading and adhesion of anchorage-dependant cells (reviewed by Zipfel *et al.,* 1999).

1.6 CFH and disease mechanisms in AMD

Following on from the studies implicating CFH polymorphism with increased risk of developing AMD, many studies have been carried out to investigate a function for CFH in AMD. Studies have focused on roles for CFH in the healthy retina as well as how the Y402H polymorphism affects the protein function.

1.6.1 CFH expression and CFH localisation in the eye

A study by Mandal *et al.* (2006a) was carried out investigating CFH expression and localisation within the mouse eye. CFH was detectable in the eye at P1, with no difference in expression levels at P30. However, at P180 expression was significantly higher, and at P300 higher still. Analysis of different eye tissues revealed CFH expression was mainly in the posterior tissues of the RPE, choroid and sclera, with low levels observed in the iris-ciliary body and lens. Minimal expression was observed in the retina, and none was in the cornea. Immunohistology of mouse

ocular tissues showed CFH localising to the RPE, ciliary epithelium, outer plexiform layer, inner plexiform layer, ganglion cell layers and in the limiting membranes, although it is acknowledged that labelling in the inner plexiform layer could be migratory ganglion cells. Another study (Chen *et al.,* 2006) showed, by immunohistology of mouse eye cryosections, that CFH was present in the choroidal vessels, Bruch's membrane and RPE cells. A diffuse punctate distribution was also observed in the interphotoreceptor matrix, although no staining was observed at any other localisation within the eye.

1.6.2 CFH expression by the RPE

CFH/FHL-1 is produced and secreted by mouse and human RPE cells (Chen *et al.,* 2006). Because a major function of the RPE is phagocytosis of rod outer segments, and lipofuscin accumulation has been suggested to be caused by phagocytosis of oxidised ROS (ox-ROS), the effects on CFH production by RPE due to exposure to ROS and oxidised ROS were investigated. Although short-term (2 hour) exposure to ROS and ox-ROS had no effects on CFH synthesis, after 24 hours exposure to ox-ROS CFH synthesis decreased. Normal ROS had no effect on levels of synthesis, although 24 hour exposure to both ROS and ox-ROS did lower intracellular CFH levels suggesting that CFH secretion is stimulated. It is postulated that ox-ROS may damage the cells and impair their ability to produce CFH, and that this could be a gradual process exacerbated by an ageing RPE, resulting in less CFH secretion. CFH secretion was also shown to be reduced in RPE cells by exposure to tumour necrosis factor α (TNF-α) and IL-6, both inflammatory cytokines. As low-level inflammation is associated with AMD, it is suggested there are potential implications for this result in AMD pathogenesis too (Chen *et al.,* 2006).

Oxidative stress has also been shown to affect CFH expression by the RPE (Wu *et al.,* 2007). Whilst interferon-γ (INF-γ) increases CFH expression, as shown by Western blot of cell lysates, oxidative stress due to exposure to H_2O_2, paraquat or $FeSO_4$ reduced this effect. The mechamism was shown to involve the activator signal transducers and activators of transcription 1 (STAT1) and repressor forkhead box 03 (FOXO3), with INF-γ inducing FOXO3 translocation to the nucleus and

binding to STAT1, and oxidative stress acetylating FOXO3 resulting in its preferential binding to the CFH promoter, reducing CFH expression.

1.6.3 CFH knockout mouse and retinal phenotype

A comparison was carried out between normal and age-matched CFH knockout ($CFH^{-/-}$) mice. Phenotypic observations included a reduction in visual acuity, increased photoreceptor dysfunction and increased sub-retinal autofluorescence when compared with the wild-type mouse. In wild-type mice, C3 deposits are observed in Bruch's membrane but not the RPE or retina, whereas in $CFH^{-/-}$ mice C3 deposits were also observed fragmented in Bruch's membrane, extending into the RPE, and also in the neuroretina. Ultrastructural phenotypes included reduced sub-RPE electron dense material and reduced Bruch's membrane thickness. It should be noted that this is the opposite of that observed in AMD patients. It was suggested that in the $CFH^{-/-}$ mice increased C3 deposition leads to increased deposit clearance. In addition, the RPE-ROS boundary is disrupted, with reduced apical microvilli and ROS misalignment. The apical/basal polarity of RPE organelles also appears to be disrupted.

1.6.4 Effects of the Y402H polymorphism on CFH function

The Y402H polymorphism occurs in SCR7 of CFH. This is a region which is involved in binding to GAGs and CRP. Studies have been carried out to see if these functions are affected by this polymorphism and to gain insight into possible disease mechanisms. Clark *et al.* (2006) investigated interactions of recombinant SCR6-8 (402Y and 402H alleles) with different heparins. It was found that the two alleles showed different binding properties dependant upon which heparin was present. Interactions were investigated by plate binding assay and heparin affinity columns, using various differently desulphated heparins. It was hypothesised that age-related changes in GAG composition affect CFH binding and so have implications for AMD disease mechanisms. Further investigation of the interaction with heparin was carried out by Herbert *et al.* (2007). It was shown that SCR7 adopts an elongated structure with respect to neighbouring SCR6 and SCR8, exposing the Y402H residue, and that the structures were the same for the two variants. The histidine

allele of SCR7 was found to have a higher affinity for heparin affinity columns and also gel mobility shift assays (GMSA) found it showed greater retardation of different size-fractionated heparins when compared to the tyrosine allele. No differences were observed when SCR6-8 was used. Fernando *et al.* (2007) however, provided data suggesting that SCR6-8 actually forms a bent-back structure, where SCR6 and SCR8 approach each other, with the heparin binding residues exposed on the outside curvature of the molecule, and that binding of heparin was likely to alter this structure slightly. Prosser *et al.* (2007) determined the crystal structure of SCR6-8 (histidine allele) in complex with sucrose octasulphate (SOS). They showed that the Y402H residue is directly involved in GAG binding, in combination with other residues within SCR6-8. They propose a model where these GAG binding residues are contained within a groove formed from modules 6-8, capable of interacting with a single GAG molecule. Full length CFH is predicted to interact with this GAG molecule via modules 6-8 and 20, where it is localised to the surface and able to hold C3b in a pincer. Having a tyrosine at residue 402 would alter the GAG specificity of the binding site.

Laine *et al.* (2007) have reported differences between the two alleles in their ability to bind CRP. CRP binding sites in CFH have been mapped to SCR7 and SCR8-11. They investigated the ability of either recombinant modules 5-7 (both alleles) or full length CFH (purified from plasma of either AMD patients homozygous for the histidine allele, or unaffected controls homozygous for the tyrosine allele). They found that in both cases the histidine allele showed reduced binding affinity to CRP. This difference was greater for the recombinant modules SCR5-7, as would be expected due to the additional CRP binding site in full length CFH SCR8-11. They suggest that a reduced binding affinity for CRP could reduce the ability of the CFH-CRP complex to promote non-inflammatory debris clearance, leading to accumulation of debris and inflammation. Other studies looking at the effects of the Y402H polymorphism of CFH ligand binding confirmed the reduced binding affinity of the histidine allele for CRP (Sjoberg *et al.,* 2007, Skerka *et al.,* 2007). Skerka *et al.* also showed that the histidine allele of FHL-1 has reduced CRP binding ability, as well as to heparin. Elevated levels of deposited CRP have been observed in the

choroidal stroma of individuals homozygous for the histidine allele (Johnson *et al.,* 2007). No differences were observed for CFH or albumin, suggesting that the deposition is CRP-specific rather than a result of leaky choroidal capillaries. It is proposed that this observation is due to a state of chronic inflammation due to altered complement inhibition as a result of the Y402H polymorphism.

1.6.5 CFH mutations and kidney disease

Mutations in CFH have also been associated with the kidney diseases membranoproliferative glomerulanephritis type II (MPGNII) and atypical haemolytic uraemic syndrome (aHUS). MPGNII presents with complement-containing dense deposits in the basement membrane of the glomerular capillary wall, whereas aHUS presents with hemolytic anemia, glomerular endothelial cell damage, alternative pathway activation and progression to end-stage renal disease (Zipfel *et al.,* 2006). Also associated with MPGNII are Bruch's membrane deposits similar in structure and composition to the drusen observed in AMD (Mullins *et al.,* 2001, Montes *et al.,* 2008). Patients with MPGNII have low plasma CFH levels, as well as low C3 levels thought to be the result of CFH-deficient alternative complement pathway activation. C3 deposition is observed along the glomerular capillary walls and C3c was shown by immunohistology to be a primary component of the glomerular dense deposits, supporting this dysregulation of complement activation (Abrera-Abeleda *et al.,* 2005, Montes *et al.,* 2008). MPGNII disease mechanisms are therefore thought to be the result of low plasma CFH causing systemic alternative pathway activation and dense deposit deposition on both Bruch's memebrane and the kidney glomerular basement membrane. This is supported by the observation that both pigs and mice deficient for CFH develop symptoms similar to MPGN II (Hogasen *et al.,* 1995, Pickering *et al.,* 2002).

Disease-causing mutations in aHUS tend to occur in the C-terminal SCR19-20. This is the region involved in initial cell-surface polyanion binding, and it is thought that the disease-causing mutations compromise this ability. This then results in surface complement activation and the subsequent aHUS-associated tissue damage (Jokiranta *et al.,* 2005, Herbert *et al.,* 2006). Further structural analysis of the CFH

C-terminal polyanion binding site revealed that aHUS-associated mutations directly affected this binding site (Herbert *et al.,* 2006). In addition to mutations within CFH, aHUS can arise due to non-homologous recombination within the RCA gene cluster resulting in a *CFH/CFHR1* hybrid gene, consisting of the first 21 exons of *CFH* and the last 2 exons of *CFHR1* (Venables *et al.,* 2006). Further aHUS-associated non-homologous recombinations within the RCA gene cluster have resulted in deletions of *CFHR3* and *CFHR1*, whilst leaving *CFH* intact, suggesting that CFHR3 and/or CFHR1 have roles in regulating complement activation on cell and tissue surfaces (Zipfel *et al.,* 2007) (see Section 1.5.6).

1.7 Late-onset retinal macular degeneration

Late-onset retinal macular degeneration (L-ORMD) is a rare, autosomal dominant disease characterised by extensive sub-RPE deposits, leading to progressive loss of central and then peripheral vision (Duval *et al.,* 1986, Brosnahan *et al.,* 1994, Kuntz *et al.,* 1996, Milam *et al.,* 2000, Jacobson *et al.,* 2001). The disease is similar to AMD with punctate yellow-white lesions observed in the retina of affected individuals. First reported disease symptoms are visual disturbances and difficulty in dark adaptation from about the fifth decade. A study looking at 3 affected families testing 17 individuals at 50:50 risk of developing L-ORMD found such dark adaptation abnormalities to be an early phenotypic marker for disease progression (Jacobson *et al.,* 2001). Investigations revealed rod adaptation kinetics to be affected, resulting in a reduction in rod electroretinography (ERG) b-wave kinetics (Kuntz *et al.,* 1996, Milam *et al.,* 2000). These dark adaptation abnormalities were more pronounced in the macula than in the peripheral retina (Figure 1.7) (Hayward *et al.,* 2003). Affected individuals have also been reported to have long anterior lens zonules (Ayyagari *et al.,* 2005).

1.7.1 Diseased retinal structure

Post-mortem examination was carried out on donated eye from elderly affected individuals, revealing posterior retinal disruption affecting the photoreceptors, RPE and Bruch's membrane, although the retina anterior to this did not appear to be

greatly affected. There was thinning of the retina, photoreceptor loss, retinal atrophy and a hyper-pigmented macula. New blood vessels were formed extending from the choriocapillaris through Bruch's membrane, and disciform scarring was also observed indicating old CNV (Kuntz *et al.,* 1996, Milam *et al.,* 2000). Studies on eyes donated from two affected brothers showed retinal atrophy except in the peripheral retina and only the occasional photoreceptor in the macula. Rod outer segments were shortened with disorganised disc membranes, with this disorganisation being greater in the central retina (Duval *et al.,* 1986). A donated eye from an affected individual aged 80 years showed extensive deposits between the RPE and Bruch's membrane, with associated degeneration of the neural retina including loss of cells and normal retinal structure (Figure 1.7) (Hayward *et al.,* 2003).

1.7.2 Sub-RPE deposits in L-ORMD

Extensive deposits were observed between Bruch's membrane and the RPE, ending anteriorly at the *ora serrata* and posteriorly at the edge of Bruch's membrane at the optic nerve head. In places the deposits were greater than 50μm thick and extended from the basal lamina of the RPE to the inner collagenous layer of Bruch's membrane (Kuntz *et al.,* 1996). These deposits were found to have many components including collagen, lipids, amyloid P, lysozyme, elastin, apolipoprotein B-100, calcium, esterified and unesterified cholesterol and rhodopsin, with Muller cell processes also observed in some regions (Kuntz *et al.,* 1996, Milam *et al.,* 2000). Duval *et al.* (1986) carried out light microscopy analysis of deposits showing occasional mononuclear cells and lipofuscin autofluorescence. Electron microscopy revealed fibrous growth, with deposits anteriorly showing amorphous material with electron dense material inclusions and posteriorly showing more granular material and possible macrophages. Further microscopy studies were carried out by Milam *et al.* (2000). Light microscopic analysis of sections of a donated eye revealed spheres of deposits, elevating overlying RPE cells (Figure 1.8), with thick laminated deposits formed by coalescence of these spherical deposits (Figure 1.8). Electron microscopy confirmed the apical displacement of RPE cells by spherical deposits, which consisted of basal lamina-like surface shells and cores containing wide-spaced

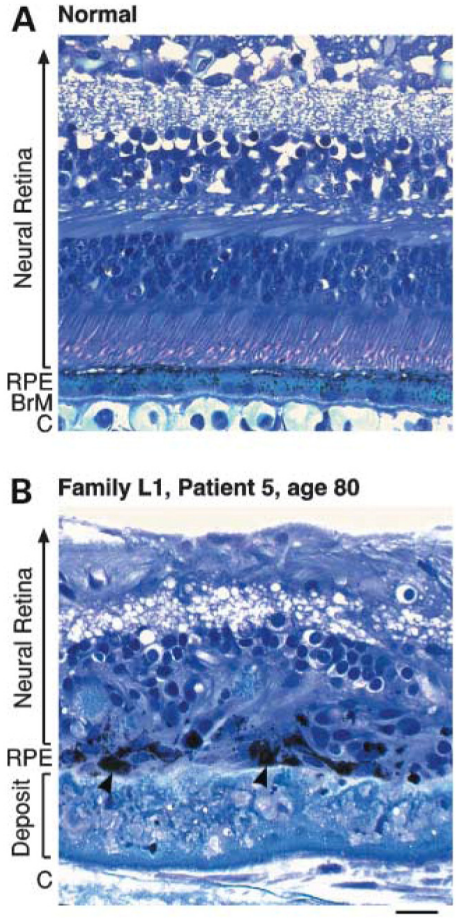

Figure 1.7: Sub-RPE deposits observed in L-ORMD patients.
(Hayward *et al.,* 2003)

Patients with L-ORMD have extensive sub-RPE deposits.
The normal retina (A) has a thin Bruch's membrane (BrM) and healthy neural retina.
The L-ORMD retina (B) has a thick layer of extracellular deposits, with heavily pigmented RPE cells (arrow). The neural retina is also degenerate. Bar: 100µm

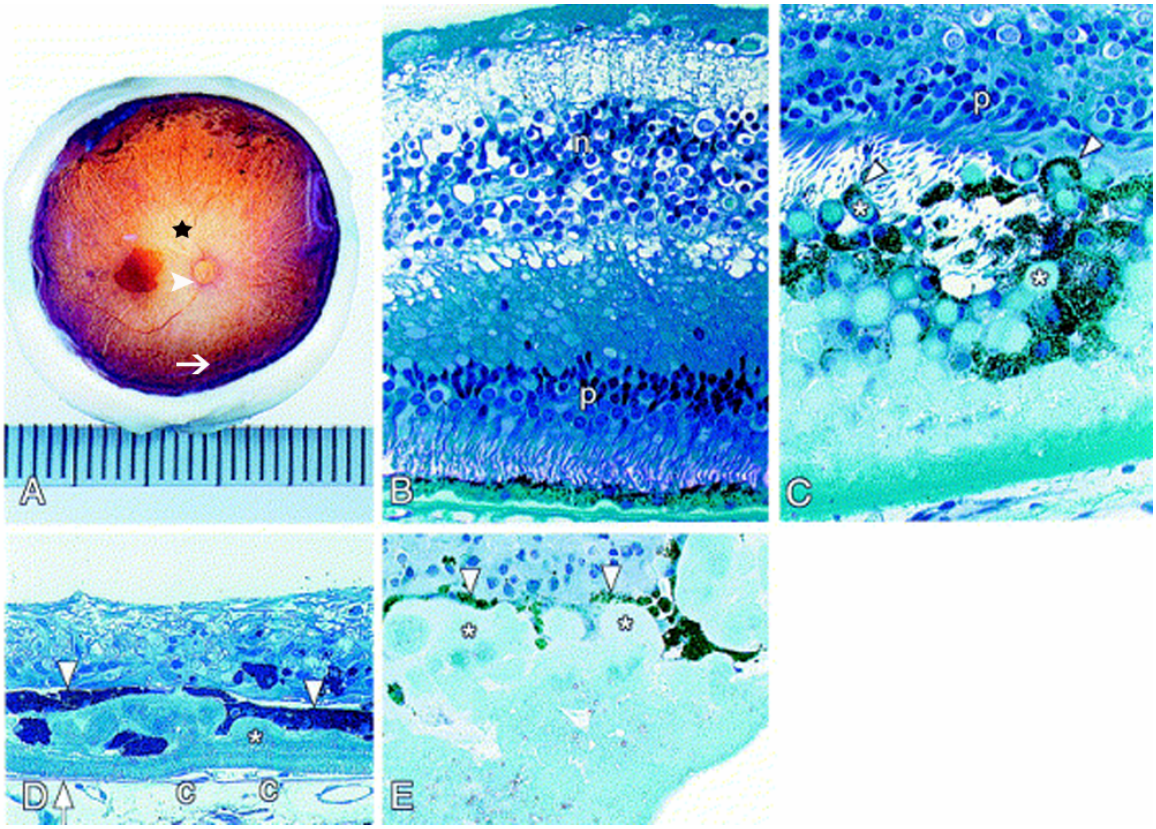

Figure 1.8: Microscopic analysis of L-ORMD deposits
(source: Milam *et al.,* 2000)

A - Pathology of a donor L-ORMD eye, showing atrophic retina and optic nerve (arrow head), thinned retina and hyperpigmented macula (*). Pigment deposits are observed in the far peripheral retina (arrow).
B – Bruch's membrane (B) is thickened and there is a decreased number of photoreceptors (p) (n – inner nuclear layer).
C – Far peripheral retina showing spherical deposits (*) elevating overlying RPE cells (arrowhead) (p – photoreceptor nuclei).
D – Midperipheral retina, showing thick laminated deposits (*) between the RPE (arrowhead) and the elastin layer of Bruch's membrane (arrow), c indicates new capillaries. No photoreceptros are present.
E – Sub-RPE deposits are formed by coalescence of sherical deposits seen in C (arrowheads – RPE cells).

collagen. Basal processes from the RPE extended into the deposits and observed omega-shaped profiles suggested exocytosis of packets of fibrillar material into the deposits. The deposits were described as resembling the BlamD but not the BlinD seen in AMD.

1.7.3 Identification of a disease-causing mutation in *C1QTNF5*

With initial patient diagnosis that of an autosomal dominant retinitis pigmentosa screening was carried out for mutations in rhodopsin, peripherin and TIMP3, however no mutations were found (Kuntz *et al.,* 1996). Genetic analysis was subsequently carried out looking at 14 affected families to identify a disease-causing mutation. The mutation was found to be a serine to arginine (Ser163Arg) mutation in *C1q and tumour necrosis factor related protein 5* (*C1QTNF5*), with 7/14 affected families and 0/100 control families showing the mutation (Hayward *et al.,* 2003). *C1QTNF5* is located in chromosomal region 11q23, and is contained entirely within the 3' untranslated region of the *MFRP* gene. *MFRP* encodes a protein of unknown function which shares homology with the Frizzled family of receptors (see Section 1.7.9). It was shown by PCR amplification of retinal DNA that both genes are co-expressed as a bicistronic transcript. *C1QTNF5* consists of 3 exons, with the disease-causing C to G transversion occurring in the third exon. The mutation occurs in a highly conserved residue, showing conservation from mammals to birds and fish (Hayward *et al.,* 2003).

1.7.4 C1QTNF5 shares homology with short chain collagens

C1QTNF5 shares homology with other C1q-like proteins and the tumour necrosis factor (TNF) superfamily, which are both thought to share an evolutionary link (Shapiro *et al.,* 1998). These proteins form the C1q and TNF superfamily (Kishore *et al.,* 2004). C1q proteins contain a globular C1q (gC1q) domain, usually at the carboxyl terminus of a collagen stalk, with the gC1q domain involved in trimerisation and the collagen stalk enabling multimerisation of the trimers to form bouquets. The TNF family also contains gC1q domains which trimerise, but they have stalks which, although rich in glycine and proline residues, are not collagenous (Shapiro *et al.,* 1998). Other members of C1q and TNF superfamily include C1q,

EMILIN-1, collagen types VIII and X and adiponectin (see Figure 1.9). In homologous proteins containing the gC1q domain, an aromatic motif is responsible for initial trimer assembly (Brass *et al.,* 1992, Chan *et al.,* 1999), followed by the formation of a central solvent-filled channel stabilised by Ca^{2+} clusters providing strong ionic bonds (Kishore *et al.,* 2004, Bogin *et al.,* 2002). C1q family members actually share only five conserved residues, each of which is contained within the hydrophobic core of the trimeric molecule. Of the proteins whose gC1q domain structures have been determined, each contains a ten-strand β-sandwich fold with a jelly-roll topography, consisting of two five-stranded β-sheets, each made of antiparallel strands (Kishore *et al.,* 2004).

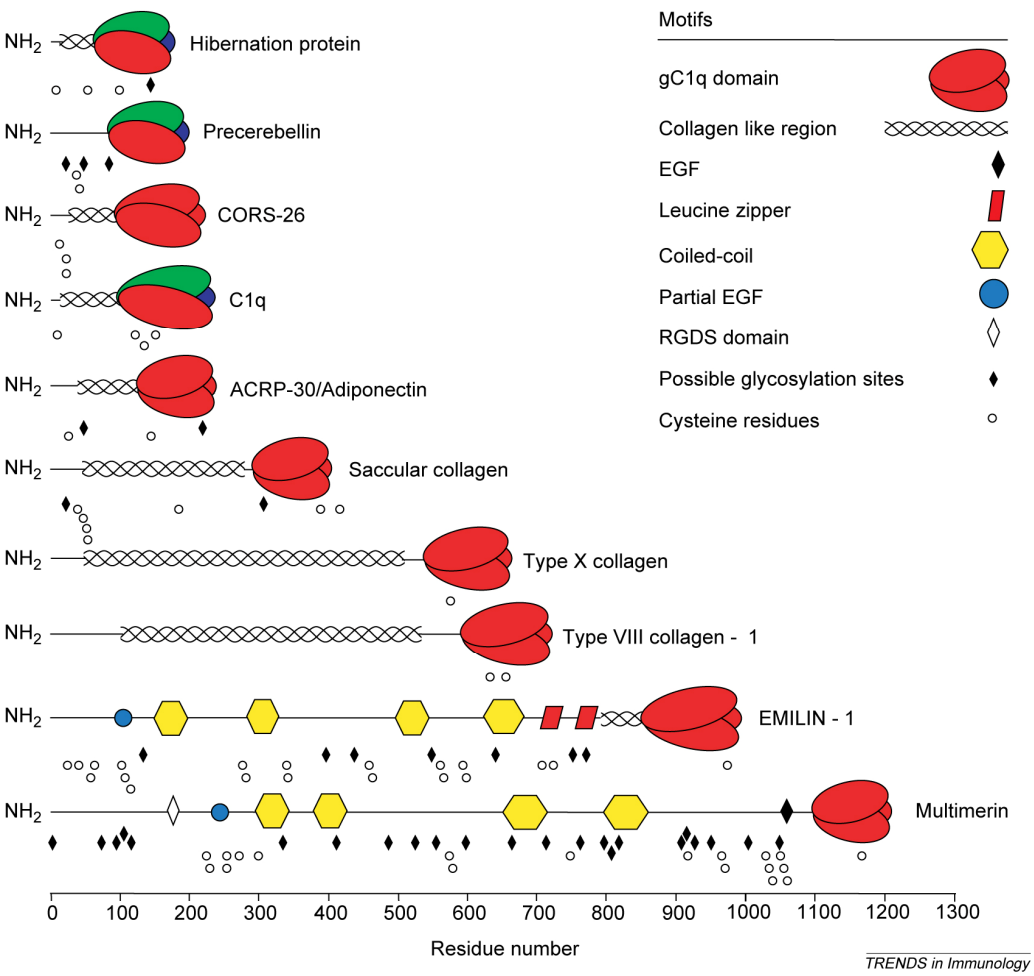

Figure 1.9: The C1q and TNF superfamily.
(source: Kishore *et al.,* 2004)

Members of the C1q and TNF superfamily: All members contain a C-terminal gC1q domain involved in trimerisation of the molecule, and trimers can be homotrimeric or heterotrimeric. Most members also contain a triple-helical Gly-X-Y collagen domain.

1.7.5 C1QTNF5 protein properties

C1QTNF5 is a 25kDa protein with three domains: a signal peptide, a collagen domain and a globular C1q domain. The disease-causing mutation occurs in the gC1q domain and is predicted to alter the surface charge. Functional studies have been carried out looking at *E. coli*-produced recombinant gC1q domain, with comparisons made between the wild type and mutant proteins. The solubility of the purified wild-type and mutant gC1q was investigated at 37°C. The wild type protein was found to be soluble up to 24 hours whilst the mutant protein had a tendency to form insoluble aggregates. In addition, although both wild type and mutant gC1q showed predominantly monomeric protein when analysed by reducing sodium dodecyl sulphate polyacrylamide gel eletrophoresis (SDS-PAGE), under native conditions the wild type protein was found to be present mainly as trimeric with weak hexameric forms, whilst the mutant protein would not migrate through the gel. It was concluded that the Ser163Arg mutation causes misfolding and aggregation of the mutant protein (Hayward *et al.,* 2003). Further biochemical analysis was carried out on the gC1q domain looking at the multimeric state of the protein (Shu *et al.,* 2006b). Both proteins were shown to oligomerise readily even under reducing conditions, with the wild-type forming monomers, dimers and trimers but the mutant showing only monomers and dimers. It was suggested this was due to instability of the mutant protein, making it more susceptible to reducing conditions. Further investigation into the effects of the Ser163Arg mutation and trimer assembly was carried out by Shu *et al*. (2006a). Pull-down experiments using glutathione *S*-transferase (GST)-tagged wild-type gC1q and His-tagged wild-type or mutant gC1q showed that it is the gC1q domain which is involved in self assembly and trimer formation, and that the wild type protein can interact with the mutant, with this result confirmed by yeast-two-hybrid experiments. The gC1q domain contains a conserved aromatic motif homologous to aromatic motifs found in other C1q-like proteins, which are predicted to be important for self-assembly of multimeric species (Brass *et al.,* 1992, Chan *et al.,* 1999). Using recombinant gC1q produced in *E. coli* and site-directed mutagenesis to introduce point mutations, it was shown that the aromatic motif in the gC1q domain is important for such self-assembly. Deletion of this

region resulted in a complete loss of self-assembly of the multimers, as did introducing missense mutations of the conserved residues.

1.7.6 C1QTNF5 tissue expression

Mandal *et al.* (2006c) investigated C1QTNF5 tissue expression in the mouse at different stages of development, with tissue expression studied in both embryonic and adult mice. Embryonic expression was first observed at E11, continuing up to E17, the last stage investigated. In the post-natal eye, expression was highest at P1 and declined until P5, after which expression levels remained steady. In 33 week old mice expression was highest in the posterior segment of the eye, followed by the iris-ciliary body. Low level expression was also observed in the brain, retina, lens, liver, lungs, heart, spleen, kidney, skeletal muscle, skin, testes and uterus. Cellular expression was also investigated using *in situ* hybridisation with a C1QTNF5 sequence-specific probe. At E14.5 it was detected in the layer of neural crest and cranial paraxial mesoderm marking the anlage of the ciliary body and iris stoma, and at E18.5 it was detected in the presumptive iris and ciliary body. In the adult mouse, C1QTNF5 was detected in the lateral plasma membrane of the RPE, the RPE apical processes, ganglion cells, ciliary body apical membranes and the plasma membrane of the lens epithelial cells. In the RPE apical processes it co-localised with ezrin. However, no co-localisation was observed with TIMP-3, a marker for Bruch's membrane. Immunostaining of mouse RPE sections showed co-localisation with the tight junction protein 1, ZO-I, suggesting association with tight junctions, and immunostaining of Madin-Darby canine kidney (MDCK) cells also showed such ZO-I co-localisation in the lateral plasma membranes. Immunoelectron microscopy confirmed the C1QTNF5 plasma membrane localisation, with levels being highest where the cells juxtapose, and along the lateral membrane and apical processes which interdigitate with the ROS.

1.7.7 The effects of the Ser163Arg mutation on C1QTNF5 in a cellular system

It has been shown that C1QTNF5 is expressed in the RPE, and that C1QTNF5 forms multimeric species. It has also been shown that the Ser163Arg mutation affects

multimerisation of the gC1q domain, causing aggregation of the protein. Several studies have investigated the mutation using full length C1QTNF5 and how this affects the protein in mammalian cellular systems.

1.7.7.1 Wild-type C1QTNF5 is secreted but the mutant protein is not

It was shown by Hayward *et al.* (2003) that C1QTNF5 is expressed by the RPE and is predicted to be secreted. To investigate C1QTNF5 secretion and the effects of the Ser163Arg mutation in a mammalian cellular model, HEK293-EBNA cells were stably transfected with wild-type or mutant His-tagged C1QTNF5 (Shu *et al.,* 2006b). In both cases, C1QTNF5 was detected in the cell lysate by Western blot, confirming its expression. However, only wild-type C1QTNF5 was detected in the culture media. Also, when cell lysates were analysed by native polyacrylamide gel electrophoresis (PAGE), the wild-type protein migrated through the gel whereas the mutant protein did not. From these results it was concluded that the mutant protein is not secreted but is retained within the cells as a high molecular weight aggregate (Hayward *et al.,* 2003).

A similar study was carried out using C-terminal V5-tagged C1QTNF5, transfected into COS-7 cells (Mandal *et al.,* 2006a). Cell lysate membrane and hydrophilic fractions, and culture media were analysed by Western blot under reducing and non-reducing conditions. Wild type C1QTNF5 was found to be present in all samples, whereas mutant C1QTNF5 was present only in the cell lysates and could not be detected in the culture media. When analysed by reducing SDS-PAGE and Western blot both the wild type and mutant proteins were present as monomers. However, under non-reducing conditions the wild type also formed dimers whereas again the mutant would not migrate through the gel. From this it was also concluded that the Ser163Arg mutation in C1QTNF5 causes aggregation and lack of secretion of the mutant protein.

1.7.7.2 Different cellular trafficking of the mutant protein

ARPE-19, a spontaneously transformed human RPE-derived cell line, was transiently transfected with green fluorescent protein (GFP)-tagged wild-type or mutant

C1QTNF5 (Shu *et al.,* 2006b). Immunostaining analysis was carried out looking at the cellular localisation of the proteins. Wild-type C1QTNF5 showed a diffuse cytoplasmic distribution, whereas the mutant appeared to show formation of intracellular aggregates. Co-localisation immunostaining was carried out with the endoplasmic reticulum (ER) markers calreticulin and protein disulphide isomerase (PDI). The mutant co-localised with both these markers whereas the wild-type did not. From this it was concluded that the wild-type protein undergoes normal cellular trafficking for a secreted protein whereas the mutant is retained within the ER. In addition, further immunostaining showed no co-localisation between mutant C1QTNF5 and the Golgi apparatus 58K protein, whereas it was observed for the wild-type, providing further evidence for the wild-type protein only travelling through the secretory pathway. To test whether either protein was preferentially degraded by the proteosome, stably transfected ARPE-19 cells were incubated with the proteosome inhibitors MG132 and MG115. Levels of both proteins, detected by Western blot in cell lysates, increased following treatment. However, when the cells were treated with cycloheximide to block protein synthesis, the mutant protein had a reduced half life when compared with the wild-type. This suggests it is preferentially degraded by the proteosome. Disease mechanisms have been suggested in which the mutant protein is retained within the ER as a high molecular weight aggregate, resulting in either a loss of function due to haploinsuffuciency, or a gain of function due to protein aggregation. As mutant C1QTNF5 has been shown to interact with the wild-type, then such interactions occurring intracellularly could significantly reduce the amount of wild-type protein secreted too, raising the possibility of a dominant negative effect.

1.7.7.3 C1QTNF5 and RPE cell adhesion to Bruch's membrane

To investigate a possible function for C1QTNF5 as an extracellular matrix protein, stably transfected HEK293-EBNA cells expressing either wild-type or mutant proteins were plated on laminin- or fibronectin-coated microtitre plates. Mutant C1QTNF5-expressing cells showed significantly reduced adhesion when compared with the wild-type to laminin-coated plates, but no difference in adhesion was observed to fibronectin. It was postulated that one role of C1QTNF5 could be in

adhesion of the RPE to Bruch's membrane, and that the Ser163Arg mutation resulted in reduced adhesion which facilitated the build up of the extracellular debris seen in the L-ORMD (Shu *et al.,* 2006b). It was suggested that *in vivo* wild-type C1QTNF5 multimerises to form a hexagonal lattice, as some other short chain collagens have been shown to do, and that this ability is affected by the Ser163Arg mutation (Hayward *et al.,* 2003).

1.7.8 C1QTNF5 interacts with CFH

Preliminary studies have shown there to be an interaction between CFH and C1QTNF5. Due to the similarities in phenotype between L-ORMD and AMD, and the expression of both CFH and C1QTNF5 by the RPE, it was investigated in this lab whether an interaction between CFH and C1QTNF5 could be observed. Initial results, carried out by Dr X. Shu, suggested this was the case (unpublished data). Surface plasmon resonance (SPR) was carried out between recombinant gC1q and plasma-purified CFH, with an interaction observed when gC1q was immobilised to the chip and CFH was added in the fluid phase. ^{125}I-labelled proteins were used in plate binding assays which showed an interaction between gC1q and CFH domains SCR6-8Y and SCR6-8H and it was shown by gel mobility shift assays and heparin affinity columns that gC1q, like CFH, is capable of binding polyanions.

1.7.9 C1QTNF5 and obesity

C1QTNF5 has been identified as playing a role in obesity. Microarray profiling was carried out looking at adipocytes from abdominal subcuteanceous adipose deposits in Pima Indians, which showed that most differentially expressed genes between obese and non-obese individuals are involved in inflammation, with a larger proportion showing up-regulation than down-regulation (Lee *et al.,* 2005). C1QTNF5 and CD90 were up-regulated, with both located in chromosomal region 11q22-q24. This region showed peak linkage with obesity in the population studied. It is suggested that up the regulation of genes involved in inflammation (it is assumed this is the case for C1QTNF5) is perhaps not surprising due to adipose tissue inflammation and macrophage infiltration being associated with obesity. Another study was carried out to identify polymorphisms in a Japanese population that confer susceptibility to

metabolic syndrome which identified a T101A polymorphism in C1QTNF5 showing significant association (Yamada *et al.,* 2008).

1.7.10 Membrane-type Frizzled-Related Protein (MFRP)

MFRP is a type II membrane protein consisting of 579 amino acids. It contains a C-terminal domain which is homologous to the Wnt-binding cysteine-rich domains (CRD) of the Frizzled family of transmembrane proteins, two Tolloid repeats (comprising globular domains related to cubulin and the low-density lipoprotein receptor) which are homologous to the Tolloid metalloprotease family, and a membrane-spanning domain (Katoh, 2001, Sundin *et al.,* 2005) (Figure 1.10). The Frizzled family of proteins consist of receptors for Wnt binding and signalling, with the first Frizzled gene identified as a polarity-determining gene in *Drosophila* (Adler, 1992).

1.7.10.1 *MFRP* mutation and expression in the mouse eye

MFRP is mutated in the mouse retinal degeneration 6 (*rd6*), which is an autosomal recessive trait causing discrete spots across the retina, progressive photoreceptor degeneration and subsequent retinal dysfunction (Kemeya *et al.,* 2002). MFRP is expressed in the RPE, cillary body and testis of the adult mouse, and has been found expressed as a bicistronic transcript with C1QTNF5 (Kameya *et al.,* 2002, Mandal *et al.,* 2006b). Looking at expression levels within the embryo, MFRP was detected by quantitative real time polymerase chain reaction (qRT-PCR) at E11 to E17, peaking at E15. In adult mouse whole eyes, expression levels were highest at P1, declining by around 75% by P5. Expression levels were slightly lower still at P7, and remained unchanged up to P30. This data indicates that MFRP has roles not only in eye development but also in maintenance as the eye ages. Within the adult retina, MFRP localises to the apical and basal membranes of the RPE, although not the apical processes, as no co-localisation with ezrin was detected. Immunostaining of MDCK cells, which endogenously express low levels of MFRP and C1QTNF5, showed MFRP to be localised to the apical membranes, where it showed co-localisation with C1QTNF5. However, whereas C1QTNF5 was also found localised to the lateral membranes, this was not the case for MFRP (Mandal *et al.,* 2006b). In

the *rd6* mouse, *MFRP* expression levels in the embryo were similar to those in control mice. However, expression levels were markedly lower after birth and, although expression levels rose up to a peak at P28, this peak was much later than in the control mice where expression peaked at around P14 after which it declined slightly (Won *et al.,* 2008). This pattern of expression in the control mouse differs from that reported previously (Mandal *et al.,* 2006b).

Again comparing wild-type and mutant mice, immunohistology was carried out on the retina. In the wild-type animals, MFRP was found to be localised to the cillary body and RPE apical but not basal membranes. No protein was detected in the mutant mice, and after carrying out Western blot analysis this was found to be due to truncation of the mutant MFRP. Photoreceptor development peaks at around P7, so histological analysis was carried out on retinas from P7 through to P28. In the mutant mice ROS were shortened and disorganised, although they did not appear to be reduced in number. By P28 the thickness of the ONL is reduced and there is thinning of the ROS. Electron microscopy of mutant retina revealed areas where there was disorganisation and a reduction in numbers of apical microvilli (Won *et al.,* 2008). ERG analysis was carried out on wild-type and *rd6* mice, with aberrant ERG responses in mutant mice revealing rod dysfunction. One function of the RPE is the daily phagocytosis of ROS, initiated by the onset of light (LaVail, 1976). To determine if this was affected in the *rd6* mice, levels of rhodopsin in the RPE were measured 1 hour after the onset of light. These were found to be reduced when compared to wild-type. In addition, levels of phosphorylated MerTK were reduced, suggesting that these mice have deficiencies in ROS phagocytosis. Due to the homology between MFRP and the Frizzled family of receptors, it was also investigated whether any evidence could be found for MFRP localisation with β-catenin. None was found, suggesting MFRP is not involved in signal transduction via this pathway (Won *et al.,* 2008).

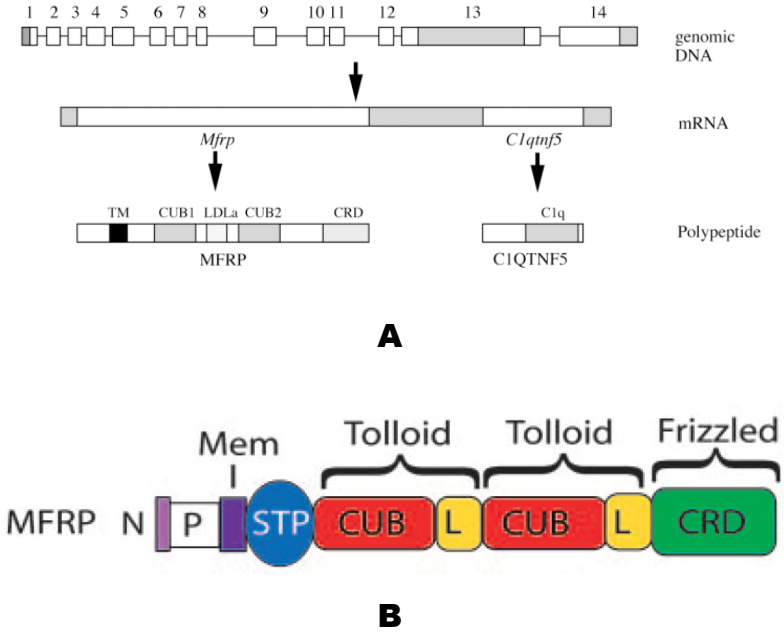

Figure 1.10: C1QTNF5 and MFRP are expressed as a bicistronic transcript. (source: Sundin *et al.,* 2005, Kameya *et al.,* 2005)

MFRP is expressed as a bicistronic transcript with C1QTNF5.
A - C1QTNF5 is contained with in the last two exons (13 and 14) of the MFRP transcript. Genomic DNA and mRNA: white represents coding regions, shaded represents untranslated regions (individual exons are numbered). Polypeptide: different domains are indicated by labels and shading (TM - transmembrane domain, CUB1 / CUB2 - cubulin-related 1 and 2, LDLa - low-density lipoprotein receptor-related, CRD - cystein-rich domain).
B – MFRP: N, amino terminus; C, carboxyl terminus; P, proline-rich interval; Mem, membrane spanning helix; STP, serine-threonine-proline-rich interval; CUB, cubilin-related; L, low-density lipoprotein receptor-related. CRD, Frizzled-related CRD.

1.7.10.2 MFRP mutation in the human eye

In humans, *MFRP* mutation (the result of a frameshift insertion in exon 10) has been reported associated with extreme hyperopia, and although some dark adaptation difficulties were observed, there was no retinal degeneration (Sundin *et al.,* 2005). Other reports have found mutations in *MFRP* associated with a syndrome resulting in nanophthalmos, retinitis pigmentosa, foveoschisis and optic disc drusen, caused by frame shift mutations, the result of either a 1 base pair insertion or deletion in exon 5 (Ayala-Ramirez *et al.,* 2006, Crespi *et al.,* 2008). It is interesting to note that no reduction in eye size is observed in the *rd6* mouse, suggesting that MFRP functions may differ between the two species. Whilst the mouse is an excellent model for human disease, there are distinct differences with humans. For instance the mouse eye is adapted for nocturnal vision and so has slightly fewer cone photoreceptors and does not have a macula containing increased numbers of rods (Sundin, 2005).

1.7.10.3 MFRP interacts with C1QTNF5

MFRP and C1QTNF5 are expressed as a bicistronic transcript, suggesting that they are functionally related. MFRP contains two cubulin (CUB) domains, which can also be found on complement components C1s and C1r. The CUB domains participate in the interaction of these proteins with C1q, which contains a gC1q domain homologous to that found in C1QTNF5. Several studies have confirmed an interaction between MFRP and C1QTNF5. Mandal *et al.* (2006b) co-immunoprecipitated both proteins from human RPE-choriod and whole mouse eye extract. In addition they co-transfected COS-7 cells with C-terminal V5-tagged C1QTNF5 and N-terminal Xpress-tagged MFRP, and were able to pull down the complexed proteins using immunoprecipitation. Shu *et al.* (2006b) used full-length C1QTNF5 as bait to screen a human brain yeast two-hybrid cDNA library and identified MFRP-containing clones. Further investigation was carried out looking at gC1q interactions with the CUB domain, with pull-down experiments confirming an interaction between the two recombinant proteins. Yeast two-hybrid again confirmed that the domains interact, and co-transfection of HEK-293T cells showed the proteins to co-localise.

1.8 Aims of this study

Age-related macular degeneration is a complex disease. It impacts upon many people's lives, not only those affected but their carers and society too, and its incidence is increasing. Due to its complexity and many contributing factors it is difficult to gain insights into the underlying disease mechanisms. Also, although individuals have donated eyes for research, these tend to be in the later stages of the disease and therefore ascertaining what observations are causative and what are the result of other initiating factors can be difficult. Some mouse models have been found which replicate some of the symptoms of human disease, and some inherited diseases have been identified which result in retinal degenerations, both of which are useful for increasing our understanding. L-ORMD is one such inherited disease, with patients presenting the extensive sub-retinal deposits, CNV and retinal degeneration observed in AMD. The disease-causing mutation and resulting protein product have been identified, making this a good target to study. It is hoped that understanding disease mechanisms in L-ORMD with help to unravel what is occurring in AMD.

In order to understand these processes, this study aims to investigate the effects of the Ser163Arg mutation in both a mammalian cellular system and on recombinant protein properties. Using a physiologically relevant cell line, the effects of stable C1QTNF5 over-expression will be investigated, using both the wild-type and mutant proteins. The observation that C1QTNF5 may be involved in RPE cell adhesion will be studied, as will the effects of mutant C1QTNF5 over-expression on the cellular system. The interaction between C1QTNF5 and CFH will be further investigated, aiming to identify which regions of CFH are involved. Also, due to the reported interaction between MFRP and C1QTNF5, and the involvement of MFRP in ROS phagocyotsis, the stably transfected cell lines will also be used to determine if any role for C1QTNF5 can be found in ROS phagocytosis.

2 CHAPTER 2

:

MATERIALS & METHODS

2.1 Cell culture procedures

2.1.1 Mammalian cell culture

Unless otherwise specified, all ARPE-19 and EBNA293 cells were cultured at 37°C, 5% CO_2, using the following tissue culture media. For stock solution concentrations, see Section 2.8.3. All cell cultures were checked and confirmed negative for mycoplasma infection (carried out by HGU Technical Services).

ARPE-19:	**Reagent**	**Volume**
	DMEM F12	500ml
	FCS	50ml
	Penicillin/streptomycin	5ml

EBNA293:	**Reagent**	**Volume**
	DMEM (with L-glutamate)	500ml
	FCS	50ml
	Penicillin/streptomycin	5ml
	MEM vitamins	5ml
	Sodium pyruvate	5ml
	Non-essential amino acids	5ml
	L-glutamate	5ml

For 25cm^2 tissue culture flasks, cells were passaged once they had reached 80% confluence. This involved washing the cells twice with PBS, adding 1 pastette volume of trypsin/EDTA (1:1 mixture of stock solutions provided by HGU technical services, see Section 2.8.3) and incubating at 37°C for 2-3 minutes or until the cells had detached. Three pastette volumes of culture media were then added to neutralise the trypsin. To a fresh 25cm^2 tissue culture flask, 2 pastette volumes of media were added, followed by 1 pastette volume of cell suspension. For other flask sizes, volumes were adjusted accordingly.

2.1.2 Bacterial cell culture

Escherichia coli cultures were used to produce recombinant His-gC1q. Unless otherwise specified, all *E. coli* cultures were incubated 37°C, rotated at 225rpm, with cultures maintained in Lauria Broth (LB), supplied by HGU technical services. Bacterial clones were supplied by and bacterial culture protocols had previously been optimised by Dr X. Shu (MRC Human Genetics Unit).

Large-scale cultures were grown from glycerol stocks stored at -80°C. These were streaked onto an LB-agar plate containing ampicillin (provided by HGU technical services) and incubated overnight at 37°C to obtain individual colonies. One colony was then transferred to 5ml LB containing 0.1mg/ml ampicillin and incubated overnight as before. These were then added to 1.2l LB and incubated until an OD_{595} 0.6-1.0 was reached. IPTG was then added to a concentration of 1mM, the temperature reduced to 20°C and the culture incubated overnight to allow for expression of recombinant protein.

2.1.3 Yeast cell culture

Pichia pastoris cultures were used to produce recombinant SCR modules. In all instances, basic minimal media plus glycerol (BMG) and basic minimal media plus methanol (BMM) were prepared as described below, with solutions sterile filtered prior to use.

BMG: 100mM potassium phosphate pH6.0
1.34% yeast nitrogen base with ammonium sulphate
4×10^{-5}% biotin
1% glycerol

BMM: 100mM potassium phosphate pH6.0
1.34% yeast nitrogen base with ammonium sulphate
4×10^{-5}% biotin
1% methanol

Stabs of each clone were provided by Dr A. Herbert (University of Edinburgh), which were streaked onto a yeast extract peptone dextrose medium plus sorbitol (YPDS) agar plates and incubated overnight at 37°C enabling individual colonies to be obtained. YPDS plates were prepared using the following in 1l distilled water, which was autoclaved prior to pouring the plates:

YPDS: 10g yeast extract
182.2g sorbitol
20g peptone
20g agar

The individual colonies obtained were used to inoculate 5ml BMG, and incubated at 37°C, 225 rpm for 48 hours, until the culture turned milky-white. The cultures were then added to 100ml BMG, in a 500ml shaker flask, and incubated overnight at 37°C, 225 rpm. The 100ml cultures were then added to 1l BMG, divided into 2 x 2l flasks and incubated as before until an OD_{595} 10.0 was reached. The cell pellets were collected by centrifugation at 500g for 10 minutes, resuspended in 200ml BMM and transferred to a 1l shaker flask. Cultures were incubated at 25°C, 225rpm for 4 days, with 1% methanol by volume (2ml) added every 24 hours to induce recombinant protein expression.

2.2 Stably transfected cell line creation

Stably transfected ARPE-19 or EBNA293 cell lines were created, over-expressing recombinant His-tagged C1QTNF5 (His-C1QTNF5). ARPE-19 cell lines expressed either wild-type or mutant His-C1QTNF5, with the required plasmid vectors created in this study. EBNA293 cell lines were created which expressed wild-type His-C1QTNF5, with plasmid vectors created and supplied for use by Dr X. Shu (MRC Human Genetics Unit, Edinburgh).

2.2.1 Creating ARPE-19 cell lines stably expressing wild-type and mutant His-C1QTNF5

Creation of the cell lines involved making plasmid constructs with *His-C1QTNF5* inserts, subsequent transfection of ARPE-19 with the vectors and then screening of the ARPE-19 clones for His-C1QTNF5 expression.

2.2.1.1 Creating pEGFP-C1-C1QTNF5 (minus *EGFP*) constructs

The vectors were created using the pEGFP-C1 plasmid, with *pEGFP* removed and replaced with *His-C1QTNF5.*

2.2.1.1.1 DNA separation and purification by agarose gel electrophoresis

Several stages in the creation of the pEGFP-C1-C1QTNF5 inserts required separation and/or purification of DNA by agarose gel electrophoresis. Unless otherwise specified, this was carried out using the following method.

1g agarose was dissolved in 100ml 0.5x TBE buffer (20x stock: 216g Tris base, 110g boric acid, 18.6g EDTA, to make 1l with dH_2O) by heating in a microwave until boiling. 0.2mg/ml ethidium bromide was added once the liquid had cooled a little. DNA samples were diluted in 1x loading buffer (6x stock: 25µg bromophenol blue, 25µg xylene cyanol, 3ml glycerol, 6.95ml dH_2O) before loading on to the gel immersed in 0.5x TBE buffer. Gels were run at 150V until suitable separation had occurred. The DNA standard size marker used was bacteriophage lambda digested with HindIII (DNA marker X, Roche).

DNA was purified from the agarose gel using the QIAquick PCR Purification Kit (Qiagen) as follows. All centrifugation steps were carried out using a benchtop microcentrifuge. Using the pre-prepared buffers supplied, 3 volumes of buffer PB was added to 1 volume of DNA-containing agarose gel (excised from the main gel) (100mg ~ 100µl) in a microcentrifuge tube. The mixture was incubated at 50°C for 10 minutes to dissolve the gel, and then loaded to the QIAquick column via centrifugation for 1 minute with the flow-through discarded. The column was

washed by addition of 0.5ml Buffer QG and centrifugation for 1 minute with the flow-through discarded, followed by addition of 0.75ml Buffer PE, centrifugation for 1 minute and the flow-through again discarded. An additional centrifugation ensured complete removal of wash buffers from the column. DNA was eluted by placing the QIAquick column in a fresh microcentrifuge tube, adding 30µl sterile H_2O, leaving to stand for 1 minute and then centrifugation for 1 minute, with the elution retained and the column discarded.

2.2.1.1.2 Plasmid amplification in Escherichia coli

At several stages in the preparation of the pEGFP-C1-His-C1QTNF5 constructs, it was necessary to amplify plasmids in *E. coli*. Each stage follows the standard method of transfection, culture and purification as described below.

E. coli TOP-10 cells (Invitrogen) show no resistance to ampicillin, and both the pGEM-T-Easy and pEGFP-C1 vectors confer resistance to this antibiotic. 3µl of purified vector was added to 1 vial of competent cells as provided by the supplier and only just obtained from -80 ºC freezer. These were incubated on ice for 30 minutes before heat shocking at 42ºC for 30 seconds and placing on ice for a further 2 minutes. 250µl super optimal broth with catabolite repression (SOC) medium (provided with the cells) was added, and the mixture incubated at 37 ºC on rotation for 1 hour. 30µl cell suspension was then spread on LB-agar plates containing ampicillin (provided by HGU technical services), with 100µl per plate 100mM IPTG and 50µl per plate 50mg/ml 5bromo-4-chloro-3-indolylbeta-D-galactopyranoside (X-gal). The plates were incubated overnight at 37ºC to allow for individual colonies to grow. Six white colonies were selected for each insert, as selection criteria meant these rather than blue colonies contained plasmids with inserts disrupting the *lac Z* gene. The colonies were amplified overnight at 37 ºC in 5ml LB containing 0.1mg/ml ampicillin, and cell pellets collected by centrifugation at 3000g for 5 minutes.

The plasmids were purified from the cell pellets using the QIAprep Spin Miniprep Kit (Qiagen), as follows. All centrifugation steps were carried out using a benchtop

microcentrifuge. Using the pre-prepared buffers supplied, the cell pellet was resuspended in 250µl Buffer P1 plus RNase A and transferred to a microcentrifuge tube. To this was added 250µl Buffer P2 and the tube inverted 4 times to mix. 350µl Buffer N3 was added and the tube was again inverted 4 times to mix, followed by centrifugation at 13,000 rpm for 10 minutes. The supernatant was then added to a QIAprep spin column followed by centrifugation at 13,000 rpm for 60 seconds. The flow through was discarded. The column was then washed, firstly with 0.5ml Buffer PB followed by centrifugation at 13,000 rpm for 60 seconds, and then with 0.75ml Buffer PE again followed by centrifugation at 13,000 rpm for 60 seconds. An additional centrifugation was carried out to remove any residual wash buffer. The flow through was discarded after each centrifugation step. The plasmid was then eluted from the column in 30µl dH_2O, incubating for 1 minute, before placing the spin column in a fresh microcentrfuge tube and centrifuging at 13,000 rpm for 60 seconds.

2.2.1.1.3 PCR amplification of *C1QTNF5* inserts

C1QTNF5 inserts were created with restriction sites suitable for insertion into pEFGP-C1, minus *EGFP* (*enhanced green fluorescent protein*). The N-terminal restriction site was for NheI and the C-terminal site was for BamHI. The following primers were used for creation via polymerase chain reaction (PCR) of both the wild type and mutant *C1QTNF5* inserts:

N-terminal: GCT AGC ATG GCG ATG AGG CCA CTC CTC GTC
C-terminal: GGA TCC CTA ATG GTC ATG GTG ATG ATG AGC AAA GAC TGG GGA GCT

The N-terminal primer includes a Kozak sequence (G/ANNATGG) and start codon, and the C-terminal primer contains a hexa-histidine ('His')-tag sequence for addition of this tag to the C-terminal of the recombinant C1QTNF5, and a stop codon. Inserts were created via polymerase chain reaction (PCR) amplification of a human complementary DNA (cDNA) template, provided by Dr X. Shu (Human Genetics Unit, Edinburgh), using the Expand High Fidelity PCR System (Roche), and primers

were commercially produced (Sigma). The following reaction criteria were followed:

Reagent	Volume	Concentration
N-terminal primer	2.0µl	10µM
C-terminal primer	2.0µl	10µM
cDNA template	0.5µl	Provided by Dr X Shu
dNTP	2.0µl	20µM
10x reaction buffer M	2.5µl	N/A
Polymerase	0.2µl	N/A
DMSO	1.25µl	N/A
dH2O	9.55µl	N/A

Temperature	Time
1. 95 °C	60 seconds
2. 95 °C	30 seconds
3. 58 °C	60 seconds
4. 72 °C	90 seconds
5. Go to step 2, 34 times	
6. 72 °C	600 seconds

PCR products were purified using 1% agarose gel electrophoresis, with complete PCR reaction mixtures loaded. The appropriate bands were excised from the gel and then purified using the QIAquick PCR Purification Kit (QIAGEN), eluting in 30µl sterile H_2O, to give purified inserts ready for ligation into the pGEM-T-Easy vector and amplification in *E. coli* TOP10. Ligation was carried out using the Rapid DNA Ligation Kit (Roche) and by incubating 5µl 2x reaction buffer, 3µl *C1QTNF5* insert, 1µl vector and 1µl T4 ligase overnight at 16°C. Plasmds were then amplified in *E. coli* TOP-10 as described in Section 2.2.1.1.2.

2.2.1.1.4 Selection of *C1QTNF5* inserts

A sample of each purified plasmid was then analysed to check for the presence of a

C*1QTNF5* insert with the correct sequence. Plasmids were first digested with the restriction enzymes *NheI* and *BamHI* using the following reaction mixture and incubation for 3 hours at 37 ºC.

Reagent	**Volume**
BamH1	0.5ul
Nhe1	0.5ul
Reaction buffer M	1ul
Plasmid	3µl
dH_2O	Up to 10ul

Digestion reactions were then analysed by 1% agarose gel electrophoresis to check for the presence of bands of approximately 700bp, corresponding to inserts for His-tagged *C1QTNF5*. Plasmids showing inserts of this size were then sequenced to check this was correct. Sequencing was carried out by HGU technical services.

2.2.1.1.5 Preparation of the pEGFP-C1 vector and *C1QTNF5* inserts

The pEGFP-C1 vector was prepared for ligation with the *C1QTNF5* inserts by digestion with NheI and BamHI to remove the region encoding EGFP, and the *C1QTNF5* inserts were removed from the pGEM-T-Easy constructs by digestion with the same enzymes. The following digestion reactions were incubated at 37 ºC for 3 hours:

Reagent	**Volume**
BamHI	0.5µl
NheI	0.5µl
Reaction buffer M	1µl
Plasmid	5.0µl
dH_20	Up to 10µl

Following digestion, the plasmid and inserts were purified using 1% agarose gel electrophoresis and gel extraction as described previously.

2.2.1.1.6 Ligation, selection and screening of the pEGFP-C1-C1QTNF5 (minus *EGFP*) constructs

Ligations were set up between vector and either wild-type or mutant *C1QTNF5* insert using the Rapid DNA Ligation Kit (Roche). Following the manufacturers' instructions, 4µl *C1QTNF5* insert and 1µl pEGFP-C1 vector were incubated with 2µl 5x dilution buffer and 3µl H_2O for 10 minutes at room temperature. To this was then added 10µl 2x ligation buffer and 1µl T4 ligase, and the reaction incubated overnight at 16°C. The resulting plasmid constructs were then used to transform *E. coli* TOP-10, amplified and purified as described previously. Following the same method as Section 2.2.1.1.4, a sample of each was taken to test for the presence of the correct sized insert via digestion with NheI and BamHI, and suitable constructs with inserts of the correct size were chosen to test for expression of His-C1QTNF5 in ARPE-19.

2.2.1.2 Checking expression of His-C1QTNF5 in ARPE-19

Transient transfection and immunostaining were carried out to check that His-C1QTNF5 was expressed in ARPE-19 when using the pEGFP-C1-C1QTNF5 constructs. ARPE-19 cells were grown to <50% confluency on glass slides in 6-well tissue culture plates, and then transfected with either the wild-type or mutant C1QTNF5 constructs as follows. 4ul FuGene (Roche) were added to 100ul serum-free media and incubated at room temperature for 5 minutes. 3µl DNA was then added and the mixture incubated at room temperature for 15 minutes. Fresh culture media was added to the cells, followed by the FuGENE mixture. Cells were allowed to grow overnight, slides were then washed twice with PBS and cells fixed to the slides with ice-cold methanol for 5 minutes and again washed twice with PBS. Immunohistochemistry was carried out as described in Section 2.3, using the anti-His primary and anti-mouse Texas Red secondary antibodies.

2.2.1.3 Determination of correct G418 concentration

In order to select stably transfected ARPE-19 cells, it was necessary to determine the correct G418 concentration. ARPE-19 cells were grown to confluence in 6 well tissue culture plates, after which time culture media was changed for that containing

0, 300, 400, 500, 600 or 700µg/ml G418. Cells were incubated for 2 weeks, changing the culture media for fresh G418-containing culture media every three days. After this time the media was changed back to standard ARPE-19 culture media and the cells incubated for a further week. It was then determined by light microscopy whether any live cells remained. The minimum concentration required for no live cells to remain (500µg/ml) was selected for future use.

2.2.1.4 Transfection and screening of ARPE-19 colonies

Following clarification by immunohistochemistry that His-C1QTNF5 was expressed in ARPE-19 following transient transfection with the pEGFP-C1QTNF5 constructs, stably transfected cell lines were created. Transfection of ARPE-19 was carried out using the microporator and supplied buffers as this has an optimised protocol for high-efficiency tansfection of many cell lines, including ARPE-19.

ARPE-19 cells were grown to 80% confluence and detached using 1 volume of trypsin. Following trypsin neutralization with 3 volumes of culture media containing 10% FCS, cell number was counted using a haemocytometer and a suspension volume containing 56 x 10^5 cells was aliquoted into a 15ml Falcon tube. This was centrifuged at 3000g to obtain a cell pellet which was resuspended in 1ml Buffer R. 5µg DNA (wild type or mutant pEGFP-C1-C1QTNF5 vector) was added to 100µl cell suspension and gently mixed. Cells were tranfected using microporator with the following parameters: 1350 V/ 20 ms/ 2 pulses.

Each transfection reaction was then divided between three 30cm^2 tissue culture dishes containing ARPE-19 selection media (DMEM-F12, FCS, P/S, 500ug/ml G418) and incubated for 2 weeks or until cell death occurred of the untransfected cells, leaving only transfected cells. Media was changed for fresh every 3 days. The plates were incubated for a further week to allow the transfected cell colonies to become viable. Individual colonies were then detached with trypsin/EDTA, transferred to 24 well plates and subsequently amplified into 25cm^3 flasks. Each cell line was maintained under selection with G418 to ensure continued plasmid presence, following the method described in Section 2.1.1. After the first passage,

the remaining cells from each flask were screened via Western blot for the expression of His-C1QTNF5 using the mouse anti-His primary antibody (see Section 2.6.5).

2.2.2 Creating an EBNA293 cell line stably expressing wild-type His-C1QTNF5

EBNA293 were transfected with the pCEP-Pu vector containing a wild-type *His-C1QTNF5* insert, created by and supplied for use by Dr X. Shu (MRC Human Genetics Unit, Edinburgh). pCEP-Pu contains a puromycin resistance gene for selection of transfected cell lines. Culture media puromycin concentrations had previously been optimised by Dr X .Shu.

2.2.2.1 Transfection and screening of EBNA293 colonies

EBNA293 were grown to <50% confluence in 1 well of a 6 well tissue culture plate. The cells were then transfected with the pCEP-Pu construct using FuGENE as described in Section 2.2.1.2. Following transfection, cells were incubated overnight and then detached with trypsin/EDTA and transferred to two 30cm^2 tissue culture dishes containing EBNA293 culture media plus 500µg/ml puromycin. The plates were incubated for two weeks ensuring only transfected cells remained. Individual colonies were detached with trypsin/EDTA and transferred to 24 well tissue culture plates. Once they had reached confluence these were transferred to 25cm^2 tissue culture flasks. After the first passage the remaining cells from each flask were screened by Western blot for His-C1QTNF5 expression using the mouse anti-His primary antibody (see Section 2.6.5).

2.2.3 Checking secretion of His-C1QTNF5 in the transfected cell lines

Secretion of His-C1QTNF5 in the stably transfected ARPE-19 and EBNA293 cell lines was tested, with samples analysed by Western blot. In all instances the primary antibody used was mouse anti-His and the secondary antibody was horse raddish peroxidase (HRP)-labelled rabbit anti-mouse (see Section 2.6.5).

2.2.3.1 Checking secretion in the ARPE-19 transfected cell lines

Secretion of His-C1QTNF5 was first tested in 2 wild-type and 2 mutant His-C1QTNF5 stably transfected ARPE-19 cell lines. Each cell line was grown to confluence in 3 wells of a 6-well tissue culture plate. Culture media was then changed to serum free and the cells incubated for a further 3 days. Culture media for each cell line was then pooled and centrifuged at 3000g for 5 minutes, with the supernatant retained. The culture media were diluted 1:2 with 20% trichloroacetic acid (TCA) and left on ice for 20 minutes to enable precipitation of any proteins, followed by centrifugation at 3,000 rpm with the supernatant discarded. The protein pellets were then analysed by reducing SDS-PAGE and subsequent Western Blot as described in Section 2.6.4 and Section 2.6.5, with primary antibody mouse anti-His, secondary antibody HRP-labelled rabbit anti-mouse and the standard ECL detection reagents used.

2.2.3.1.1 Comparing secretion levels in the ARPE-19 cell lines

Levels of His-C1QTNF5 secretion were compared between the selected wild-type and mutant stably transfected ARPE-19 cell lines, GFWT19 and GFMT22. Cell lines were each grown to confluence in 1 well of a 24 well tissue culture plate, after which the media was replaced with 1ml serum free media and the cells incubated for a further 5 days. Culture media were collected and set aside. Cells were then detached in 250µl trypsin/EDTA, followed by the addition of 750µl media containing serum to neutralise the trypsin. Cell concentrations were then determined using a haemocytometer, with an aliquot from each cell solution taken up to the maximum volume possible so that each contained the same number of cells. Aliquots of the culture media were then taken and placed in microcentrifuge tubes, with volumes also adjusted to reflect the same number of cells in each sample and centrifuged at 13,000 rpm for 1 minute in a benchtop microcentrifuge, with the supernatant then transferred to fresh microcentrifuge tubes. To the centrifuged aliquots, 10µl Ni-NTA bead suspension (Qiagen) was added (having previously been washed twice with 1ml PBS and resuspended to the same volume prior to washing), and the samples incubated on rotation for 1 hour. The beads were then allowed to settle, the liquid

aspirated from the tube and the beads washed twice with 1ml PBS allowing them to settle in between washes. After the final wash had been removed from the tube, the beads were centrifuged at 13,000rpm for 1 minute to collect a compact pellet and the excess liquid removed. Bead samples and cell samples were then resuspended in reducing SDS-PAGE loading buffer and analysed by reducing SDS-PAGE and subsequent Western Blot as described in Section 2.6.4 and Section 2.6.5, with primary antibody mouse anti-His, secondary antibody HRP-labelled rabbit anti-mouse and the ECL$^+$ detection reagents used.

A secretion time line was also carried out, comparing levels of His-C1QTNF5 secretion after 1, 2 or 3 days. Three wells of cells for each cell line were cultured and samples prepared as described above, with 1 well samples taken after 1, 2 or 3 days incubation. Cell samples were not collected, but media samples were analysed as described above.

2.2.3.2 Checking secretion in the EBNA293 transfected cell lines

Secretion of His-C1QTNF5 in the stably-transfected EBNA293 cell line was tested by TCA precipitation of the culture media proteins, as described in Section 2.2.3.1.

2.2.3.2.1 Secretion time line in the EBNA293 cell lines

Secretion of wild-type and mutant His-C1QTNF5 was compared in the stably transfected EBNA293 cell lines. Cell lines were each grown to confluence in 3 wells of a 24 well tissue culture plate, after which the media was replaced with 1ml serum free media and the cells incubated for a further 1, 2 or 3 days, with culture media then collected into microcentrifuge tubes and centrifuged at 13,000 rpm for 1 minute on a benchtop centrifuge. Supernatants were then transferred to fresh tubes and 10µl Ni-NTA bead suspension was added (having previously been washed twice with 1ml PBS and resuspended to the same volume prior to washing), and the samples incubated on rotation for 1 hour. The beads were then allowed to settle, the liquid aspirated from the tube and the beads washed twice with 1ml PBS allowing them to settle in between washes. After the final wash had been removed from the tube, the beads were centrifuged at 13,000 rpm for 1 minute to collect a compact pellet and the

excess liquid removed. Bead samples and cell samples were then resuspended in reducing SDS-PAGE loading buffer and analysed by reducing SDS-PAGE and subsequent Western Blot as described in Section 2.6.4 and Section 2.6.5, with primary antibody mouse anti-His, secondary antibody HRP-labelled rabbit anti-mouse and the ECL$^+$ detection reagents used.

2.3 Immunohistochemistry

Unless otherwise specified, immunohistochemical analysis of adherent cells was carried out using the following method. Tables 2.1 and 2.2 give the concentrations of all primary and secondary antibodies used.

Table 2-1: Primary antibodies used in immunohistochemistry

Antibody	Species	Supplier	Dilution
Anti-His	Mouse	Invitrogen	1:400
Anti-β-catenin	Rabbit	Sigma	1:2000
Anti-calreticulin	Rabbit	StressGen	1:400
Anti-C1QTNF5	Goat	R&D Systems	1:400
Anti-PDI	Mouse	StressGen	1:400

Table 2-2: Secondary antibodies used in immunohostochemistry

Antibody	Species	Supplier	Dilution
Anti-mouse Texas Red	Donkey	Jackson Labs	1:400
Anti-rabbit FITC	Donkey	Jackson Labs	1:400
Anti-goat Texas Red	Donkey	Santa Cruz	1:400
Anti-mouse FITC	Donkey	Jackson Labs	1:400

2.3.1 General immunostaining method

Cells were grown to 60-80% confluency on glass slides in 6 well tissue culture plates using the appropriate culture media. Media was then aspirated from the wells and the cells washed twice with PBS. Cells were then fixed to the slides in ice-cold methanol for 5 minutes, followed by two further washes in PBS. Slides were

blocked for 1 hour with 10mg/ml BSA in PBS at room temperature and again washed twice with PBS. Cells were then incubated with the primary antibody, diluted in PBS to the specified concentration, for 1 hour at room temperature, and washed 3 times for 5 minutes with PBS. Fluorescent-labelled secondary antibody was added, again diluted in PBS to the appropriate concentration, followed by incubation for 1 hour at room temperature and then 3 washes for 5 minutes with PBS. Slides were mounted in mounting medium (Vectashield) containing 4',6-diamidino-2-phenylindole (DAPI) and analysed by fluorescent microscopy.

2.3.2 Transient transfection and immunostaining of ARPE-19 for cellular trafficking of C1QTNF5

Using the pEGFP-C1-C1QTNF5 constructs, ARPE-19 cells were transfected as described in Section 2.2.1.4, using 10µl cell suspension and 0.5µg DNA per reaction. Following transfection, each reaction was transferred to separate wells of a 6 well tissue culture plate, each containing a glass slide and ARPE-19 culture media. Cells were incubated for 48 hours at 37°C. Media was then aspirated from the wells and cells washed twice with PBS. Cells were fixed with ice-cold methanol for 5 minutes and again washed twice with PBS. Immunohistochemistry was then carried out as described in Section 2.3.1, using primary antibodies of mouse anti-His and rabbit anti-β-catenin and secondary antibodies of anti-mouse Texas Red and anti-rabbit FITC.

2.4 Cell culture assays

The following cell culture assays were carried out on untransfected ARPE-19, the ARPE-19 stably transfected cell lines, untransfected EBNA293 and the EBNA293 stably transfected cell lines. The ARPE-19 stably transfected cell line over-expressing His-C1QTNF5 were produced in this study, as was the EBNA293 stably transfected cell line over-expressing wild-type His-C1QTNF5. However, the mutant His-C1QTNF5-expressing EBNA293 cell line was produced by Dr X. Shu (MRC Human Genetics Unit) and supplied for use in this study.

2.4.1 Apoptosis (TUNEL) assays

The terminal deoxynucleotidyl transferase (TdT)-mediated dUTP nick-end labelling (TUNEL) assay was carried out to detect levels of apoptosis in ARPE-19 cells, either of untransfected ARPE-19 where apoptosis had been induced with H_2O_2 or of the transfected cell lines. Once cells had been prepared, the TUNEL assay was carried out following the same method in each instance.

2.4.1.1 Inducing apoptosis in ARPE-19

ARPE-19 cells were grown to confluence on glass slides in 3 wells of a 6-well tissue culture plates. 1 well of cells was then incubated for a further 12 hours in media containing 0.5μM H_2O_2, with the remaining two wells incubated for a further 2 hours in normal culture media. These provided the apoptosis-induced, positive and negative control samples respectively. Following the further incubation, the cells were washed twice with PBS and fixed to the slides with 4% methanol-free PFA for 25 minutes at 4°C, followed by two 5 minute washes with PBS at room temperature. The slides were then ready for analysis using the TUNEL assay.

2.4.1.2 Culturing the APRE-19 transfected cell lines prior to apoptosis detection

ARPE-19 and wild-type or mutant His-C1QTNF5-expressing APRE-19 cells were grown to confluence on glass slides in 6-well tissue culture plates in culture media containing 10% FCS. This was then changed to serum-free media and the cells incubated for a further 1, 2 or 3 days. The slides were then washed twice with PBS and the cells fixed to the slides with 4% methanol-free paraformaldehyde (PFA) for 25 minutes at 4°C, followed by two 5 minute washes with PBS at room temperature. In addition, 2 extra untransfected ARPE-19 slides were prepared, incubating in serum-free media for 3 days post confluence. These provided positive and negative control slides.

2.4.1.3 The TUNEL assay

TUNEL assay analysis was carried out using the DeadEnd Fluorimetric TUNEL System (Promega) and following the manufacturers' instructions. Unless otherwise specified, all steps were carried out at room temperature. Cells were permeabilised with 0.2% Triton X-100 solution in PBS for 5 minutes, and then washed for 5 minutes with PBS. After removing excess liquid, cells were covered with 100µl equilibration buffer and incubated at room temperature for at least 10 minutes. Whilst the cells were equlibriating, the rTdT incubation buffer and positive control slides were prepared. To prepare the positive control slides, following permeabilisation and washing, the cells were covered with 100µl DNase I buffer and incubated for 5 minutes. The liquid was then tapped off and 100µl DNase buffer I containing 10 units/ml DNase I was added followed by incubation for 10 minutes. Slides were then washed by immersing 3-4 times in dH_2O. The rTdT buffer was prepared by mixing 45µl equilibration buffer, 5µl nucleotide mix and 1µl rTdT enzyme per sample and positive control slide. For the negative control slides, rTdT buffer was prepared in the same manner but omitting the rTdT enzyme. Following draining of excess liquid, 50µl of the appropriate rTdT buffer was then added to each slide and incubated in the dark at 37°C for 1 hour, ensuring that the slides do not dry out. Meanwhile, 20x saline-sodium citrate (SSC) was diluted 1:10 to create a 2x SSC solution. Following sufficient incubation, the slides were then immersed in the 2x SSC for 15 minutes, and subsequently washed 3 times for 5 minutes in PBS. Slides were then mounted in Vectashield plus DAPI and analysed by fluorescence microscopy as before.

2.4.2 Cell adhesion assay

Cell adhesion assays were carried out following the optimised cell adhesion assay method (Section 2.4.2.2).

2.4.2.1 Optimising the cell adhesion assay

Optimisation was required to obtain a reproducible cell adhesion assay method. Optimised stages included blocking the plate, determining correct cell number, washing to remove non-adherent cells and fixing of adherant cells.

2.4.2.1.1 Blocking the plate

It was investigated whether bovine serum albumin (BSA), heat-inactivated BSA (both using a high 98% purity or low 96% purity grade of BSA) or using 1% skimmed milk would be most suitable as a blocking solution.

Heat-inactivated PBS-BSA (HI-PBS/BSA) was prepared by dissolving 10 mg/ml BSA in PBS and filtering through a 2 µm disposable filter (Schleicher) to remove any large undissolved particles. Any concentration greater than 10 mg/ml would form a solid gel when heat-inactivated, which is unsuitable for blocking wells. The solution was heated in a 90°C water bath until it went cloudy but not white indicating that the protein was denatured but had not formed large aggregates. High grade and low grade BSA were used to prepare HI-PBS/BSA solutions. Blocking solutions were also prepared using high and low grade BSA at 3 % solution in PBS without heat inactivation, 1 % skimmed milk in dH_2O or PBS alone.

Two hundred microlitres of each blocking solution was added to the wells of a 96-well microtitre plate and incubated at room temperature for 2 hours. After washing two times with 200µl per well PBS, 100µl ARPE-19 cell suspension at 5×10^5 cells/ml in standard ARPE-19 culture media was added to each well and incubated at 37°C for 1 hour. Wells were washed three times with 200µl per well PBS and the number of adherent cells determined by staining with crystal violet (see Section 2.4.2.2).

2.4.2.1.2 Determination of correct cell number and washes

The concentration of cells added to the wells and the number of washes required were investigated. Too vigorous washing could remove adherent cells from the wells, and too few washes or too high a cell concentration could mean non-adherent cells remain.

Using 96-well microtitre plates, 100µl 10.0mg/ml laminin, diluted in PBS, was added to each well and incubated overnight at 4°C. The wells were washed once with 200µl PBS using a multichannel pipette, with all liquid aspirated from the wells.

Blocking was then carried out using 200µl per well HI-PBS/BSA (low grade) for 2 hours at room temperature, followed by three washes with 200µl PBS as before. 100µl ARPE-19 cell suspension containing $2.5x10^5$, $5.0x10^5$, $7.5x10^5$ or $1.0x10^6$ cells/ml diluted in culture media was added to the wells and the plate incubated for 1 hour at 37°C. The cell suspension was then aspirated from the wells using the multichannel pipette. In this and all subsequent washing stages, care was taken not to dislodge loosely adhered cells. Pipette tips were placed gently against the edge of the well base and liquid was applied or removed slowly. Wells were either washed 1, 2 or 3 times, with the number of adherant cells determined by staining with crystal violet (see Section 2.4.2.2). The assay was carried out in triplicate to test which combination of cell concentration and number of washes gave the most reproducible results.

2.4.2.1.3 Investigating different fixatives

To investigate the effects of different fixatives, 96 well microtitre plates were coated with increasing concentrations of laminin in PBS. These were then blocked for 2 hours with low-grade HI-PBS/BSA (prepared as before) and washed with 200µl per well PBS. 100µl cell suspension at $5.0x10^5$ cells/ml in culture media was added to each well and incubated for 1 hour at 37°C. Wells were washed twice with 200µl per well PBS and then fixed with 100µl per well of either 5% aqueous glutaraldehyde, methanol or not fixed (PBS alone added) for 20 minutes at room temperature. Wells were washed twice with 200µl per well PBS and the degree of cell adhesion measured using crystal violet (see Section 2.4.2.2).

2.4.2.2 Optimised cell adhesion assay

A 96 well microtitre plate was coated overnight at 4°C with the desired extracellular matrix proteins (1µg/well of laminin, fibronectin, His-C1QTNF5 or His-gC1q) diluted in PBS. The solution was then aspirated from wells, 200µl per well HI-BSA added and the plate incubated at room temperature for 2 hours. The wells were washed three times with 200µl per well PBS, and 100µl cell suspension at $5.0x10^5$ cells/ml in culture media was added per well. The plate was then incubated for 1 hour (unless otherwise specified) at 37°C. Following this, undetached cells were

carefully removed from the wells by aspiration, ensuring pipette tips did not detach cells from the wells. The wells were then washed twice with 200µl per well PBS, again ensuring minimal detachment of the attached cells. One hundred microlitres of 5% aqueous glutaraldehyde was added to each well to fix the adherent cells, and the plate was incubated at room temperature for 20 minutes. To determine the level of adherant cells, wells were then washed three times with 200µl per well PBS, 100µl 0.1% crystal violet (in 0.2M MES, pH6.0) was added to each well and the plate incubated at room temperature for 10 minutes. The wells were then washed three times with 200µl per well PBS, 100 µl 10% acetic acid was added to each well and, after mixing, the OD_{595} measured.

2.4.3 Cell spreading assay

96 well microtitre plates were coated overnight with 100µl per well of 10mg/ml laminin or fibronectin diluted in PBS. Wells were then washed three times with PBS and 100µl cell suspension at a concentration of $5.0x10^5$ cells/ml in culture media was added to each well. The plates were incubated at 37°C for 2 hours, after which time images were taken of the cells using a light microscope from which to determine the number of spread cells.

2.4.4 Phagocytosis assays

Phagocytosis assays were carried out to compare levels of FITC-labelled ROS phagocytosis in the different ARPE-19 cell lines. Levels of phagocytosis were determined by flow cytometry.

2.4.4.1 Preparing and FITC-labelling rod outer segments

Bovine retinas were stored at -80°C until required. Following defrosting on ice, each retina was resuspended in 1ml sucrose homogenizing medium (34% sucrose, 65mM NaCl, 2mM $MgCl_2$, 5mM tris-acetate pH7.4, 1x protease inhibitor tablet) and shaken vigorously for 1 minute to detach the ROS. Following centrifugation at 4,600 rpm for 4 minutes using a benchtop microcentrifuge, the supernatant was removed and diluted with 2 volumes 10mM tris-acetate pH7.4. The pellet was resuspended in 1ml sucrose homogenizing medium, homogenized with a loose-fitting pestle (4-5 passes)

and centrifuged as before at 4,600 rpm for 4 minutes. The supernatant was removed and diluted with 2 volumes tris-acetate pH7.4. The supernatants were pooled and centrifuged at 2,600 x g for 4 minutes. The supernatant was discarded and ROS pellet resuspended in 1ml 0.1M sodium bicarbonate pH9.0

To fluorescently-label the ROS, 10µl FITC (10mg/ml in 0.1M sodium bicarbonate pH9.0) was added to the ROS suspension and incubated overnight at 4°C in the dark. Prior to use, FITC-labeled ROS (FITC-ROS) were centrifuged at 2,600g for 4 minutes, the supernatant removed and the ROS pellet resuspended in 2ml 0.1M sodium bicarbonate pH9.0.

2.4.4.2 Measuring phagocytosis of FITC-ROS by ARPE-19 cells using flow cytometry

The following general method was adapted for each phgoytosis assay. When investigating the effects of an anti-gC1q antibody (supplied by Dr X. Shu), the antibody was added to the cells after 3 days incubation in serum-free media and the addition of fresh culture media, diluting to a concentration of 0.1mg/ml. When investigating the effects of additional CFH this was added in the same manner at concentrations of 0, 1, 5, 10, 50 and 100µg/ml. In both instances, cells were then incubated at 37°C for 1 hour prior to the addition of FITC-ROS.

Cells were grown to 80% confluence in 6 well plates in normal culture medium. The medium was then changed to serum free for 3 days. After 3 days, the serum was changed for fresh serum free medium and 120µl FITC-ROS suspension was added to the appropriate wells, and the cells incubated for the allocated incubation time with FITC-ROS for up to 48 hours. Cells were then washed twice with PBS and detached using 1ml trypsin/EDTA. Three ml normal culture medium was added to neutralize the trypsin and cell pellets were collected by centrifugation at 3000g for 5 minutes. Cell pellets were then washed twice in PBS and resuspended in 2ml PBS. Cell suspensions were then analysed by flow cytometry.

2.5 Human blood procedures and assays

All methods were optimised by and carried out with the assistance of Aisleen McColl (MRC Centre for Inflammation Research, Edinburgh).

2.5.1 Isolation and maturation of macrophages from whole blood

Monocytes were isolated from whole blood and macrophages prepared for use by Aisleen McColl. The monocytes were plated onto 6 well tissue culture plates and incubated at 37˚C for 1 week to allow their differentiation into macrophages. Some of the cells were steroid-treated with dexamethasone, as this enhances their phagocytic activity.

Mature macrophages were washed twice with PBS and detached from the wells using 5 mM EDTA, 0.1% BSA on ice for 30 minutes. It was not possible to use trypsin as this blocks phagocytosis. Vigorous pipetting was carried out to assist in detaching the cells, which were then collected, centrifuged and resuspended to a concentration of 0.7 x 10^6 cells/ml in Iscove's modified Dulbecco's medium (IMDM), with or without autologous serum.

2.5.2 Neutrophil preparation

Neutrophils (purified from whole blood by Aisleen McColl) were cultured in IMDM, with or without 10% autologous serum at 37˚C for 22 hours at a concentration of 4 x 10^6 cells/ml. Neutrophils undergo apoptosis when left in culture, although if left for longer periods of time they will become necrotic. Neutrophils were then incubated with AnnexinV, with a 10 minute incubation at 37˚C to allow for labelling of the apoptotic neutrophils.

2.5.3 Macrophage phagocytosis of apoptotic neutrophils with autologous serum

24-well tissue culture plates were coated overnight at 4°C with 1µg/well His-C1QTNF5, His-gC1q or CFH diluted in 100µl PBS. The coated wells were washed with PBS and the liquid removed from the wells. 500µl of macrophage suspension with autologous serum was added to each well and the plates incubated at 37 ˚C for

45 minutes. After incubation, the media and non-adherant cells were removed from the wells, which were then washed once with IMDM. 400µl per well of labelled neutrophil suspension was added and the plates incubated at 37 ˚C for 30 minutes. Following incubation, the liquid was removed from the wells and the cells detached by addition of trypsin/EDTA and incubated on ice for 10 minutes. Cells were then analysed by flow cytometry to determine the degree of phagocytosis by the macrophages of the labelled neutrophils.

2.5.4 Macrophage phagocytosis of apoptotic neutrophils without autologous serum

500µl macrophage suspension without autologous serum and containing either CFH, wild-type or mutant His-C1QTNF5 or 10% autologous serum as a positive control was added to wells of a 24-well tissue culture plate. The plates were incubted at 37°C for 45 minutes to allow the macrophages to adhere to the wells. Media was then aspirated from the wells, which were then washed once with IMDM. 400µl per well of labelled neutrophil suspension was added, containing either CFH, wild-type or mutant His-C1QTNF5 or 10% autologous serum positive control, and the plates incubated at 37 ˚C for 30 minutes. Following incubation, the liquid was removed from the wells and the cells detached by addition of trypsin/EDTA and incubation on ice for 10 minutes. Cells were then analysed by flow cytometry to determine the degree of phagocytosis by the macrophages of the labelled neutrophils.

2.6 Protein procedures

2.6.1 Ni-NTA affinity purification of His-C1QTNF5 from mammalian cell culture media

Unless otherwise specified, the following method was used for purification of His-C1QTNF5 from the culture media of both the stably-transfected EBNA293 and ARPE-19 cell lines. Cells were grown to 80% confluence in media containing 10% FCS. This was then changed to serum-free media and the cells incubated for a further 5 days. The culture media was then collected and clarified by centrifugation

at 10,000g for 10 minutes. To the culture media was then added 30mM NaH_2PO_4, 150mM NaCl, 10mM imidazole and the pH adjusted to 8.0. 2ml per litre of culture media of Ni-NTA bead suspension was washed twice with an excess of PBS and then added to the culture media and incubated on rotation at 4°C for 2 hours. This was then poured down a chromatography column, collecting the beads within the column. These were washed with 20ml per 2ml bead suspension of 30mM NaH_2PO_4, 150mM NaCl, 20mM imidazole pH8.0, followed by 20ml per 2ml bead suspension of 30mM NaH_2PO_4, 150mM NaCl, 50mM imidazole pH8.0. His-C1QTNF5 was then eluted from the beads in 1ml fractions of 1M imidazole, pH10.0, with 10µl from each elution analysed by reducing SDS-PAGE for the presence of pure His-C1QTNF5. Appropriate elution fractions were pooled and dialysed for 24 hours against 1l PBS using dialysis tubing, with the buffer replaced for fresh after 12 hours.

2.6.2 Ni-NTA affinity purification of His-gC1q from *E. coli*

Recombinant His-gC1q was purified from *E. coli* cell pellets, cultured as follows, unless otherwise specified. Cell pellets were collected by centrifugation at 3000rpm for 10 minutes.

Cell pellets were resuspended in 5ml per gram of 50mM NaH_2PO_4, 300mM NaCl, 10mM imidazole, pH8.0 plus 1mg/ml lysozyme and incubated on rotation for 30 minutes. The cells were then lysed using 2 passes through a French press. The lysed mixture was centrifuged at 10,000g for 30 minutes to remove cellular debris, with the supernatant retained. Ni-NTA beads were washed twice in PBS with 1ml bead suspension per 100ml supernatant used. The beads were then added to the supernatant and incubated on rotation for 2 hours at 4°C. This was then poured down a chromatography column, collecting the beads within the column. These were washed with 20ml per 2ml bead suspension of 30mM NaH_2PO_4, 150mM NaCl, 20mM imidazole pH8.0, followed by 20ml per 2ml bead suspension of 30mM NaH_2PO_4, 150mM NaCl, 50mM imidazole pH8.0. His-gC1q was then eluted from the beads in 1ml fractions of 1M imidazole pH10, with 10µl from each elution analysed by reducing SDS-PAGE. Appropriate elution fractions were pooled and

dialysed for 24 hours against 1l PBS using dialysis tubing, with the buffer replaced after 12 hours.

2.6.3 Purification of SCR modules from *Pichia pastoris* culture media by SP-Sepharose ion exchange chromatography

P. pastoris cultures were grown according to the standard method, with secreted SCR proteins purified from the culture supernatant. All purification methods had been optimised previously by Dr A. Herbert (University of Edinburgh).

2.6.3.1 Purification of SCR7-8Y and SCR7-8H

Culture supernatants were collected via centrifugation at 2,500g for 15 minutes, with the cell pellets discarded. 5mM EDTA was added to each before diluting 1:6 with distilled water. The diluted supernatants were loaded to 5ml SP-Sepharose columns and subsequently washed with 10ml, 20mM potassium phosphate pH6.0. Protein was eluted in 2ml fractions of 1M NaCl, 20mM potassium phosphate pH6.0, which were then screened by SDS-PAGE for the presence of protein. Fractions containing the appropriate protein were pooled and dialysed for 24 hours against 1l PBS using dialysis tubing, with the buffer replaced after 12 hours.

2.6.3.2 Purification of SCR19-20

The same purification method was followed as for SCR7-8Y/H, however protein was eluted from the column in 1M NaCl, 20mM potassium phosphate pH7.0

2.6.4 Reducing and non-reducing SDS-PAGE

Reducing and non-reducing sodium dodecyl sulphate polyacrylamide gel electrophoresis (SDS-PAGE) were carried out using pre-cast NuPAGE Novex Bis-Tris Gels (Invitrogen), NuPAGE running and sample buffers (Invitrogen) and the XCell SureLock Mini-Cell system (Invitrogen). Protein and cell samples were prepared by incubating with 4x NuPAGE LDS Sample Buffer, 10x NuPAGE Reducing Agent (omitted for non-reducing gels) and dH_2O up to a volume of 20µl at 70°C for 10 minutes. Gels (4-12% or 10%) were immersed in either NuPAGE MOPS (3-(N-morpholino)propanesulfonic acid) or MES (2-(*N*-

morpholino)ethanesulfonic acid) running buffer, samples and SeeBlue Plus 2 protein standard marker (Invitrogen) were loaded and the gels run for 60 minutes at 180V constant voltage. If required, proteins were then visualised by immersing the gel in Coomassie stain for 1 hour followed by washing overnight in dH_2O, changing for fresh as required.

2.6.5 Western blot

Following protein separation, transfer to Hybond-P membranes was carried out using the XCell SureLock Mini-Cell Blot Module system (Invitrogen). 1 piece of Hybond-P membrane was cut to the size of the gel, with this and the gel being sandwiched between two pieces of Whatman filter paper, also cut to the size of the gel and soaked in transfer buffer (1.46g Tris base, 7.2g glycine, made up to 1l with dH_2O). The blot module was then assembled, sufficient amounts of transfer buffer added and the transfer run for 60 minutes at 30V constant voltage. The membrane was then blocked overnight at 4°C in 1% skimmed milk powder dissolved in PBS, 0.01% TWEEN20. The blot was then incubated with primary antibody diluted to the appropriate concentration in PBS, 0.01% TWEEN20 (see Table 2.3) for 1 hour at room temperature, followed by 3x 5 minute washes in PBS, 0.01% TWEEN20. Secondary antibody was diluted to the appropriate concentration in the same buffer and incubated with the blot for 1 hour at room temperature followed by 3x 5 minute washes as before.

Table 2-3: Primary and secondary antibodies used for Western blots.

Primary antibodies	**Supplier**	**Dilution**
Anti-His	Sigma	1:3000
Anti-gC1q	Dr X Shu	1:1000
Secondary antibodies	**Supplier**	**Dilution**
HRP-labelled rabbit anti-mouse	GE Healthcare	1:4000
HRP-labelled goat anti-rabbit	GE Healthcare	1:4000

Secondary antibody detection was carried out using the Enhanced Chemiluminescence (ECL) or Enhanced Chemiluminescence Plus (ECL^+) Western blotting detection reagents (Amersham Biosciences). Following washing, excess liquid was drained from the membrane which was then covered in detection reagent

(diluted following the manufacturers' instructions) and incubated for 1 minute (ECL) or 5 minutes (ECL^+). Following draining of the detection reagent from the membrane, detection was then carried out using an X-ray film exposure cassette and Kodak X-Omat AR imaging film. Following exposure, the film was then developed using a phosphorimager X-ray machine (Konica Minolta).

2.6.6 Isoelectric focusing gel electrophoresis

Isoelectric focusing (IEF) gel electrophoresis was carried out using pre-cast Novex pH3-10 IEF Gels (Invitrogen), the Novex IEF pH3-10 Buffer Kit (Invitrogen) and the XCell SureLock Mini-Cell system (Invitrogen). Protein samples were prepared by mixing with 2x Novex Sample Buffer pH3-10 and dH_2O up to a volume of 20µl. The gel tank was assembled using 1x IEF anode buffer (20x stock, Invitrogen) and 1x IEF cathode buffer pH3-10 (50x stock, Invitrogen). Samples and IEF pH3-10 markers (Invitrogen) were loaded to the gel, which was run at 100V constant voltage for 60 minutes, then at 200V constant voltage for 60 minutes and finally at 500V constant voltage for 30 minutes. Proteins were then fixed to the gel by immersion in 12% TCA for 30 minutes, followed by washing with adequate H_2O. Proteins were then visualised by immersing the gel in coomassie stain for 1 hour followed by washing overnight in dH_2O, changing for fresh as required.

2.6.7 Native PAGE

Native PAGE was carried out using the Hoefer SE600 Vertical Slab Unit, following the standard Laemmli system. Resolving gels of 8%, 10% or 12% were poured (see Table 2.4 for formulations), overlaid with 5% stacking gels (see Table 2.4). Protein samples were diluted in running buffer (5x stock: 15.1g Tris base, 72g glycine, make up to 1l with dH_2O), with protein standard samples of lactalbumin, carbonic anhydrase, ovalbumin and BSA obtained from the Molecular Weight Marker Kit for Non-denaturing PAGE, 14,000 – 500,000 range (Sigma). Gels were run in 1x running buffer for 8 hours at 30V constant voltage, with proteins visualised by Coomassie staining followed by adequate washing overnight in dH_2O, changing for fresh as required.

Table 2-4: Native PAGE resolving and stacking gel formulations.
All volumes are in millilitres.

	Resolving gel			Stacking gel
Gel percentage	**8%**	**10%**	**12%**	**5%**
dH_2O	9.3	7.9	6.6	2.7
30% acrylamide mix	5.3	6.7	8.0	0.67
1.5M Tris pH8.8	5.0	5.0	5.0	/
1.0M Tris pH6.8	/	/	/	0.5
10% ammonium persulphate	0.2	0.2	0.2	0.04
TEMED	0.012	0.008	0.008	0.004

2.6.8 Bradford assay

The Bradford assay was used to determine the concentration of protein solutions. Standard samples were prepared by diluting a stock solution of 10mg/ml BSA in PBS to 0, 0.078, 0.156, 0.313, 0.625, 1.25 and 2.5µg/ml. 0.98ml Bradford reagent was added to disposable 1ml cuvettes and 20µl of either standard sample or protein solution was added to this. These were then mixed and left at room temperature for 10 minutes. The OD_{595} of each was then measured and the OD_{595} of the standard samples was used to create a standard curve from which the concentrations of the protein solutions could be determined.

2.6.9 Protein solubility assay

Wild-type and mutant His-C1QTNF5 were incubated at 37°C for 10 minutes, followed by centrifugation at 13,000 rpm using a benchtop centrifuge at 37°C to remove any insoluble protein, with the protein concentration then determined by Bradford assay. Each was then diluted to 200µg/ml in PBS at 37°C up to a volume of 2ml. The protein solutions were then incubated at 37°C, with 200µl samples taken after 0, 2, 4, 6, 10 and 36 hours and placed into separate microcentrifuge tubes. Each sample tube was then immediately centrifuged at 13,000 rpm on a benchtop centrifuge for 10 minutes at 37°C, after which time the OD_{280} of each sample was taken and a 20µl aliquot prepared for analysis by reducing SDS-PAGE.

2.6.10 MALDI-TOF M/S

MALDI-TOF M/S analysis was carried out by Dr J. Creanor (University of Edinburgh), using the Voyager-DE STR Biospectrometry Workstation**.**

2.7 Protein interaction assays

Protein interaction assays were carried out investigating interactions between wild-type and mutant His-C1QTNF5 or wild-type His-gC1q and either CFH, recombinant SCR modules or CRP. All His-C1QTNF5 and His-gC1q was produced in this study, as were SCR7-8Y, SCR7-8H and SCR19-20. CFH was purified from whole blood and supplied by Professor R. Sim (University of Oxford), SCR3-4 was recombinantly produced in *P. pastoris* and supplied by Dr H. Hocking (University of Edinburgh) and CRP was purchased commercially (Sigma).

2.7.1 Plate binding assays

An initial plate binding assay was carried out using the unoptimised method, as follows. 96-well microtitre plates were coated with 1µg/well His-gC1q diluted in PBS overnight at 4°C. Wells were then washed 3 times with 200µl per well PBS, 0.01% TWEEN20. Wells were blocked with 100µl per 10mg/ml BSA diluted in PBS for 2 hours at room temperature, followed again by washing with 200µl per well PBS, 0.01% TWEEN20. CFH was diluted to the desired concentrations in PBS and 100µl added per well. The plates were incubated at room temperature for 1 hour, and the wells then washed 3 times with 200µl per well PBS, 0.01% TWEEN20. Primary antibody, OX23, stock solution (340µg/ml) was diluted to 10µg/ml in PBS and 100µl added to each well. The plates were incubated for 1 hour at room temperature, followed by washing with 200µl per well PBS, 0.01% TWEEN20 as before. Secondary antibody, alkaline phosphatase-labelled rabbit anti-mouse (Sigma), was diluted 1:1000 in PBS and 100µl added to each well. The plates were again incubated at room temperature for 1 hour followed by 3 washes with 200µl per well PBS, 0.01% TWEEN20. Secondary antibody was then detected using the p-nitrophenyl phosphate tablet kit (Sigma) with 100µl reagent added per well and after 20 minutes incubation at room temperature the OD_{450} measured was using the plate

reader. Control assays were also carried out following the same method but rather than coating with His-gC1q, 200µl PBS alone was added to the wells. Measurements from wells with a His-gC1q coat gave readings for total binding, measurements form wells without a His-gC1q coat gave readings for background binding and specific binding was calculated by deduction of specific binding from total binding for each CFH concentration.

2.7.1.1 Plate binding assay optimisation

The plate binding assay was optimised with regards to primary antibody concentration, dilution buffer pH and His-gC1q coat concentration.

2.7.1.1.1 Optimising primary antibody concentration

96-well microtitre plates were coated and blocked as described in Section 2.7.1. CFH was diluted in PBS and added to the wells and the plate incubated at room temperature for 1 hour as before. Wells were then washed 3 times with 200µl per well PBS, 0.01% TWEEN20 and 100µl per well OX23 solution was added, diluted from stock to 1:34, 1:340, 1:1000 or 1:3400 in PBS. The plates were incubated at room temperature for 1 hour, and then washed, secondary antibody applied, washed again and detection solution applied as described previously. The plates were incubated with detection reagent for 10, 20 or 30 minutes prior to OD_{450} measurements being taken.

2.7.1.1.2 Optimising pH

The plate binding assay was carried out as described in Section 2.7.1. However, a primary antibody dilution of 1:340 was used with a 20 minute detection time, and only one CFH concentration of 0.5µg/ml was used, diluting in 10mM MES at pH6.0 or pH6.5, or PBS. Following the addition of CFH, all subsequent wash stages and antibody incubations were carried out in either 10mM MES at pH6.0 or pH6.5, or PBS, with or without 0.01% TWEEN20, as appropriate.

2.7.1.1.3 Optimising His-gC1q concentration

The plate binding assay was carried out as described in Section 2.7.1. However, plates were coated with His-gC1q diluted to 0, 0.001, 0.01, 0.1, 1.0 or 10.0µg/ml in PBS. Also, a primary antibody dilution of 1:340 was used with a 20 minute detection time and CFH was diluted in 10mM MES pH6.5 with all subsequent wash and antibody incubation stages carried out using this buffer with or without TWEEN20.

2.7.1.1.4 The optimised plate binding assay method

96-well microtitre plates were coated with 1µg/well His-gC1q diluted in PBS overnight at 4°C. Wells were washed 3 times with 200µl per well PBS, 0.01% TWEEN20. To each well was then added 200µl 10mg/ml BSA diluted in PBS and the plates incubated at room temperature for 2 hours. The wells were then washed 3 times with 200µl per well PBS, 0.01% TWEEN20. CFH was diluted to the appropriate concentration in 10mM MES pH6.5, with 100µl added per well and the plate incubated for 1 hour at room temperature. Wells were washed 3 times with 200µl per well 10mM MES pH6.5, 0.01% TWEEN20. Primary antibody was diluted 1:340 in 10mM MES pH6.5 and 100µl was added to each well followed by incubation at room temperature for 1 hour. Wells were subsequently washed 3 times as before and secondary antibody added, diluted 1:1000 in 10mM MES pH6.5. Following incubation at room temperature for 1 hour, wells were washed 3 times as before. To each well was added 100µl detection reagent and the plates incubated at room temperature for 20 minutes prior to taking OD_{450} measurements using the plate reader.

2.7.1.2 His-gC1q and CFH plate binding assay

The optimised plate binding assay method was followed, coating the plates with His-gC1q and adding CFH in the fluid phase.

2.7.1.3 His-C1QTNF5 and CFH plate binding assay

The optimised plate binding assay was followed, except plates were coated with 1µg/well of either wild-type or mutant His-C1QTNF5. CFH was again added in the fluid phase.

2.7.1.4 CFH and CRP plate binding assay

The optimised plate binding assay was followed, except plates were coated with 1µg/well CRP. CFH was again added in the fluid phase.

2.7.1.5 CRP and His-gC1q/His-C1QTNF5 plate binding assay

The optimised plate binding assay was followed, except plates were coated with 1µg/well CRP. Wild-type or mutant His-C1QTNF5 were added in the fluid phase, with a primary antibody of mouse anti-His (Sigma) used diluted in 1:1000 in PBS.

2.7.2 Surface plasmon resonance

All SPR experiments were carried out using the Biacore T100 machine and Biacore T100 Control software, with all analysis carried out using the Biacore T100 Evaluation software. In all instances, pH scouting, coating the chips and kinetic assays were carried out using the software wizards provided. All buffers and protein samples used were at 37°C and at all stages the Biacore T100 sample compartment and operating temperature were maintained at 37°C, and in all instances running buffer was 10mM HEPES pH7.4, 150mM NaCl, 0.005% P20 (supplied by Biacore).

2.7.2.1 pH scouting and coating of the CM5 chips

pH scouting was carried out in order to determine the optimal buffer conditions for coating of wild-type and mutant His-C1QTNF5 to the CM5 chips. Chips were prepared prior to use by 3x 1 minute injections with 50mM NaOH (Biacore) at a flow rate of 1µl per minute, to remove any unwanted ions or uncoupled dextran. Following this, the chip was washed with running buffer for 5 minutes at a flow rate of 10µl per minute. pH scouting was then carried out to determine the optimal buffer pH for either wild-type or mutant His-C1QTNF5, giving the weakest conditions for a high level of attraction of protein to the chip surface which rapidly dissociates once

conditions return to physiological (running buffer alone). This was carried out following the immobilisation pH scouting wizard and using only the flow cells which were to be coated with protein. His-C1QTNF5 was diluted to a concentration of 25mM in 10mM acetate pH4.5, 5.0 or 5.5 (Biacore), or 10mM HEPES pH6.0, 6.5 or 7.0. 120 second injections at a flow rate of 10µl per minute were used, washing between each stage with 50mM NaOH. The optimal buffers were selected as 10mM HEPES pH6.5 for wild-type His-C1QTNF5 and 10mM HEPES pH6.0 for the mutant protein.

Immobilisation of His-C1QTNF5 to the CM5 chips was carried out using the immobilisation wizard, following the protocol for amine coupling. The appropriate chip type and blank or reference flow cells were selected, and the desired levels of bound response units set at either 200RU or 1000RU. EDC (1-ethyl-3-(3-dimethylaminopropyl) carbodiimide hydrochloride) (Biacore) and NHS (*N*-hydroxysuccinimide) (Biacore) were used to activate the chip surface and, once sufficient protein was bound, ethanolamine was used to quench any uncoupled sites. Ethanolamine alone was used for the blank flow cells. The chip was then washed with running buffer at 50µl per minute to remove any loosely bound protein.

2.7.2.2 SPR analysis of His-C1QTNF5 interactions with CFH, SCR7-8Y/H, SCR19-20, SCR3-4 and CRP

SPR analysis of His-C1QTNF5 interactions with CFH, SCR7-8Y/H, SCR19-20, SCR3-4 and CRP were all carried out using the kinetics/affinity wizard facility. Following the wizard protocol, the chips were normalised with glycerol prior to beginning each run, 3 start-up cycles were run, injection times were 30 seconds and dissociation times were either 2000 seconds for CFH or 300 seconds for the SCR modules and CRP. An internal repeat was carried out for each run, taking a mid-range dilution and, for each protein, experiments were run on at least one 200RU and one 1000RU chip for both wild-type and mutant His-C1QTNF5 chips. Experimental data was analysed using the Biacore T100 Evaluation software kinetics/affinity application.

2.7.3 Isothermal titration calorimetry

Isothermal titration calorimetry (ITC) was carried out using the AutoITC MicroCal and the DRV 2000 auto ITC software. To set up the instrument, the reference cell was washed 3 times with 2ml H_2O, and then filled to the indicated level with PBS. Samples were then added to the sample tray, allowing for reactions involving macromolecule (CFH) and ligand (His-gC1q), and macromolecule (CFH) and PBS only. When investigating reactions with a predicted kD in the nM range, 2ml CFH was added at a concentration of 0.5µM in PBS and 0.7ml His-gC1q was added at 7.5µM in PBS. When investigating reactions with a predicted kD in the µM range, 2ml CFH was added at a concentration of 5µM and 0.7ml His-gC1q was added at 125µM in PBS. The instrument and sample drawer were then left to equilibriate to 37°C. Reaction parameters when investigating nM kD interactions were 25 injections of 4.8µl and a 9.8 second equilibration period. Reaction parameters when investigating µM interactions were 42 injections of 4.8µl and a 9.8 second equilibriation period.

2.7.4 His-C1QTNF5 co-factor assays

It was investigated whether His-C1QTNF5 had any effect on CFH co-factor activity with FI, adapting a method supplied by Professor R. Sim (University of Oxford). His-C1QTNF5 was produced in this study, whilst C3b, CFH and FI were provided by Prof. R. Sim.

2.7.4.1 Fluid-phase co-factor assay

The following reagents were incubated together in PBS at 37°C up to a total volume of 20µl; C3b (5µg), CFH (0.5µg), FI (0.1µg) and wild-type or mutant His-C1QTNF5 (0.5µg). In addition, control reactions were also set up omitting CFH, FI, His-C1QTNF5 or combinations thereof. Following incubation, total reactions were analysed by reducing SDS-PAGE as described in Section 2.6.4. Co-factor activity was confirmed by the presence of C3b degradation products, visible after Coomassie staining of the SDS-PAGE gel, at 43kDa and 46kDa.

2.7.4.1.1 Fluid-phase co-factor assay time course

The following reagents were incubated together in PBS at 37°C up to a total volume of 100µl; C3b (25µg), CFH (2.5µg), FI (0.5µg) and wild-type or mutant His-C1QTNF5 (2.5µg). In addition, control reactions were also set up omitting His-C1QTNF5. 20µl samples were taken after 0, 1, 5 and 15 minutes and immediately prepared for analysis by reducing SDS-PAGE by addition of LDS sample buffer and reducing agent (as described in Section 2.6.4). This was to prevent any further co-factor activity from occurring. Samples were then analysed by reducing SDS-PAGE. Co-factor activity was confirmed by the presence of C3b degradation products, visible after Coomassie staining of the SDS-PAGE gel, at 43kDa and 46kDa.

2.7.4.2 Solid phase co-factor assay

A 96-well microtitre plate was coated overnight in 1µg/well wild-type or mutant His-C1QTNF5 in 100µl PBS, or 100µl PBS alone, as illustrated in Figure 2.1. The wells were then washed 3 times with 200µl per well PBS, 0.01% TWEEN20 and blocked at room temperature for 2 hours with 200µl per well 10mg/ml BSA in PBS, again followed by 3 washes with 200 µl per well PBS, 0.01% TWEEN20. To the wells was then added CFH, diluted in PBS to concentrations of 0, 0.5 and 2.0µg/ml, as illustrated in Figure 2.1. The plate was incubated for 2 hours at room temperature and washed 3 times as before with PBS, 0.01% TWEEN20. To each well was then added C3b (20µg) and FI (0.4µg) up to a final volume of 80µl in PBS. The plate was incubated at 37°C, with 20µl samples taken after 30, 60 and 90 minutes. Immediately after taking, each sample was prepared for analysis by reducing SDS-PAGE by incubating with LDS sample buffer and reducing agent at 70°C, as described in Section 2.6.4. Samples were then analysed by reducing SDS-PAGE, with C3b degradation product visualised by Coomassie staining.

	CFH ug/ml		
	0	0.5	2
Protein coat	Wild-type His-C1QTNF5		
	Mutant His-C1QTNF5		
	PBS		

Figure 2.1: Solid phase co-factor assay plate layout.

2.8 Equipment, consumables and reagents

2.8.1 Equipment

Equipment	Type/model	Supplier
Balance	Toledo	Metler
Benchtop microcentrifuge	Biofuge fresco	Heraeus
Heated benchtop microcentrifuge	S417R	Eppendorf
Cassettes for film development		Amersham
Centrifuge	Legend RT	Sorval
Chromatography column		BioRad
Fluorescence microscope		
French press	French Pressure CellPress	Thermo
Gel tank	Origo H3-SET	Amersham
Incubator	HERA cells 240	Hereaus
ITC machine	AutoITC	MicroCal
Light microscope	DMIL	Leica
Microporator	MP-100	Digital Biotech
Microwave	Super Showerwave	Sanyo
Multichannel pipette	Finnpipette	Thermo
Nanodrop spectrophotometer	ND100	NanaDrop
Plate reader	Multiskan Spectrum	Thermo
Rotating incubator	Innova 4250	New Brunswick
PCR machine	PTC-225	MJ Research
pH meter	Hydrus 400	Fisher scientifc
Medical film processor	SRX-101A	Konica Minolta
Spectrophotometer	UV1101	BiotechPhotometer
Tissue culture hood	LaminAir HB2448	Heraeus
Water bath	GD120	Grant
Water purification system	Milli-Q	Millipore

2.8.2 Consumables

Consumable	Supplier
Agar plates (plus ampicillin)	HGU technical services
CM5 chips	Biacore
Dialysis tubing	BioDesign
Falcon tube	Cellstar
Glass slide	VWR International
Hybond-P membrane	Amersham Biosciences
Microcentrifuge tube	Anachem
Microtitre plates (96 well)	Greiner Bio-One
Pastette	Alpha Labs
Plates (for agar)	Nunc
Shaker flask (500ml and 1l)	HGU technical services
Sterile filter	Elkay Lab Products
Syringe	BD Plastipak
Tissue culture dish	Greiner Bio-One
Tissue culture flasks	Greiner Bio-One
Tissue culture plate (24 and 6 well)	Greiner Bio-One
Whatman filter paper	Whatmann
X-ray film	Kodak

2.8.3 Reagents

Reagent	Supplier	Stock concentration
Acrylamide mix	Severn Biotech	30%
Agar	Duchefa Biochemie	
Agarose	Biogene	
Ammonium persulphate	Sigma	
Ampicillin	Sigma	
BamHI	Boehringer Mannheim	40u/µl
Biotin	Sigma	
Boric acid	Sigma	

Bradford reagent	BioRad	5x
Bromophenol blue	BDH	
BSA (98%)	Sigma	
BSA (96%)	Sigma	
Coomassie stain	Pierce	
Crystal violet	Sigma	
DMEM (with L-glutamate)	Gibco	
DMEM F12	Gibco	
DMSO	Sigma	
DNTP	Invitrogen	
EDTA	BDH AnalaR	
EDTA solution	HGU technical services	0.4g/l
Ethidium bromide	Sigma	
FCS	HGU technical services	
Fibronectin	Sigma	
FITC	Sigma	
FuGENE	Roche	
G418	Sigma	
Glutaraldehyde	Sigma	
Glycerol	BDH	
Glycine	Sigma	
HEPES	Sigma	
Hydrogen peroxide	Sigma	
IMDM	Gibco	
Imidazole	Sigma	
IPTG	Sigma	
Laminin	Sigma	
Luria broth	HGU technical services	
LB-agar plus ampicillin	HGU technical services	
L-glutamate	HGU technical services	30g/l
Lysozyme	Sigma	
Magnesium chloride	Sigma	

MEM vitamins	Gibco	100x
MES	Sigma	
Methanol	Fisher	
NheI	Boehringer Mannheim	10u/µl
Non-essential amino acids	Sigma	100x
Paraformaldehyde	BDH	
PBS	HGU technical services	
Penicillin/streptomycin	HGU technical services	7.0g/l and 13.0g/l
Peptone	Difco	
PFA	Sigma	
Protease inhibitor tablets	Roche	
Potassium phosphate	AnalaR	
Puromycin	Sigma	10mg/ml
Reaction buffer M	Boehringer Mannheim	
Skimmed milk	Marvel	
Sodium bicarbonate	Sigma	
Sodium chloride	BDH	
Sodium dihydrogen orthophosphate	Sigma	
Sodium pyruvate	Gibco	
Sorbitol	Sigma	
SP-Sepharose	Sigma	
Sucrose	Sigma	
TCA	AnalaR	
TEMED	Invitrogen	
Tris base	Sigma	
Triton X-100	Sigma	
Trypsin	HGU technical services	2.0g/l
TWEEN20	Sigma	
Vectashield	Vector	
X-gal	Sigma	
Xylene cyanol	Fisher chemicals	

Yeast extract Yeast nitrogen base plus ammonium sulphate	Gibco Difco	

3 CHAPTER 3

:

CREATING STABLY TRANSFECTED CELL LINES EXPRESSING C1QTNF5

3.1 Introduction

This chapter discusses the creation and analysis of stably transfected ARPE-19 cell lines expressing wild-type or mutant His-tagged C1QTNF5 (His-C1QTNF5). C1QTNF5 is expressed in the RPE, with immunostaining of mouse tissue sections showing C1QTNF5 to be located apically between the RPE and ROS, and basally between the RPE and Bruch's membrane (Mandal *et al.,* 2006b). Studies into the effects of the Ser163Arg mutation in C1QTNF5 using stably transfected EBNA293 showed that the wild type but not the mutant protein is secreted, whilst immunostaining of transiently transfected ARPE-19 cells suggested that the mutant protein aggregates and is retained within the endoplasmic reticulum (Shu *et al.,* 2006b). ARPE-19 is a spontaneously transformed human RPE-derived cell line which retains many features of the RPE such as the ability to form morphologically polarised monolayers and to phagocytose rod outer segments (Dunn *et al.,* 1998, Finnemann *et al.,* 1997). Mandal *et al.* (2006c) also found the wild type protein to be secreted but not the mutant when investigating V5-tagged C1QTNF5 expressed in COS-7 cells. Stably transfected EBNA293 expressing mutant C1QTNF5 also showed reduced adhesion to laminin-coated plates compared with wild-type C1QTNF5 expressing cells (Shu *et al.* 2006b). Such studies have used either the mouse, transiently transfected ARPE-19 or COS-7 (a transformed African green monkey kidney cell line) or stably transfected human EBNA293 cells (embryonic kidney in origin) to study C1QTNF5. This study will use stably transfected ARPE-19 cell lines to investigate the function of the Ser163Arg mutation. C1QTNF5 is expressed by the RPE so ARPE-19 is therefore physiologically relevant for studying C1QTNF5 expression and the effects of the Ser163Arg disease-causing mutation in L-ORMD. Creation of stably transfected ARPE-19 cell lines allows for functional assays to be carried out as stably transfected cells show constant expression levels. Comparisons can be made looking at the effects of over-expression of wild-type or mutant C1QTNF5 which could give insights into disease mechanisms in L-ORMD and possibly AMD.

3.2 Creating stably transfected ARPE-19 cell lines

In order to create stably transfected ARPE-19 cell lines, plasmid vector constructs were made containing either wild-type or mutant *C1QTNF5* inserts, with expression confirmed via transient transfection in ARPE-19. Stably transfected cells were then selected for with G418 and individual colonies screened for His-C1QTNF5 expression.

3.2.1 Creation of pEGFP-C1 constructs containing *C1QTNF5*

The transfected ARPE-19 cell lines expressing wild type or mutant His-C1QTNF5 were created using pEGFP-C1 plasmid vector constructs. pEGFP-C1 can be used for expression of recombinant proteins in mammalian cell lines, and contains the neomycin/G418 selectable marker, allowing for selection of transfected cells. Figure 3.1 shows the vector map for pEGFP-C1, with the cytomegalovirus (CMV) promoter upstream of *EGFP* (encoding the enhanced green fluorescent protein, EGFP) and the multiple cloning site (MCS). *EGFP* was removed by restriction enzyme digestion and replaced with the *C1QTNF5* inserts containing an additional C-terminal His-tag.

3.2.1.1 PCR amplification of *C1QTNF5* inserts

Wild-type or mutant *C1QTNF5* inserts were created by PCR amplification of human cDNA templates (supplied by Dr X. Shu, MRC Human genetics Unit, Edinburgh), with N-terminal NheI and C-terminal BamHI restriction enzyme sites for ligation into pEGFP-C1. PCR products were separated by agarose gel electrophoresis and bands corresponding to approximately 750bp were excised and purified from the gel (Figure 3.2, lanes 1 and 4). The PCR would only work in the presence of dimethyl sulfoxide (DMSO) (Figure 3.2, no DMSO lanes 2 and 5).

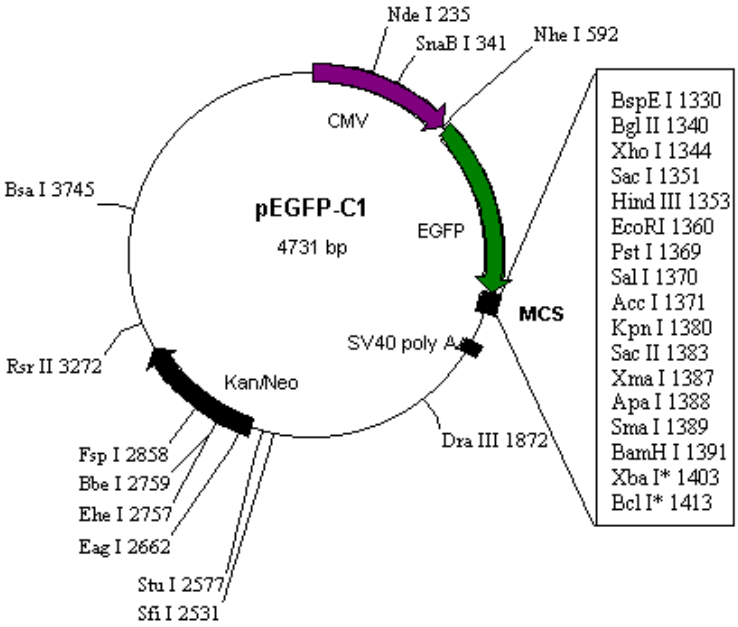

Figure 3.1: Vector map of the pEGFP-C1 plasmid.
(Source: www.biocenter.helsinki.fi/.../EGFP-C1.htm)

3.2.1.2 Selection of *C1QTNF5* inserts

Purified *C1QTNF5* inserts were ligated into pGEM-T-Easy and amplified in *E. coli* TOP10 cells. Individual colonies (5 for each construct) were selected and amplified. The plasmids were then extracted and samples digested with restriction enzymes to check for the presence of inserts of the correct size for *C1QTNF5,* with analysis by agarose gel electrophoresis (see Figure 3.3). Constructs corresponding to lanes 2 – 6 and 8 – 10 were selected for sequence analysis to check that the inserts matched the published *C1QTNF5* sequence with or without the 163Arg mutation as appropriate.

3.2.1.3 Preparation of the pEGFP-C1 vector and *C1QTNF5* inserts

pEGFP-C1 was restriction enzyme digested with NheI and BamHI and separated by agarose gel electrophoresis to obtain the pEGFP-C1 vector minus its *EGFP* insert, which was then purified from the gel (Figure 3.4A). *C1QTNF5* inserts showing the correct sequence were restriction enzyme digested to remove them from pGEM-T-Easy, then separated and purified by agarose gel electrophoresis (Figure 3.4B).

3.2.1.4 Construction, amplification and screening of *C1QTNF5*-containing pEGFP-C1 (minus *EGFP*) constructs

C1QTNF5 inserts were ligated into pEGFP-C1 minus *EGFP* and the constructs amplified in pGEM-T-Easy. Six colonies from each were selected, amplified by overnight culture and the plasmids purified, with the presence of *C1QTNF5* inserts of the correct size checked by agarose electrophoresis (Figure 3.5). One construct for mutant *C1QTNF5* and one for wild-type *C1QTNF5* was selected for use in creating the stably transfected ARPE-19 cell lines, with the inserts checked by sequencing prior to use.

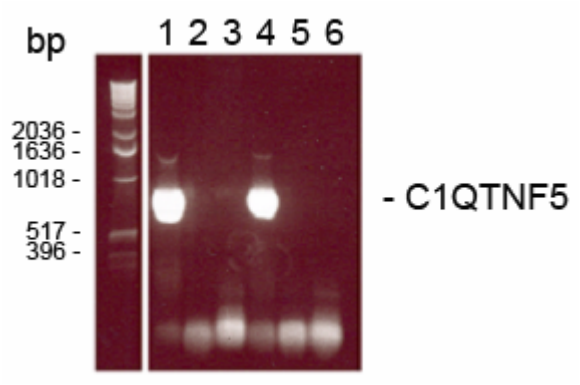

Figure 3.2: Agarose gel electrophoresis showing wild-type and mutant C1QTNF5 inserts created by PCR

Lanes: 1 – Wild-type *C1QTNF5* plus DMSO, 2 – Wild-type *C1QTNF5* minus DMSO, 3 – Wild-type *C1QTNF5* no template, 4 – Mutant *C1QTNF5* plus DMSO, 5 – Mutant *C1QTNF5* no DMSO, 6 – Mutant *C1QTNF5* no template.
Bands of approximately 700bp (base pairs) were excised and purified from lanes 1 and 4. The relative molecular mass markers and corresponding size in base pairs are shown.

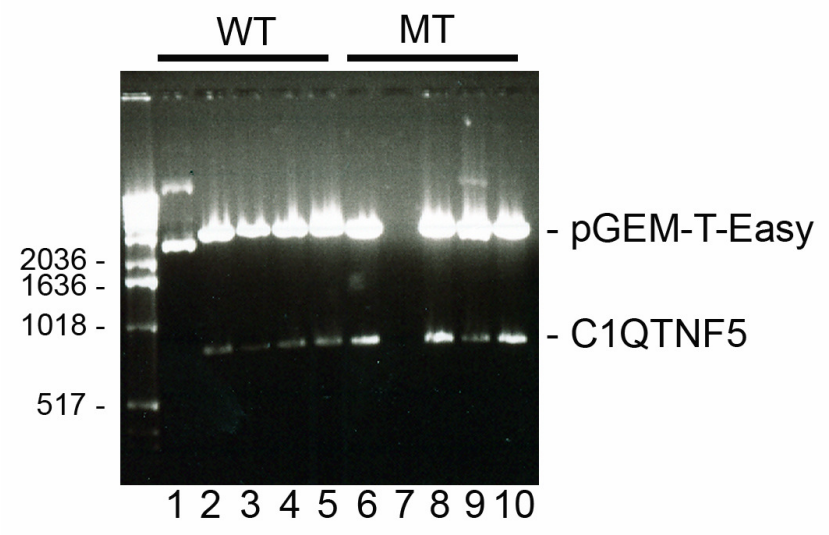

Figure 3.3: Agarose gel electrophoresis showing restriction enzyme digestion of pGEM-T-Easy constructs to check for the presence of wild-type or mutant *C1QTNF5* inserts.

C1QTNF5 are seen as bands of approximately 750bp (base pairs). The relative molecular mass markers and corresponding size in base pairs are shown on the left.

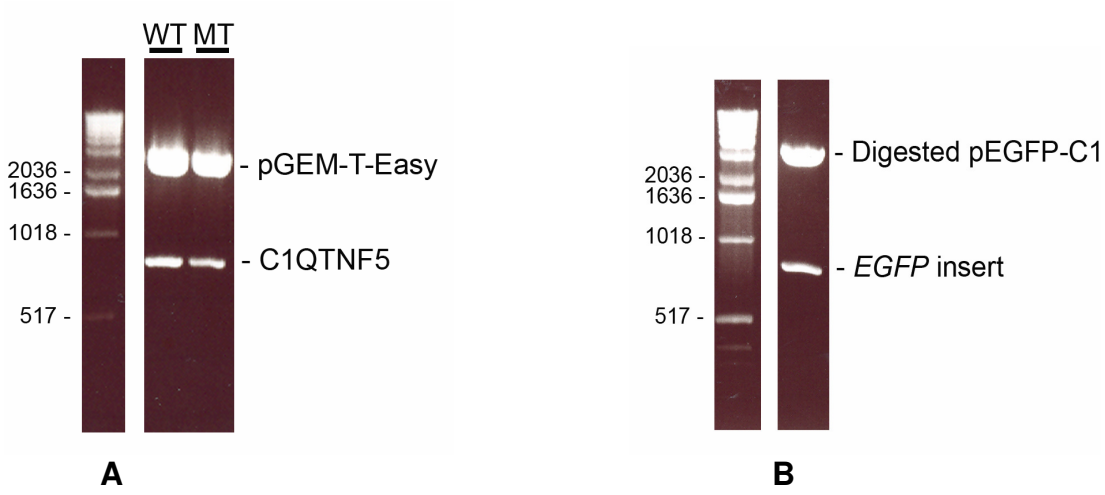

Figure 3.4: A – Restriction enzyme digestion of wild type and mutant constructs, separated by agarose gel electrophoresis.

Bands at approximately 750bp corresponding to wild-type (WT) and mutant (MT) *C1QTNF5* were purified for ligation into pEGFP-C1 minus *EGFP*.
B – Restriction enzyme digestion of pEGFP-C1 to remove the *GFP* insert. Band corresponding to digested pEGFP-C1 was purified from the gel for ligation with *C1QTNF5* inserts. The relative molecular mass markers and corresponding size in base pairs are shown on the left.

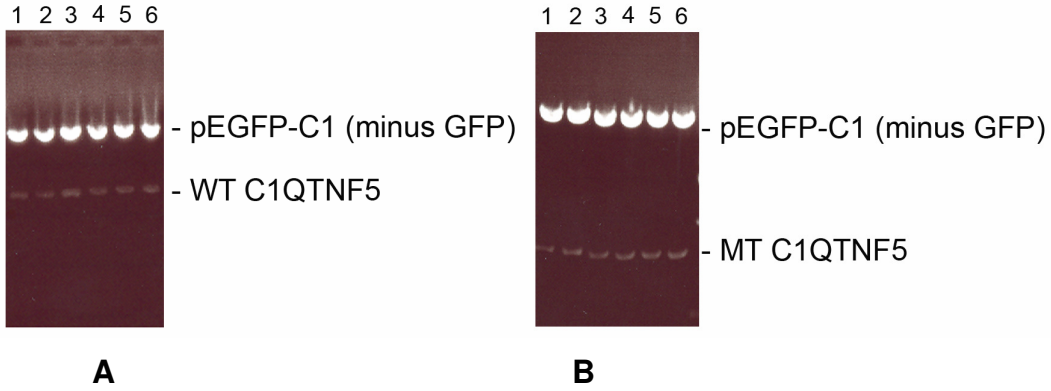

Figure 3.5: Agarose gel electrophoresis showing restriction enzyme digested pEGFP-C1 constructs (minus EGFP) checking for the presence of wild-type (WT) C1QTNF5 (A) or mutant (MT) C1QTNF5 (B) inserts

C1QTNF5 are seen as bands of approximately 750bp.

3.2.2 Checking expression of His-C1QTNF5 in ARPE-1 cells using pEGFP-C1-C1QTNF5

Before commencing with creation of the stably transfected ARPE-19 cell lines, it was necessary to ascertain that His-C1QTNF5 was expressed when the selected constructs were transiently transfected into ARPE-19. Transfection was carried out using FuGENE, and His-C1QTNF5 expression confirmed by immunostaining. Figure 3.6 shows ARPE-19 cells expressing either wild-type or mutant His-C1QTNF5, as well as untransfected ARPE-19 cells.

3.2.3 Stable cell line creation and screening

As His-C1QTNF5 was expressed when ARPE-19 were transiently transfected with the pEGFP-C1-C1QTNF5 constructs, these were deemed suitable for use in creation of the stably transfected ARPE-19 cell lines.

3.2.3.1 Determination of correct G418 concentration

G418 is an aminoglycoside antibiotic which blocks peptide elongation during translation and so polypeptide synthesis in prokaryotic and eukaryotic cells. pEGFP-C1 contains the G418/neomycin selectable marker, conferring G418 resistance to transfected cells. In order to select for transfected cells, it was necessary to determine the minimum concentration of G418 required for toxicity to ARPE-19 cells.

ARPE-19 cells were cultured for 2 weeks in 0 – 700µg/ml G418, after which time the G418 was removed and, following a further week's incubation, it was determined if any live cells remained. Table 3.1 shows the results obtained. 500µg/ml was the minimum concentration required to kill ARPE-19 cells. Toxicity was determined by the absence of live cells following culture.

Table 3-1: G418 concentration requirement in media to kill cultured ARPE-19 cells.

G418 µg/ml	0	300	400	500	600	700
Live cells	Yes	Yes	Yes	No	No	No

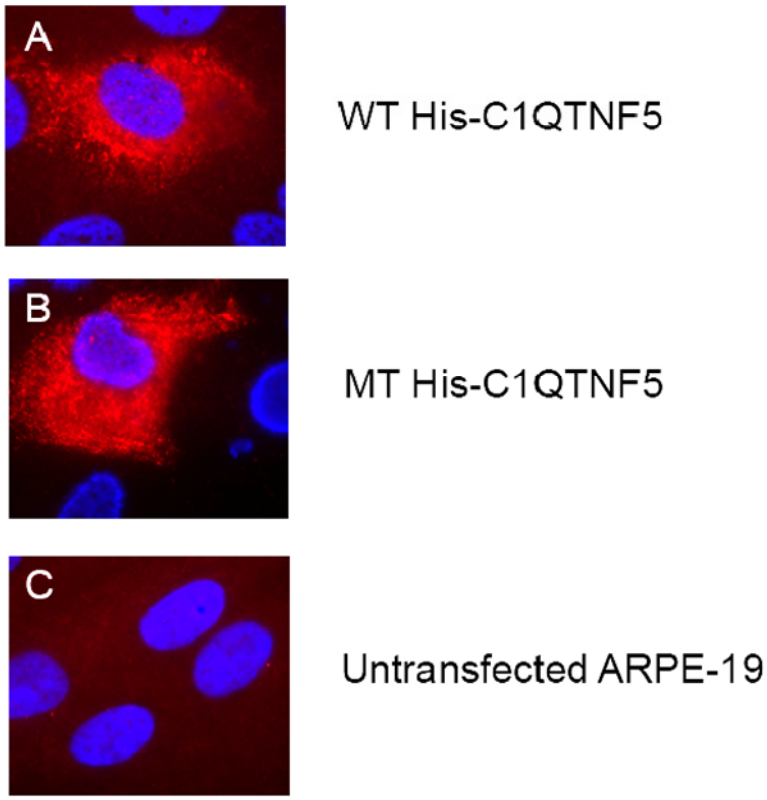

Figure 3.6: Immunostaining of ARPE-19 cells transiently transfected with the wild-type (WT) (A) and mutant (MT) (B) pEGFP-C1-C1QTNF5 constructs showing expression of His-tagged protein.

His-tagged protein is shown in red. Primary antibody: mouse anti-His, secondary antibody: rabbit anti-mouse TxRed. DAPI-stained nuclei are shown in blue.

3.2.3.2 Transfecting and screening of ARPE-19 colonies

Transfections were carried out using the microporator rather than FuGENE as this has been optimised for ARPE-19 transfection and shown previously in this lab to have greater transfection efficiency than FuGENE. Even so, it should be noted that in this instance transfection levels were not high and screening did not reveal many suitable cell lines. Individual clones were amplified and samples of cell lysate screened for His-C1QTNF5 expression by Western blot.

Individual clones were amplified into 25cm^2 flasks in culture media containing 10% serum, with the entire cell pellet used to screen for His-C1QTNF5. This was due to low His-C1QTNF5 expression levels requiring a greater cell mass for detection. Figure 3.7 shows a Western blot for 8 screened cell pellets corresponding to 8 separate clones. The band at approximately 28kDa in lane 2 is His-C1QTNF5, indicating that this particular cell line is expressing the recombinant protein.
In total, 18 wild-type and 15 mutant cell lines were screened. Only 2 wild-type (GFWT19 and GFWT29) and 2 mutant (GFMT4 and GFMT22) cell lines were found to be expressing His-C1QTNF5.

3.2.3.3 Checking for His-C1QTNF5 secretion in selected cell lines

Previous studies had indicated that wild-type but not mutant C1QTNF5 was secreted, and that the mutant protein was retained within the cell. TCA precipitated proteins from the culture media of the 2 wild-type and 2 mutant His-C1QTNF5 expressing cell lines were analysed by Western blot for the presence of His-C1QTNF5. As can be seen from Figure 3.8, His-C1QTNF5 was found to be present in the culture media of all four cell lines, indicating that both the wild-type and mutant proteins are secreted.

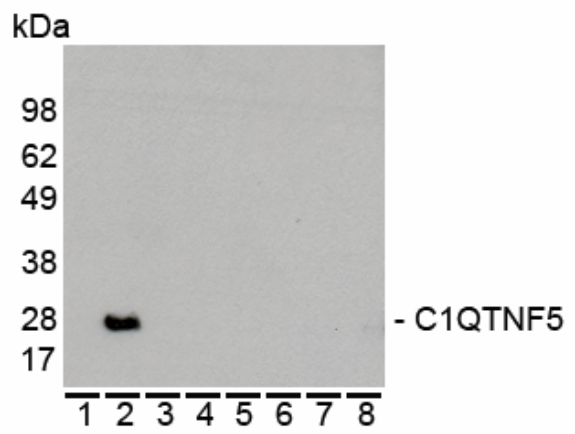

Figure 3.7: Western blot of cell lysates from selected ARPE-19 transfections, screening for His-C1QTNF5.

In the above figure, lanes 1-8 represent individual cell lines. The band at approximately 28kDa in lane 2 is His- C1QTNF5. This cell line was selected as showing His-C1QTNF5 expression. Primary antibody: mouse anti-His; secondary antibody: HRP labelled rabbit anti-mouse. kDa: relative molecular mass.

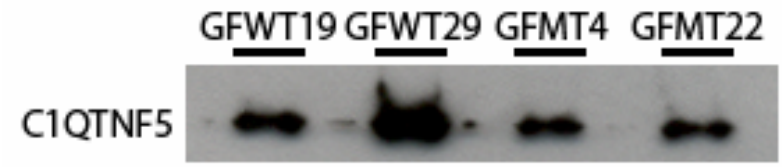

Figure 3.8: Western blot of TCA precipitated media proteins from culture media of stably transfected ARPE-19 cell lines expressing wild-type His-C1QTNF5 (GFWT19 and GFWT29) or mutant His-C1QTNF5 (GFMT4 andGFMT22).

Bands correspond to His-C1QTNF5. Primary antibody: mouse anti-His; secondary antibody: HRP-labelled rabbit anti-mouse.

3.3 Checking secretion levels

Figure 3.8 indicates that wild type and mutant His-C1QTNF5 are secreted in the stably transfected ARPE-19 cell lines. It had previously been observed (Shu *et al.* 2006b; Mandal *et al.* 2006c) that wild-type C1QTNF5 but not the mutant is secreted in EBNA293 cells. However, these studies were either carried out in less physiologically relevant cell lines (Mandal *et al.* 2006c) and/or the C1QTNF5 recombinant protein had a large GFP tag (Shu *et al.* 2006b)

Before investigating this observation further, it was necessary to determine that the wild type (GFWT19) and mutant (GFMT22) cell lines to be used in future experiments are secreting His-C1QTNF5 at similar levels. Post-confluent cells were cultured for 5 days in serum-free media, with cell pellets and culture media collected for analysis. After adjusting lysate and culture media volumes for cell number, His-tagged protein was affinity purified using Ni-NTA beads. Due to the low levels of His-C1QTNF5 produced this was considered to be a highly sensitive method of protein detection suitable for accurate comparisons. Figure 3.9 shows a Western blot of the culture media eluates, with similar intensities observed for the His-C1QTNF5 bands at approximately 28kDa, corresponding to GFWT19 and GFMT22 respectively. This indicates that these cell lines are secreting His-C1QTNF5 to similar levels. However, His-C1QTNF5 was not observed in the cell lysate sample eluates for either GFWT19 or GFMT22, even when using ECL^{+} for detection, indicating that not enough protein was retained within the cells of either cell line to allow detection by Western blot, under these conditions.

3.3.1 His-C1QTNF5 secretion time course

As the previous experiment was carried out over 5 days, a secretion time course was carried out to determine if any differences in levels of secretion between the cell lines could be observed over shorter time periods. Media samples were taken at specified time intervals and, after normalising for cell number as before, analysed by Western blot for His-C1QTNF5 (see Figure 3.10). Both cell lines showed His-C1QTNF5 secretion after 1, 2 and 3 days. Expression levels were similar, although

slightly higher in GFWT19. This was not considered great enough to prevent future comparisons being made between the two cell lines.

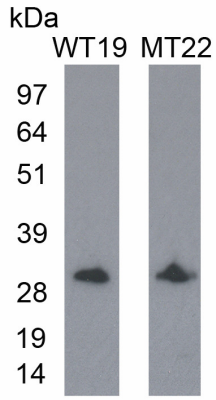

Figure 3.9: Western blot of Ni-NTA affinity purified culture media proteins from cell lines GFWT19 and GFMT22.

Culture media volumes were adjusted for cell number prior to purification. Both cell lines show similar expression levels of His-C1QTNF5, indicated by bands at approximately 28kDa. Primary antibody: mouse anti-His, secondary antibody: HRP-labelled rabbit anti-mouse. kDa: relative molecular mass

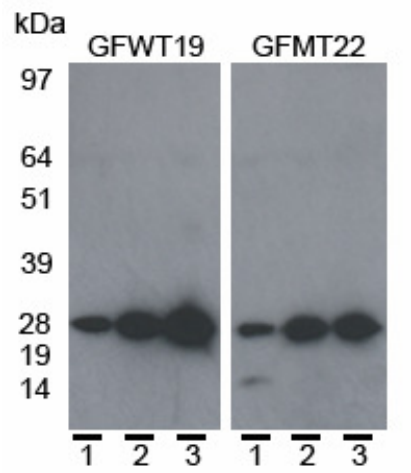

Figure 3.10: Western blot of Ni-NTA affinity purified culture media proteins from cell lines GFWT19 and GFMT22.

Samples were taken 1, 2 and 3 days post-confluence in serum free media. Culture media volumes were adjusted for cell number prior to purification. GFWT19 shows slightly higher expression levels of His-C1QTNF5, indicated by bands at approximately 28kDa. Primary antibody: mouse anti-His, secondary antibody: HRP-labelled rabbit anti-mouse. kDa: relative molecular mass

3.4 Cellular trafficking of His-C1QTNF5

Previous studies investigating GFP-tagged recombinant C1QTNF5 using transiently transfected ARPE-19 cells had shown the wild-type protein to have a diffuse cellular localisation, as would be expected for a secreted protein, whereas mutant C1QTNF5 aggregated and was retained within the endoplasmic reticulum. It had also been shown that mutant GFP-tagged C1QTNF5 was not secreted when stably expressed in EBNA293 although the wild-type protein was (Shu *et al.,* 2006b). V5-tagged mutant C1QTNF5 was also not secreted when transiently over-expressed in COS7 cells (Mandal *et al.,* 2006c). However, results from Section 3.2 show that mutant and wild-type His-C1QTNF5 are secreted when stably over-expressed in ARPE-19 cells. Expression levels can differ between transiently and stably transfected cells, and the protein expressed in this instance had a His rather than the larger GFP or V5 epitope tag. Therefore it was necessary to determine whether the cellular trafficking of wild-type and mutant His-C1QTNF5 differed between cell lines GFWT19 and GFMT22.

3.4.1 Immunostaining of stably transfected ARPE-19 cell lines

Immunostaining was carried out on cell lines GFWT19 and GFMT22, which showed similar secretion levels of C1QTNF5, and untransfected ARPE-19 cells. Primary antibodies used were against the endoplasmic reticulum markers calreticulin and protein disulphide isomerase (PDI), beta-catenin and either the C-terminal His-tag or C1QTNF5. Calreticulin and PDI have both been used previously when investigating C1QTNF5 cellular trafficking (Shu *et al.* 2006b). Calreticulin binds misfolded proteins within the ER preventing their translocation to the Golgi apparatus. PDI is a chaperone which is located in the ER and catalyses the formation and breakage of disulphide bonds, facilitating the correct folding of proteins. Beta-catenin is a subunit of the cadherin protein complex and is involved in *Wnt* signalling. It is commonly observed to be associated with the plasma membrane.

3.4.1.1 Immunostaining for beta-catenin and His-C1QTNF5

Beta-catenin is located at the plasma membrane and so enables detection of cellular boundaries. Figure 3.11 shows stably transfected cell lines GFWT19 and GFMT22,

with beta-catenin immunostaining seen in green and anti-His immunostaining in red. His- C1QTNF5 shows a diffuse cytoplasmic localisation in both cell lines. No differences were observed between GFWT19 or GFMT22 cell lines.

3.4.1.2 Immunostaining for calreticulin and His-C1QTNF5

Calreticulin is localised in the ER. If a protein is aggregated and retained within the ER, it would be expected to co-localise with calreticulin. As can be seen from Figure 3.12, in both GFWT19 and GFMT22, diffuse cytoplasmic association was observed between calreticulin (green) and His-tagged C1QTNF5 (red), with no apparent aggregated protein retained within the ER. No differences were observed between GFWT19 or GFMT22 cell lines, with the same calreticulin distribution observed in untransfected ARPE-19.

3.4.1.3 Immunostaining for PDI and C1QTNF5

PDI is located within the ER. If a protein were aggregated and retained within the ER, it would be expected that this would co-localise with PDI. As can be seen from Figure 3.13, in both GFWT19 and GFMT22, a diffuse cytoplasmic localisation was observed for C1QTNF5 (green), with no apparent aggregated protein retained within the ER and limited co-localisation of C1QTNF5 and PDI (red). No differences were observed between GFWT19 or GFMT22 cell lines, with the same PDI distribution observed in untransfected ARPE-19. It should be noted that the same distribution is seen when anti-C1QTNF5 and anti-His primary antibodies are used (Figures 3.12 and 3.13).

3.4.2 Immunostaining of transiently transfected ARPE-19

Immunostaining of the stably transfected cell lines did not highlight any differences between GFWT19 and GFMT22 cell lines with respect to His-C1QTNF5 cellular trafficking, suggesting that mutant His-C1QTNF5 is not aggregated or retained within the ER. It is possible that expression levels are lower in stably transfected cells compared to transiently transfected. At higher expression levels, it is possible that an increased tendency to aggregate for either the wild-type or mutant protein may be detected. At higher expression levels, the cellular machinery and protein-

folding pathways are under greater stress, meaning that the cell may be less able to cope with misfolded proteins, which then accumulate within the ER. ARPE-19 cells were therefore transiently transfected with either the wild type or mutant C1QTNF5 pEGFP-C1 (minus *EGFP*) constructs. Immunostaining for beta-catenin and His-C1QTNF5 was carried out. Twelve images were analysed for wild-type and mutant His-C1QTNF5 expressing cells and the distributions of His-C1QTNF5 compared (Figures 3.14 and 3.15). No differences were observed between cells expressing wild-type or mutant C1QTNF5.

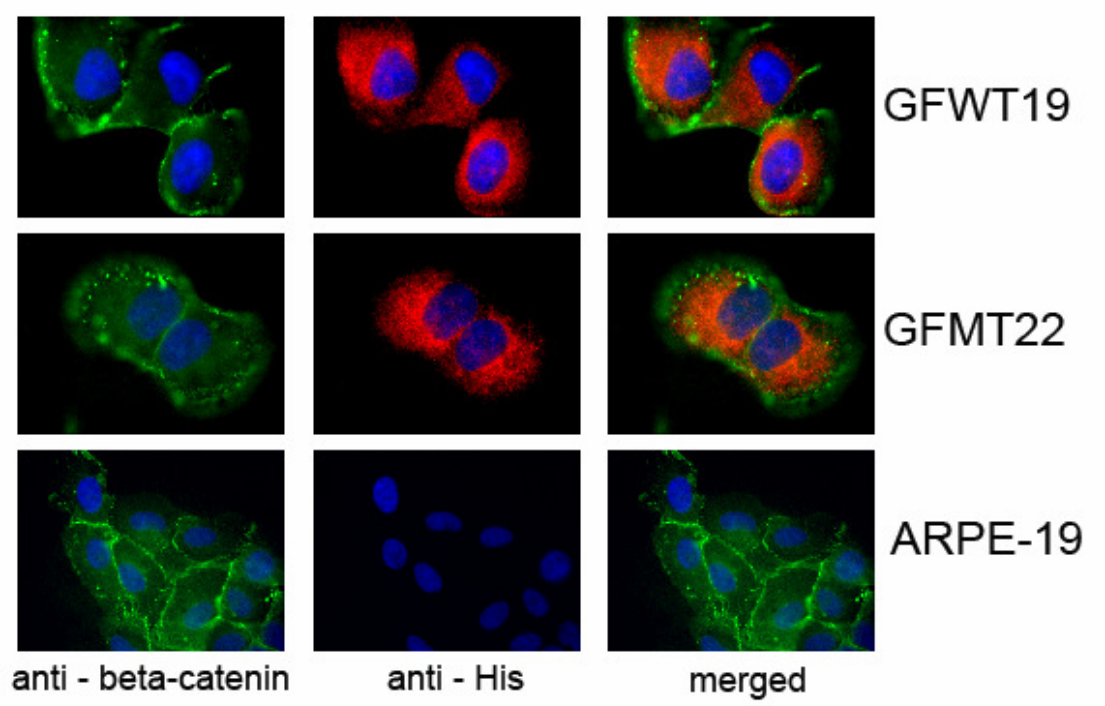

Figure 3.11: Immunostaining of cell lines GFWT19 (expressing wild-type His-C1QTNF5), GFMT22 (expressing mutant His-C1QTNF5) and untransfected ARPE-19 cells.

Anti-beta-catenin staining is seen in green. Anti-His staining, corresponding to His-C1QTNF5, is seen in red. In both GFWT19 and GFMT22 His-C1QTNF5 shows diffuse cytoplasmic localisation.

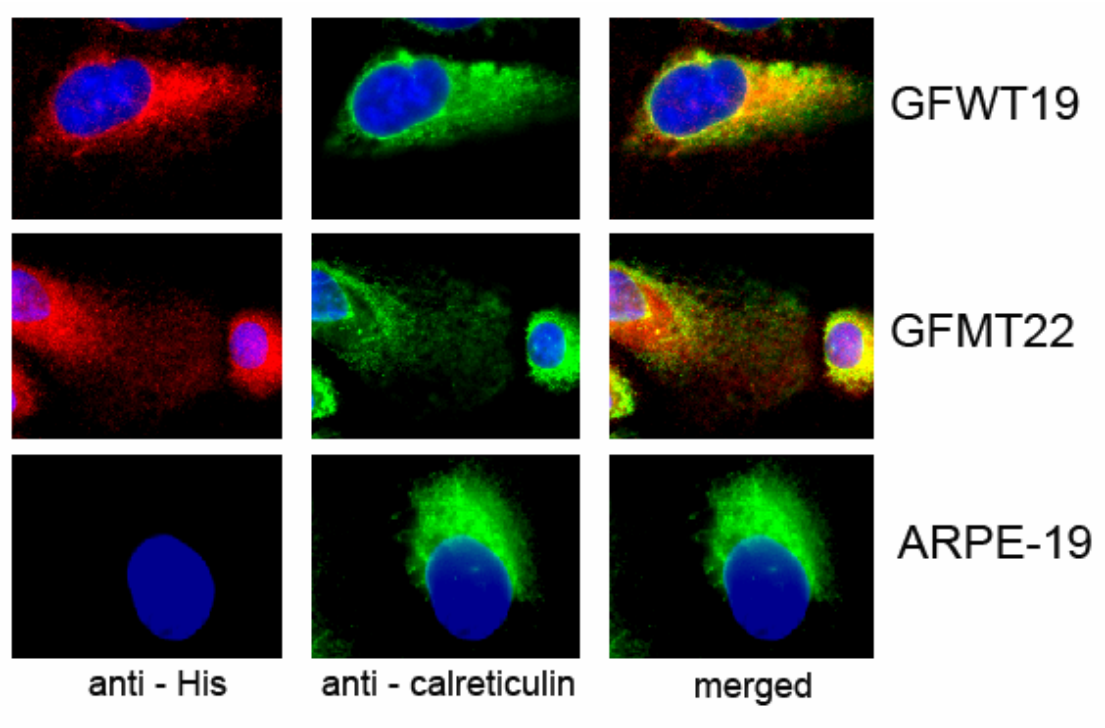

Figure 3.12: Immunostaining of cell lines GFWT19 (expressing wild-type His-C1QTNF5), GFMT22 (expressing mutant His-C1QTNF5) and untransfected ARPE-19.

Anti-calreticulin staining is seen in green. Anti-His staining, corresponding to His-C1QTNF5, is seen in red. In both GFWT19 and GFMT22 His-C1QTNF5 shows a diffuse cytoplasmic localisation. No co-localisation was observed between His-C1QTNF5 and calreticulin in either cell line.

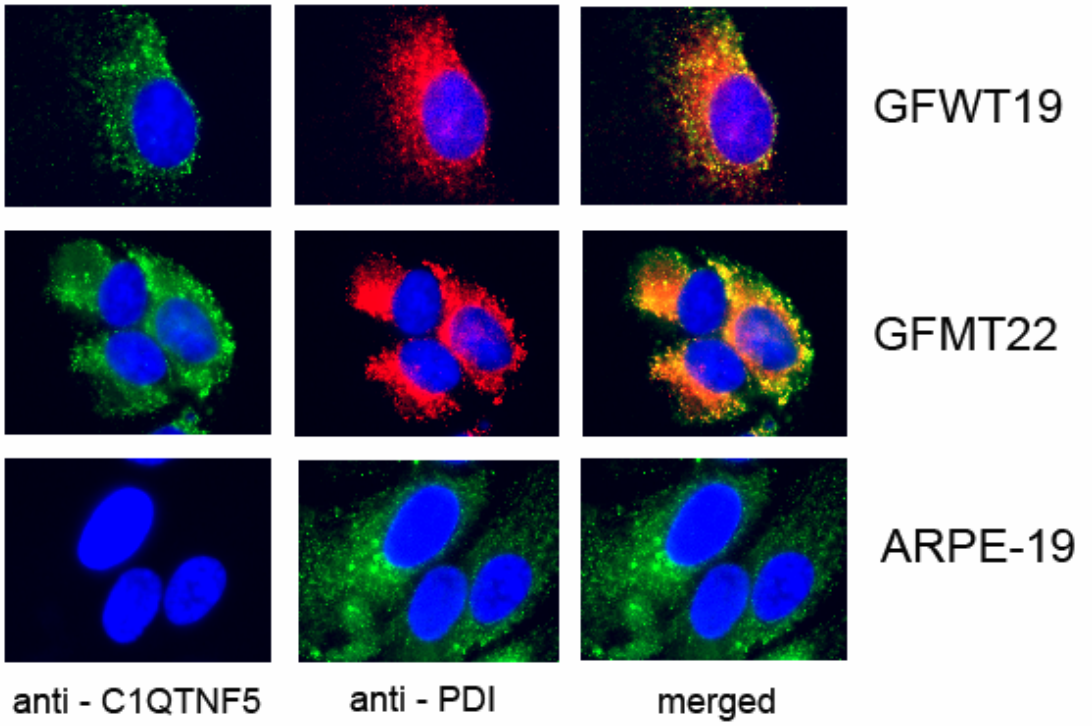

Figure 3.13: Immunostaining of cell lines GFWT19 (expressing wild-type His-C1QTNF5), GFMT22 (expressing mutant His-C1QTNF5) and untransfected ARPE-19.

Anti-PDI staining is seen in red, anti-C1QTNF5 staining is seen in green. In both GFWT19 and GFMT22 C1QTNF5 shows diffuse cytoplasmic localisation. No co-localisation was observed between C1QTNF5 and PDI in either cell line.

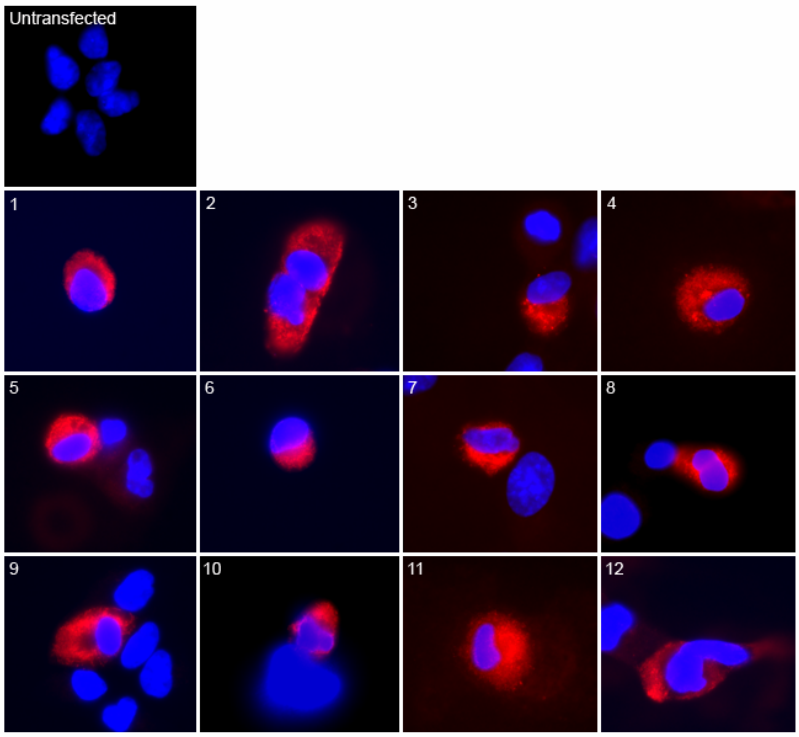
Untransfected
1
2
3
4
5
6
7
8
9
10
11
12

A

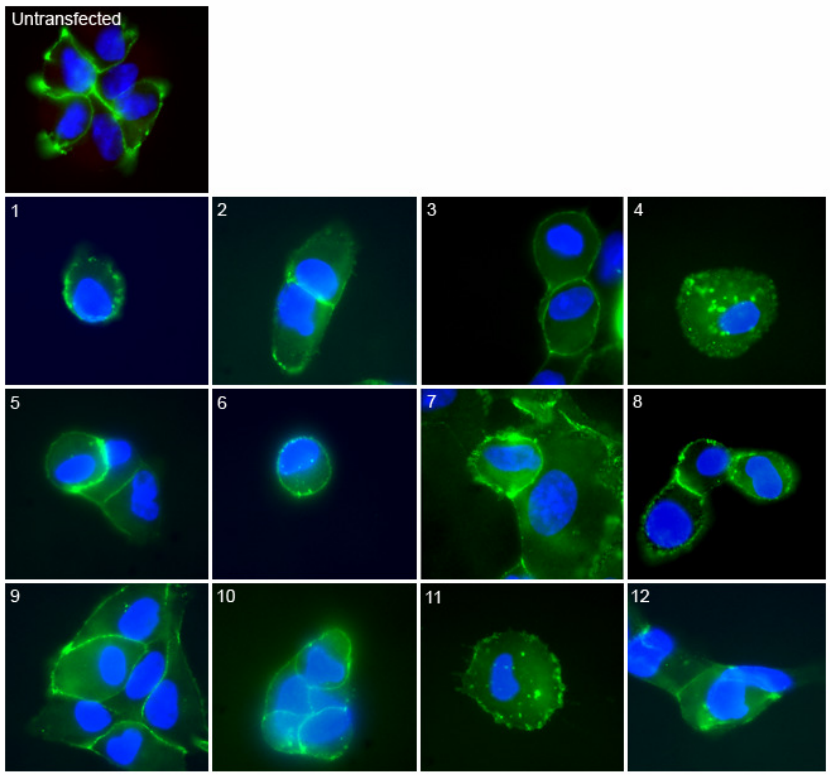
Untransfected
1
2
3
4
5
6
7
8
9
10
11
12

B

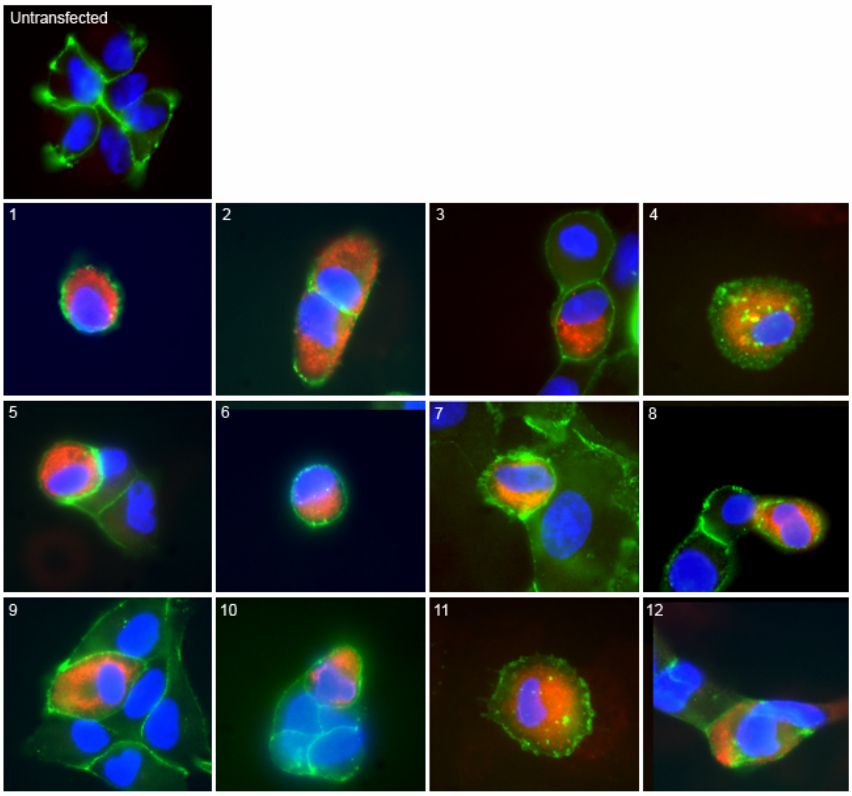

C

Figure 3.14: Immunostaining of transiently transfected ARPE-19 cells expressing wild-type His-C1QTNF5 (images 1-12) and untransfected ARPE-19.

Images were taken of different transfected ARPE-19 cells, with untransfected cells shown in box 1.
A: Nuclear staining (blue) with DAPI, anti-His immunostaining (red) showing cytoplasmic distribution of His-C1QTNF5, B: Anti-beta-catenin (green) showing cellular boundaries, C: Merged anti-His and anti-beta-catenin showing showing cellular boundaries and cytoplasmic distribution of His-C1QTNF5.

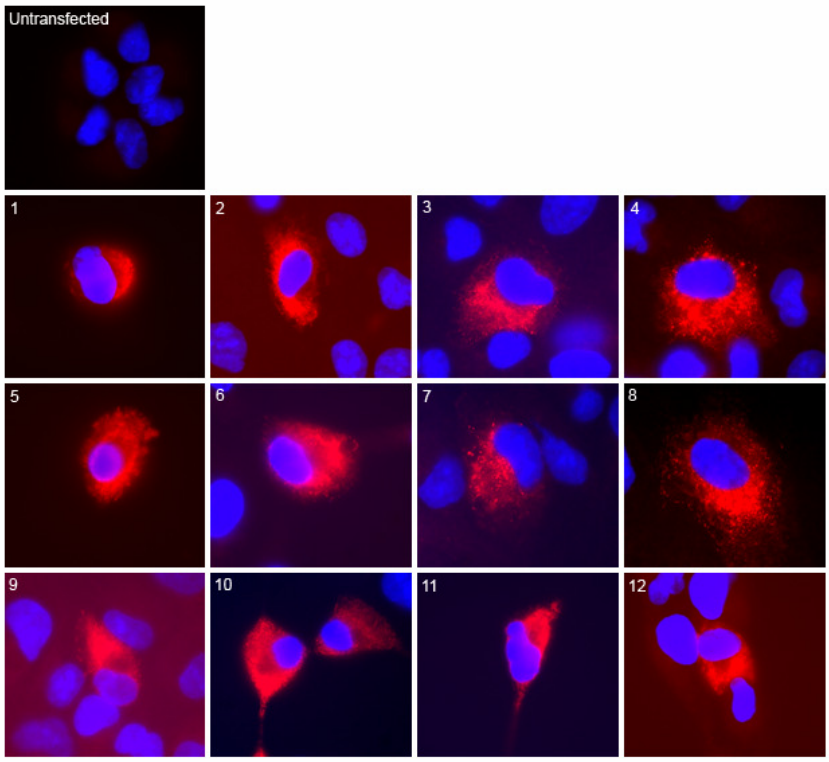
Untransfected
1
2
3
4
5
6
7
8
9
10
11
12

A

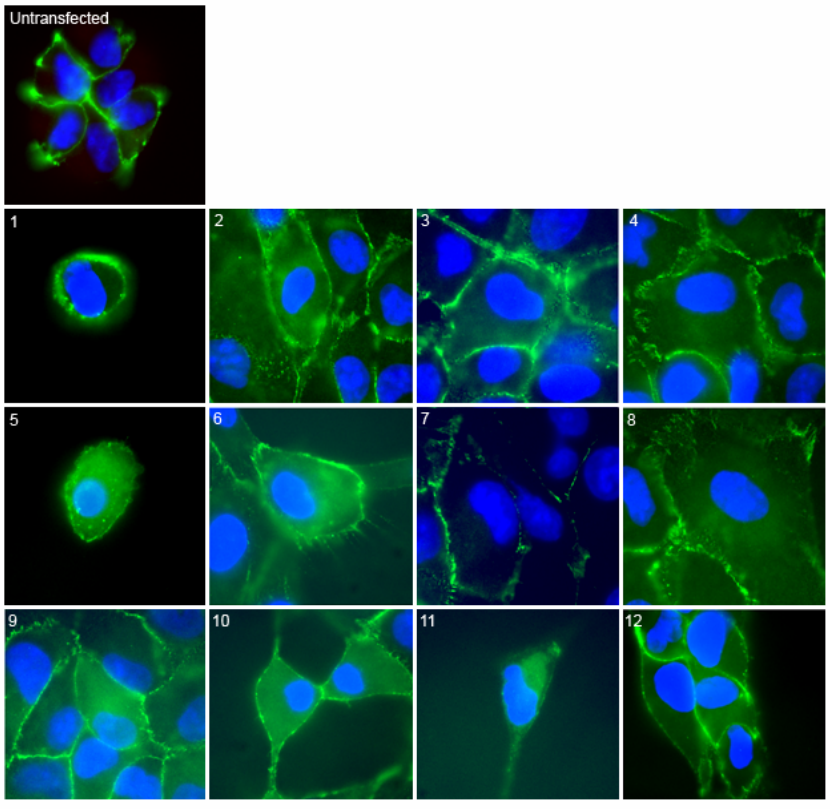
Untransfected
1
2
3
4
5
6
7
8
9
10
11
12

B

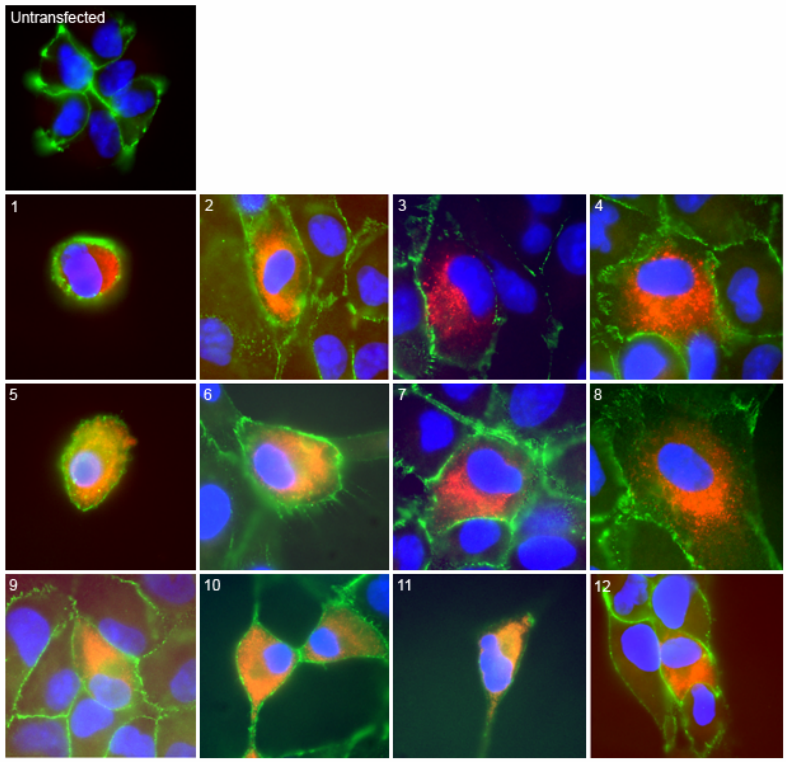

C

Figure 3.15: Immunostaining of transiently transfected ARPE-19 cells expressing mutant His-C1QTNF5 (images 1-12) and untransfected ARPE-19.

Images were taken of different transfected ARPE-19 cells, with untransfected cells shown in box 1.
A: Nuclear staining (blue) with DAPI, anti-His immunostaining (red) showing cytoplasmic distribution of His-C1QTNF5, B: Anti-beta-catenin (green) showing cellular boundaries, C: Merged anti-His and anti-beta catenin showing cellular boundaries and cytoplasmic distribution of His-C1QTNF5.

3.5 Checking apoptosis levels

It is possible that over-expression of mutant His-C1QTNF5 may reduce cell viability and so increase levels of apoptosis, and this could release His-C1QTNF5 into the medium, perhaps accounting for at least part of the His-C1QTNF5 detected in the culture media of GFMT22 cells. After confirming that apoptotic ARPE-19 cells could be detected using the TUNEL assay, levels of apoptosis were compared between untransfected ARPE-19, GFWT19 and GFMT22.

3.5.1 The TUNEL assay

The TdT-mediated dUTP nick-end labelling (TUNEL) assay allows for the detection of single apoptotic cells within a larger cell population. Cells undergoing apoptosis generate fragments of DNA 180-200 base pairs in length (Bortner *et al.,* 1995). The TUNEL assay fluorescently labels the 3' OH ends of such DNA strands. The DeadEnd™ Fluorometric TUNEL System (Promega) used in this study labels these 3' OH ends with fluorescein-12-dUTP using recombinant terminal deoxynucleotide transferase, (rTDT), allowing for their detection by fluorescence microscopy or flow cytometry.

3.5.2 Inducing and detecting apoptosis in ARPE-19 cells

Hydrogen peroxide has been shown to induce apoptosis in cultured human retinal pigment epithelial cells (Jin, 2001). Cultured ARPE-19 cells were treated with hydrogen peroxide, and then apoptotic cells detected using the TUNEL assay described above. Figure 3.16 shows hydrogen peroxide treated ARPE-19 cells, positive and negative control cells. Apoptotic cells are shown in green. The results indicate that it is possible to detect apoptotic cells in confluent ARPE-19 using this method.

3.5.3 Detecting apoptosis levels in the ARPE-19 transfected cell lines

Apoptosis levels of confluent cells were measured after 1, 2 or 3 days post-confluence in serum-free media using the TUNEL assay. Five images were taken at each time point for ARPE-19, GFWT19 or GFMT22 cultures at 10X magnification and the number of apoptotic cells in each image scored. As can be seen from Table

3.2, there were no differences in the levels of apoptosis between the cell lines, and apoptosis levels were negligible in all cases.

	Number of apoptotic cells		
Day	**ARPE-19**	**GFWT19**	**GFMUT22**
1	0	0	0
2	0	1	1
3	2	1	2

Table 3-2: Total number of apoptotic cells in 5 images of confluent cell lines ARPE-19, GFWT19 and GFMT22 after 1, 2 or 3 days post-confluence in serum-free media.
Levels of apoptosis were negligible in all cases.

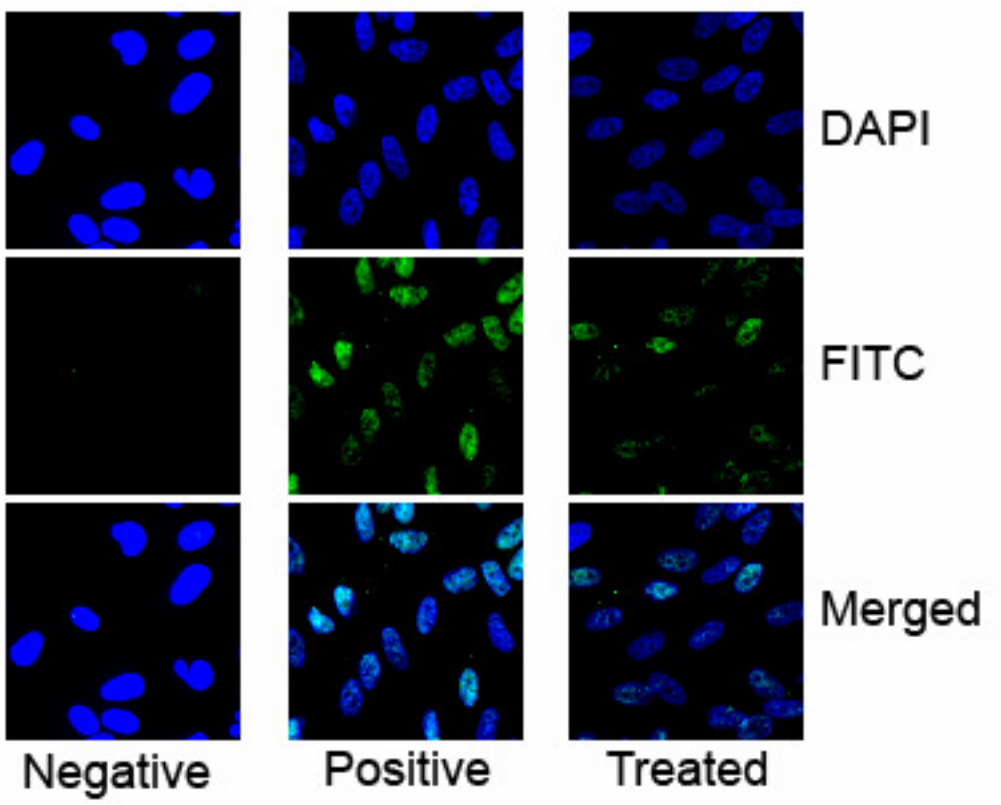

Figure 3.16: TUNEL assay staining of ARPE-19 cells.

Nuclei (DAPI staining) are shown in blue. Apoptotic nuclei are shown in green. Images are for negative control cells (negative), positive control cells (positive) and cells where apoptosis has been induced with hydrogen peroxide (treated). The images show that it is possible to detect apoptotic ARPE-19 cells using the TUNEL assay.

3.6 Cell adhesion assays

A previous study suggested that C1QTNF5 might be involved in RPE cell adhesion, in particular to Bruch's membrane (Shu *et al.,* 2006b). The study had been carried out using stably transfected EBNA293 cell lines expressing GFP-tagged wild type or mutant C1QTNF5, with the mutant cell line showing reduced adhesion to laminin- but not fibronectin-coated microtitre plates.

Laminin and fibronectin are extracellular matrix proteins. Laminin consists of α, β and γ chains which create a framework that interacts with collagens, other ECM components and cell surface receptors such as integrins and some proteoglycans. Laminin provides a structural extracellular framework and, through its interactions with cell surface receptors, can influence signal transduction, migration and focal adhesion (Alberts *et al.,* 2002, Miner, 2008). Fibronectin is a dimer consisting of two polypeptide chains, and can be found in various isoforms as a result of alternative splicing. Each polypeptide chain contains several domains involved in collagen-binding, cell attachment (via the RGD motif and cell surface integrins), heparin binding and interactions with cell surface receptors. Fibronectin provides a structural framework for cell attachment and spreading, and also has roles in signal transduction (Alberts *et al.,* 2002).

C1QTNF5 shares homology with other collagens such as collagen IV, which has a globular head group and has been shown to form a polygonal lattice, providing a basement membrane framework (Yurchenco, 1987), and collagen X, which forms a hexagonal lattice and has been shown to be involved in cell adhesion via the α2β1 integrin, amongst others (Kwan *et al.,* 1991, Luckman *et al.,* 2003). Laminin and fibronectin have also been shown to interact with collagens. It was therefore investigated whether ARPE-19 shows adhesion to C1QTNF5 or its gC1q domain, or whether ARPE-19 cells stably expressing either wild type or mutant His-C1QTNF5 would show any differences in adhesion to laminin- or fibronectin-coated plates, which might suggest that C1QTNF5 is involved in cell-extracellular matrix interactions and adhesion.

3.6.1 Optimising the assay

It was necessary to optimise the cell adhesion assay since initial results obtained following the described assay of Shu *et al.* (2006b) were variable. Several studies have been carried out using cell adhesion assays to test cell adhesion to extracellular matrices (Qi *et al.,* 2002, Luckman *et al.,* 2003, Humphries *et al.,* 2001, Bax *et al.,* 2003). Stages from these assays were investigated and combined to obtain a repeatable method for determination of cell adhesion to use with the stably transfected ARPE-19 cell lines. The stages involved in the cell adhesion assay included coating the plate, blocking non-specific binding sites, addition and incubation of cells, washing, fixing and detection of adherant cells. The stages optimised in the method were blocking the plate, determination of correct cell number, washing and fixing.

3.6.1.1 Blocking the plate

Following coating of the microtitre plate with the desired extracellular matrix, it was necessary to block the plate to prevent non-specific cell adhesion. Blocking solutions used previously include 3% BSA in PBS (Qi *et al.,* 2002) and 10mg/ml heat denatured BSA in PBS (Bax *et al.,* 2003, Luckman *et al.,* 2003, Humphries, 2001). These two blocking solutions were investigated, using high (98%) and low (96%) grade BSA, as well as 5% skimmed milk in PBS.

As can be seen from Figure 3.17, heat-inactivated 10mg/ml low grade BSA in PBS was effective in preventing ARPE-19 adhering to the plate. This blocking solution was used in all future assays.

3.6.1.2 Determination of correct cell number and washes

Whilst it is necessary to use a high enough cell concentration in the assay to enable comparisons to be made between levels of cell adhesion, too high a cell concentration may affect the reliability of results. In addition, whilst it is necessary to remove non-adherant cells from the wells following incubation, care has to be taken so that loosely adherant cells are not removed as well. Comparisons were

made between different cell concentrations and the number of washes to determine which combination produced the most reliable results.

Previous studies have used cell concentrations of $5x10^4$ cells/ml (Luckman *et al.,* 2003),$1x10^5$ cells/ml (Qi 2002) and $5x10^5$ cells/ml (Humphries, 2001, Bax *et al.,* 2003). This study chose to investigate concentrations of $2.5x10^5$, $5.0x10^5$, $7.5x10^5$ and $1.0x10^6$ cells/ml, and 1, 2 or 3 washes of 200µl per well PBS. Figure 3.18 shows the results obtained. A cell concentration of $5x10^5$ cells/ml and 2 washes was chosen for use in all future assays.

3.6.1.3 Investigating different fixatives

It is possible that the variable results obtained when following the previously described assay were caused by removal of adherant cells during the detection phase of the assay, where cells are stained with crystal violet and wells are washed repeatedly to remove excess stain. In order to prevent this from happening, adherant cells can be fixed to the wells. 5% (w/v) glutaraldehyde has been described as a suitable fixative for use in cell adhesion assays (Bax *et al.,* 2003, Humphries, 2001), and ice-cold methanol has been used as a fixative when carrying out immunostaining (section 3.1.2). These two fixatives were compared and the most reproducible were results obtained when 5% (w/v) glutaraldehyde was used (Figure 3.19). This fixative was chosen for use in future assays.

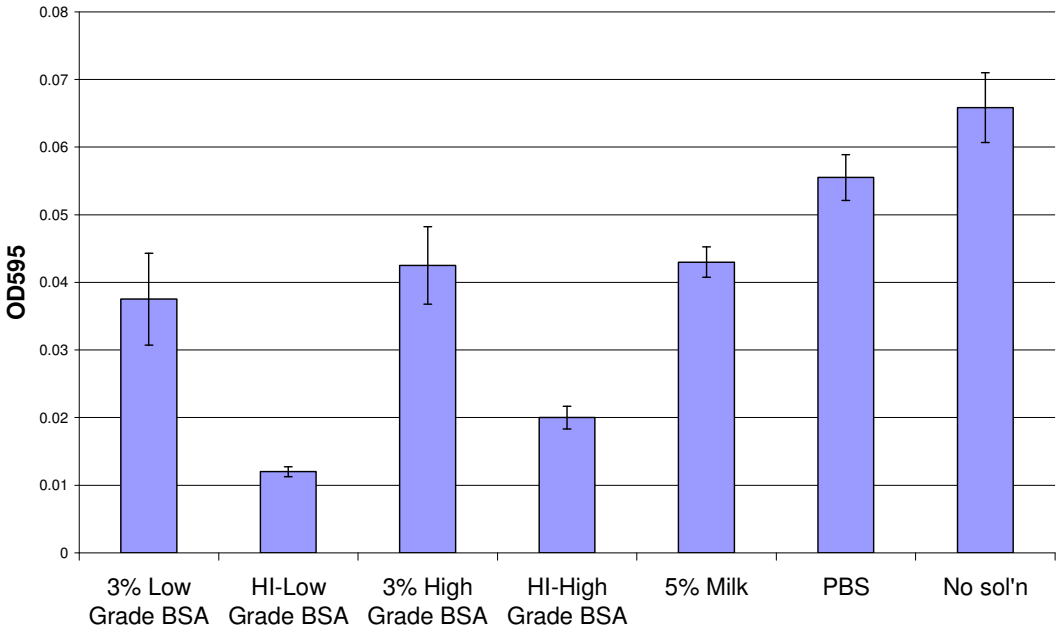

Figure 3.17: Bar chart showing the effectiveness of different blocking solutions to prevent ARPE-19 cells from adhering to 96 well microtitre plates.

OD_{595} corresponds to the degree of cell adhesion. 10mg/ml heat-inactivated low grade BSA in PBS (HI-Low Grade BSA) was most effective at inhibiting cell adhesion.

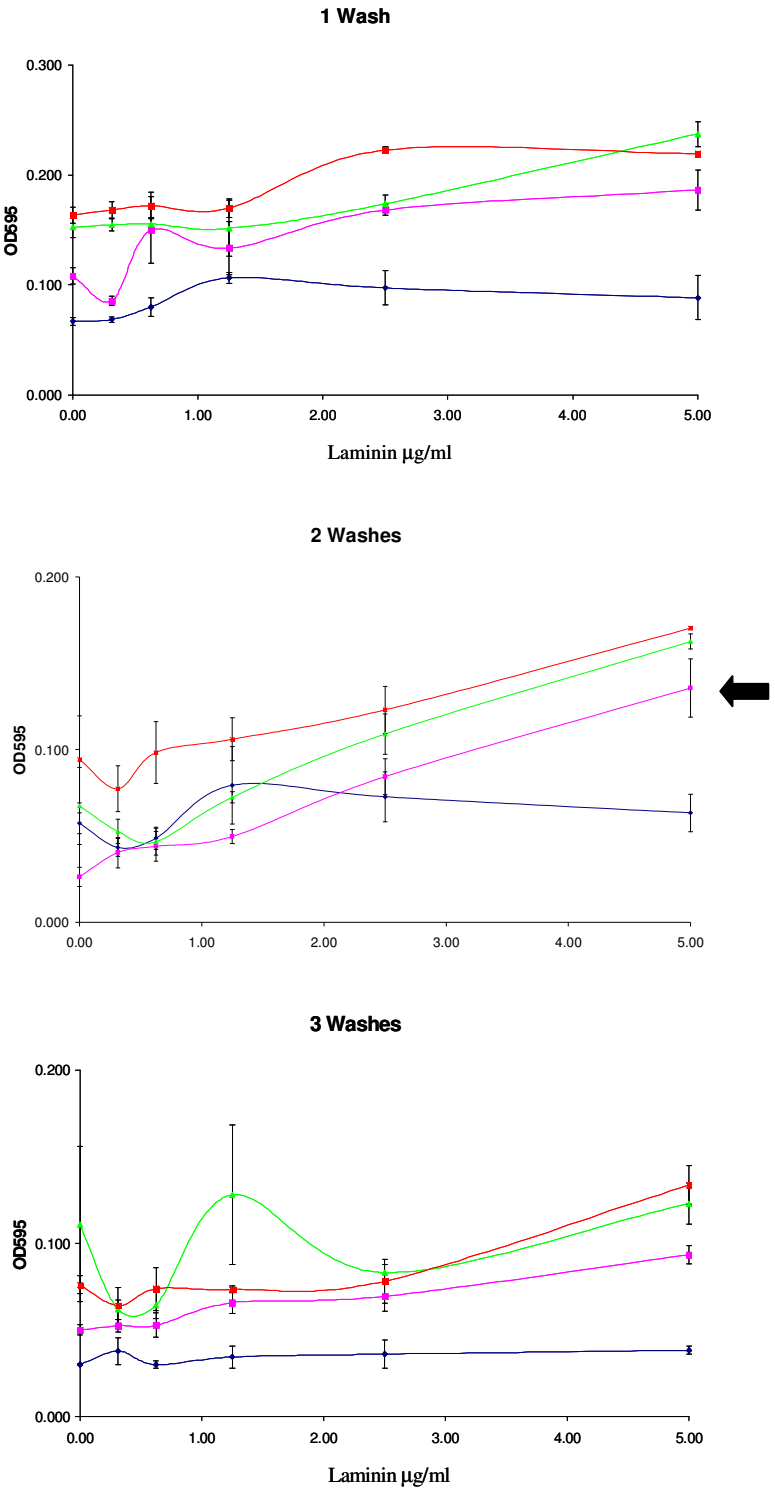

Figure 3.18: ARPE-19 cells adhesion to increasing concentrations of laminin.

Different cell concentrations and number of washes were investigated to obtain the most reproducible results. The optimal conditions were $5.0x10^5$ cell/ml and 2 washes, indicated by an arrow. Blue: $2.5x10^5$ cell/ml; pink: $5.0x10^5$ cell/ml; green: $7.5x10^5$ cell/ml; red: $10.0x10^5$ cell/ml

3.6.2 Cell adhesion assays

The optimised cell adhesion assay was used to investigate ARPE-19 adhesion to C1QTNF5 and its gC1q domain. Adhesion of the stably transfected cell lines GFWT19 and GFMT22 to either laminin- or fibronectin-coated plates was also investigated.

3.6.2.1 ARPE-19 adhesion to C1QTNF5 and gC1q

It was investigated whether ARPE-19 would adhere to C1QTNF5- or gC1q-coated microtitre plates. Laminin was used as a positive control. As can be seen from Figure 3.20, ARPE-19 cells adhered to laminin in a dose-dependant manner. However, no adhesion of ARPE-19 cells was observed to C1QTNF5, gC1q or BSA.

3.6.2.2 Adhesion to laminin-coated plates

Using the optimised cell adhesion assay, adhesion of ARPE-19, GFWT19 and GFMT22 cells to laminin-coated plates was investigated over increasing time periods. This was to determine if there was any difference in both total adhesion and rate of adhesion between the cell lines. Figure 3.21 shows the results obtained. No differences were observed between the cell lines for each of the incubation times.

3.6.2.3 Adhesion to fibronectin-coated plates

Using the optimised cell adhesion assay, adhesion of ARPE-19, GFWT19 and GFMT22 to fibronectin-coated plates was investigated over increasing time periods. Figure 3.22 shows the results obtained, with OD_{595} being indicative of the total cell number. No differences were observed between the cell lines for each of the incubation times.

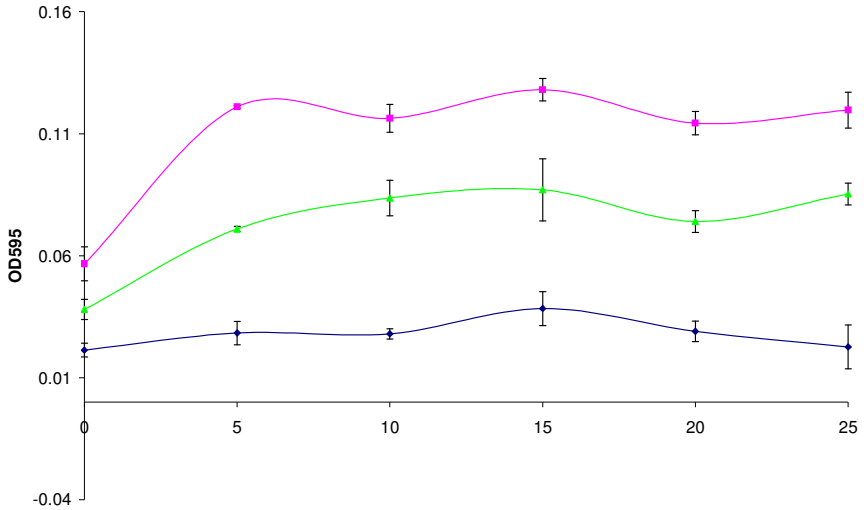

Figure 3.19: The effects of different fixatives on the total number of adherant cells.

5% (w/v) glutaraldehyde gave the least reduction in adherant cells. Pink – 5% (w/v) glutaraldehyde, Green – methanol, Blue – no fixative

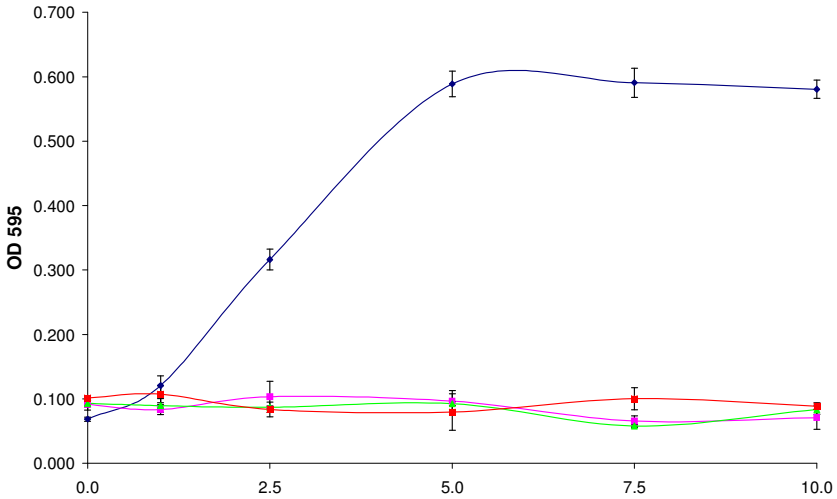

Figure 3.20: Adhesion of ARPE-19 cells to increasing concentrations of different extracellular matrices.

No adhesion was observed to C1QTNF5 (pink), gC1q (green) or BSA (red). A dose-dependant adhesion to laminin was observed (blue), with adhesion levels increasing up to 5µg/ml laminin.

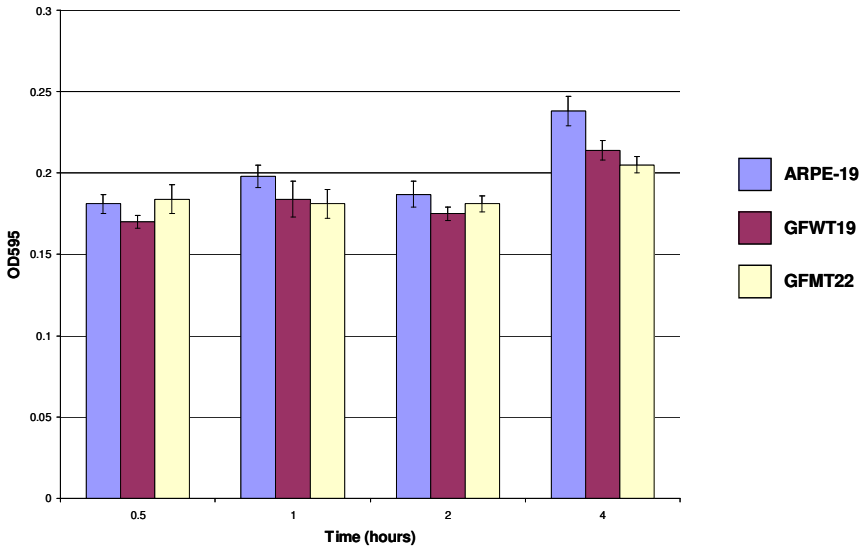

Figure 3.21: Adhesion of ARPE-19, GFWT19 and GFMT22 to laminin-coated microtitre plates using varying incubation times.

No differences were observed in levels of adhesion between the cell lines at any of the incubation times.

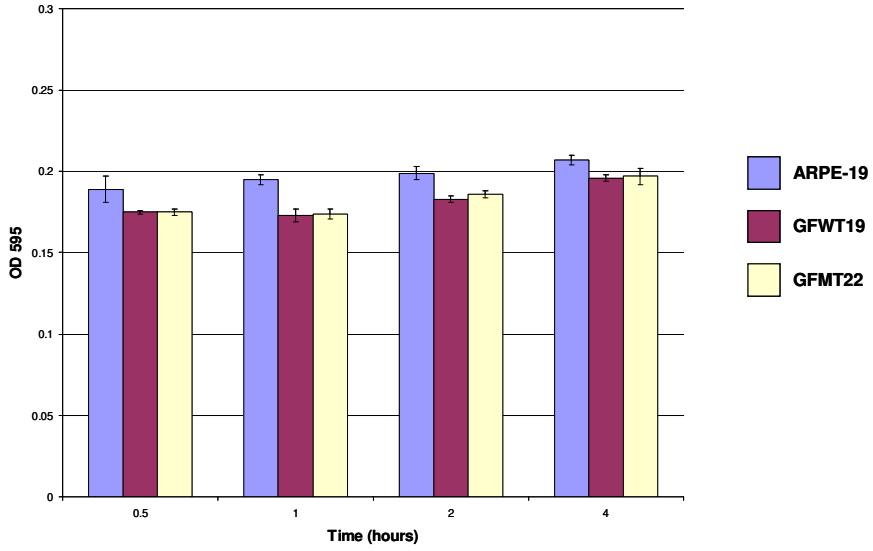

Figure 3.22: Adhesion of ARPE-19, GFWT19 and GFMT22 to fibronectin-coated microtitre plates using varying incubation times.

No differences were observed in levels of adhesion between the cell lines at any of the incubation times.

3.7 Cell spreading

It was also investigated whether there are differences in cell spreading between the ARPE-19 cell lines. Cell-ECM contacts are not only required for adhesion but also affect cell morphology, polarity and viability. Cell spreading involves cytoskeletal re-organisation and the formation of focal contacts, so that differences in ability to spread can be indicative of a cell's ability to change its morphology, to become polarised and to interact with its environment (Hynes, 1999). It was therefore investigated whether any differences in cell spreading could be observed between the cell lines.

3.7.1 Cell spreading assays

Cell spreading of ARPE-19 has previously been investigated, using fibronectin-coated plates (Elib *et al.*, 2005). The method was adapted for use in this study using laminin-coated plates. Figure 3.23 shows spread and non-spread cells. Non-spread cells retain a rounded morphology (indicated by the black arrow) whereas spread cells show a cytoplasmic halo and can have cellular projections (white arrow).

3.7.1.1 Cell spreading on laminin

Cell lines ARPE-19, GFWT19 and GFMT22 were allowed to spread on laminin-coated 96-well microtitre plates for 2 hours, after which time the number of spread cells was determined. Figure 3.24 shows images of the three cell lines after two hours incubation and spreading on laminin. Spread cells can be seen for both ARPE-19 and GFWT19, which in some cases have produced cellular projections, whereas GFMT22 remain spherical and shows little spreading. Two hundred cells were counted for each and scored as either spread or non-spread and with or without cellular projections. The assay was repeated three times and the results pooled. As can be seen from Figure 3.25, GFMT22 showed a significant reduction in cell spreading on laminin coated plates, χ^2 (2-sided, N = 200) = 21.7, $p < 0.001$, and GFWT19 showed a significant increase in cellular projections, χ^2 (2, N = 200) = 43.8, $p < 0.001$.

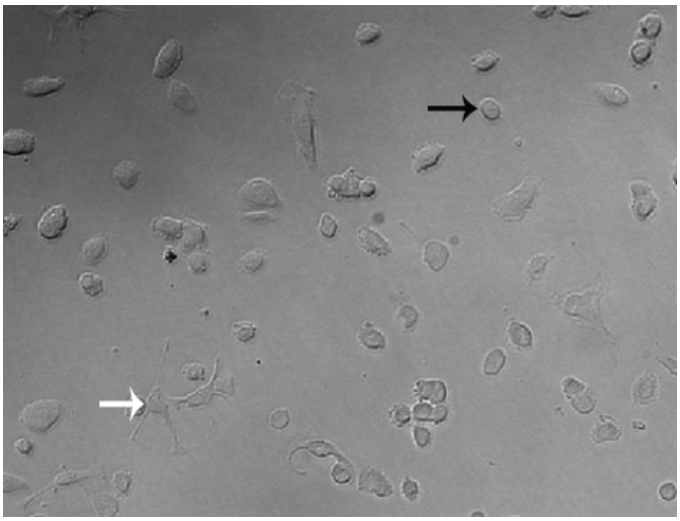

Figure 3.23: ARPE-19 cells spread on laminin.

White arrow indicates a spread cell with cellular projections.
Black arrow indicates a non-spread cell.

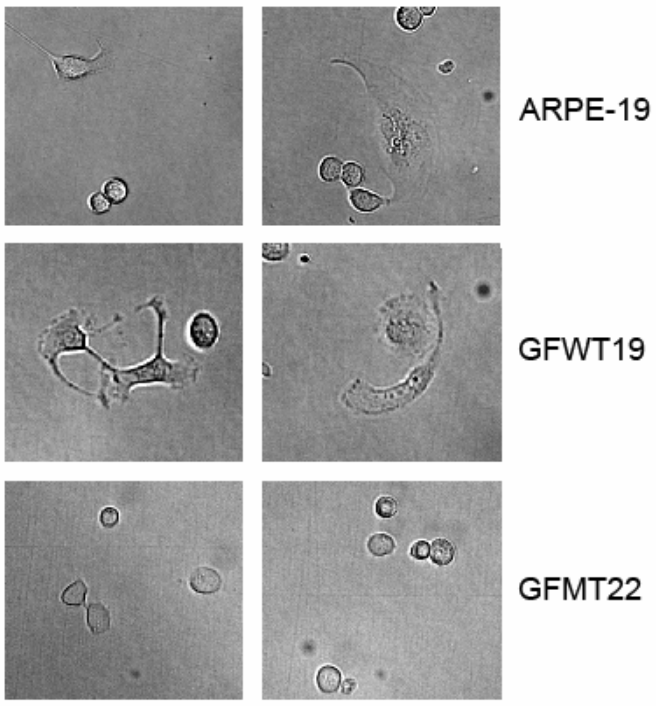

Figure 3.24: 20x magnification of cell lines ARPE-19, GFWT19 and GFMT22 spread on laminin.

ARPE-19 and GFWT19 can be seen as spread cells, whereas GFMT22 remains spherical and shows minimal spreading. GFWT19 also shows increased cellular projections.

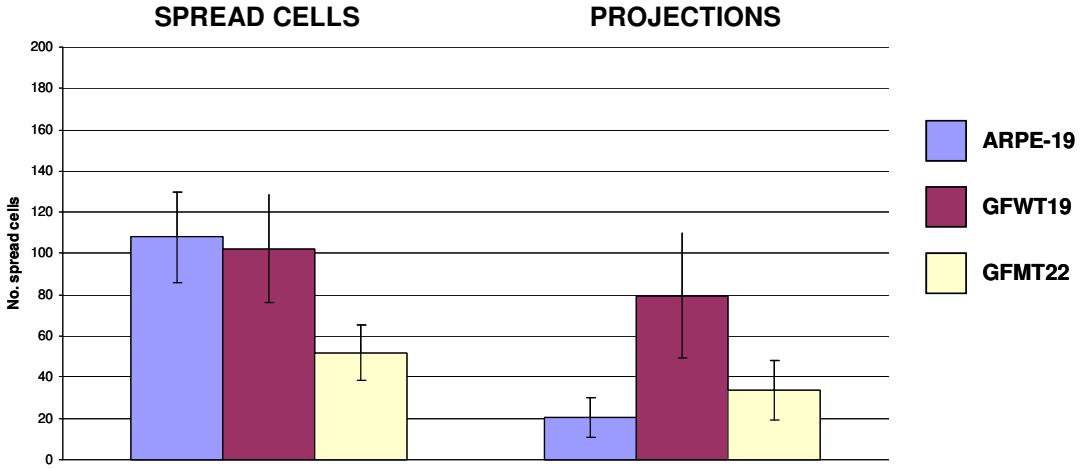

Figure 3.25: Number of spread cells for cell lines ARPE-19, GFWT19 and GFMT22 on laminin-coated plates.

The total number of spread cells was counted out of 200, as were the number showing cellular projections. The assay was repeated 3 times, and standard errors are shown.

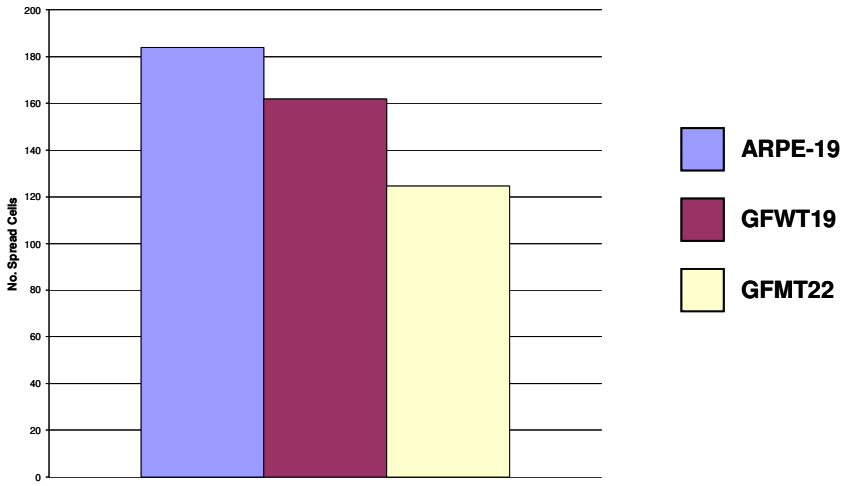

Figure 3.26: Number of spread cells for cell lines ARPE-19, GFWT19 and GFMT22 on fibronectin-coated plates.

The total number of spread cells was counted out of 200. The assay was not repeated so standard errors were not calculated.

3.7.1.2 Cell spreading on fibronectin

The cell spreading assay was repeated using fibronectin-coated microtitre plates and the number of spread cells scored for each cell line out of a total of 200. As can be seen from Figure 3.26, ARPE-19 and GFWT19 show similar levels of spreading whereas this is significantly reduced in GFMT22, χ^2 (2-sided, N = 200) = 11.3, $p <$ 0.01.

3.8 Discussion

Stably transfected ARPE-19 cell lines expressing wild type or mutant His-C1QTNF5 have been created. ARPE-19 cells are physiologically relevant for use in investigating the effects of C1QTNF5 over-expression and the Ser163Arg mutation. An advantage of using the stably transfected cell lines over transient ones is that expression levels can be determined and remain constant. Few cell lines were created due to the low transfection efficiency of ARPE-19, as previously observed in this lab. It is likely that this is simply a feature of ARPE-19 rather than due to over-expression of C1QTNF5. However, C1QTNF5 expression in the stably transfected cell lines was difficult to detect due to the low expression levels. This could be coincidence, or might indicate that high levels of C1QTNF5 are detrimental to the cells.

Whereas previously it had been shown that wild-type but not mutant C1QTNF5 is secreted (Shu *et al.,* 2006b, Mandal *et al.,* 2006c), this study has shown that both forms of the protein are secreted. In addition there does not appear to be high levels of retention of either protein within the cells, since His-C1QTNF5 was difficult to detect in both GFWT19 and GFMT22 cell lysates by Western blot. Shu *et al.* (2006b) were using stably transfected EBNA293 cells expressing His-C1QTNF5 to investigate secretion, rather than ARPE-19, so it is possible that His-C1QTNF5 is simply not secreted in that cell line. It is also possible that an insufficient volume of culture medium was analysed, or that the cells were not incubated for long enough to allow for sufficient secretion. Mandal *et al.* (2006c) were investigating V5-tagged

C1QTNF5 expression in transiently transfected COS-7 cells and analysed culture media after 48 hours' incubation. It is possible again that insufficient culture medium was analysed, or that either the V5 tag or expression in COS-7 does not allow for secretion of mutant C1QTNF5.

Levels of apoptosis were compared between GFWT19, GFMT22 and ARPE-19 cells, and found to be negligible in each cell line after 5 days post-confluence in serum free media. This would support any His-C1QTNF5 detected in the culture media being present as a result of secretion rather than via release from dying cells.

Secreted proteins are synthesised in the ER before they travel to the Golgi apparatus to be packaged for secretion. However, misfolded proteins are retained within the ER and subsequently subject to ER-associated degradation via translocation to the cytosol, ubiquitination and degradation by proteosomes (Ellgaard *et al.,* 2003). Therefore, the observation that mutant but not wild type C1QTNF5 co-localised with calreticulin and PDI, and that wild type but not mutant C1QTNF5 co-localised with the Golgi apparatus (Shu *et al.,* 2006b) would appear to support wild type C1QTNF5 travelling through the secretory pathway whilst the mutant was retained within the ER. However, in the present study immunostaining was carried out in stably transfected cell lines looking at the sub-cellular distributions of His-C1QTNF5 and the presence or absence of co-localisation with the ER markers calreticulin and PDI. No differences were observed between the two cell lines, and no retention of protein within the ER was observed. The previous study was carried out using transiently transfected ARPE-19 expressing GFP-tagged protein whereas this study used stably transfected cells expressing His-tagged protein. It is possible that expression levels differed between transiently and stably transfected cells and that this could have an effect on the tendency to aggregate or the inability to secrete. ARPE-19 cells were therefore transiently transfected with the pEGFP-C1 (minus EGFP)-C1QTNF5 constructs and the sub-cellular distribututions of His-C1QTNF5 analysed by immunostaining. However, no differences were observed between wild-type- or mutant-His-C1QTNF5 expressing cells. Therefore, it is likely that the difference observed between this and the previous study was not due to differences in

C1QTNF5 expression levels resulting from transient expression of C1QTNF5. It is possible that having a GFP tag promotes aggregation or impairs secretion of mutant but not wild-type C1QTNF5, and this may explain the differences observed.

It has been suggested that C1QTNF5 may be involved in RPE-extracellular matrix adhesion, possibly to Bruch's membrane, and that the C1QTNF5 mutation could cause a reduction in adhesion, possibly due to haploinsufficiency (Hayward *et al.,* 2003). Secretion experiments have shown that wild type and mutant protein are both secreted and undergo similar cellular trafficking in ARPE-19 cells, so haploinsufficiency is unlikely to be an issue. However, it was investigated whether differences between the wild-type and mutant proteins could affect cell adhesion, either of ARPE-19 cells directly to C1QTNF5 or of C1QTNF5-expressing cell lines to extracellular matrix proteins. C1QTNF5 shares homology with other collagens such as collagens VI and X, which form extracellular lattices and bind to cells via integrin interactions with their helical collagen domains and globular head groups (Yurchenco *et al.,* 1987, Kwan *et al.,* 1991, Luckman *et al.,* 2003). However ARPE-19 cells did not show adhesion to either C1QTNF5 or gC1q, suggesting that C1QTNF5 is unlikely to be directly involved in RPE-extracellular matrix adhesion. It was also investigated whether ARPE-19 cells stably over-expressing wild type or mutant C1QTNF5 shows any differences in adhesion to laminin or fibronectin when compared with untransfected cells. Again, no differences in levels of adhesion were observed. This suggests that C1QTNF5 is unlikely to have an indirect effect on RPE-extracellular matrix adhesion. It is possible that C1QTNF5 may still be involved but that another downstream factor is limiting and therefore cancels out any effects of wild-type C1QTNF5 over-expression. However, over-expression of mutant C1QTNF5 did not reduce cell adhesion, as might be expected if it was involved, as the wild-type and mutant proteins have been shown to interact (Shu *et al.,* 2006b) and over-expression of mutant could therefore alter the effects of endogenous wild type protein.

Cell-extracellular matrix interactions are not only involved in cell adhesion, but can also have effects on cellular morphology, polarisation and cytoskeletal organisation.

Cell spreading involves cytoskeletal re-organisation and the formation of focal contacts, so differences in ability to spread can be indicative of a cell's ability to change morphology, become polarised and interact with its environment (Hynes, 1999). Cell spreading was investigated by looking at the transfected cell lines on laminin-coated plates, and a reduction in spreading was seen in the mutant cell line GFMT22. In addition, an increase in the percentage of spread cells showing cellular projections was seen in the wild type cell line GFWT19. This would suggest that C1QTNF5 is involved (either directly or indirectly) in interactions with the ECM and ECM-mediated alterations in cell morphology. The RPE is a polarised epithelium, and forms apical microvilli which interdigitate with ROS, facilitating their phagocytosis upon shedding. C1QTNF5 has been shown to be localised to this boundary, and to co-localise with ezrin (Mandal *et al.,* 2006c). Ezrin has been shown to be involved in the formation of these apical microvilli, along with basal infoldings (where C1QTNF5 is also localised) (Bonhilha *et al.,* 1999, Mandal *et al.,* 2006c). CFH knockout mice show a disrupted RPE-ROS boundary (Coffey *et al.,* 2007), and MFRP, with which C1QTNF5 has been shown to interact (Shu *et al.,* 2006b, Mandal *et al.,* 2006c), has recently been shown to be involved in RPE microvilli formation, maintenance of the ROS-RPE boundary and ROS phagocytosis (Won *et al.,* 2008). It is tempting to suggest that C1QTNF5 could be involved in the formation or maintenance of the RPE-ROS boundary *in vivo*. Mutation in C1QTNF5 has been shown to reduce the morphological changes in ARPE-19 cells when plated on laminin and fibronectin *in vitro. In vivo* it is possible that affected individuals could have a disrupted RPE-ROS boundary. It is not possible to confirm this in donated eyes as only aged eyes have been donated, which show many other features of L-ORMD, so cause and effect cannot be established. Further investigation into the nature of the morphological changes observed is required, for instance to establish what receptors are involved and if there are any effects of C1QTNF5 over-expression or mutation on the phagocytic capabilities of the transfected cell lines.

4 CHAPTER 4

:

PRODUCTION AND ANALYSIS OF RECOMBINANT C1QTNF5

4.1 Introduction

Several studies have already been carried out looking at C1QTNF5 properties and the effects of the Ser163Arg mutation. To summarise, C1QTNF5 is a 25kDa secreted protein which shares homology with short chain collagens (Hayward *et al.,* 2003). It consists of 3 domains: a secretory domain, a collagen domain and a globular C1q (gC1q) region. The gC1q region has been shown to be involved in self-assembly of the protein to form trimers and hexamers under native conditions, with an aromatic motif conserved within the C1q superfamily essential for intiating the assembly. The Ser163Arg disease-causing mutation in L-ORMD is located in the gC1q region and is predicted to alter the surface charge of this head group. Wild type and mutant proteins have been shown to interact and form multimeric species, indicating that the Ser163Arg mutation does not affect this property (Shu *et al.,* 2006b). Using *E. coli* expressed protein, it has been shown that mutant gC1q forms an insoluble, high molecular weight aggregate whereas wild-type gC1q is soluble (Hayward *et al.,* 2005). Mandal *et al.* (2006c) found that recombinant full length V5-tagged mutant C1QTNF5 produced using a mammalian expression system (COS-7) had an increased tendency to form aggregates which would not migrate through an SDS-PAGE gel under reducing or non-reducing conditions. When His-tagged C1QTNF5 was stably expressed in EBNA293 cells it was reported that the wild type protein was secreted and formed trimers and hexamers under native conditions, whereas the mutant protein was not secreted and formed a high molecular weight aggregate (Shu *et al.,* 2006b). Therefore, the published data so far would suggest a disease mechanism in L-ORMD caused by aggregation and/or lack of secreted C1QTNF5.

It has been shown in Chapter 3 that wild-type and mutant His-C1QTNF5 are both secreted when stably expressed in ARPE-19, and that neither protein appears to form an aggregate or to be retained within the cell. Due to the contradiction between this result and the published data, further investigation is required into the effects of the Ser163Arg mutation on C1QTNF5. In particular, it needs to be determined whether

the mutant protein does indeed form insoluble aggregates and whether the 163Arg mutation affects multimerisation.

4.2 Producing recombinant C1QTNF5

In order for comparisons to be made between wild-type and mutant C1QTNF5, it was necessary to produce reasonable quantities of the recombinant proteins. When recombinant wild type and mutant His-C1QTNF5 were stably produced in ARPE-19 with small C-terminal His tags, the secreted proteins were found to be present in the culture medium. However, recombinant His-C1QTNF5 is produced at very low levels in ARPE-19, meaning that these cell lines would not be practical for large scale protein production. EBNA293 is a human embryonic kidney derived cell line which has been used previously as a mammalian expression system to produce recombinant proteins, for instance EMILIN-1, which is an extracellular matrix protein containing a self-interacting gC1q domain homologous to C1QTNF5 (Spessotto *et al.,* 2003). Therefore, a stably transfected EBNA293 cell line producing wild-type His-tagged C1QTNF5 was produced from which to purify recombinant protein. A stably transfected EBNA293 cell line producing mutant His-tagged C1QTNF5 had previously been created and was supplied for use by Dr X. Shu.

4.2.1 Creating an EBNA293 cell line stably expressing wild type C1QTNF5

EBNA293 cells were transfected with a pCEP-Pu vector construct containing *His-C1QTNF5* insert, supplied by Dr X. Shu. This vector has been used previously for expression of recombinant proteins in EBNA293 (Hopf *et al.,* 2001) and contains a selectable marker for selection of transfected cells with puromycin.

4.2.1.1 Transfection, selection and screening of EBNA293 for stable transfection and expression of His-C1QTNF5

Following transfection, EBNA293 were maintained in culture media containing 2µg/ml puromycin. Individual colonies were amplified and cell lysates screened by

Western blot for His-C1QTNF5 expression. Figure 4.1 is an example of a screening Western blot. Lanes A to H contain cell lysate samples from individual colonies. The band at approximately 28kDa seen in lanes A, C, D, E, G and H is His-C1QTNF5. The additional band at approximately 14kDa is most likely to be degraded His-C1QTNF5, possibly the gC1q domain which is 15kDa in size. Cell line A was selected for use in future assays.

4.2.1.2 Checking secretion of His-C1QTNF5

TCA precipitated culture medium proteins from the selected cell line were analysed by Western blot to check whether His-C1QTNF5 was secreted. As can be seen from Figure 4.2, His-C1QTNF5 (approximately 28kDa) was present in both the cell lysate and precipitated culture medium protein samples, indicating that it is secreted.

4.2.1.3 Immunostaining of wild-type and mutant His-C1QTNF5 expressing cell lines

Immunostaining was carried out on the above cell line and also on the mutant His-C1QTNF5 expressing EBNA293 cell line supplied by Dr X. Shu (Figure 4.3). Anti-His antibodies confirmed the expression of His-C1QTNF5 in both cell lines. A diffuse cytoplasmic distribution of His-C1QTNF5 was observed in both, suggesting similar cellular trafficking between the cell lines and no aggregation or retention of His-C1QTNF5 within the ER. Beta-catenin staining indicates cellular boundaries.

4.2.2 Secretion of mutant His-C1QTNF5

When carrying out the above immunostaining, the C1QTNF5 aggregation and retention within the ER described previously (Shu *et al.,* 2006b) was not observed. It was therefore investigated whether mutant His-C1QTNF5 was actually secreted from this cell line. Culture media from the wild type and mutant His-C1QTNF5-expressing EBNA293 cell lines were analysed by Western blot at 1, 2 and 3 days post-confluence, after replacing the media with serum free medium to allow accumulation of secreted protein in the culture medium. His-C1QTNF5 was purified using Ni-NTA affinity chromatography beads allowing for detection of low levels of protein. His-C1QTNF5 was found to be present in the culture media of both cell

lines, increasing from 1 to 3 days (see Figure 4.4). Samples were not normalised for cell number and cell lines were not selected for similar expression levels, so the apparent differences in levels of His-C1QTNF5 expression between the cell lines cannot be taken as indicative of any inherent differences between the wild-type and mutant proteins.

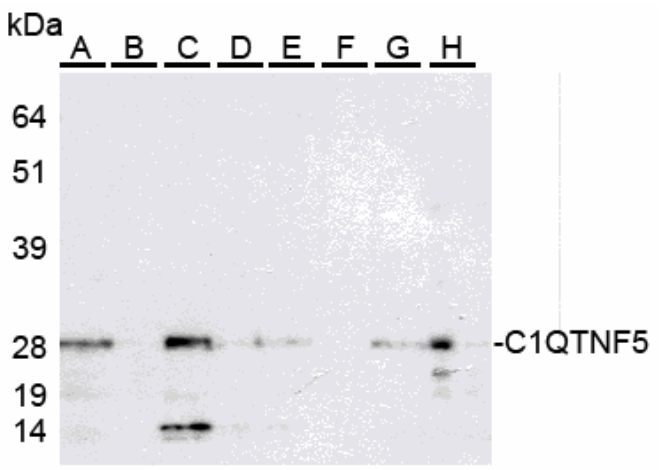

Figure 4.1: Western blot showing cell lysate samples from screened transfected EBNA293 cell lines checked for expression of His-C1QTNF5.

His-C1QTNF5 can be seen at approximately 28kDa. The band in lane C at approximately 14kDa is most likely partially degraded protein. Primary antibody – mouse anti-His; secondary antibody – rabbit anti-mouse HRP. kDa: relative molecular mass

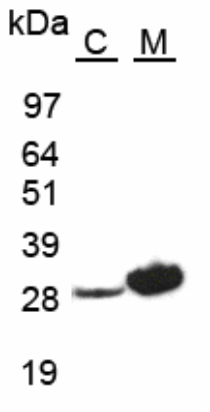

Figure 4.2: Western blot of cell lysate (C) and TCA precipitated culture media protein (M) samples from the wild type His-C1QTNF5 expressing EBNA293 cell line.

The band at approximately 28kDa is His-C1QTNF5. The figure shows that His-C1QTNF5 is present in the cell lysates and is secreted into the culture medium. Primary anitbody – mouse anti-His; secondary antibody – rabbit anti-mouse HRP. kDa: relative molecular mass

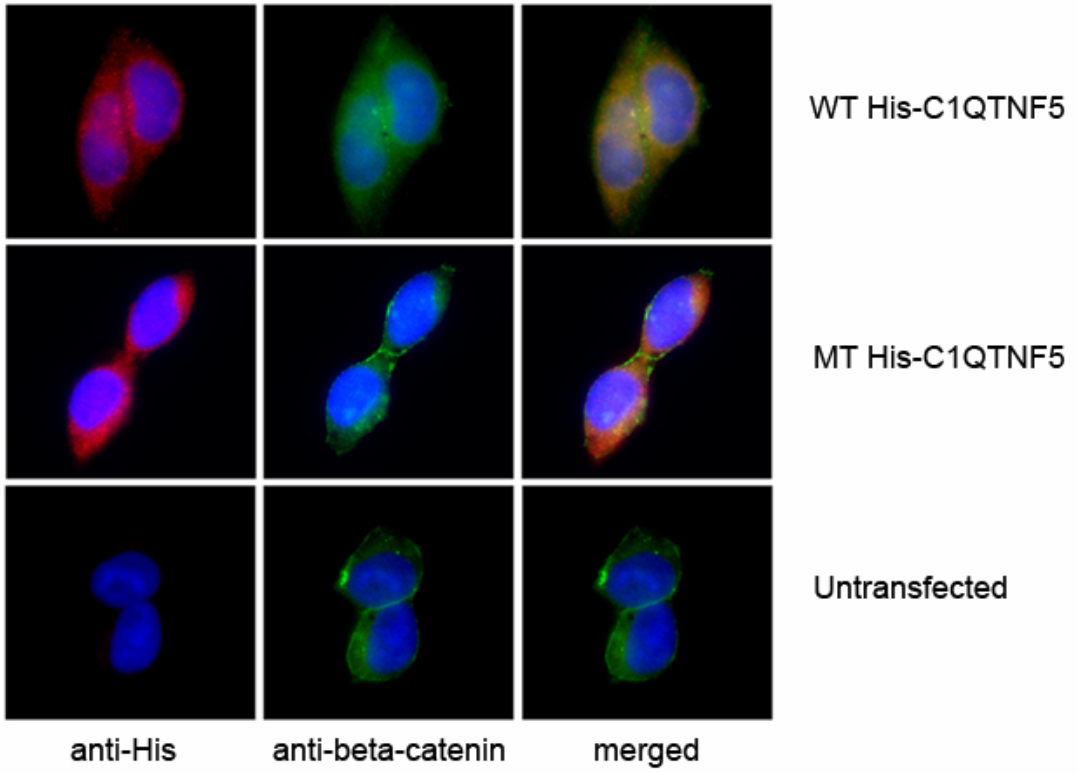

Figure 4.3: Immunostaining of stably transfected EBNA293 expressing wild type (WT) or mutant (MT) His-C1QTNF5 and untransfected EBNA293. Anti-beta catenin staining seen in green. Anti-His staining, corresponding to His-C1QTNF5, is seen in red. In both WT His-C1QTNF5 and MT His-C1QTNF5, His-C1QTNF5 shows diffuse cytoplasmic localisation.

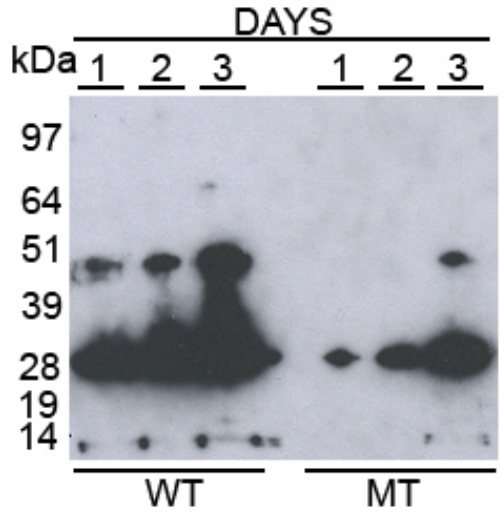

Figure 4.4: Western blot of Ni-NTA purified culture media proteins from transfected EBNA293 stably expressing wild-type or mutant His-C1QTNF5. Samples were taken at 1, 2 or 3 days post confluence in serum free media. Bands at approximately 28kDa are His-C1QTNF5 monomer, and bands at approximately 50kDa are His-C1QTNF5 dimer. Primary anitbody – mouse anti-His; secondary antibody – rabbit anti-mouse HRP. kDa: relative molecular mass

4.2.3 Purifying recombinant His-C1QTNF5 from transfected EBNA293

Wild-type and mutant His-C1QTNF5 are both secreted from the stably transfected EBNA293 cell lines. Larger quantities of the protein are secreted from these cell lines than the transfected ARPE-19 cell lines GFWT19 and GFMT22, making feasible large-scale production and purification of His-C1QTNF5 for use in future assays.

Cells were grown to confluence in media containing 10% serum, and then incubated in serum-free media for 5 days to allow accumulation of secreted protein in the culture media. His-C1QTNF5 was affinity purified from culture medium supernatants using Ni-NTA affinity chromatography, with His-C1QTNF5 eluted in 1 ml fractions using 1M imidazole, pH10. Figure 4.5 shows reducing SDS-PAGE of elution fractions for wild type His-C1QTNF5 (A) and mutant His-C1QTNF5 (B). Bands corresponding to His-C1QTNF5 monomers, dimers and trimers can be observed. Additional bands were also observed in the mutant fractions, highlighted by the black arrow.

Elution fractions were pooled and dialysed into PBS. Figure 4.6 shows reducing SDS-PAGE and Western blot analysis of the pooled proteins. It can be seen that even under reducing conditions both wild type and mutant His-C1QTNF5 are present as monomeric, dimeric and trimeric species. In addition, the extra bands observed only for the mutant protein in Figure 4.5 are observed here too, although it was necessary to load excess protein onto the gel to enable detection.

4.3 Producing His-gC1q in *E. coli*

As well as producing full length His-C1QTNF5 using a mammalian expression system, His-tagged globular C1q domain (His-gC1q) was produced using a bacterial expression system. The clones had been created and supplied by Dr X. Shu. Such recombinant *E. coli*-produced gC1q domains have been used in previous studies looking at C1QTNF5 (Shu *et al.,* 2006a).

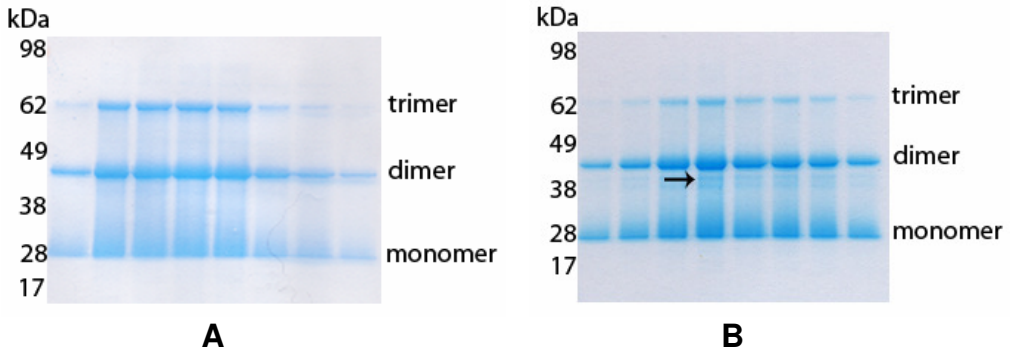

Figure 4.5: Reducing SDS-PAGE of successive elution fractions for wild-type (A) and mutant (B) His-C1QTNF5 purified from the culture media of the stably transfected EBNA293 cell lines.

Protein was eluted in 1M imidazole, pH10, with 10µl eluant loaded per well.
The arrow indicates additional bands present in the mutant. kDa: relative molecular mass

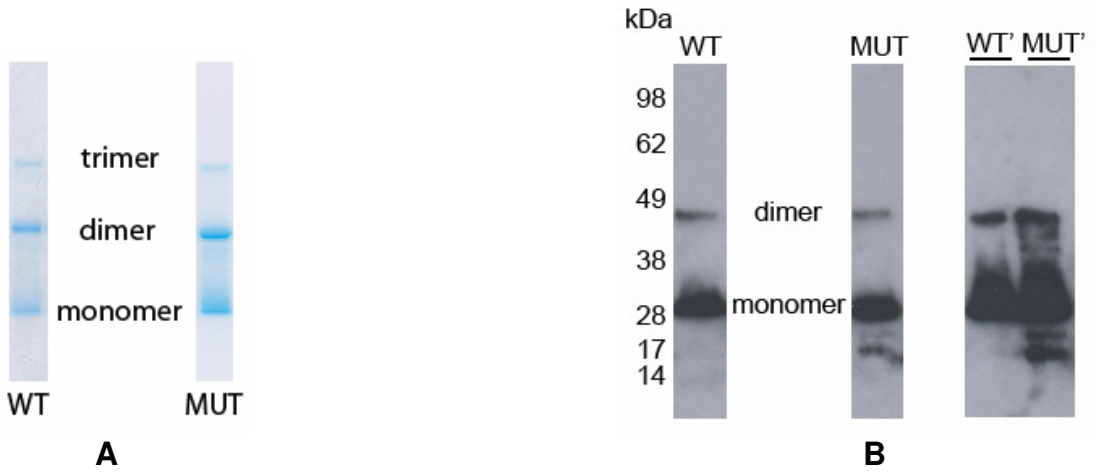

Figure 4.6: Reducing SDS-PAGE (A) and Western blot (B) of pooled and dialysed wild type (WT) and mutant (MUT) His-C1QTNF5

Additional bands are observed for the mutant when excess protein is loaded to the gel (WT' MUT'). Primary antibody – mouse anti-His; secondary antibody – rabbit anti-mouse HRP. kDa: relative molecular mass

4.3.1 Purifying wild-type His-gC1q from *E. coli*

Wild-type His-gC1q-expressing *E. coli* was cultured at 37°C until sufficient biomass had been reached, whereupon the temperature was reduced to 20°C and expression was induced by addition of IPTG. Reducing the temperature slowed the rate of protein production, which is high in *E. coli*, to help facilitate correct protein folding and prevent the formation of inclusion bodies. This was especially important as the construct does not contain a secretion signal peptide and so the protein remains intracellular. Figure 4.7 (A and B) shows sample cell lysates analysed by SDS-PAGE and Western blot of induced (I) and non-induced (NI) cultures. His-gC1q can be seen at between 15 and 20kDa in induced samples.

Following large-scale culture and cell lysis, intracellular His-gC1q was purified from clarified lysates by Ni-NTA affinity chromatography, with the protein eluted in 1M imidazole, pH10. Figure 4.7 (C) shows a reducing SDS-PAGE of the eluted fractions, with monomeric, dimeric and trimeric species present. All the fractions were then pooled and dialysed into PBS. Figure 4.7 (D and E) shows a reducing SDS-PAGE and Western blot for the pooled and dialysed protein. Multimeric species can again be observed.

4.3.2 Purifying mutant His-gC1q from *E. coli*

E. coli clones expressing mutant His-gC1q were also supplied by Dr X. Shu. However, it was not possible to purify protein from the cell lysates due to the formation of insoluble inclusion bodies. Figure 4.8 shows the elution fractions obtained, analysed by reducing SDS-PAGE. In addition to possible multimeric His-gC1q, many contaminating bands are present. Therefore it was decided not to pursue the production of mutant His-gC1 in *E. coli* any further.

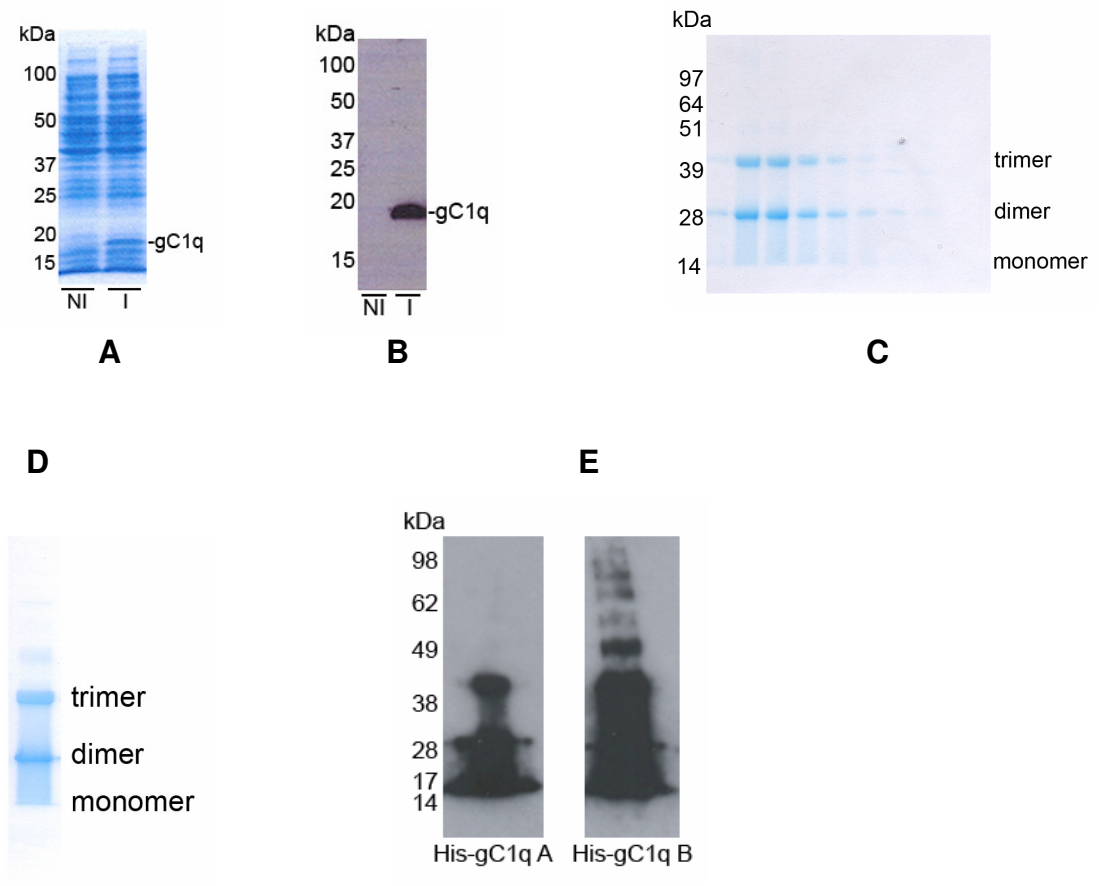

Figure 4.7: A – Reducing SDS-PAGE of non-induced (NI) and induced (I) *E. coli* cultures showing expression of wild-type His-gC1q in the induced culture.

B – Western blot of A, showing His-gC1q expressing in the induced culture.
C – Reducing SDS-PAGE of elution fractions purified from a large scale culture. Monomeric, dimeric and trimeric His-gC1q can be seen.
D – Reducing SDS-PAGE of pooled His-gC1q elution fractions, showing monomeric, dimeric and trimeric protein.
E – Western blot of D with low (His-gC1q A) and high (His- gC1q B) concentrations of protein loaded to the gel. Monomeric, dimeric and trimeric species are present with higher order multimers in His-gC1q B.
For Western blots: Primary anitbody – mouse anti-His; secondary antibody – rabbit anti-mouse HRP. kDa: relative molecular mass

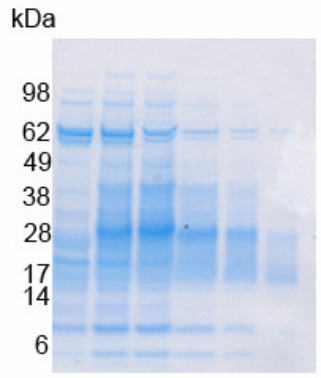

Figure 4.8: Reducing SDS-PAGE of successive mutant His-gC1q eluted fractions purified from transfected *E. coli* cell lysates by Ni-NTA affinity chromatography.

It was not possible to obtain pure protein, indicating that mutant His-gC1q is forming inclusion bodies.

4.4 Comparing wild-type and mutant His-C1QTNF5

Previous studies indicated that differences existed relating to the solubility and aggregation of wild-type and mutant C1QTNF5. However, the results from the previous chapter indicated that this was not necessarily the case, so further investigations were carried out, looking at solubility and multimerisation of the recombinant proteins, to determine what differences could be observed between the wild-type and mutant.

4.4.1 Bradford assay

All protein concentrations were determined by Bradford assay. Bovine serum albumin sample solutions of known concentration were analysed to give a standard curve, from which the recombinant protein concentrations were determined. The standard curve process was repeated each time the assay was carried out. Figure 4.9 gives an example of such a standard curve and subsequent calculation of protein concentration.

4.4.2 Investigating C1QTNF5 solubility

Previous studies had indicated that mutant but not wild-type C1QTNF5 formed insoluble aggregates. Soluble protein concentrations of wild-type and mutant gC1q had been determined after incubation at 37°C for up to 24 hours, and it was found that the mutant protein showed a total decrease in soluble protein concentration of approximately 85% compared with a roughly 15% decrease in the wild type (Hayward *et al.,* 2003). However, this result was obtained using *E. coli* expressed wild-type and mutant gC1q domains and it has been shown in section 4.3.2 that, when expressed in *E. coli,* the mutant protein forms insoluble inclusion bodies. Therefore, the result obtained may have been due to an impure, misfolded mutant gC1q rather than the Ser163Arg mutation. The assay was repeated using wild-type and mutant His-C1QTNF5 purified from the stably transfected EBNA293 cell lines. Both proteins were shown to be soluble in PBS up to 36 hours, with no observable reduction over this time period when samples were analysed by reducing SDS-PAGE (Figure 4.10). OD_{280} measurements were also taken and although both proteins

showed a slight reduction in soluble protein over this time course, there was no difference between the wild-type and mutant samples (Figure 4.11). It should however be noted that mutant His-C1QTNF5 precipitates at room temperature in PBS but the wild-type does not, although the mutant protein will enter solution again upon re-heating.

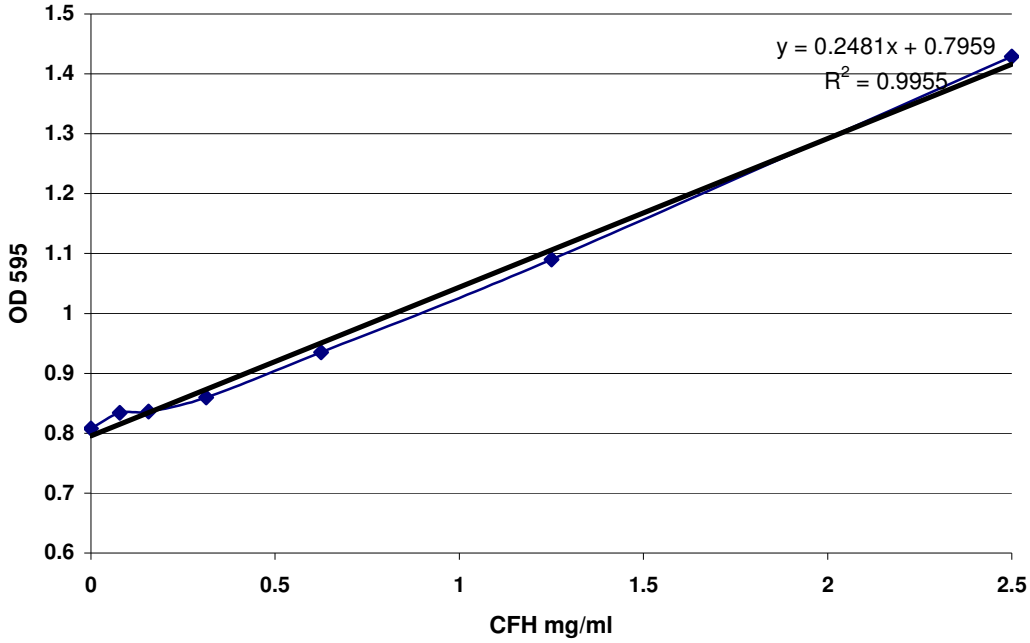

Sample calculation:

y = sample OD_{595}

= 1.35

x = sample concentration

$y = 0.2481x + 0.7959$

So, $x = (y - 0.7959) / 0.2481$

Therefore, $x = (1.35 - 0.7959) / 0.2481$

= 2.23 mg/ml

Figure 4.9: Sample Bradford assay standard curve and calculation of protein sample concentration.

The standard curve OD_{595} values were obtained using PBS/BSA standard solutions of known concentration in Bradford assay reagent.

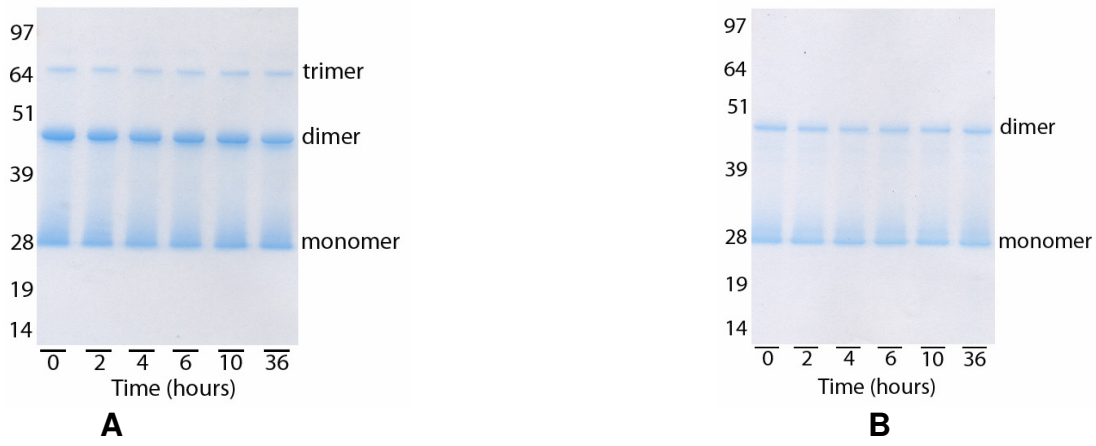

Figure 4.10: Reducing SDS-PAGE of wild type (A) and mutant (B) His-C1QTNF5.

Proteins were incubated at 37℃ with samples taken for analysis for up to 36 hours. Samples were centrifuged at 13,000 rpm for 10 minutes prior to gel loading to remove any insoluble protein.

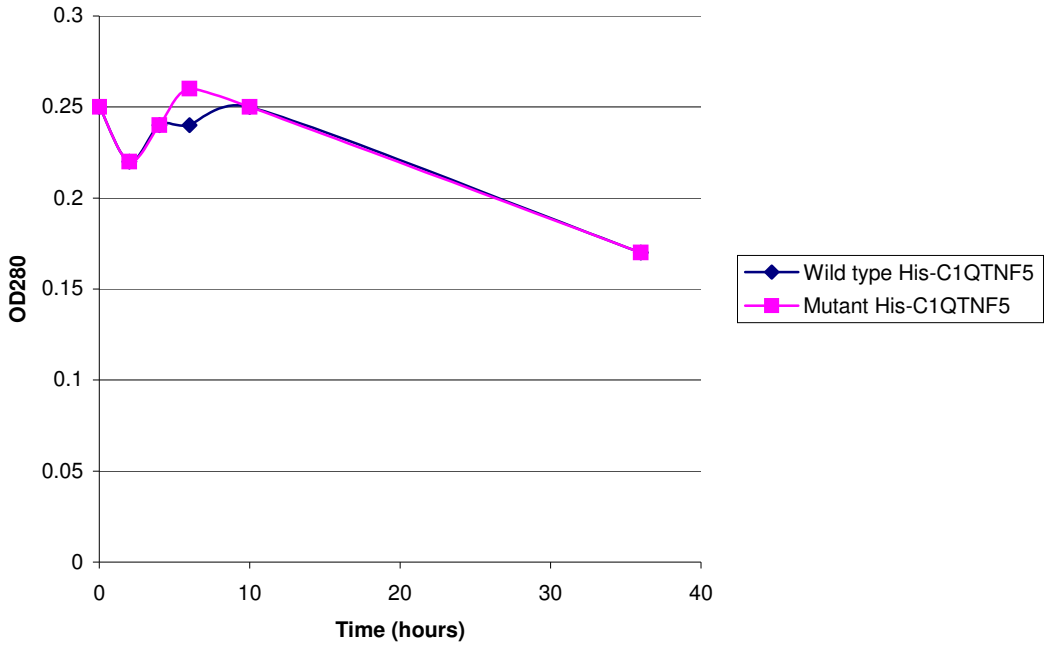

Figure 4.11: OD_{280} readings for wild type and mutant His-C1QTNF5 at 37℃ in PBS for up to 36 hours.

Samples were centrifuged at 13,000 rpm for 10 minutes prior to analysis to remove any insoluble protein.

4.4.3 Polyacrylamide gel electrophoretic analysis of C1QTNF5 and gC1q

When analysing purified His-C1QTNF5 by reducing SDS-PAGE it was observed that both the wild-type and mutant proteins formed monomeric, dimeric and trimeric species, and these did not appear to differ between the proteins. Other gC1q-containing proteins such as C1q and collagens X and VIII have been shown to form trimeric species which are highly resistant to reducing conditions, and it has been suggested this is due to buried Ca^{2+} clusters providing stability to the trimers (Kishore *et al.,* 2004a, Kishore *et al*., 2004b, Bogin *et al.,* 2002, Stephan *et al.,* 2004). It has been proposed that in homologous proteins containing the gC1q domain, an aromatic motif is responsible for initial trimer assembly (Brass *et al.,* 1992, Chan *et al.,* 1999), followed by the formation of a central solvent-filled channel stabilised by Ca^{2+} clusters providing strong ionic bonds (Kishore *et al.,* 2004b). Supramolecular assembly differs between gC1q-containing proteins. Exposed aromatic strips at the surface of the trimers promote hydrophobic interactions for supramolecular assembly of collagen X and VIII (Stephan *et al.,* 2004, Kishore *et al.,* 2004b). However, interactions between the collagen domains of C1q and MBL (which contains a gC1q-like domain) cause these proteins to form tulip-like clusters (Kishore *et al.,* 2004a).

Polyacrylamide gel electrophoresis separates proteins according to their electrophoretic mobility, which can be dependant upon protein molecular weight, higher order structure and post-translation modifications. Analysis by reducing SDS-, non-reducing SDS- or native PAGE was carried out to give insight into the nature of the bonds and molecular interactions involved in C1QTNF5 multimerisation.

4.4.3.1 Reducing and non-reducing SDS-PAGE

Protein samples for reducing SDS-PAGE were prepared by heating in the presence of SDS and dithiothreitol (DTT). SDS is an anionic detergent which denatures secondary and non-disulphide-linked tertiary structures and gives proteins a uniform

negative charge in proportion to their mass. DTT reduces disulphide bridges found in protein tertiary structure. Prior treatment with both of these chemicals should allow for protein separation due to mass alone. Proteins undergoing non-reducing SDS-PAGE were prepared by heating in the presence of SDS alone. Gel migration is therefore dependant upon mass and disulphide-linked tertiary structure.

Figure 4.12 shows reducing and non-reducing SDS-PAGE gels for wild-type and mutant His-C1QTNF5 and wild-type His-gC1q. Under reducing conditions, both wild-type and mutant His-C1QTNF5 and wild type His-gC1q show monomeric, dimeric and trimeric species, the latter two of which show resistance to reducing conditions. Faint additional bands can be observed in the mutant, as noted previously (Figure 4.5/Section 4.2.3). Faint bands for higher order multimers can also be seen in His-gC1q and were observed previously by Western blot (Figure 4.7, E). Under non-reducing conditions, wild-type and mutant His-C1QTNF5 form monomeric, dimeric, trimeric and higher order multimeric species, indicating the presence of disulphide-linked tertiary structures.

4.4.3.2 Native PAGE

During native PAGE analysis, protein migration is dependant upon charge, protein size and oligomeric state. No SDS or DTT is present therefore the protein has only its native charge, which will affect the rate at which it migrates through the gel. Samples are not heated or denatured so native protein size and oligomeric state will also affect migration rate. The distance migrated is dependant upon these factors in combination with the gel pore size. Therefore, native PAGE analysis can show the native oligmeric state of the protein under the conditions investigated.

In this study, native discontinuous electrophoresis and subsequent generation of a molecular weight standard curve (Ferguson plot) was carried out following the method described by Gallagher (2000). This requires standard proteins of known molecular weight to be separated on gels of varying acrylamide plus bisacrylamide concentration (%T). The distance migrated, or relative mobility (R_f) for each protein and each %T is calculated. Plotting the log R_f against %T for each protein gives a

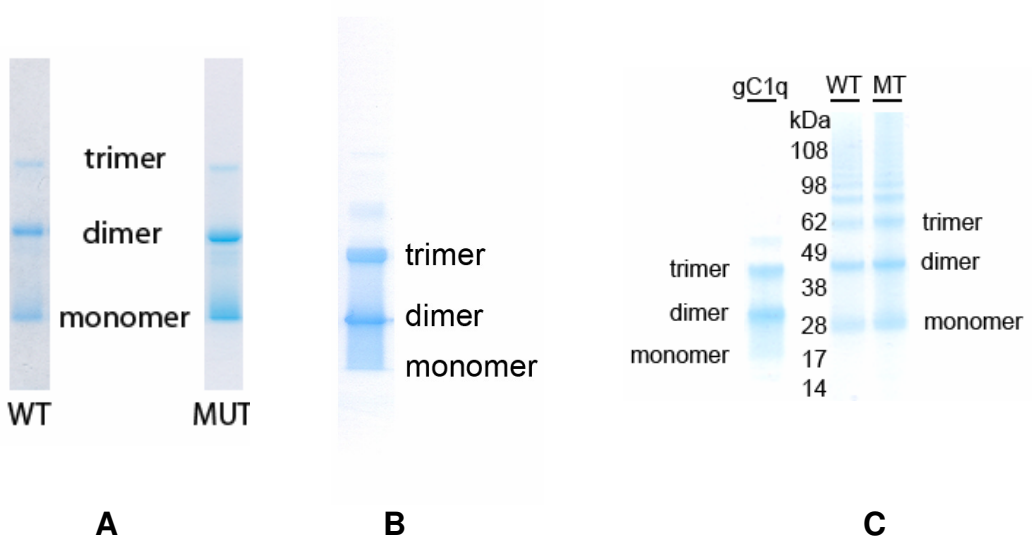

Figure 4.12: Reducing versus non-reducing SDS-PAGE of His-C1QTNF5 and His-gC1q protein.

A - Reducing SDS-PAGE of wild-type (WT and mutant (MUT) His-C1QTNF5, showing monomeric, dimeric and trimeric protein
B – Reducing SDS-PAGE of wild type His-gC1q, showing monomeric, dimeric and trimeric protein.
C – Non-reducing SDS-PAGE of wild type His-gC1q (gC1q) and wild type (WT) and mutant (MT) His-C1QTNF5. His-gC1q can be see as monomeric, dimeric and trimeric protein. His-C1QTNF5 can be seen as monomeric, dimeric, trimeric and higher order multimeric protein, and is the same for both wild type and mutant.
kDa: relative molecular mass

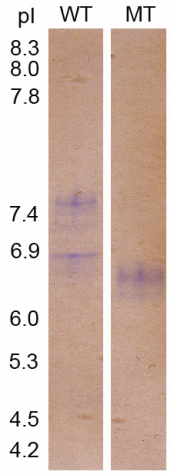

Figure 4.13: Isoelectric focusing gel for wild type (WT) and mutant (MUT) His-C1QTNF5.

Wild type protein is present as two species with pI's aproximately 7.5 and 6.8, and the mutant protein is present as a single species with a pI of aproximately 6.5. pI - relative protein pI.

slope with a gradient, K_r. This is the retardation coefficent for that protein, and is a measure of how effectively the protein is slowed by an increase in %T. Plotting log K_r against log MW for the standard proteins gives a standard curve from which unknown molecular weights can be determined. This method does however assume that protein shape does not significantly alter protein migration between either the standard or sample proteins. C1QTNF5 is a relatively small protein with a known globular domain, so it was assumed that protein shape would not be an issue in this instance. Also, ideally, standard proteins should be used which have a similar pI to the sample protein.

4.4.3.2.1 pI determination

As migration through a native PAGE gel relies partially upon the native charge of a protein, it is necessary to determine the pI of the proteins to be investigated. These were determined by isoelectric focusing PAGE (Figure 4.13), with wild-type His-C1QTNF5 existing as two species of pI 7.5 and 6.8 and the mutant existing as a single species of pI 6.5. Native gel conditions used were appropriate for proteins of pI 8.0 or below.

4.4.3.2.2 Native PAGE standard gels

Before running the His-C1QTNF5 samples, calibration was required against proteins for which the molecular weight and oligomeric state are already known, using gels ranging in pore size. Ferguson plots could then be obtained against which His-C1QTNF5 migration could be compared. All gels were run at 37°C because at this temperature both wild-type and mutant His-C1QTNF5 were found to be soluble.

Figure 4.14 shows standard proteins lactalbumin (A), carbonic anhydrase (B), ovalbumin (C) and BSA (D) run on 8%, 10% and 12% polyacrylamide gels. Distance migrated was plotted against gel concentration for each of the proteins and the gradients calculated (Figure 4.15). Protein molecular weight was then plotted against the log of the gradients to give the native PAGE standard curve (Ferguson plot) (Figure 4.16).

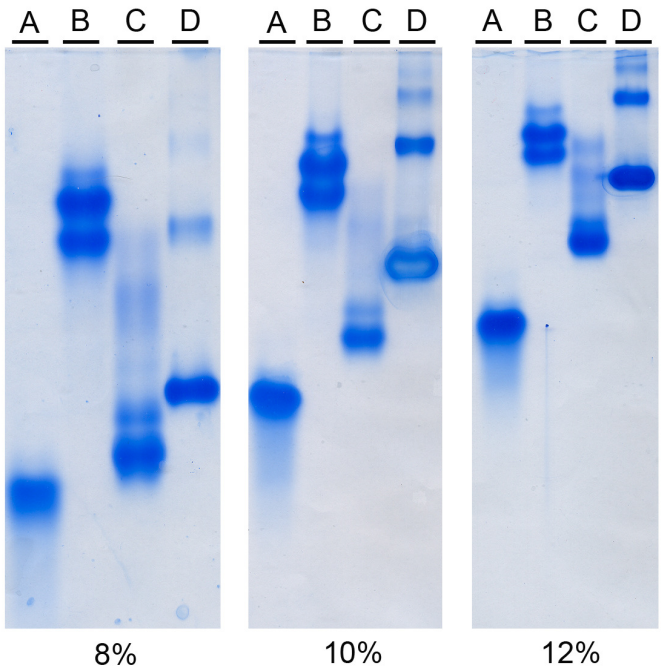

Figure 4.14: Native PAGE analysis of standard proteins lactalbumin (A), carbonic anhydrase (B), ovalbumin (C) and BSA (D), run 8%, 10% and 12% polyacrylamide gels.

Distances migrated by each protein, including multimeric forms, were used to calculate relative mobilities and to plot a native PAGE standard curve (see Figures 4.15 and 4.16).

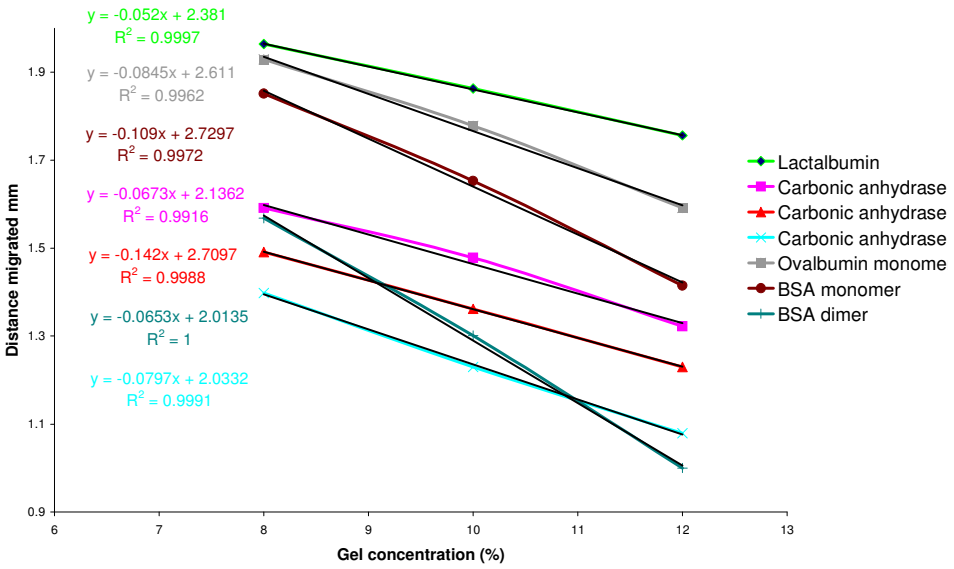

Figure 4.15: Native protein relative mobilities (mm) were plotted against gel concentration, and the gradients (Kr) calculated for each of the standard proteins.

These were used to plot the native PAGE standard curve (Figure 4.16).

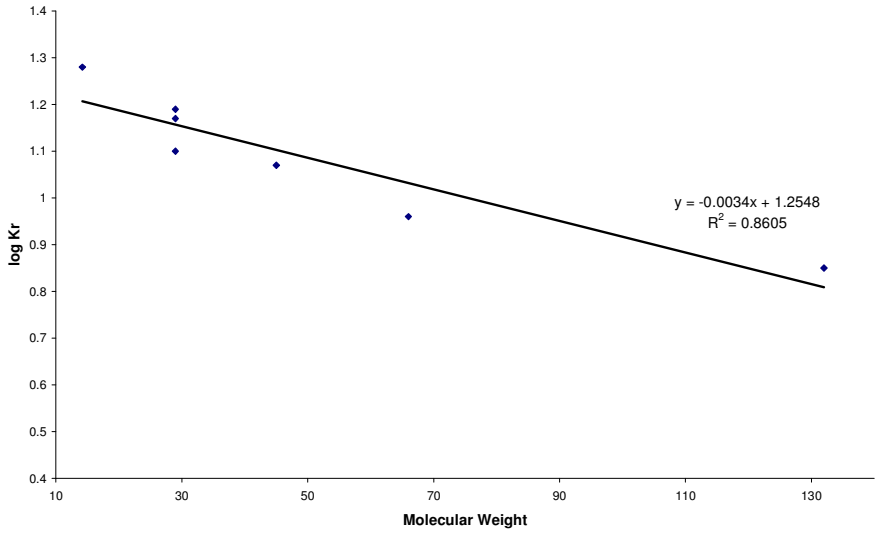

Figure 4.16: Log of the gradients from Figure 4.15 (log Kr).

This was plotted against molecular weight for each of the native protein standards to give the native PAGE standard curve, from which native molecular weights for His-C1QTNF5 were calculated.

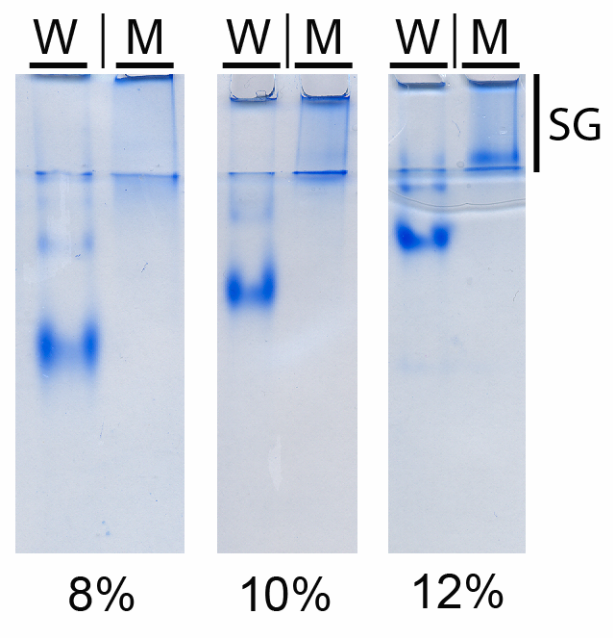

Figure 4.17: Native PAGE analysis of wild-type (W) and mutant (M) His-C1QTNF5 on 8%, 10% and 12% polyacrylamide gels.

Wild-type protein is present predominantly as two species. Distance migrated for each species through each of the gels was used to calculate the relative mobility (Figure 4.18). Mutant His-C1QTNF5 would not migrate through the gel. SG - stacking gel.

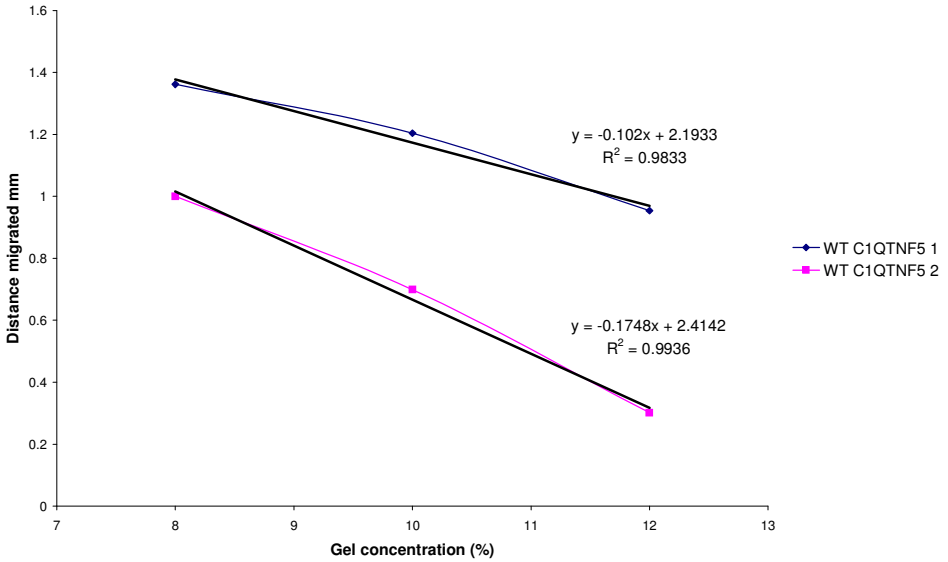

Figure 4.18: Native protein relative mobilities (mm) plotted against gel concentration for both of the two wild-type His-C1QTNF5 species, showing calculated gradients (Kr) for each.

Kr values were then used to calculate molecular weight using the native PAGE standard curve (Figure 4.16).

4.4.3.2.3 Native PAGE analysis of His-C1QTNF5

Wild-type and mutant His-C1QTNF5 were analysed on 8%, 10% and 12% polyacrylamide gels under native conditions (Figure 4.17). Wild-type His-C1QTNF5 migrated as two species. The distance migrated for each species was plotted against the gel concentration (Figure 4.18). The gradients for each were then compared to the native PAGE standard curve to give predicted molecular weights of 77.88kDa and 145.53kDa, indicating the protein is present as a major trimeric and weak hexameric species (assuming a monomeric molecular weight of approximately 25kDa). Mutant His-C1QTNF5 would not migrate through the gel.

4.4.4 Post-translational modification of C1QTNF5

C1QTNF5 is a secreted protein and therefore unlikely to undergo post-translational modifications such as phosphorylation or ubiquitination. Secreted proteins can undergo N- or O-glycosylation and alterations in this could account for the additional bands seen in the mutant. Prediction of N-glycosylation sites was carried out on C1QTNF5 (http://www.cbs.dtu.dk/services/NetNGlyc/) and no predicted sites were identified. However, prediction sites for O-glycosylation were identified (http://www.cbs.dtu.dk/services/NetOGlyc/), as shown in Figure 4.19, with these occurring in the collagen and N-terminal of the gC1q domains.

4.4.5 Matrix-assisted laser desorption/ionisation time-of-flight mass spectrometry comparison of wild type and mutant C1QTNF5

Matrix-assisted laser desorption/ionisation time-of-flight mass spectrometry (MALDI-TOF MS) is a technique used for the accurate mass analysis of biomolecules (Karas and Hillenkamp, 1988). Applications include predicting protein identity, *de novo* peptide sequencing, investigating post-translational modifications and comparing recombinant and endogenous proteins, and the technique can be used for both purified proteins and complex mixtures (Zaluzec *et al.,* 1995, Hortin, 2006). In this study, MALDI-TOF MS was used to determine the identity of the additional bands seen on reduced SDS-PAGE of mutant His-C1QTNF5 (see Figure 4.5) and to investigate any differences between the wild-type and mutant recombinant proteins.

.

```
MRPLLVLLLLGLAAGSPPLDDNKIPSLCPGHPGLPGTPGHHGSQGLPGRDGRDGRDGAPGAPGEKGEGGRPGLPGPRGDP
GPRGEAGPAGPTGPAGECSVPPRSAFSAKRSESRVPPPSDAPLPFDRVLVNEQGHYDAVTGKFTCQVPGVYYFAVHATVY
RASLQFDLVKNGESIASFFQFFGGWPKPASLSGGAMVRLEPEDQVWVQVGVGDYIGIYASIKTDSTFSGFLVYSDWHSSP
VFA
_______________.....................T.........................................
..........T......S....S..S...S.S.....................................................
.....................................................................................
...
```

Name	S/T	Pos	G-score	I-score	Y/N
Sequence	S	16	0.205	0.097	.
Sequence	S	26	0.456	0.064	.
Sequence	T	37	0.511	0.127	T
Sequence	S	43	0.401	0.066	.
Sequence	T	92	0.694	0.687	T
Sequence	S	99	0.549	0.042	S
Sequence	S	104	0.616	0.026	S
Sequence	S	107	0.611	0.053	S
Sequence	S	111	0.565	0.027	S
Sequence	S	113	0.561	0.036	S
Sequence	S	119	0.449	0.451	.
Sequence	T	144	0.273	0.053	.
Sequence	T	158	0.203	0.022	.
Sequence	S	163	0.164	0.032	.
Sequence	S	174	0.157	0.021	.
Sequence	S	177	0.198	0.026	.
Sequence	S	190	0.255	0.066	.
Sequence	S	192	0.277	0.089	.
Sequence	S	220	0.170	0.253	.
Sequence	T	223	0.243	0.056	.
Sequence	S	225	0.209	0.026	.
Sequence	T	226	0.312	0.054	.
Sequence	S	228	0.229	0.057	.
Sequence	S	234	0.352	0.050	.
Sequence	S	238	0.396	0.070	.
Sequence	S	239	0.386	0.032	.

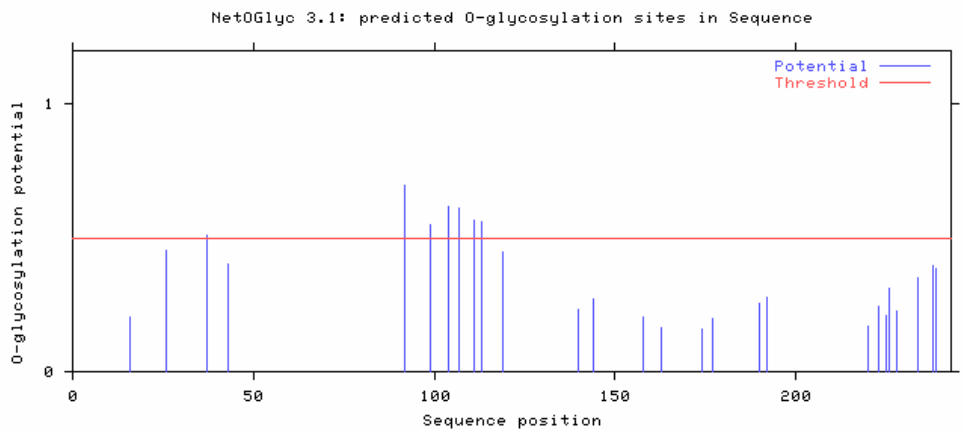

Figure 4.19: Predicted O-glycosylation sites for C1QTNF5.
(http://www.cbs.dtu.dk/services/NetOGlyc/)
The G-score is the score from the best general predictor; the I-score is the score from the best isolated site predictor. If the G-score is >**0.5** the residue is predicted as glycosylated; the higher the score the more confident the prediction. For threonines an additional score is used: if the G-score is <**0.5** but the I-score >**0.5** and there are no predicted neighbouring sites (distance <**10 residues**) the residue is also predicted as glycosylated. There are 2 predicted glycosylation sites within the collagen domain (red) and 5 predicted sites within the gC1q domain (green).
The secretory domain is shown in blue.

4.4.5.1 MALTI-TOF MS

When undergoing MALDI-TOF MS analysis, crystallised samples are ionised using lasers, changing from the solid phase into gaseous, charged molecules. Because non-volatile organic molecules do not readily absorb energy at the wavelength required for ionisation to occur, they are co-crystallised with an energy absorbing matrix. This enables desorption/ionisation to take place. Once ionised, molecules are accelerated along a flight tube until they reach a detector. The time taken between ionisation and detection is dependant upon the ion's molecular mass and charge (Karas and Hillenkamp, 1988). Due to the relationship between flight time and mass-to-charge ratio (m/z), identification of proteins by MALDI-TOF MS can be carried out using peptide mass mapping. Proteins are digested with a known enzyme such as trypsin to produce peptide fragments. These are then analysed by MALDI-TOF MS and the spectra obtained is compared to protein databases with predicted proteolytic peptide masses. This technique allows for identification of proteins within complex mixtures as well as for analysis of purified proteins (Zaluzec *et al.,* 1995, Hortin, 2006). Post-translational modifications such as glycosylation can also be predicted by MALDI-TOF MS due to alterations in peptide mass from that predicted by the amino acid sequence, although accurate predictions cannot always be made as oligosaccharide structures can be removed from glycopeptides during analysis (Zaluzec *et al.,* 1995).

4.4.5.2 Analysis of trypsin-digested wild-type and mutant His-C1QTNF5

In order to confirm the recombinant proteins produced were His-C1QTNF5, and to identify any possible differences between the wild-type and mutant proteins, MALDI-TOF MS analysis was carried out on the trypsin digested proteins. Firstly, the proteins underwent reducing SDS-PAGE, with bands corresponding to monomers and dimers excised from the gel (Figure 4.20). The additional bands observed in the mutant were also excised. Proteins were then purified, digested with trypsin and subsequently analysed. Each band was identified as C1QTNF5 by peptide mass mapping.

Table 4.1 shows the predicted peptide fragment masses for trypsin digested wild-type His-C1QTNF5, and Table 4.2 shows the same for the mutant. Figure 4.21 shows the spectra obtained for band 1 (dimeric, wild-type protein) and band 3 (dimeric mutant protein) seen in Figure 4.20. Peaks in the spectra were compared with the predicted peptide mass fragments to enable their identification. Table 4.3 and Table 4.4 show whether the predicted fragments could be identified in their corresponding spectra. Some fragments were identified as single peaks with a m/z ratio of 1, such as fragment 18 which was has a predicted mass of 1866.934Da and was identified as m/z peaks of 1866.8875 and 1866.8854 in the wild-type and mutant spectra respectively. Such fragments can be identified with a high degree of confidence. The identification of other fragments can be predicted if they are assumed to be joined, and if these conjoined fragments are doubly charged. For instance the peak at m/z of 1772.8695 in the wild-type spectra could be fragment 29 joined to fragment 16 with a charge of 2+. However, such peaks must be identified with caution as this peak could also correspond to fragment 14 attached to fragment 9 with a double charge.

The Ser163Arg mutation has created an extra trypsin cleavage site in the mutant, as can be seen from tables 4.3 and 4.4. Fragments which differ between the two proteins are highlighted in yellow. It is possible to identify m/z peaks which differ between the wild-type and mutant spectra, and which could be the result of different cleavages between the two proteins. For instance, the m/z peak at 815.4352 in the wild-type could contain one such fragment (fragment 25), with this peak not present in the mutant spectra. The m/z peak at 2016.8932 present in the mutant is of the correct size to contain fragments 25 or 26, which contain the 163Arg mutation and are not found in the wild-type.

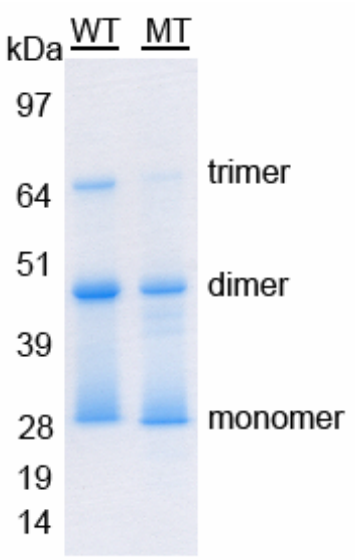

Figure 4.19: Reducing SDS-PAGE of wild type (WT) and mutant (MT) His-C1QTNF5.

Bands corresponding to momoner and dimer were excised from the gel for analysis by MALDI-TOF MS. The additional bands seen in the mutant at approximately 40kDa were also excised and analysed. kDa: relative molecular mass

	Mass	Position	Missed cleavages	Peptide sequence
1	885.4312	1-8	0	SPPLDDNK
2	3392.692	1-34	1	SPPLDDNKIPSLCPGHPGLP
3	2526.278	9-34	0	IPSLCPGHPGLPGTPGHHGS QGLPGR
4	2854.428	9-37	1	IPSLCPGHPGLPGTPGHHGS
5	675.3168	35-40	1	DGRDGR
6	1226.576	38-50	1	DGRDGAPGAPGEK
7	898.4264	41-50	0	DGAPGAPGEK
8	2029.021	41-62	1	DGAPGAPGEKGEGGRPGLPG PR
9	1149.612	51-62	0	GEGGRPGLPGPR
10	1728.889	51-68	1	GEGGRPGLPGPRGDPGPR
11	598.2943	63-68	0	GDPGPR
12	2386.12	63-88	1	GDPGPRGEAGPAGPTGPAGE CSVPPR
13	1806.844	69-88	0	GEAGPAGPTGPAGECSVPPR
14	2398.146	69-94	1	GEAGPAGPTGPAGECSVPPR SAFSAK
15	610.3195	89-94	0	SAFSAK
16	766.4206	89-95	1	SAFSAKR
17	634.3267	95-99	1	RSESR
18	1866.934	96-112	1	SESRVPPPSDAPLPFDR
19	1407.727	100-112	0	VPPPSDAPLPFDR
20	3018.532	100-127	1	VPPPSDAPLPFDRVLVNEQG HYDAVTGK
21	1629.823	113-127	0	VLVNEQGHYDAVTGK
22	3831.895	113-146	1	VLVNEQGHYDAVTGKFTCQV
23	2221.09	128-146	0	FTCQVPGVYYFAVHATVYR
24	3222.644	128-155	1	FTCQVPGVYYFAVHATVYRA SLQFDLVK
25	1020.572	147-155	0	ASLQFDLVK
26	3946.995	147-183	1	ASLQFDLVKNGESIASFFQF
27	2945.44	156-183	0	NGESIASFFQFFGGWPKPAS LSGGAMVR
28	5604.794	156-207	1	NGESIASFFQFFGGWPKPAS LSGGAMVRLEPEDQVWVQV
29	2678.371	184-207	0	LEPEDQVWVQVGVGDYIGIY ASIK
30	5009.42	184-228	1	LEPEDQVWVQVGVGDYIGIY
31	3173.37	208-228	0	TDSTFSGFLVYSDWHSSPVF AHHHHHH

Table 4-1: Predicted peptide fragments for trypsin digested wild type His-C1QTNF5.

Fragment masses are calculated assuming no post-translational modifications. Fragment sizes were calculated assuming cleavage occurred at every (black) or every other (blue) predicted trypsin cleavage site.

	mass	position	#MC	peptide sequence
1	885.4312	1-8	0	SPPLDDNK
2	3392.692	1-34	1	SPPLDDNKIPSLCPGHPGLP GTPGHHGSQGLPGR
3	2526.278	9-34	0	IPSLCPGHPGLPGTPGHHGS QGLPGR
4	2854.428	9-37	1	IPSLCPGHPGLPGTPGHHGS QGLPGRDGR
5	675.3168	35-40	1	DGRDGR
6	1226.576	38-50	1	DGRDGAPGAPGEK
7	898.4264	41-50	0	DGAPGAPGEK
8	2029.021	41-62	1	DGAPGAPGEKGEGGRPGLPG PR
9	1149.612	51-62	0	GEGGRPGLPGPR
10	1728.889	51-68	1	GEGGRPGLPGPRGDPGPR
11	598.2943	63-68	0	GDPGPR
12	2386.12	63-88	1	GDPGPRGEAGPAGPTGPAGE CSVPPR
13	1806.844	69-88	0	GEAGPAGPTGPAGECSVPPR
14	2398.146	69-94	1	GEAGPAGPTGPAGECSVPPR SAFSAK
15	610.3195	89-94	0	SAFSAK
16	766.4206	89-95	1	SAFSAKR
17	634.3267	95-99	1	RSESR
18	1866.934	96-112	1	SESRVPPPSDAPLPFDR
19	1407.727	100-112	0	VPPPSDAPLPFDR
20	3018.532	100-127	1	VPPPSDAPLPFDRVLVNEQG HYDAVTGK
21	1629.823	113-127	0	VLVNEQGHYDAVTGK
22	3831.895	113-146	1	VLVNEQGHYDAVTGKFTCQV PGVYYFAVHATVYR
23	2221.09	128-146	0	FTCQVPGVYYFAVHATVYR
24	2448.228	128-148	1	FTCQVPGVYYFAVHATVYRA R
25	1089.642	147-155	1	ARLQFDLVK
26	862.5032	149-155	0	LQFDLVK
27	3788.926	149-183	1	LQFDLVKNGESIASFFQFFG GWPKPASLSGGAMVR
28	2945.44	156-183	0	NGESIASFFQFFGGWPKPAS LSGGAMVR
29	5604.794	156-207	1	NGESIASFFQFFGGWPKPAS LSGGAMVRLEPEDQVWVQVG
30	2678.371	184-207	0	LEPEDQVWVQVGVGDYIGIY ASIK
31	5009.42	184-228	1	LEPEDQVWVQVGVGDYIGIY ASIKTDSTFSGFLVYSDWHS
32	3173.37	208-228	0	TDSTFSGFLVYSDWHSSPVF AHHHHHH

Table 4-2: Predicted peptide fragments for trypsin digested mutant His-C1QTNF5.

Fragment masses are calculated assuming no post-translational modifications. Fragment sizes were calculated assuming cleavage occurred at every (black) or every other (blue) predicted trypsin cleavage site.

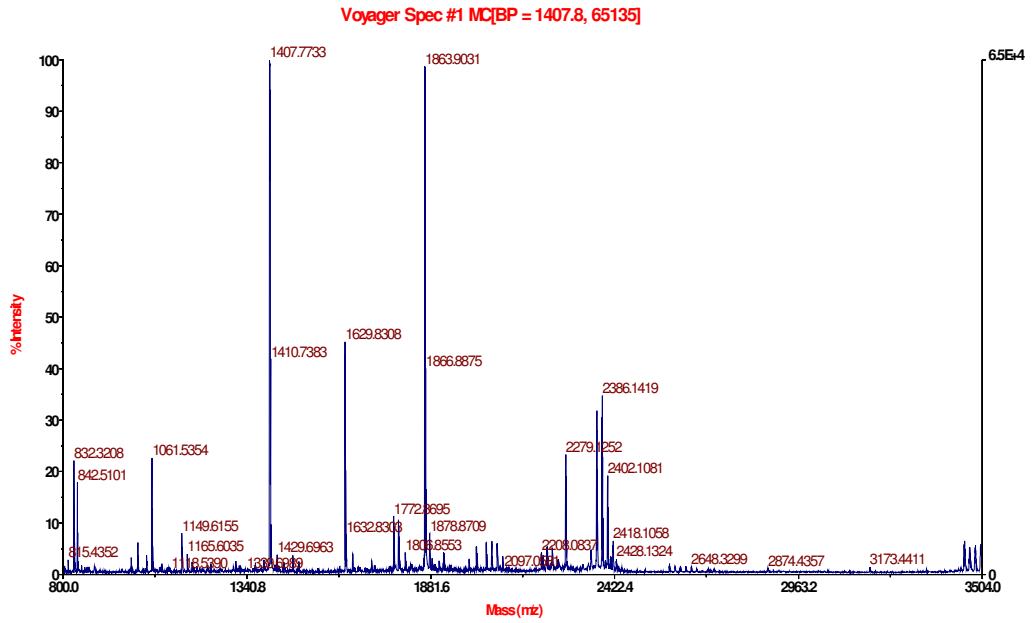

(A)

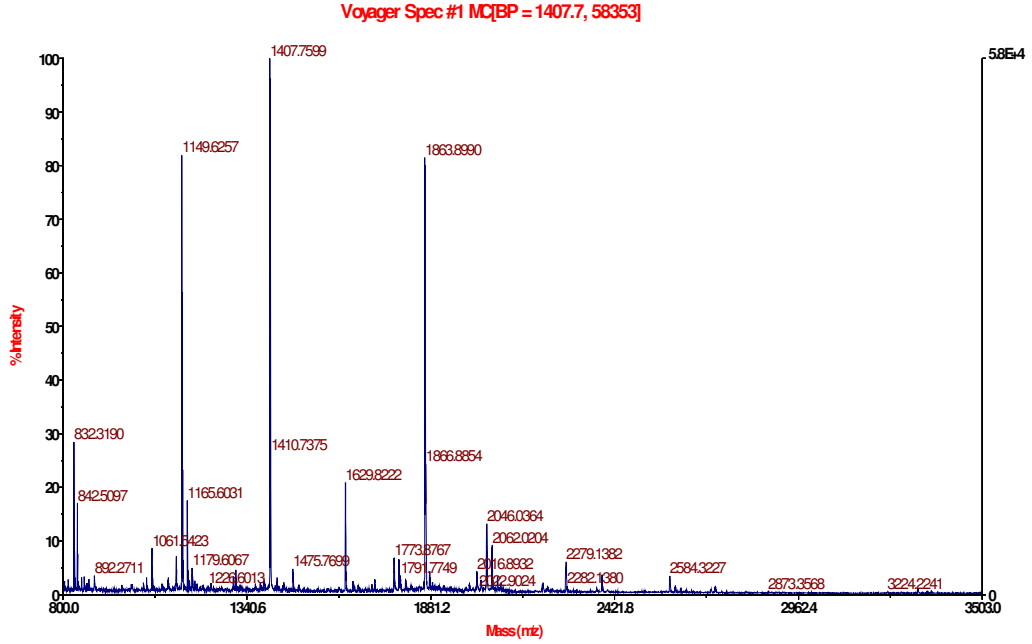

(B)

Figure 4.21: MALDI-TOF MS spectra for dimeric wild type (A) and dimeric mutant (B) His-C1QTNF5.

Proteins were excised from a reducing SDS-PAGE gel (Figure 4.19, bands 1 and 3) and digested with trypsin prior to MALDI-TOF MS analysis.

	Mass	Identified	Peak	Additional
1	885.4312	No		
2	3392.692	No		
3	2526.278	Possibly	2874.4357	Attached to fragment 24, charge 2+
4	2854.428	No		
5	675.3168	No		
6	1226.576	No		
7	898.4264	Possibly	832.3208	Attached to fragment 16, charge 2+
8	2029.021	Possibly	2208.037 1878.8709	Attached to fragment 12, charge 2+ Attached to fragment 11, charge 2+
9	1149.612	Yes	1149.6155 1772.8695*	Single peak, charge 1+ Attached to fragment 14, charge +
10	1728.889	No		
11	598.2943	Possibly	1878.8709 1808.8553	Attached to fragment 8, charge 2+ Attached to fragment 20, charge 2+
12	2386.12	Yes	2386.1419 2208.0837 2097.0581	Single peak, charge 1+ Attached to fragment 8, charge 2+ Attached to fragment 13, charge 2+
13	1806.844	Possibly	2097.0581	Attached to fragment 12, charge 2+
14	2398.146	Possibly	1772.8695*	Attached to fragment 9, charge 2+
15	610.3195	Possibly	2278.1252 815.4352	Attached to fragment 26, charge 2+ Attached to fragment 2, charge 2+
16	766.4206	Possibly	832.3208 1772.8695*	Attached to fragment 7, charge 2+ Attached to fragment 29, charge 2+
17	634.3267	No		
18	1866.934	Yes	1866.8875	Single peak, charge 1+
19	1407.727	Yes	1407.7733 1878.8709	Single peak, charge 1+ Attached to fragment 31, charge 2+
20	3018.532	Possibly	1808.8553	Attached to fragment 11, charge 2+
21	1629.823	Yes	1629.8308	Single peak, charge 1+
22	3831.895	No		
23	2221.09	No		
24	3222.644	Possibly	2874.4357	Attached to fragment 3, charge 2+
25	1020.572	Possibly	815.4352	Attached to fragment 15, charge 2+
26	3946.995	Possibly	2279.1252	Attached to fragment 15, charge 2+
27	2945.44	Possibly	2648.3299	Attached to fragment 31
28	5604.794	No		
29	2678.371	Possibly	1772.8695*	Attached to fragment 16, charge 2+
30	5009.42	No		
31	3173.37	Yes	3173.4411 1878.8709 2648.3299	Single fragment, charge 1+ Attached to fragment 19, charge 2+ Attached to fragment 27, charge 2+

Table 4-3: Comparative analysis of predicted fragments of trypsin digested wild type His-C1QTNF5 against peaks obtained by MALDI-TOF MS analysis of trypsin digested dimeric wild type His-C1QTNF5.

In the above table, some fragments were predicted to be present as single charged species (highlighted in red), whilst some were predicted to be joined to other fragments and to be present as doubly charged species. * indicates where one peak could be identified by more than one set of conjoined fragments. Fragments in grey are contained within the gC1q domain. Fragments in yellow differ between the wild type and mutant proteins due to an extra trypsin cleavage site in the mutant.

	Mass	Identified	Peak	Additional
1	885.4312	No		
2	3392.692	No		
3	2526.278	No		
4	2854.428	No		
5	675.3168	No		
6	1226.576	No		
7	898.4264	Yes	1226.6013 832.319	Single fragment, charge 1+ Attached to fragment 17, charge 2+
8	2029.021	No		
9	1149.612	Yes	1149.6257 2046.0364 1773.8769	Single fragment, charge 1+ Attached to fragment 28, charge 2+ Attached to fragment 15, charge 2+
10	1728.889	No		
11	598.2943	No		
12	2386.12	No		
13	1806.844	No		
14	2398.146	No		
15	610.3195	Possibly	1773.8767	Attached to fragment 9, charge 2+
16	766.4206	No		
17	634.3267	Possibly	832.319	Attached to fragment 7, charge 2+
18	1866.934	Yes	1866.8854	Single fragment, charge 1+
19	1407.727	Yes	1407.7599	Single fragment, charge 1+
20	3018.532	No		
21	1629.823	Yes	1629.8222	Single fragment, charge 1+
22	3831.895	No		
23	2221.09	Possibly	2584.3227	Attached to fragment 28, charge 2+
24	2448.228	No		
25	1089.642	Possibly	2016.8932*	Attached to fragment 28, charge 2+
26	862.5032	Possibly	2016.8932*	Attached to fragment 32, charge 2+
27	3788.926	No		
28	2945.44	Possibly	2046.0364 2584.3227 2016.8932*	Attached to fragment 9, charge 2+ Attached to fragement 23, charge 2+ Attached to fragement 25, charge 2+
29	5604.794	No		
30	2678.371	No		
31	5009.42	No		
32	3173.37	Possibly	2016.8932*	Attached to fragment 26, chage 2+

Table 4-4: Comparative analysis of predicted fragments of trypsin digested mutant His-C1QTNF5 against peaks obtained by MALDI-TOF MS analysis of trypsin digested dimeric mutant His-C1QTNF5.

In the table above, some fragments were predicted to be present as single charged species (highlighted in red), whilst some were predicted to be joined to other fragments and to be present as doubly charged species. * indicates where one peak could be identified by more than one set of conjoined fragments. Fragments in grey are contained within the gC1q domain. Fragments in yellow differ between the wild type and mutant proteins due to an extra trypsin cleavage site in the mutant.

4.4.5.3 MALDI-TOF MS analysis of native His-C1QTNF5

MALDI-TOF MS analysis was also carried out on undigested His-C1QTNF5 to ascertain if any differences could be observed between the native multimeric states of the wild-type and mutant proteins. Figure 4.22 shows the spectra obtained, with similar peaks observed for both proteins. Due to the measurements being taken close to the maximum possible m/z for the machine, background noise levels are high. Peaks at approximately 25000, 50000, 75000, 100000 and 125000 m/z correspond to multimeric His-C1QTNF5. It is not possible to say whether these correspond to monomeric, dimeric, trimeric etc species because, for instance, the peak at 25000 m/z could be monomeric protein with a charge of 1+ or trimeric protein with a charge of 3+. However, there were no obvious differences in the pattern of peaks obtained for the wild-type and mutant proteins.

A m/z shift was observed between the proteins, with the wild-type protein being slightly larger than the mutant protein (Figure 4.23). Table 4.5 shows the differences in m/z, before and after adjusting for the Ser163Arg mutation. It is possible these are caused by differences in post-translational modifications although it has not been possible to predict, based upon the m/z difference, what these could be.

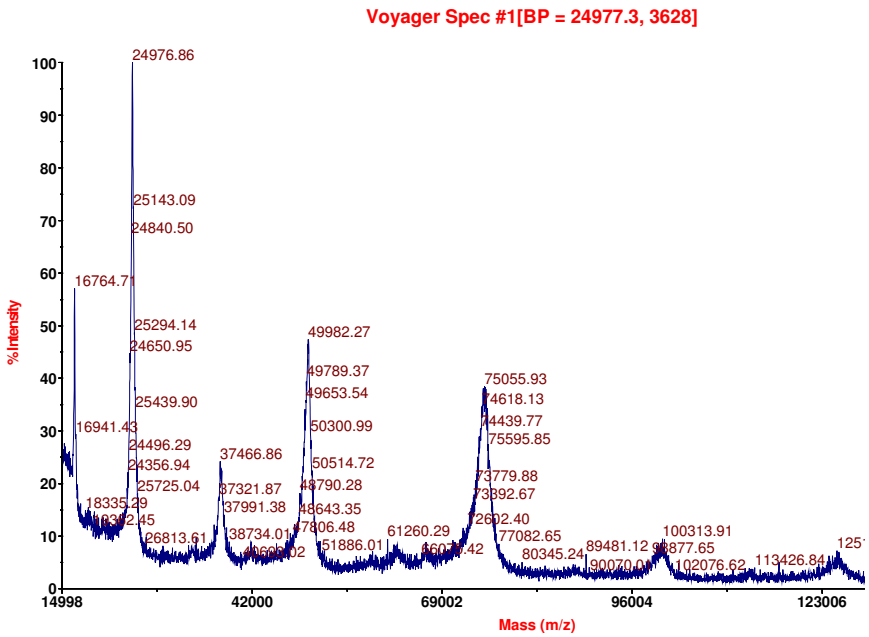

(A)

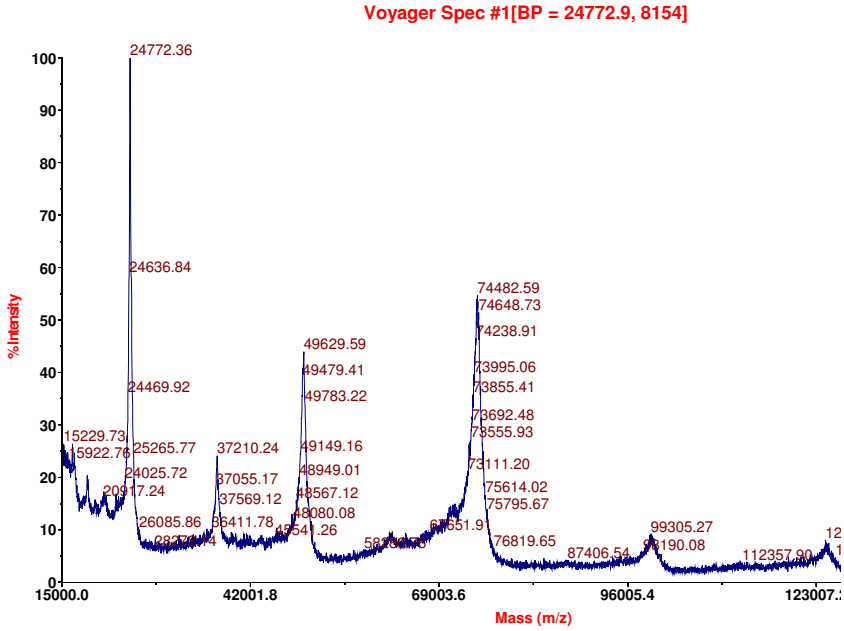

(B)

Figure 4.22: MALDI-TOF MS spectra of native wild type (A) and mutant (B) His-C1QTNF5.

Both proteins show similar multimeric species.

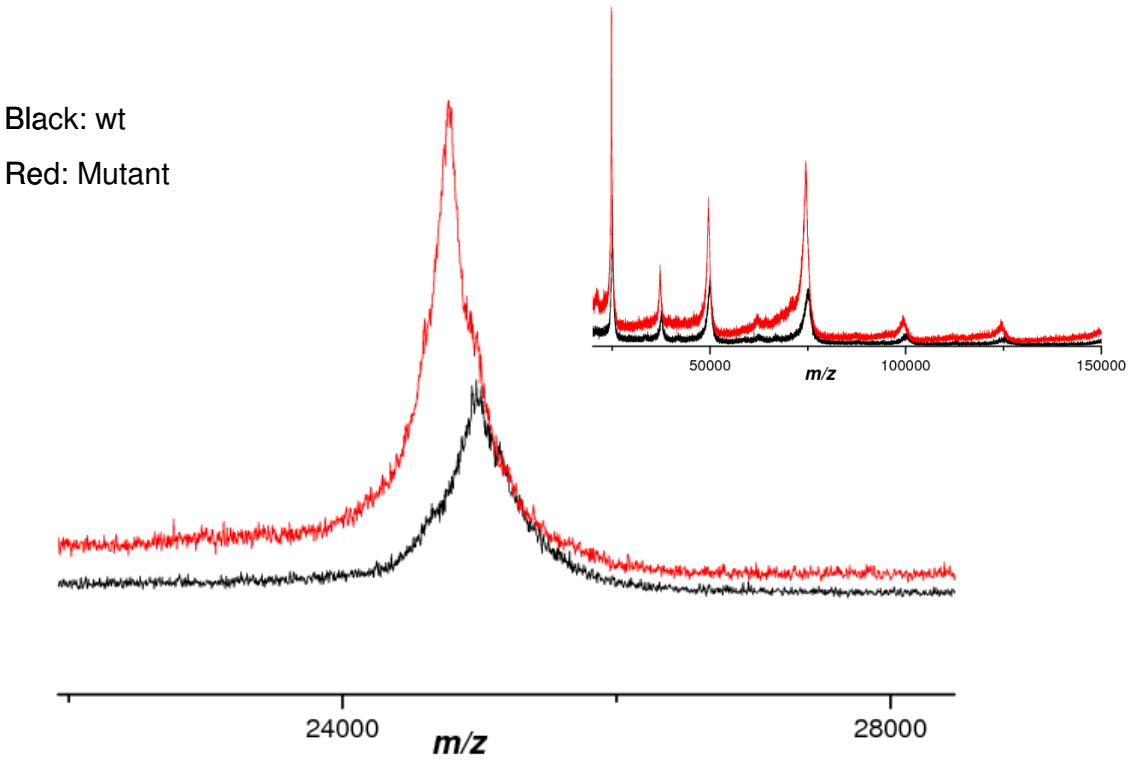

Figure 4.23: MALDI-TOF MS spectra for native wild type (black) and mutant (red) His-C1QTNF5.

A shift is observed in the m/z ration between the proteins, with the wild type protein being slightly larger.

	m/z	m/z	m/z	m/z
Wild type	24976.86	49982.27	75055.93	100313.9
Mutant	24772.36	49629.59	74482.59	99305.27
Difference	204.5	352.68	573.34	1008.64
Ser163Arg adjusted	272.8	489.28	778.24	1281.84

Table 4-5: Shows the difference in m/z for the main peaks in the wild type and mutant spectra, before and after adjusting for the Ser163Arg mutation.

4.5 Purifying His-C1QTNF5 from ARPE-19

His-C1QTNF5 has been successfully purified from stably transfected EBNA293 cells which express the protein at high levels. ARPE-19 is a physiologically relevant cell line, with stably transfected ARPE-19 cell lines created previously which express the protein at much lower levels (see Chapter 3). A small amount of wild-type and mutant His-C1QTNF5 was purified from the culture media of these cell lines and compared with the EBNA293-produced protein to see if there were any obvious differences, which may prevent the EBNA293-produced protein being suitable for use in future studies.

4.5.1 Expressing and purifying His-C1QTNF5

Stably transfected cell lines GFWT19 and GFMT22 were used to produce the protein. In both cell lines, His-C1QTNF5 has been shown to be secreted, so the protein was Ni-NTA affinity purified from culture medium following the same method as for EBNA293 produced protein. Eluted fractions were analysed by SDS-PAGE, as can be seen in Figures 4.24. Wild-type fractions were pooled and dialysed into PBS. Mutant fractions were also pooled and dialysed into PBS.

4.5.2 Reducing and non-reducing analysis of His-C1QTNF5

Reducing and non-reducing Western blots were carried out for both wild-type and mutant pooled proteins (Figure 4.25). The same banding pattern, corresponding to protein multimers, was observed for wild-type and mutant, with multimeric species observed under both reducing and non-reducing conditions. Higher order multimers (greater than trimeric) were observed under non-reducing conditions which were not observed under reducing conditions. This was the same as was observed for EBNA293-produced His-C1QTNF5.

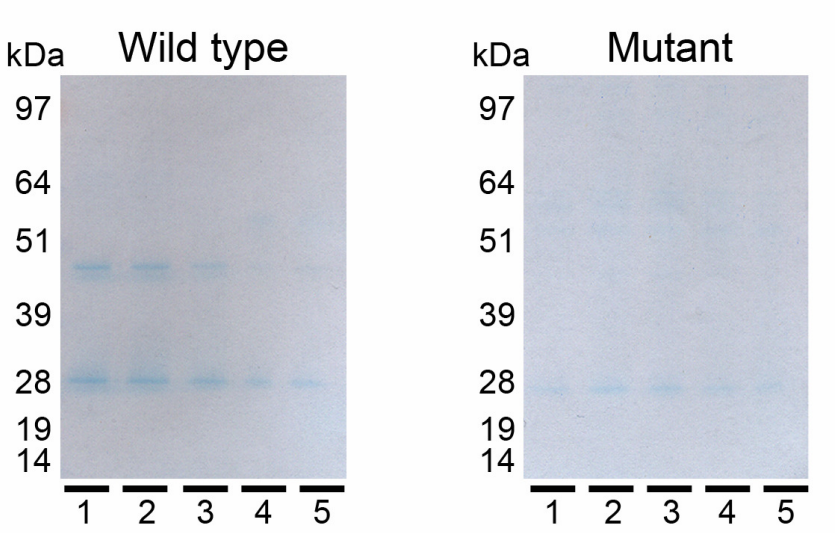

Figure 4.24: Reducing SDS-PAGE of successive eluted fractions for wild-type and mutant His-C1QTNF5 purified from stably transfected ARPE-19 cell lines.

In both instances, fractions 1 – 5 were pooled and dialysed into PBS. kDa: relative molecular mass

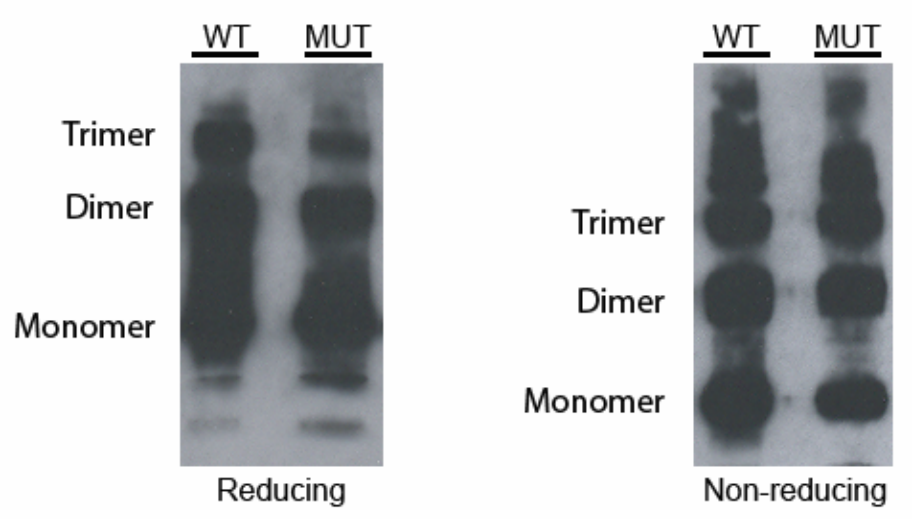

Figure 4.25: Reducing and non-reducing SDS-PAGE of pooled His-C1QTNF5 fractions for wild-type (WT) and mutant (MUT) His-C1QTNF5, purified from stably transfected ARPE-19 cell lines.

Primary anitbody – mouse anti-His; secondary antibody – rabbit anti-mouse HRP.

4.5.3 MALDI-TOF MS analysis of ARPE-19-produced His-C1QTNF5

MALDI-TOF MS analysis was carried out on native wild-type and mutant His-C1QTNF5 purified from ARPE-19. Figure 4.26 shows the spectrum obtained for the wild-type protein. The protein was very dilute and there was an insufficient amount to concentrate without losing it, so the spectra obtained is not very clear. Peaks can be observed at m/z of 24971.57, 37147.75 and 49932.44, which are almost identical to those obtained for the wild-type EBNA-produced protein. This would indicate that the EBNA protein is very similar, if not identical to the ARPE-19 protein and so suitable for use in future assays. There was insufficient mutant His-C1QTNF5 for spectra to be obtained.

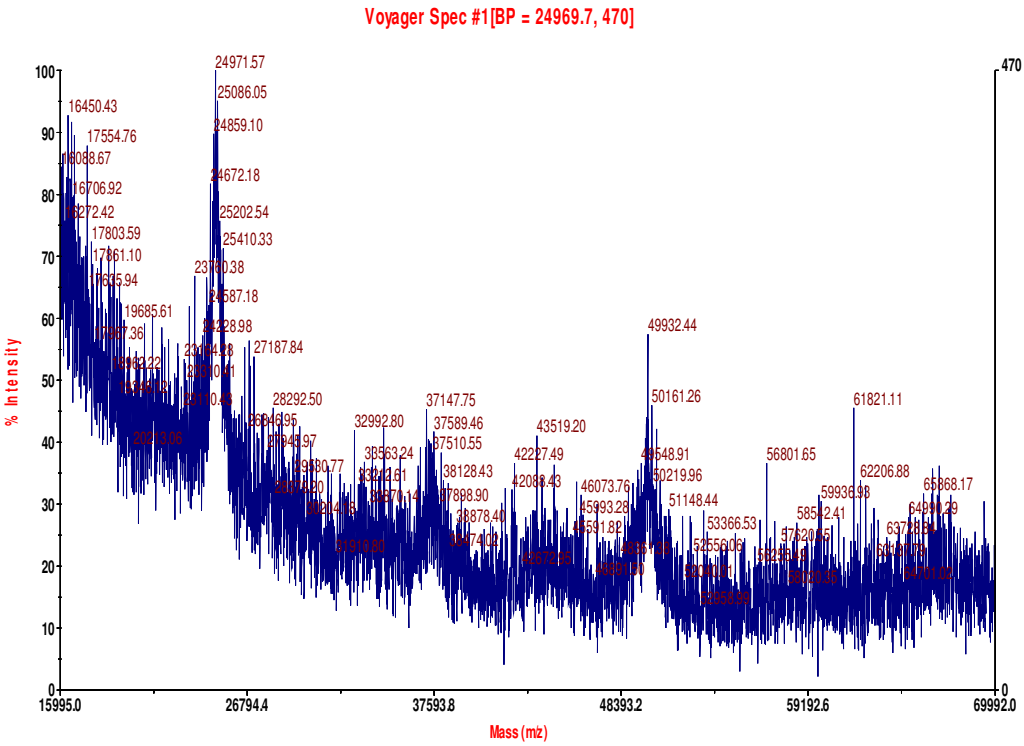

Figure 4.26: MALDI-TOF MS spectra of native wild type His-C1QTNF5 purified from the culture media of stably transfected ARPE-19.

4.6 Discussion

Recombinant, secreted wild-type and mutant His-C1QTNF5 has been purified from a mammalian expression system for use in future assays. Recombinant His-gC1q has also been purified from a bacterial expression system. Confirming the observation from Chapter 3, both wild-type and mutant His-C1QTNF5 were secreted when expressed in EBNA293. It was also shown that, when stably expressed in EBNA293, the mutant protein appears to undergo the same cellular trafficking as the wild-type and is not retained within the ER. Both these results are different from those reported previously when His-C1QTNF5 was stably expressed in EBNA293 (Shu *et al.,* 2006b). It is possilbe that secreted mutant His-C1QTNF5 was not detected in the previous study due to differences in detection methods. For instance, Shu *et al.* analysed acid-precipitated culture media proteins, whereas in this study His-tagged proteins were affinity purified using Ni-NTA beads. It is also possible that only a small amount of culture media was analysed so a low level of secreted mutant His-C1QTNF5 could not be detected. Mandal *et al.* (2006c) also reported a lack of secretion for mutant C1QTNF5. However, it is not stated how the culture medium was analysed so again it is possible that their detection method was not sensitive enough to detect a low level of protein. In the present study, mutant His-C1QTNF5 has been detected in the culture media of both stably transfected EBNA293 and ARPE-19 cells so it can be concluded that the mutant protein, like the wild type, is indeed secreted. Immunostaining of wild-type and mutant His-C1QTNF5-expressing EBNA293 was also contradictory to that reported previously (Shu *et al.,* 2006b), however it is not possible to explain how the previous result was obtained, and retention within the ER is not observed in this study. Combining these results with those from Chapter 3 makes it unlikely that the disease mechanisms in L-ORMD are due to a lack of secretion or retention of the mutant C1QTNF5 within the ER. It is more likely that altered function of the mutant protein contributes to the disease mechanisms.

Recombinant His-C1QTNF5 has been produced in order to investigate an altered function of the 163Arg mutant. Characterisation studies were carried out comparing the wild-type and mutant proteins and are summarised as follows. Both proteins were found to be soluble in PBS at 37°C, although the mutant precipitated at room temperature. SDS-PAGE analysis showed that both wild-type and mutant formed monomers, dimers and trimers under reducing conditions, with additional bands seen in the mutant, but both forms also formed higher order multimers under non-reducing conditions. His-gC1q formed monomers, dimers and trimers under reducing and non-reducing conditions, and again formed higher order multimers. Native PAGE analysis showed wild-type His-C1QTNF5 to be present as predominantly trimers but also some hexamers. The mutant protein would not migrate through the gel. However, both proteins migrated through an isoelectric focusing gel, with the wild-type protein present as two species with pI's of 7.5 and 6.8 (possibly trimers and hexamers) and the mutant as a single species with pI of 6.5. MALDI-TOF MS analysis of trypsin digested His-C1QTNF5 confirmed that both the purified recombinant proteins were C1QTNF5 and that the additional bands in the mutant were also C1QTNF5. Differences in spectra were observed between the two proteins, and possible sites of disulphide or covalent bonds were identified. Native MALDI-TOF MS showed that both forms of the protein have similar multimeric species and, although a shift was observed between them, the pattern of peaks otherwise appeared to be the same.

These protein characterisation studies highlighted several similarities and differences between the wild-type and mutant proteins. Similarities were observed when reducing SDS-PAGE analysis was carried out. The same multimeric species were observed for wild-type and mutant His-C1QTNF5 and His-gC1q, and these species also showed resistance to reducing conditions. This confirms previous studies which have identified the gC1q domain as being involved in C1QTNF5 trimerisation (Shu *et al.,* 2006a, Hayward *et al.,* 2003). The resistance of the trimers to reduction has been observed in other gC1q-containing proteins such as C1q and collagens X and VIII, and is proposed to be due to buried Ca^{2+} clusters providing ionic bonds and stability to the trimers (Kishore *et al.,* 2004a, Kishore *et al.,* 2004b, Bogin *et al.,*

2002, Stephan *et al.,* 2004). Due to the homology between C1QTNF5 and these gC1q-containing proteins, it is highly likely that the same Ca^{2+} clusters are present in this instance too.

Non-reducing SDS-PAGE showed the presence of higher order multimers for wild-type and mutant His-C1QTNF5, suggesting the presence of disulphide-linked or other tertiary structures resistant to SDS. Some higher order multimers were also present in His-gC1q, although to a much lesser degree. This suggests that the collagen domain (missing in His-gC1q) is at least partially involved in C1QTNF5 higher order multimerisation. It has been suggested that C1QTNF5 may form a hexagonal lattice similar to collagen X or VIII via interactions between the gC1q domains (Hayward *et al.,* 2003, Mandal *et al.,* 2006c). However, for these collagens, higher order multimer formation is predicted to occur via interactions between N- and C-terminal globular regions, with C-terminal C1q-like domains involved in trimerisation and the N-terminal non-collagenous domains interacting with this trimeric head group to form 3D tetrahedral structures (Bogin *et al.,* 2002, Stephan *et al.,* 2004). C1QTNF5 only has a C-terminal gC1q domain, so it is possible that C1QTNF5 forms the tulip-like clusters predicted for C1q and MBL, where the collagen tails of the trimers interact to form bunch-like structures (Kishore *et al.,* 2004b).

Native PAGE analysis of His-C1QTNF5 at 37°C showed that the wild-type protein was present as predominantly trimeric with weaker hexameric species. Such hexamers may account for the higher order multimers seen by non-reducing SDS-PAGE analysis of full length His-C1QTNF5. The mutant protein would not migrate through the gel. Both proteins however migrated through an isoelectric focusing gel, which showed them to have altered pI's. The wild-type protein was present as two species of pI 7.5 and pI 6.8, which could correspond to trimeric and hexameric protein. The mutant protein had a pI of 6.5. This implies the conditions used when carrying out native PAGE were suitable for migration of both proteins based upon their pI and another factor must be responsible for the lack of migration of the mutant. Mutant His-C1QTNF5 does have a greater tendency to precipitate than the

wild-type protein in PBS, possibly the result of an altered surface charge. Both proteins were shown to be soluble in PBS at 37°C, but only the mutant precipitated at room temperature. It is possible that the mutant protein precipitated during the running of the native PAGE, preventing it from entering the gel. It should be noted that the mutant protein migrated through the stacking gel but then halted as it reached the main gel. It is possible that the alteration in gel pH may have caused precipitation which the wild-type protein was resistant to. It has previously been suggested that the failure of the mutant protein to migrate through the native PAGE is due to its aggregation (Hayward *et al.,* 2003, Shu *et al.,* 2006b), however no evidence for aggregation has been found so far, so that this suggestion is not supported by this study. In a previous study (Hayward *et al.,* 2003), aggregation due to the Ser163Arg mutation was also shown by looking at the solubility of *E. coli*-produced gC1q domains. However, it has been shown here that the mutant gC1q forms inclusion bodies when expressed in *E. coli*. Proteins which form such inclusion bodies are inherently mis-folded and insoluble, so no conclusions can be drawn about the native state of such a protein. In fact, it has been shown in this study that mutant full length His-C1QTNF5, as well as the wild-type, is indeed soluble.

MALDI-TOF MS analysis of both proteins highlighted similarities and differences between them. When analysing trypsin digested protein, differences in the peaks were observed which could be the result of an extra trypsin cleavage site introduced in the mutant by the 163Arg mutation. Peaks were also observed which could be trypsin digested fragments joined to each other. Proteins undergoing MALDI-TOF MS analysis are subject to conditions similar to those when analysed by non-reducing SDS-PAGE (Hortin, 2006), so any covalent or disulphide linked tertiary structures should remain. Such interactions had been predicted in this study by non-reducing SDS-PAGE analysis of His-C1QNF5 and His-gC1q. In particular, covalent bonding is predicted to occur in the gC1q head region and peaks which could be identified as two fragments from this region have been found, supporting this prediction. Native MALDI-TOF MS analysis showed both proteins formed similar multimeric species, again making it unlikely that the mutant protein is aggregated. A

shift was observed between the two proteins, with the mutant being slightly smaller. It is possible this is due to differences in post translational modifications between the proteins, for instance in O-glycosylation as this has been predicted to occur.

There is plenty of scope for further work into the differences between wild-type and mutant proteins. For instance, it has not been possible to determine the native multimeric state of the mutant protein in solution in PBS. Native PAGE analysis of the wild-type protein revealed it to consist of predominantly trimeric and weaker hexameric species, however the mutant would not migrate through the gel. Dynamic light scattering may be able to solve this question as both proteins were found to be soluble in PBS at 37°C. It is possible that the change in pH prevented the mutant protein from migrating through the native PAGE gel, so further investigation could be carried out to determine whether pH affects the solubility or multimeric state of both of the proteins. It is interesting to note that both proteins were soluble in 1M imidazole which is at pH10.0. Two species were present when the wild-type protein was analysed on an IEF gel. These could correspond to trimeric and hexameric protein. 2D gel analysis could help to confirm or deny this. MALDI-TOF MS analysis of trypsin digested protein fragments revealed possible sites for covalent and disulphide bonding. Further analysis of regions which were predicted to be joined could give insight into either the tertiary structure of C1QTNF5 or the nature of the interactions between the subunits involved in multimerisation. Any effects of the 163Arg could then be investigated which would have possible implications for disease mechanisms.

5 CHAPTER 5

:

INVESTIGATING AN INTERACTION BETWEEN C1QTNF5 AND CFH

5.1 Introduction

Several haplotypes and polymorphisms in CFH have been implicated in increased risk of developing AMD (Edwards *et al.,* 2005, Haines *et al.,* 2005, Klein *et al.,* 2005, Hageman *et al.,* 2005, Li *et al.,* 2006). CFH is a regulatory protein in the alternative pathway of the innate immune system and consists of 20 modules, or SCRs. One such disease-associated polymorphism (Y402H) occurs in SCR7. This module has been shown to have involvement in binding polyanions and CRP (Blackmore *et al.,* 1996, Jarva *et al.,* 1999, Giannakis *et al.,* 2003), although CFH binding to native CRP has been disputed (Hakobyan *et al.,* 2008). Studies into the effects of this polymorphism have shown that the two alleles differ in their ability to bind such polyanions (Clark *et al.,* 2006, Prosser *et al.,* 2007, Herbert *et al.,* 2007) and CRP (Skerka *et al.,* 2007, Laine *et al.,* 2007, Yu *et al.,* 2007), and this has implications for disease mechanisms. CFH is expressed by the RPE (Chen *et al.,* 2006, Mandal *et al.,* 2006), with aged CFH-deficient mice showing severe retinal abnormalities, accumulation of autofluorescent sub-retinal deposits and visual dysfunction (Coffey *et al.,* 2007). Due to the similarities in phenotype between L-ORMD and AMD, and the expression of both CFH and C1QTNF5 by the RPE, it was investigated in this lab whether an interaction between CFH and C1QTNF5 could be observed. Initial results, carried out by Dr X. Shu, suggested this was the case (unpublished data). Surface plasmon resonance (SPR) was carried out between recombinant gC1q and plasma-purified CFH, with an interaction observed (Figure 5.1). I^{125} plate binding assays showed an interaction between gC1q and CFH domains SCR6-8Y and SCR6-8H (Figure 5.2). It was also shown by gel mobility shift assays and heparin affinity columns that gC1q, like CFH, is capable of binding polyanions (Figure 5.3). This study further investigated the interaction, in particular interactions between CFH, SCR7-8, SCR3-4, SCR19-20 or CRP and His-gC1q or His-C1QTNF5 (wild-type and mutant).

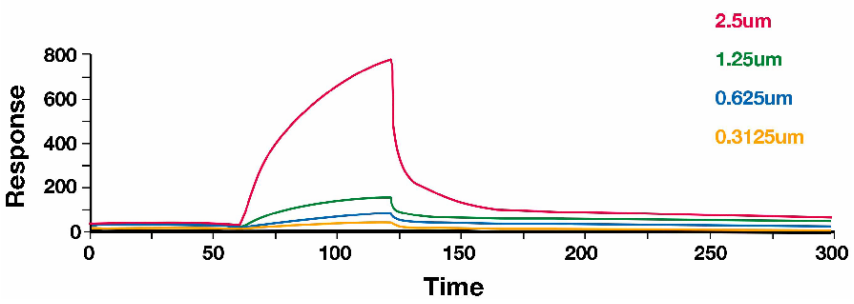

Figure 5.1: Surface plasmon resonance showing an interaction between gC1q and CFH.

gC1q was immobilized to the chip and increasing concentrations of CFH were added in the fluid phase (0.3125, 0.625, 1.25 and 2.5µM).

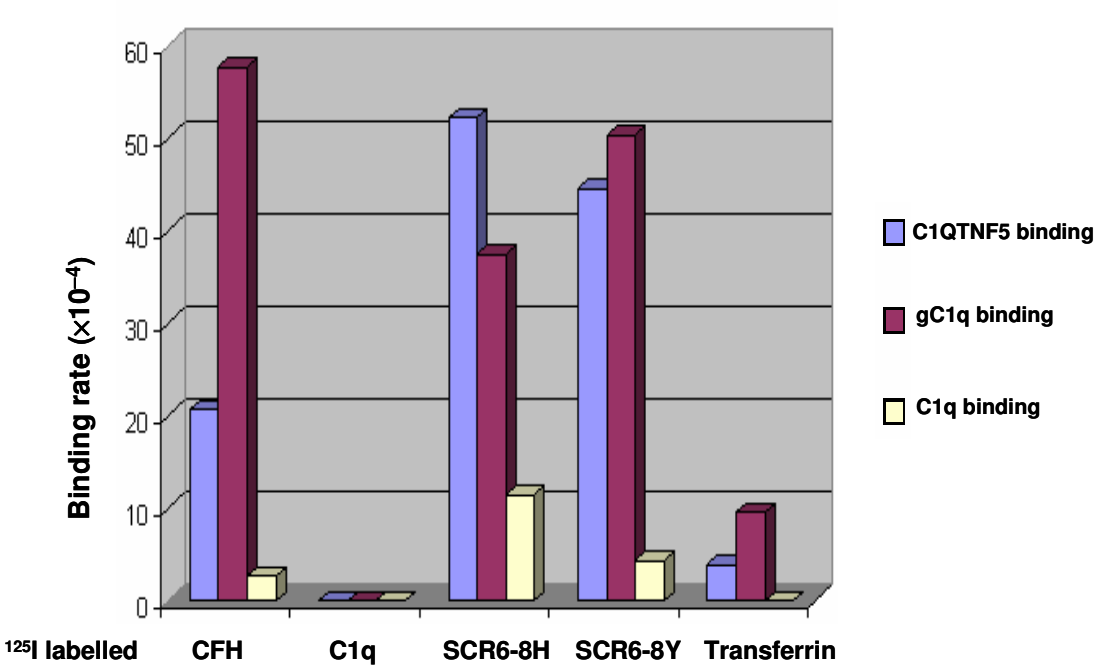

Figure 5.2: C1QTNF5 and gC1q interact with CFH, SCR6-8H and SCR6-8Y, but not C1q or transferrin.

Plates were coated with C1QTNF5, gC1q or C1q and I^{125}-labelled CFH, SCR6-8H, SCR6-8Y, C1q or transferrin were added in the fluid phase and levels of bound protein detected. Binding rates are given in counts per second and indicate levels of bound ^{125}I-labelled protein.

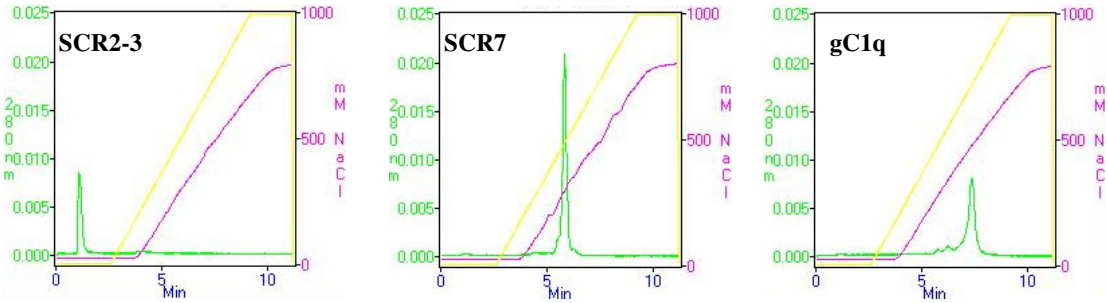

Figure 5.3: gC1q binds heparin with a higher affinity than SCR7.

The interactions were investigated using a heparin affinity column with proteins eluted in a NaCl gradient. SCR2-3 showed no interaction with the column, eluting in minimal NaCl. SCR7 showed an interaction with heparin and eluted from the column in approximately 0.5M NaCl. gC1q also showed an interaction with heparin and eluted in aproximately 0.75M NaCl, indicating it has a greater affinity for heparin than SCR7. Green - OD_{280}, Yellow - NaCl gradient, Pink - condctivity.

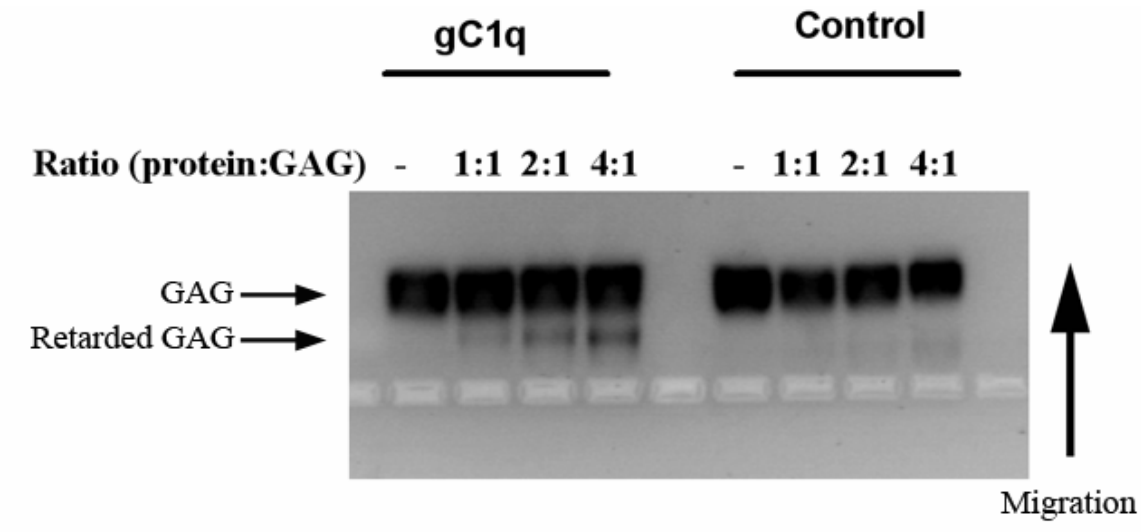

Figure 5.4: Gel mobility shift assay showing an interaction between gC1q and heparin DP12

GAG migration is retarded when it interacts with gC1q. (GAG - heparin DP12, DP - degree of polymerisation, Control: no gC1q)

5.2 Producing CFH and related proteins for use in assays

As discussed in Chapter 4, recombinant His-C1QTNF5 and His-gC1q have already been produced for use in assays. It was necessary however to produce CFH and the recombinant SCR modules to further investigate the CFH-C1QTNF5 interaction. CFH was purified from human plasma, as described previously (Sim *et al.,* 1993) and supplied by Professor R. Sim (Oxford University). *Pichia pastoris* clones expressing recombinant SCR 7-8 (tyrosine and histidine alleles) and SCR19-20 were supplied by Dr A. Herbert (Edinburgh University) and were used to express and purify these proteins. SCR3-4 had previously been produced and was supplied by Dr H. Hocking (Edinburgh University), and CRP was commercially produced (Sigma).

5.2.1 Expressing and purifying SCR7-8Y and SCR7-8H

Following large scale culture of the expressing *P. pastoris* clones and following the method optimised by Dr A. Herbert, SCR7-8Y and SCR7-8H were purified from the culture supernatants by SP sepharose ion exchange chromatography. Proteins were eluted with 1M NaCl, 20mM potassium phosphate pH6.0 and analysed by reducing SDS-PAGE. Figure 5.5 (A and B) shows elution fractions for SCR7-8Y and SCR7-8H, with the protein-containing fractions for each protein pooled. Pooled eluates were then dialysed into PBS, analysed by reducing SDS-PAGE (Figure 5.7) and protein concentration determined by Bradford assay (see section 4.4.1).

5.2.2 Expressing and purifying SCR19-20

Again following large scale culture of the expressing *P. pastoris* clone, SCR19-20 was purified from the culture supernatant by SP sepharose ion exchange chromatography. Proteins were eluted with 1M NaCl, 20mM potassium phosphate pH7.0 and analysed by reducing SDS-PAGE. Figure 5.6 shows the elution fractions. All eluates were pooled and dialysed into PBS, analysed by reducing SDS-PAGE (Figure 5.7) and protein concentration again determined by Bradford assay.

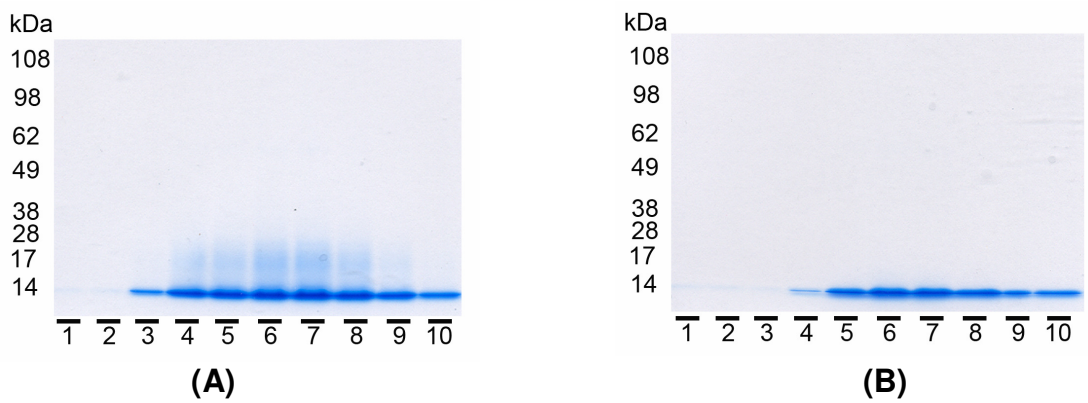

Figure 5.5: Reducing SDS-PAGE of successive elution fractions for SCR7-8Y (A) and SCR7-8H (B), purified from the culture media of transfected *P. pastoris* by SP-sepharose ion exchange chromatography.

Proteins were eluted in 2ml fractions of 1M NaCl, 20mM potassium phosphate pH6.0. Elution fractions containing protein were pooled for dialysis into PBS. kDa: relative molecular mass

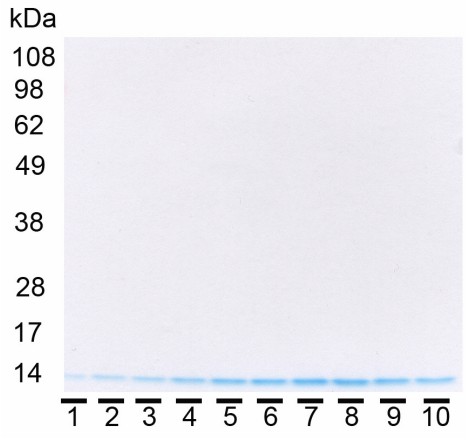

Figure 5.6: Reducing SDS-PAGE of successive elution fractions for SCR19-20 purified from the culture media of transfected *P. pastoris* by SP-sepharose ion exchange chromatography.

Proteins were eluted in 2ml fractions of 1M NaCl, 20mM potassium phosphate pH7.0. Elution fractions containing protein were pooled for dialysis into PBS. kDa: relative molecular mass

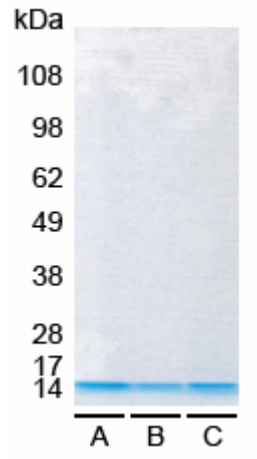

Figure 5.7: Reducing SDS-PAGE of pooled and dialysed elution fractions for SCR7-8Y (A), SCR7-8H (B) and SCR19-20 (C).

kDa: relative molecular mass

5.3 Plate binding assays

Previous I^{125} plate binding assays carried out by Dr X. Shu had shown there was an interaction between SCR6-8 and gC1q. This interaction was investigated further using full length His-C1QTNF5 (wild-type and mutant) or His-gC1q. Plates were coated overnight with a fixed concentration of His-gC1q at 4°C, or His-C1QTNF5 at 37°C (due to mutant His-C1QTNF5 being soluble at this temperature but not at 4°C). Following blocking, varying concentrations of CFH were added in the fluid phase. Bound CFH was then detected with a mouse anti-CFH primary antibody, OX23. OX23 was supplied by Prof R. Sim, and recognises both CFH and FHL-1, implying the antibody epitope is located in SCR1-7. Bound OX23 was then detected with a secondary rabbit anti-mouse alkaline phosphatase-labelled antibody and p-nitrophenyl phosphate, unless otherwise specified.

5.3.1 Plate binding assay optimisation

Following an initial, unoptimised method, it was investigated whether an interaction could be observed between His-gC1q and CFH. However, as can be seen from Figure 5.8, following 10 minutes incubation both total binding and background binding to the plate are reaching saturation. Specific binding was calculated by deducting background binding from the total binding. It was not possible to accurately detect an interaction between His-gC1q and CFH without optimising the method. Optimisation was carried out in order to reduce background binding, determine an appropriate primary (OX23) antibody concentration and optimise detection incubation time.

5.3.1.1 Optimising primary antibody concentration

Using the same amount of His-gC1q coat and CFH and secondary antibody concentrations as previously, different primary antibody (OX23) concentrations were investigated, in combination with increasing detection incubation times (Figure 5.9). Primary antibody concentrations were 1/34, 1/340, 1/1000 and 1/3400 dilutions of the stock solution (340µg/ml), and incubation times were 10, 20 and 30 minutes. A primary antibody concentration of 1:340, diluted in PBS, and an incubation time of

20 minutes were found to be suitable to give a sufficiently high signal without reaching saturation. It should be noted that the total binding appears to peak at approximately 0.5µg/ml CFH and then decline. Background binding was not deducted.

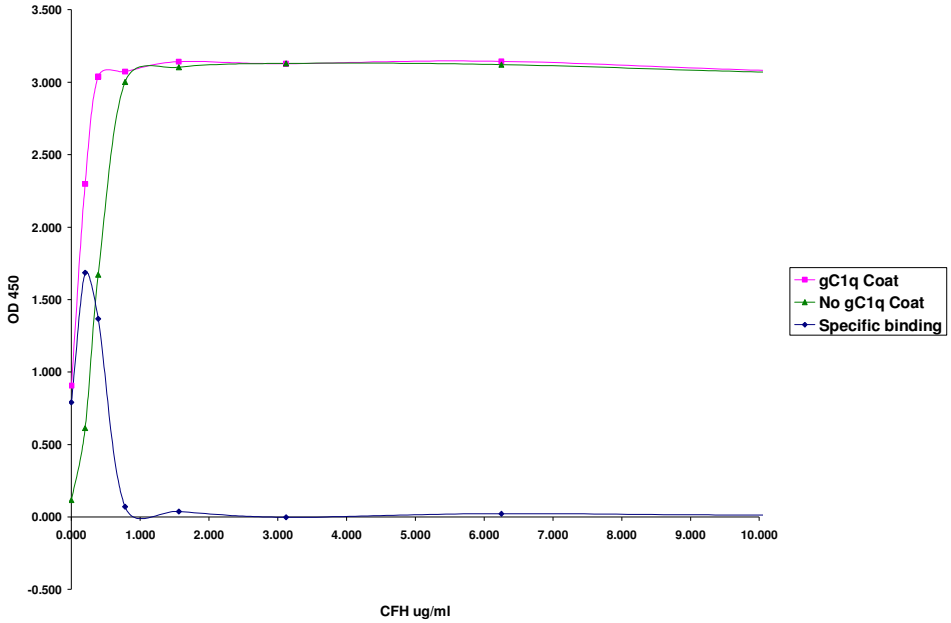

Figure 5.8: An un-optimised plate binding assay investigating an interaction between His-gC1q and CFH.

His-gC1q was immobilised to the plate and increasing concentrations of CFH were added in the fluid phase. Bound CFH was detected with OX23, which in turn was detected with alkaline phosphatase-labelled rabbit anti-mouse antibody. This was detected using p-nitrophenyl phosphate. Due to high background binding of CFH to uncoated wells and detection saturation it was not possible to accurately determine any interaction with His-gC1q. The assay required optimising.

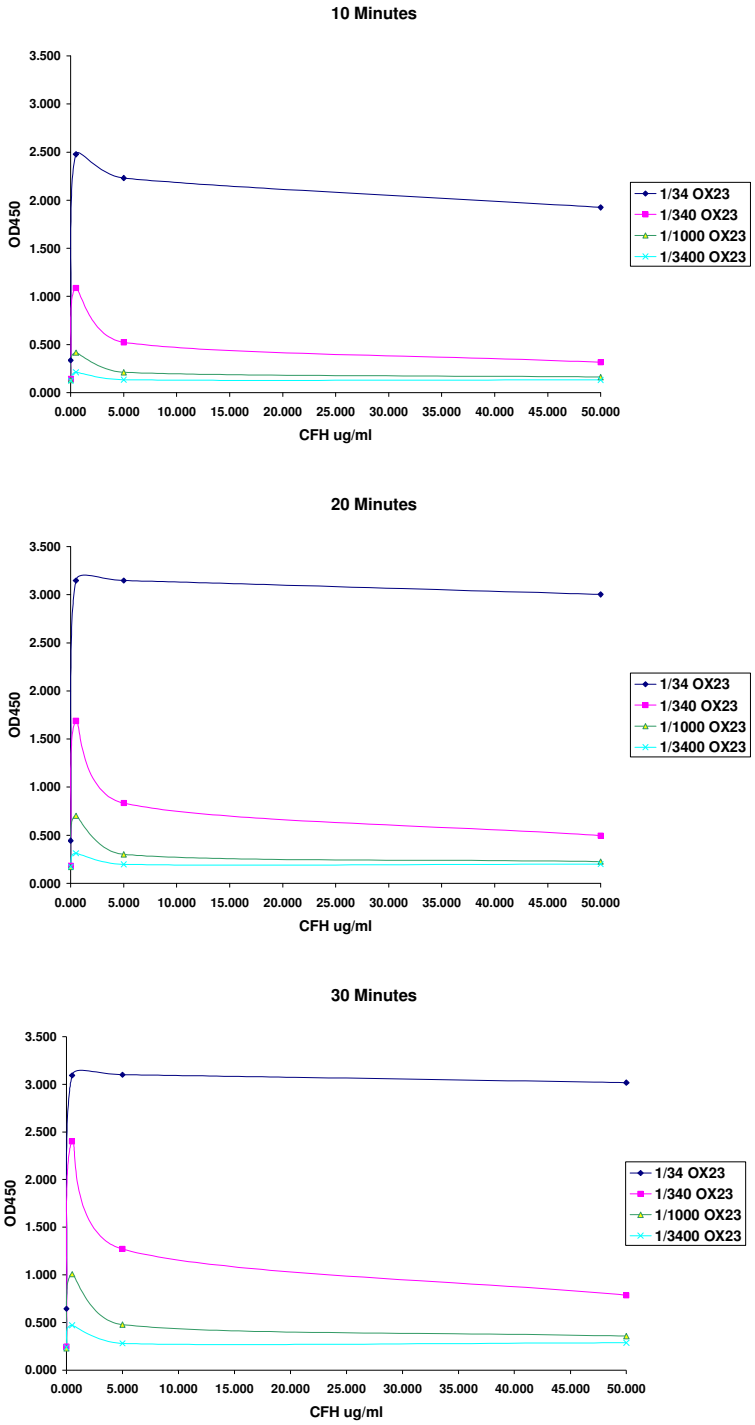

Figure 5.9: Plate binding assays optimising OX23 concentration and detection incubation time.

Increasing concentrations of CFH were added to His-gC1q-coated plates, and this was then detected with OX23 at varying dilutions of a stock solution (1/34, 1/340, 1/1000, 1/3400). Bound OX23 was detected using an alkaline phosphtase-labelled rabbit anti-mouse antibody and detected with p-nitrophenyl phosphate. Detection incubation times were 10, 20 and 30 minutes.

An OX23 dilution of 1/340 and a detection time of 20 minutes were considered optimai, with the OD_{450} remaining below 2.0. As before, CFH binding appears to increase up to a concentration of approximately 0.5µg/ml, after which it decreases. Total binding only is shown.

5.3.1.2 Optimising pH

As can be seen from Figure 5.8, background binding of CFH to the blocked wells is high. CFH was added to the wells after diluting in PBS pH7.2. It was investigated whether adding CFH diluted in 10mM MES at pH6.0 or pH6.5 would reduce the background binding whilst still allowing for the interaction with His-gC1q to occur. At pH6.5 specific binding of CFH to the His-gC1q-coated wells was the same as at pH7.2, however background binding was considerably less. At pH6.0 the background binding was reduced further still, however there was also a reduction in specific binding (Figure 5.10). All future assays were carried out diluting CFH in 10mM MES pH6.5.

5.3.1.3 Optimising His-gC1q coat concentration

The microtitre plates were coated with His-gC1q diluted in PBS at varying concentrations to determine which concentration enabled maximum CFH binding without applying an excess of His-gC1q. As can be seem from Figure 5.11, 1µg/well His-gC1q appeared to give nearly the maximum bound CFH per well. Increasing His-gC1q concentration to 10µg/ml did not greatly increase the maximum bound CFH. It should be noted again that CFH binding appears to peak and then decline. In this instance specific binding was reported, having deducted any background binding from the total. 1µg/well His-gC1q was used to coat the wells in all future assays.

5.3.2 Plate binding assay

Following the optimised conditions from Section 5.3.1, plate binding assays were carried out investigating CFH interactions with His-gC1q and His-C1QTNF5 (wild-type and mutant). Interactions were also investigated between CFH and CRP or His-C1QTNF5 and CRP.

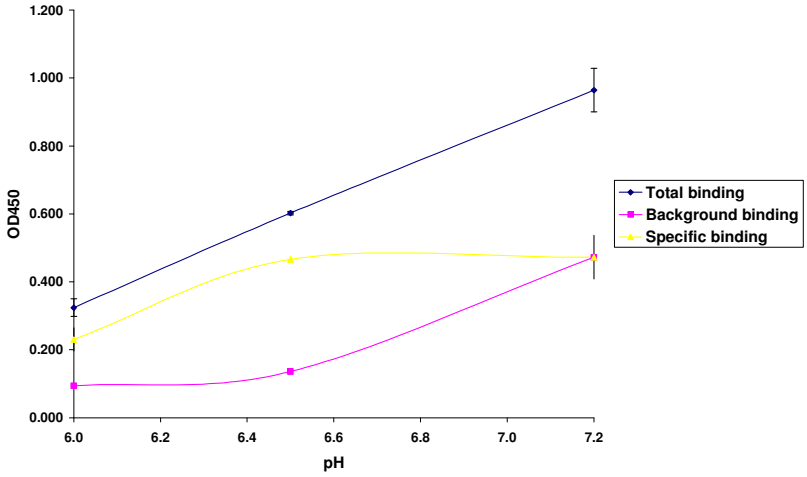

Figure 5.10: Diluting CFH in 10mM MES pH6.5 reduced background binding without reducing specific binding, when compared with PBS pH7.2.

Diluting CFH in 10mM MES pH6.0 reduced background binding further still but there was also a reduction in specific binding. Plates were coated with 1µg/well His-gC1q. Primary antibody: OX23, secondary antibody: alkaline phosphatase-labelled rabbit anti-mouse.

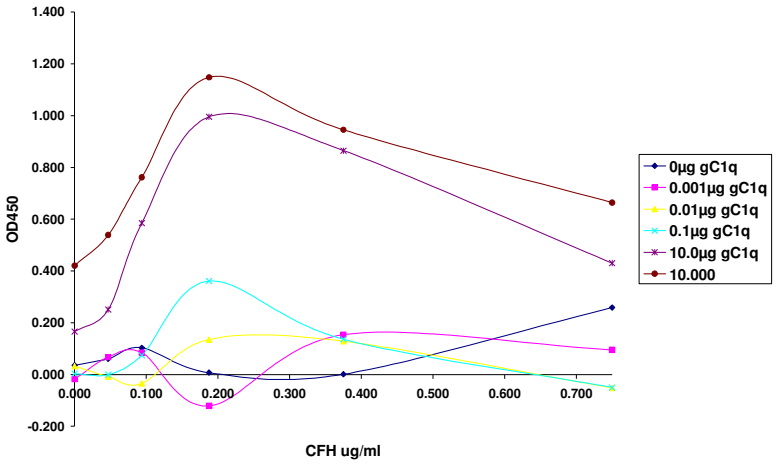

Figure 5.11: Coating the wells with 1µg/well His-gC1q is optimal for carrying out the plate binding assay.

Concentrations below this are limiting for the amount of CFH binding, and concentrations above this do not greatly increase it.

5.3.2.1 Plate binding assay investigating an interaction between His-gC1q and CFH

CFH (fluid phase) was found to bind to His-gC1q (solid phase) at pH6.5 (Figure 5.12). CFH specific binding appeared to increase up to a CFH concentration of nearly 0.5µg/ml, after which an apparent reduction in binding was observed. Specific binding is calculated by deducting the background binding from the total binding, so when background binding is greater than total binding the specific binding appears to be negative. It should be noted that no interaction could be found when CFH was in the solid phase and His-gC1q was in the fluid phase (primary antibody: mouse anti-His).

5.3.2.2 Plate binding assay investigating an interaction between CFH and His-C1QTNF5

CFH (fluid phase) was found to interact with His-C1QTNF5 (solid phase) at pH6.5 (Figure 5.13). Interactions were observed with both wild-type and mutant His-C1QTNF5 and, as observed in Figure 5.12, CFH specific binding appeared to increase up to a maximum CFH concentration (in this instance approximately 0.15µg/ml) after which an apparent reduction in binding was observed. Again, specific binding was calculated by deducting the background binding from the total binding, so when background binding is greater than total binding the specific binding appears to be negative. CFH appeared to have a greater affinity for mutant His-C1QTNF5 compared with the wild type, and the reduction in binding observed at increasing CFH concentrations was greater for the mutant too. As observed in Section 5.3.2.1, no interaction could be found when the plates were coated with CFH and His-C1QTNF5 was added in the fluid phase (primary antibody: mouse anti-His).

5.3.2.3 Plate binding assay investigating an interaction between CFH and CRP

Previous studies have reported an interaction between CFH and CRP, detected by plate binding assay (Sjoberg *et al.,* 2007). It was investigated whether this result

could be repeated, as this would provide a positive control for the plate binding assays. Such an interaction was observed (Figure 5.14), as reported previously. The apparent reduction in binding with increased CFH concentration observed when using His- gC1q/His-C1QTNF5 coated plates was not observed here, suggesting this is a phenomenon specific to that interaction.

5.3.2.4 Plate binding assay investigating an interaction between CRP and His-C1QTNF5/His-gC1q

It was also investigated whether His-C1QTNF5 or His-gC1q could interact with CRP. In this instance, plates were coated with CRP and His-gC1q or His-C1QTNF5 (wild-type) was added in the fluid phase. This is because no anti-CRP antibody was available. The primary antibody used was mouse anti-His. No interactions were observed for either His-gC1q or His-C1QTNF5 (Figure 5.15).

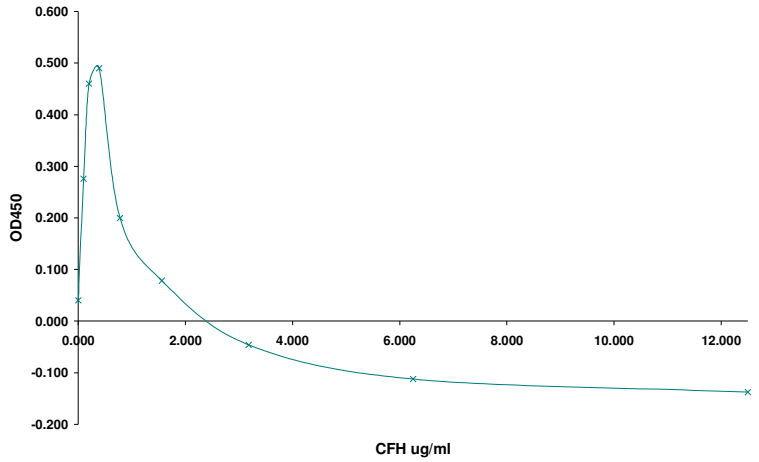

Figure 5.12: CFH binds His-gC1q.

Plates were coated with His-gC1q and increasing concentrations of CFH were added in the fluid phase. Specific binding is shown. This increases up to a CFH concentration of approximately 0.5µg/ml, after which it appears to decrease. Bound CFH was detected with primary antibody OX23 and secondary antibody alkaline phosphatase labelled rabbit anti-mouse, and this was detected with p-nitrophenyl phosphate.

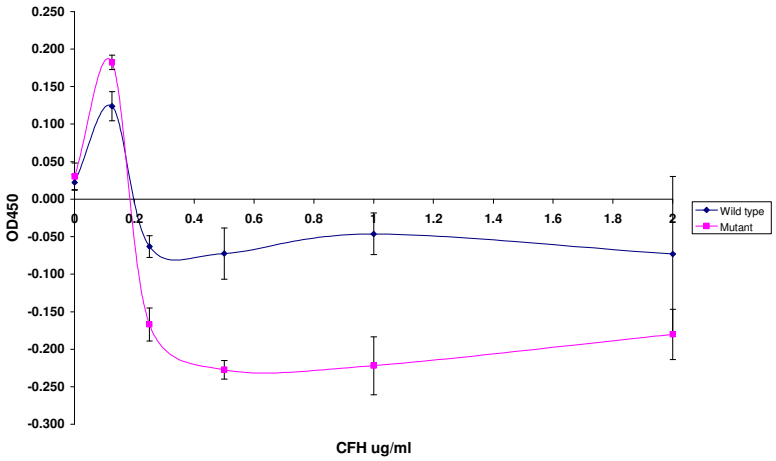

Figure 5.13: CFH binds wild-type and mutant His-C1QTNF5.

Plates were coated with His-C1QTNF5 and increasing concentrations of CFH were added in the fluid phase. Specific binding is shown. This increases up to a CFH concentration of approximately 0.15µg/ml, after which it appears to decrease. CFH shows a higher affinity for mutant His-C1QTNF5. Bound CFH was detected with primary antibody OX23 and secondary antibody alkaline phosphatase labelled rabbit anti-mouse, and this was detected with p-nitrophenyl phosphate.

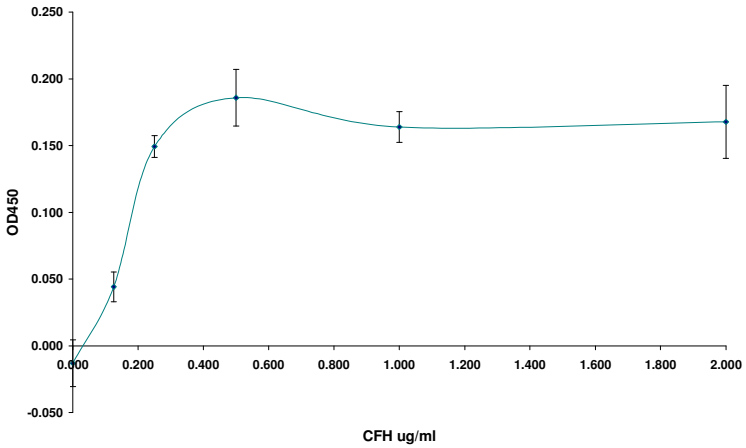

Figure 5.14: CFH binds to CRP. Plates were coated with CRP and increasing concentrations of CFH were added in the fluid phase.

Bound CFH was detected with primary antibody OX23 and secondary antibody alkaline phosphatase labelled rabbit anti-mouse, and this was detected with p-nitrophenyl phosphate.

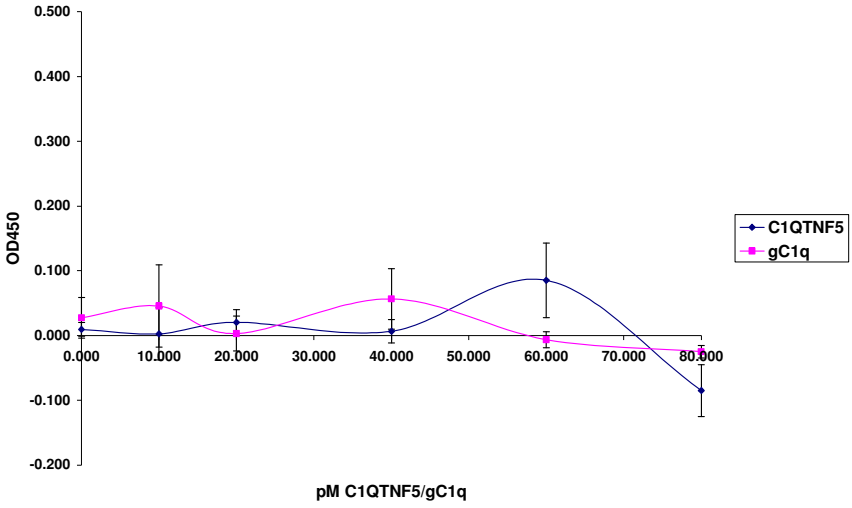

Figure 5.15: His-gC1q and His-C1QTNF5 (wild-type) do not bind CRP. Plates were coated with CRP and increasing concentrations of His-gC1q or His-C1QTNF5 were added in the fluid phase.

Bound protein was detected with primary antibody mouse anti-His and secondary antibody alkaline phosphatase labelled rabbit anti-mouse, and this was detected with p-nitrophenyl phosphate.

5.4 Surface plasmon resonance

The Biacore T100 utilises surface plasmon resonance (SPR) as a technique for detecting and analysing molecular interactions. It can be used for confirmation of protein-protein interactions and can give accurate information about reaction kinetics (McDonnell *et al.,* 2001, Wear *et al.,* 2006). The technique has been used previously to investigate interactions between complement pathway proteins (Hellwage *et al.,* 1999), and was used to investigate further the interaction between CFH and His-C1QTNF5. Analysis was carried out using His-C1QTNF5 (wild-type and mutant) and CFH, SCR7-8 Y, SCR7-8H, SCR19-20, SCR3-4 or CRP.

5.4.1 Biacore T100 and SPR theory

When using the Biacore T100 to analyse molecular interactions, alterations are measured in the parameters required for SPR to occur at the surface of a gold chip, comprising of a layer of gold film on a glass surface. Surface plasmons are a surface electromagnetic wave found on the interface between a metal surface and an external medium. When a light beam hits the metal surface at an angle it is usually totally reflected. However, at a particular wavelength and incident angle, resonance of the surface plasmons can occur . This results in a reduction in the intensity of the reflected light. The wavelength/incident angle at which SPR will occur is dependant upon the conditions at the metal surface, and any molecules on or very near the surface will affect this.

When detecting SPR, the Bicaore T100 uses monochromatic light in a wedge shape giving a broad distribution of incident angles. The incident angle giving a reduction in reflected light is detected. This will alter dependant upon what molecules are attached to the surface of the chip (Figure 5.16). In a typical experiment, the gold surface of the chip is coated with a particular molecular ligand and this surface is exposed to the flow cell. Running experimental buffer through the flow cell will give a baseline refractive index at which SPR will occur for that particular surface. When the experimental buffer subsequently contains analyte, this will attach to the surface of the chip and alter the angle at which SPR occurs. Analyte binding to

ligand will increase the refractive index, so the machine records the new position of reduced reflected light. Changes in refractive index are given as response units (RU), where a change of 1000RU corresponds to an approximately 0.1° angle change.

5.4.2 Coating CM5 chips with His-C1QTNF5

All chips used in the study were CM5 chips. These have a carboxymethyl-dextran matrix coating on the exposed gold surface, creating a hydrophilic environment upon which to attach the experimental ligand. Dextran is flexible and allows for molecular movement and so increased accessibility of the immobilised ligand. The ligand is covalently bound to the dextran matrix via amine coupling. Treatment of the chip surface with NHS and EDS prior to coating modifies around 30% of the carboxylates to succinamide esters, which are highly reactive with primary amines, forming covalent bonds. Primary amines are found on lysine residues and at the N-terminus of proteins and peptides. It should be noted that coupling of ligand to the matrix occurs at random orientations and can be via residues important for ligand binding, which may reduce the specific activity of the immobilised ligand.

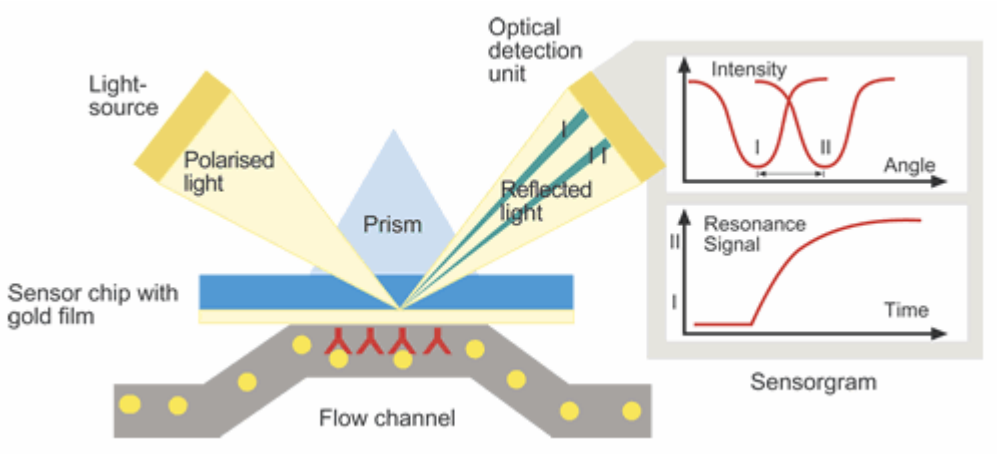

Figure 5.16: Biacore T100 measures changes in the parameters required for SPR to occur at the surface of a gold chip.
(Source: www.rci.rutgers.edu)
Monochromatic light is beamed through a prism at the sensor chip surface in a wedge shape, covering a broad distribution of incident angles. At a particular incident angle SPR will occur, resulting in a reduction in reflected light (see graph AI). With ligand attached to the chip and experimental buffer alone running through the flow cell, a baseline sensorgram reading is obtained (see graph BI). When running buffer contains analyte, this binds to the ligand altering the incident angle at which SPR will occur (AII). As increasing amounts of analyte bind to the immobilised ligand, so the incident angle increases to deviate from baseline and the sensorgram resonance signal increases (BII). Dissociation of analyte results in a reduction in resonance signal.

5.4.2.1 pH scouting

In order for the ligand to become covalently bound to the dextran matrix, sufficient amounts need to be electrostatically concentrated at the chip surface. At a pH above 3.5 the dextran matrix is negatively charged. The ligand is diluted in buffer at a pH above 3.5 but below its pI, giving it a net positive charge. This means it will be attracted to the matrix when it is flowed over in solution. To determine the optimal conditions required for concentration of sufficient ligand at the chip surface, pH scouting was carried out, with the ligand diluted in buffers covering a range of pHs. Following equilibriation of the chip in running buffer, the ligand solution was applied for 60 seconds. After this time the buffer was then changed back to running buffer. The optimal pH is that which is closest to the protein's pI and gives a high concentration of protein at the chip surface whilst still giving rapid dissociation when the buffer is changed back to running buffer. Figure 5.17 and 5.18 show the pH scouting for wild-type and mutant His-C1QTNF5. The optimal buffer for wild-type His-C1QTNF5 was 10mM acetate pH5.0, and 10mM acetate pH6.0 for the mutant.

5.4.2.2 Coating the chips

When coating chips, a theoretical maximum level of RU is aimed for (RU_{max}), from which the desired amount of bound ligand (RU_{ligand}) can be determined:

$$RU_{ligand} = RU_{max} / (MW_{analyte} / MW_{ligand})$$

For protein:protein interaction, $RU_{max} = 100$. However, a reduction in specific activity is always observed when coating chips, so an RU_{max} of at least 2-3 times this should be aimed for. Under native conditions His-C1QTNF5 is predominantly trimeric (see section 4.4.3.2). Trimeric His-C1QTNF5 has a molecular weight of approximately 75kDa. Therefore the desired amount of bound ligand is 48RU. However, due to the expected reduction in specific activity, 200RU of bound ligand was aimed for when coating the chips. In addition to this, chips were also coated with 1000RU of bound ligand to provide a comparison with the low density 200RU chips.

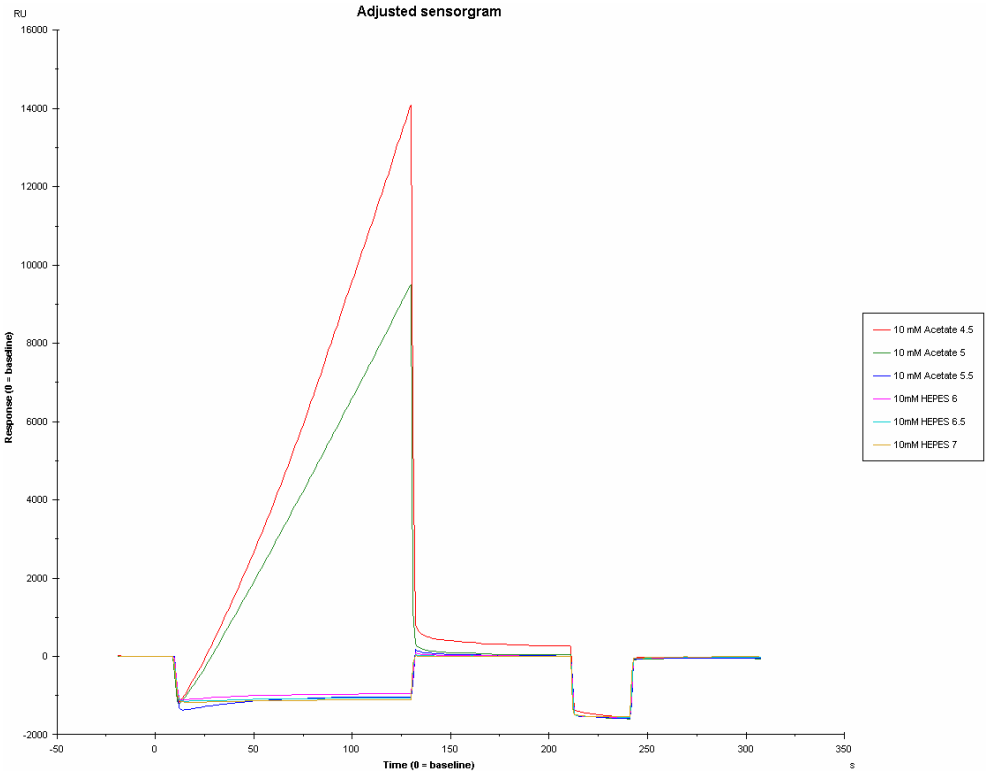

Figure 5.17: Wild-type His-C1QTNF5 pH scouting using a CM5 chip.

10mM acetate pH5.0 was selected for coating the chips.

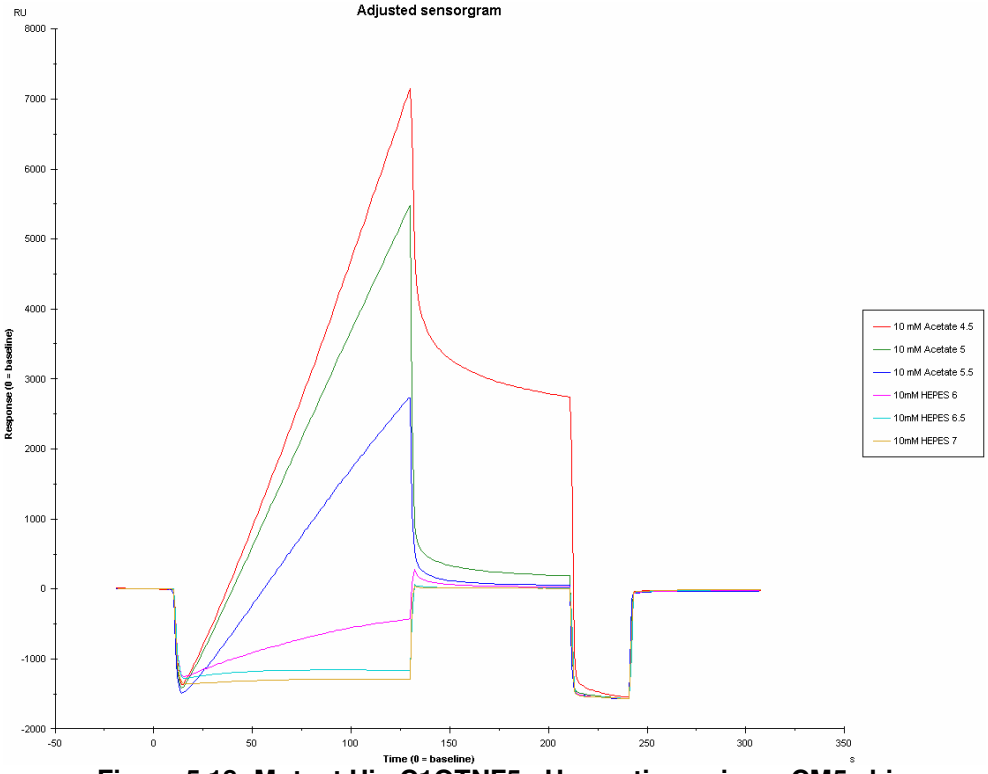

Figure 5.18: Mutant His-C1QTNF5 pH scouting using a CM5 chip.

10mM HEPES pH 6.0 was selected for coating the chips.

5.4.3 Investigating an interaction between His-C1QTNF5 and CFH by SPR

Once the chips were prepared, it was investigated whether any interactions could be observed between His-C1QTNF5 and fluid-phase CFH, SCR7-8Y, SCR7-8H, SCR19-20, SCR3-4 and CRP. Experiments and affinity calculations involving His-C1QTNF5 and CFH were carried out using the low density 200RU chips. Experiments and affinity calculations involving His-C1QTNF5 and the SCR modules were carried out using low density 200RU and high density 1000RU chips, with at least one analysis carried out using each chip.

5.4.3.1 Analysing His-C1QTNF5 interactions with CFH

Using the CM5 chips coated with 200RU wild-type or mutant His-C1QTNF5, interactions with six sequential injections containing increasing concentrations of CFH diluted in running buffer (10mM HEPES pH7.4, 150mM NaCl, 0.01% P20) were investigated. Each sample injection was for 30 seconds, followed by 2000 seconds' dissociation time where running buffer alone was flowed over the chip. A final 7^{th} injection was carried out containing the same concentration of CFH as injection 3, providing an internal control. The experimental data was then analysed using the "kinetic/affinity" software facility. Figure 5.19 shows the sensorgrams and data analysis for three repeat experiments using the wild-type His-C1QTNF5 chips. Figure 5.20 shows the sensorgrams and data analysis for two repeat experiments using the mutant His-C1QTNF5 chips. CFH shows an approximately 17.5-fold greater average affinity (kD) for mutant His-C1QTNF5 ($1.1x10^{-9}$ M) compared with the wild-type ($1.9x10^{-8}$ M). Although not significant (one-tailed t-test (3) = 0.883, p = 0.221), this result is suggestive that there may be differences in CFH binding between the two proteins. Further repeats would help to confirm any significance. The predicted model which best fitted the data for each was '2-state binding with conformational change'.

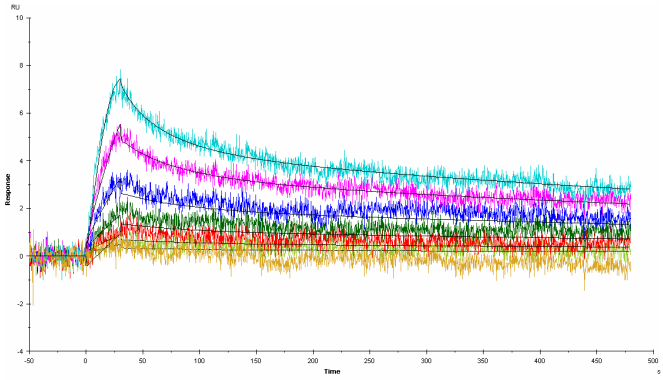

Sensorgram A:
kD: 1.1×10^{-9} M
ka1: 6.0×10^{6}
ka2: 0.01
kd1: 0.03
kd2: 0.003

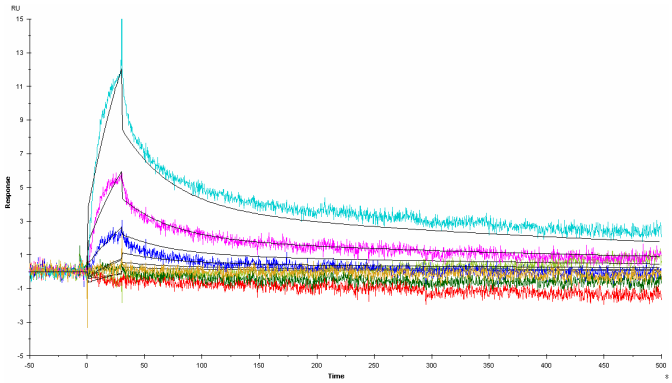

Sensorgram B:
kD: 5.0×10^{-8} M
ka1: 8.1×10^{4}
ka2: 0.02
kd1: 0.007
kd2: 0.002

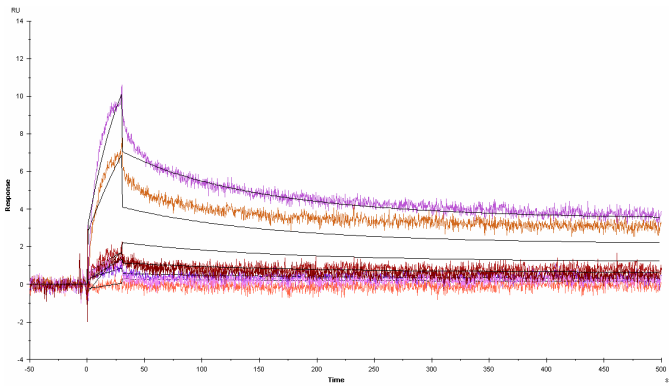

Sensorgram C:
kD: 5.6×10^{-9} M
ka1: 4.1×10^{6}
ka2: 0.02
kd1: 0.07
kd2: 0.008

Figure 5.19: SPR sensorgrams showing that CFH (fluid phase) interacts with wild-type His-C1QTNF5-coated CM5 chips.
Chips were coated with 200RU wild-type His-C1QTNF5, with three separate experiments carried out. Individual affinities (kD), association rates (ka1 – 1/ms, ka2 – 1/s) and dissociation rates (kd1 and kd2 – 1/s) for each experiment are shown. The average affinity (kD) of CFH for wild-type His-C1QTNF5 is 1.9×10^{-8} M. The predicted model which best fits the data is 'two-state binding with conformational change'. CFH was added in the fluid phase, with increased binding responses observed with increased concentrations.

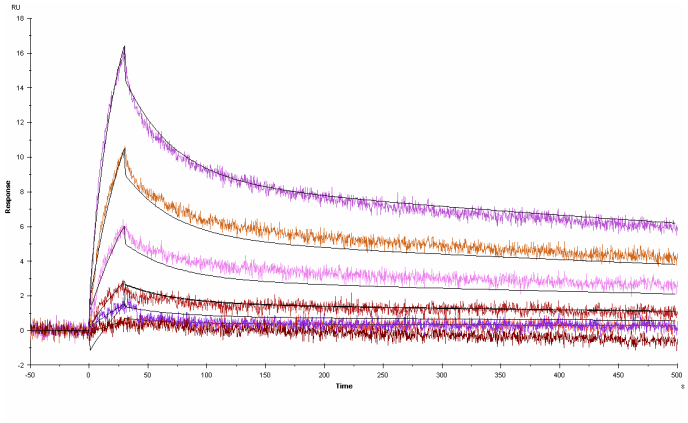

Sensorgram A:
kD: 2.1×10^{-9} M
ka1: 6.8×10^{5}
ka2: 0.01
kd1: 0.01
kd2: 0.001

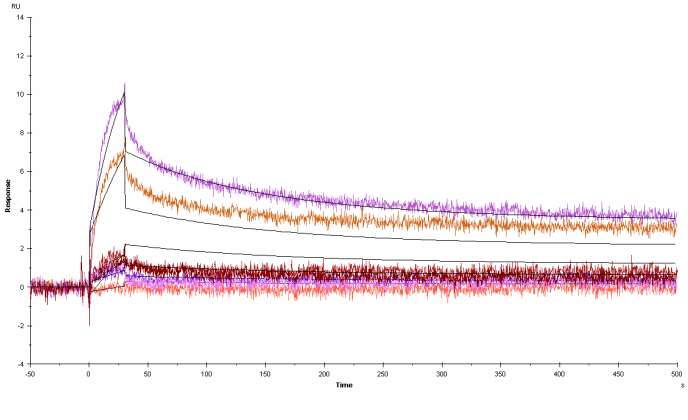

Sensorgram B:
kD: 8.3×10^{-11} M
ka1: 1.3×10^{6}
ka2: 0.004
kd1: 0.007
kd2: 5.9×10^{-5}

Figure 5.20: SPR sensorgrams showing that CFH (fluid phase) interacts with mutant His-C1QTNF5-coated CM5 chips.

Chips were coated with 200RU mutant His-C1QTNF5, with two separate experiments carried out. Individual affinities (kD), association rates (ka1 – 1/ms, ka2 – 1/s) and dissociation rates (kd1 and kd2 – 1/s) for each experiment are shown. The average affinity (kD) of CFH for mutant His-C1QTNF5 is 1.1×10^{-9} M. The predicted model which best fits the data is 'two-state binding with conformational change'. CFH was added in the fluid phase, with increased binding responses observed with increased concentrations.

5.4.3.2 Analysing His-C1QTNF5 interactions with SCR7-8Y

Using the CM5 chips coated with 200RU and 1000RU of wild-type or mutant His-C1QTNF5, interactions with six sequential injections containing increasing concentrations of SCR7-8Y diluted in running buffer were investigated. Each sample injection was for 30 seconds, followed by 300 seconds dissociation time where running buffer alone was flowed over the chip. As before, a 7th repeat injection was carried out providing an internal control. The experimental data was then analysed using the "kinetic/affinity" software facility. Figure 5.21 shows the sensorgrams and data analysis for three repeat experiments investigating interactions with wild-type His-C1QTNF5. Two experiments were carried out using the 200RU chips and one experiment was carried out using the 1000RU chip. Figure 5.22 shows the sensorgrams and data analysis for three repeat experiments investigating interactions with mutant His-C1QTNF5. Again, two experiments were carried out using the 200RU chips and one experiment was carried out using the 1000RU chip. SCR7-8Y showed similar affinities (kD) for wild-type ($9.7x10^{-6}$ M) and mutant ($2.8x10^{-6}$ M) His-C1QTNF5. The predicted model which best fitted the data for each was '1:1 binding'.

5.4.3.3 Analysing His-C1QTNF5 interactions with SCR7-8H

Using the CM5 chips coated with 200RU and 1000RU of wild-type or mutant His-C1QTNF5, interactions with six sequential injections containing increasing concentrations of SCR7-8H were investigated. Each sample injection was for 30 seconds, followed by 300 seconds dissociation time where running buffer alone was flowed over the chip. As before, a 7th repeat injection was carried out providing an internal control. The experimental data was then analysed using the "kinetic/affinity" software facility. Figure 5.23 shows the sensorgrams and data analysis for two repeat experiments investigating an interaction with wild-type His-C1QTNF5. One experiment was carried out using a 200RU chip and one experiment was carried out using a 1000RU chip. Figure 5.24 shows the sensorgrams and data analysis for three repeat experiments investigating an interaction with mutant His-C1QTNF5. Two experiments were carried out using 200RU chips and one

experiment carried out using a 1000RU chip. SCR7-8H showed similar affinities (kD) for wild-type ($4.2x10^{-6}$ M) and mutant ($1.8x10^{-6}$ M) His-C1QTNF5, and both affinites were similar to those obtained with SCR7-8Y. The predicted model which best fitted the data for each was '1:1 binding'.

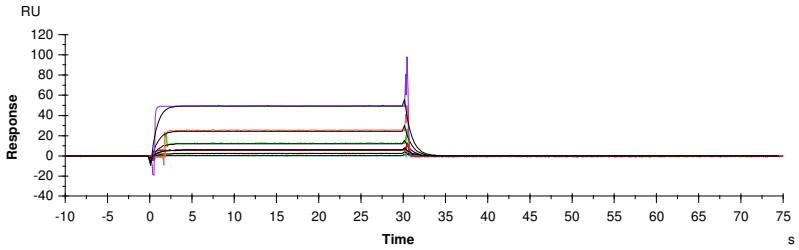

Sensorgram A:
kD: 1.2×10^{-5} M
ka: 1.0×10^{5}
kd: 1.3

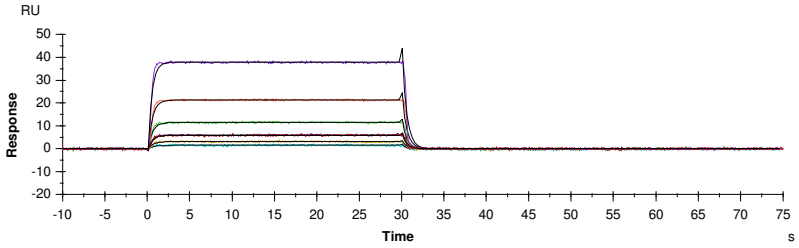

Sensorgram B:
kD: 7.8×10^{-6} M
ka: 2.4×10^{5}
kd: 1.9

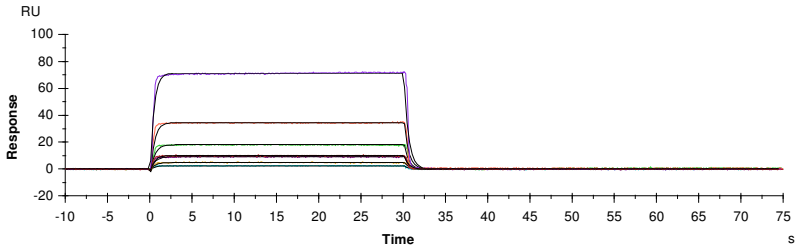

Sensorgram C:
kD: 9.3×10^{-6} M
ka: 2.1×10^{5}
kd: 1.9

Figure 5.21: SPR sensorgrams showing that SCR7-8Y (fluid phase) interacts with wild-type His-C1QTNF5-coated CM5 chips. Chips were coated with either 200RU (sensorgrams A and B) or 1000RU (sensorgram C) wild-type His-C1QTNF5. Individual affinities (kD), association rates (ka – 1/ms) and dissociation rates (kd – 1/s) for each experiment are shown. The average affinity (kD) of SCR7-8Y for wild-type His-C1QTNF5 is 9.7×10^{-6} M. The predicted model which best fits the data is '1:1 binding'. CFH was added in the fluid phase, with increased binding responses observed with increased concentrations.

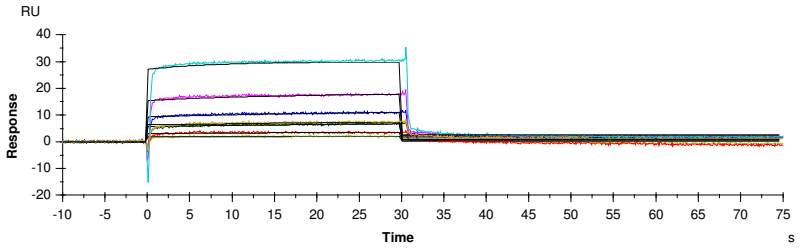

Sensorgram A:
kD: 1.7×10^{-6} M
ka: 2600
kd: 0.005

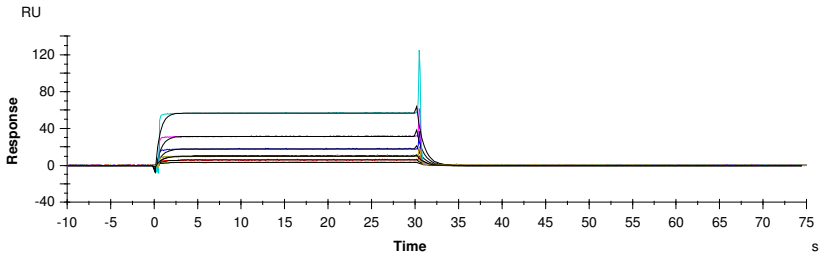

Sensorgram B:
kD: 3.9×10^{-6} M
ka: 3.3×10^{5}
kd: 1.3

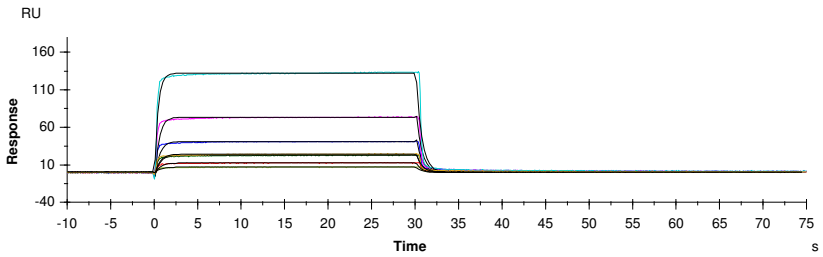

Sensorgram C:
kD: 2.9×10^{-6} M
ka: 5.4×10^{5}
kd: 1.5

Figure 5.22: SPR sensorgrams showing that SCR7-8Y (fluid phase) interacts with mutant His-C1QTNF5-coated CM5 chips. Chips were coated with either 200RU (sensorgrams A and B) or 1000RU (sensorgram C) mutant His-C1QTNF5. Individual affinities (kD), association rates (ka – 1/ms) and dissociation rates (kd – 1/s) for each experiment are shown. The average affinity (kD) of SCR7-8Y for mutant His-C1QTNF5 is 2.8×10^{-6} M. The predicted model which best fits the data is '1:1 binding'. CFH was added in the fluid phase, with increased binding responses observed with increased concentrations.

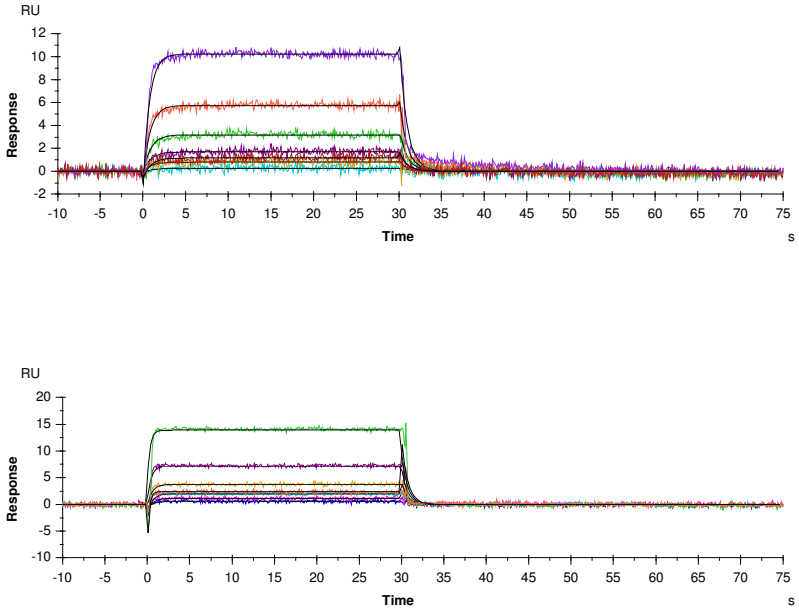

Figure 5.23: SPR sensorgrams showing that SCR7-8H (fluid phase) interacts with wild-type His-C1QTNF5-coated CM5 chips.
Chips were coated with either 200RU (sensorgram A) or 1000RU (sensorgram B) wild-type His-C1QTNF5. Individual affinities (kD), association rates (ka – 1/ms) and dissociation rates (kd – 1/s) for each experiment are shown. The average affinity (kD) of SCR7-8H for wild-type His-C1QTNF5 is 4.2×10^{-6} M. The predicted model which best fits the data is '1:1 binding'. CFH was added in the fluid phase, with increased binding responses observed with increased concentrations.

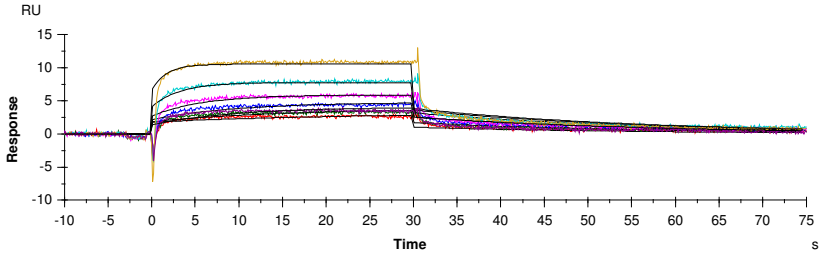

Sensorgram A:
kD: 1.3×10^{-7} M
ka: 2.8×10^{5} M
kd: 0.04

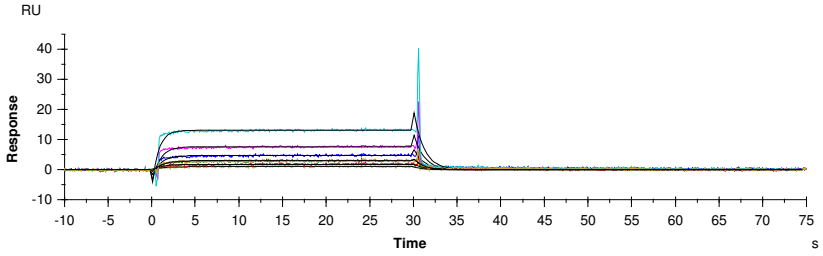

Sensorgram B:
kD: 3.3×10^{-6} M
ka: 2.6×10^{5} M
kd: 0.8

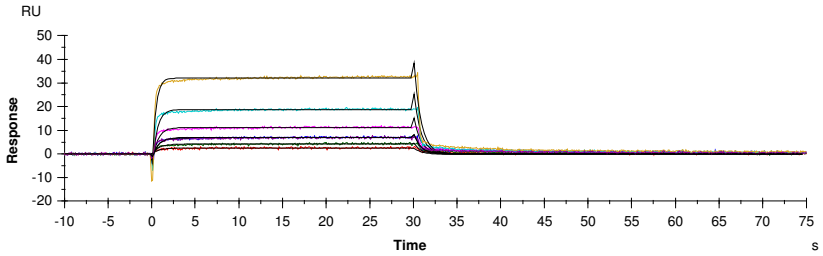

Sensorgram C:
kD: 2.1×10^{-6} M
ka: 6.1×10^{5} M
kd: 1.3

Figure 5.24: SPR sensorgrams showing that SCR7-8H (fluid phase) interacts with mutant His-C1QTNF5-coated CM5 chips.

Chips were coated with either 200RU (sensorgrams A and B) or 1000RU (sensorgram B) mutant His-C1QTNF5. Individual affinities (kD), association rates (ka – 1/ms) and dissociation rates (kd – 1/s) for each experiment are shown. The average affinity (kD) of SCR7-8H for mutant His-C1QTNF5 is 1.8×10^{-6} M. The predicted model which best fits the data is '1:1 binding'. CFH was added in the fluid phase, with increased binding responses observed with increased concentrations.

5.4.3.4 Analysing His-C1QTNF5 interactions with SCR19-20

Following the same experimental parameters as for SCR7-8Y and SCR7-8H, His-C1QTNF5 interactions with SCR19-20 were investigated. Figure 5.25 shows the sensorgrams and data analysis for three repeat experiments investigating an interaction with wild-type His-C1QTNF5. One experiment was carried out using a 200RU chip and two experiments were carried out using the 1000RU chip. Figure 5.26 shows the sensorgrams and data analysis for three repeat experiments investigating an interaction with mutant His-C1QTNF5. Two experiments were carried out using the 200RU chips and one experiment was carried out using the 1000RU chip. SCR19-20 showed a greater affinity (kD) for mutant His-C1QTNF5 ($2.0x10^{-7}$ M) compared with wild-type ($1.9x10^{-5}$ M). The predicted model which best fitted the data for each was '1:1 binding'.

5.4.3.5 Analysing His-C1QTNF5 interactions with SCR3-4

Following the same parameters as for SCR7-8 and using the 200RU-coated chips, His-C1QTNF5 interactions with SCR3-4 were investigated. No interactions were observed between wild-type or mutant His-C1QTNF5 and SCR3-4.

5.4.3.6 Analysing His-C1QTNF5 interactions with CRP

It was investigated whether an interaction between CRP and wild-type His-C1QTNF5 could be observed. Sequential injections containing increasing concentrations of CRP diluted in running buffer were investigated. It was not possible to detect an interaction.

5.4.3.7 Summary of SPR kinetic data

Tables 5.1 and 5.2 summarise the kinetic data obtained for interactions with wild-type and mutant His-C1QTNF5. In all instances, analytes showed a greater affinity (kD) for mutant His-C1QTNF5 compared to the wild-type, with the exception of SCR7-8Y where the association rate was marginally slower. For full length CFH this was a 17.5-fold increase. Modules SCR7-8Y and SCR7-8H showed only slight increases (3.4-fold and 2.3-fold respectively), whereas SCR19-20 showed a 95-fold increase. When looking at the rates of association for each analyte, these were again

greater for the mutant, and dissociation rates were slower. Two association and two dissociation rates are given for full length CFH as these were calculated based upon a two-state binding model. For the ligands CFH, SCR7-8Y and SCR7-8H association rates and dissociation rates differ only slightly between wild-type and mutant His-C1QTNF5. For SCR19-20, however, association rates show only a 2-fold increase for the mutant but dissociation rates are 173-fold slower.

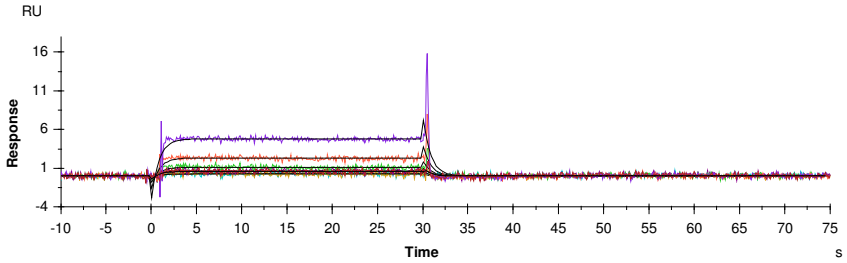

Sensorgram A:
kD: 3.5×10^{-5} M
ka: 3.3×10^{4} M
kd: 1.2

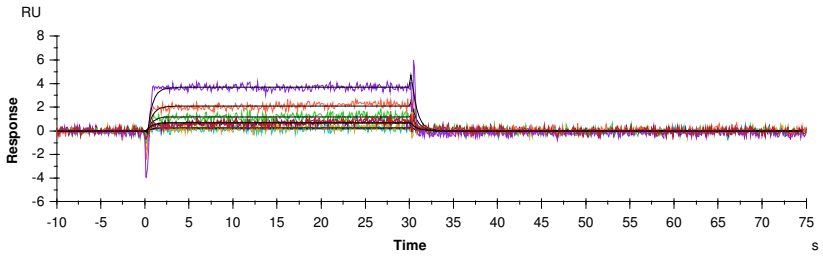

Sensorgram B:
kD: 1.7×10^{-5} M
ka: 9.6×10^{4} M
kd: 1.6

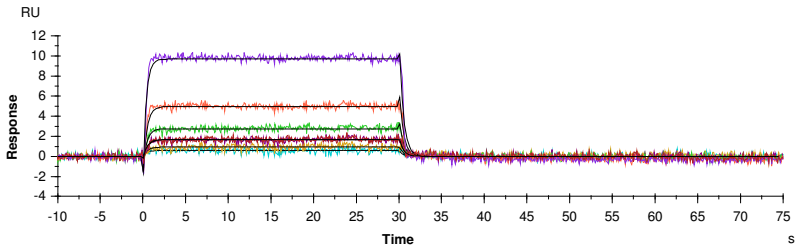

Sensorgram C:
kD: 5.6×10^{-6} M
ka:3.6×10^{5} M
kd: 2

Figure 5.25: SPR sensorgrams showing that SCR19-20 (fluid phase) interacts with wild-type His-C1QTNF5-coated CM5 chips.

Chips were coated with either 200RU (sensorgram A) or 1000RU (sensorgrams B and C) wild-type His-C1QTNF5. Individual affinities (kD), association rates (ka – 1/ms) and dissociation rates (kd – 1/s) for each experiment are shown. The average affinity (kD) of SCR19-20 for wild-type His-C1QTNF5 is 1.9×10^{-5} M. The predicted model which best fits the data is '1:1 binding'. CFH was added in the fluid phase, with increased binding responses observed with increased concentrations.

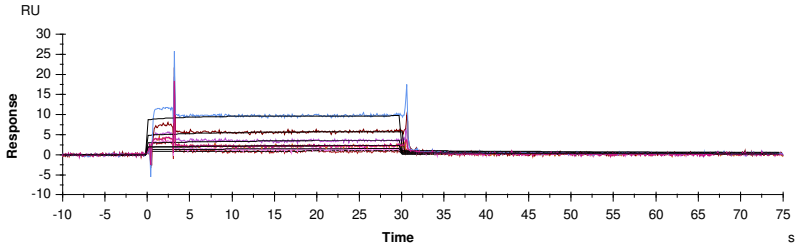

Sensorgram A:
kD: 1.3×10^{-7} M
ka: 1.0×10^{5} M
kd: 0.01

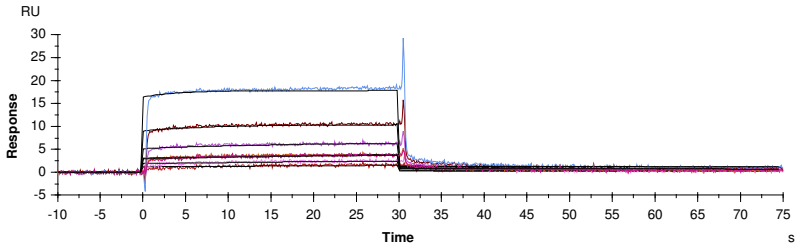

Sensorgram B:
kD: 2.6×10^{-8} M
ka: 1.3×10^{5} M
kd: 0.003

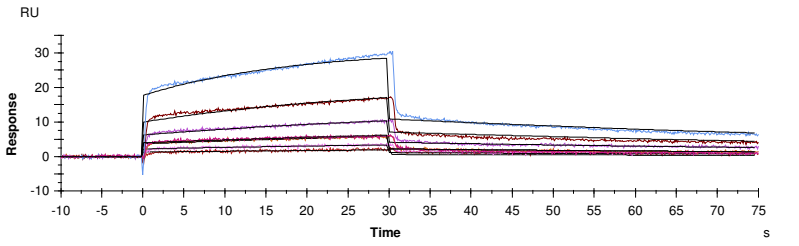

Sensorgram C:
kD: 4.4×10^{-7} M
ka: 2.4×10^{4} M
kd: 0.01

Figure 5.26: SPR sensorgrams showing that SCR19-20 (fluid phase) interacts with mutant His-C1QTNF5-coated CM5 chips.
Chips were coated with either 200RU (sensorgrams A and B) or 1000RU (sensorgram B) mutant His-C1QTNF5. Individual affinities (kD), association rates (ka – 1/ms) and dissociation rates (kd – 1/s) for each experiment are shown. The average affinity (kD) of SCR19-20 for mutant His-C1QTNF5 is 2.0×10^{-7} M. The predicted model which best fits the data is '1:1 binding'. CFH was added in the fluid phase, with increased binding responses observed with increased concentrations.

Wild-type His-C1QTNF5

kD (M)	CFH	SCR7-8Y	SCR7-8H	SCR19-20
	1.0E-09	7.8E-06	7.6E-06	3.5E-05
	4.9E-08	1.2E-05	7.4E-07	1.7E-05
	5.6E-09	9.3E-06		5.6E-06
Ave	**1.9E-08**	**9.7E-06**	**4.2E-06**	**1.9E-05**

ka (1/ms)	CFH1	CFH2 (1/s)	SCR7-8Y	SCR7-8H	SCR19-20
	6.0E+06	9.0E-03	2.4E+05	1.4E+05	3.4E+04
	8.1E+04	2.0E-02	1.0E+05	1.9E+06	9.6E+04
	4.1E+06	2.0E-02	2.1E+05		3.6E+05
Ave	**3.4E+06**	**1.0E-02**	**1.8E+05**	**1.0E+06**	**1.6E+05**

kd (1/s)	CFH1	CFH2	SCR7-8Y	SCR7-8H	SCR19-20
	2.9E-02	2.6E-03	1.9E+00	1.1E+00	1.2E+00
	7.1E-03	2.5E-03	1.3E+00	1.4E+00	1.6E+00
	7.1E-02	8.1E-03	1.9E+00		2.0E+00
Ave	**3.6E-02**	**4.4E-03**	**1.7E+00**	**1.2E+00**	**1.6E+00**

Mutant His-C1QTNF5

kD (M)	CFH	SCR7-8Y	SCR7-8H	SCR19-20
	2.1E-09	1.7E-06	1.3E-07	2.6E-08
	8.3E-11	3.9E-06	3.3E-06	1.3E-07
		2.9E-06	2.1E-06	4.4E-07
Ave	**1.1E-09**	**2.8E-06**	**1.8E-06**	**2.0E-07**

ka (1/ms)	CFH1	CFH2 (1/s)	SCR7-8Y	SCR7-8H	SCR19-20
	6.8E+05	1.1E-02	2.6E+03	2.8E+05	1.3E+05
	1.3E+06	3.6E-03	3.3E+05	2.6E+05	1.0E+05
			5.4E+05	6.1E+05	2.4E+04
Ave	**1.0E+06**	**7.4E-03**	**2.9E+05**	**3.8E+05**	**8.5E+04**

kd (1/s)	CFH1	CFH2	SCR7-8Y	SCR7-8H	SCR19-20
	1.2E-02	1.4E-03	4.6E-03	3.7E-02	3.2E-03
	6.8E-03	5.9E-05	1.3E+00	8.5E-01	1.4E-02
			1.5E+00	1.3E+00	1.0E-02
Ave	**9.6E-03**	**7.3E-04**	**9.4E-01**	**7.2E-01**	**9.1E-03**

Table 5-1: The dissociation constant (kD), association rate (ka) and dissociation rate (kd) constants of the analytes CFH, SCR7-8Y, SCR7-8H and SCR19-20 for wild-type and mutant His-C1QTNF5 as determined by SPR. The difference in mean dissociation constant for SCR19-20 between wild-type and mutant His-C1QTNF5 is significant (one-tailed t-test (4) = 2.231, p = 0.045). The difference in mean dissociation constant for CFH between wild-type and mutant His-C1QTNF5 is suggestive, and may be significant if more samples were to be obtained (one-tailed t-test (3) = 0.883, p = 0.221).

kD (M)

CFH	SCR7-8Y	SCR7-8H	SCR19-20
17.5	3.4	2.3	95.3

ka (1/ms)

CFH 1	CFH 2(1/s)	SCR7-8Y	SCR7-8H	SCR19-20
3.4	1.9	0.6	2.7	1.9

kd (1/s)

CFH 1	CFH 2(1/s)	SCR7-8Y	SCR7-8H	SCR19-20
3.7	6	1.8	1.8	173.2

Table 5-2: The fold differences in dissociation constant (kD), association rate (ka) and dissociation rate (kd) of the analytes CFH, SCR7-8Y, SCR7-8H and SCR19-20 for mutant His-C1QTNF5 compared with wild-type as determined by SPR.

In all instances, affinities and association rates were greater and dissociation rates slower for mutant His-C1QTNF5 compared with wild-type, with the exception of SCR7-8Y where the association rate was marginally less.

5.5 Isothermal titration calorimetry

Isothermal titration calorimetry (ITC) quantifies the heat absortion/evolution accompanying molecular associations in solution, from which reaction kinetics and stoichiometry can be determined (Pierce *et al.,* 1999, Okhrimenko *et al.,* 2007). Experiments were carried out investigating the interaction between His-gC1q and CFH, with calculations of experimental protein concentrations based upon affinities obtained by SPR for either full length CFH or SCR19-20 (section 5.4).

5.5.1 ITC theory

During an ITC experiment, the time-dependant power input necessary to maintain a sample and reference cell at the same temperature is measured. This is dependant upon the reaction stoichiometry, association constant, free energy, enthalpy, entropy and heat capacity of binding. ITC can therefore provide a detailed insight into the parameters of molecular interactions in solution. Both the sample and reference cells are made from highly efficient thermal conductors (e.g. hasteloy or gold) surrounded by an adiabatic jacket, with the temperature of each accurately measured. The ITC machine aims to maintain both cells at the same temperature. The sample cell contains the macromolecule in buffer solution, whereas the reference cell contains buffer alone. With constant stirring, the ligand is titrated into the sample cell and the power input required to maintain both sample and reference cell at the same temperature is recorded. This will be dependant upon whether the reaction is endothermic or exothermic. In addition, a control experiment is carried out where the ligand is titrated into buffer alone. Deducting this from the experimental data cancels out any effects of stirring or heat of dilution of the ligand (Pierce *et al.,* 1999).

5.5.2 Investigating an interaction by ITC between CFH and His-gC1q

It was investigated whether an interaction could be observed between His-gC1q and CFH by ITC. In all experiments His-gC1q was titrated into CFH. Determination of the concentration requirements for an ITC experiment can be calculated based upon the equation s = kD x [cell], where s is in the range 20-1000, and initial titrant

concentrations should be approximately 10-20 times the protein concentration in the cell, [cell]. Values for kD were obtained by SPR, as described in Section 5.4. Experimental concentrations were calculated based upon affinities of either full length CFH or SCR19-20 for wild-type His-C1QTNF5. SCR19-20 was chosen because whilst the full length protein has been shown to interact with His-C1QTNF5, it is thought that CFH initially attaches to ligands such as C3b and polyanions via its C-terminal SCR20 domain (Jokiranta *et al.,* 2005, Ferreira *et al.,* 2006), before undergoing a conformational change to make other domains accessible.

It was determined by SPR that the affinity (kD) of CFH for wild-type His-C1QTNF5 ranges from $1.0x10^{-9}$ M to $5.0x10^{-8}$ M (Section 5.4.3.1). Taking the lowest of these, 1nM, and a mid-range s value of 500 gives a CFH concentration of 0.5µM and a His-gC1q concentration 15 times that of 7.5µM. ITC was carried out using these concentrations of proteins at 25°C with 25 injections of 4.81µl. No interaction was observed (Figure 5.27).

It was also determined by SPR that the affinity (kD) of SCR19-20 for wild-type His-C1QTNF5 ranges from $1.7x10^{-5}$ M to $5.6x10^{-6}$ M (Section 5.4.3.4), with the lower of these being 5µM. It was not possible to concentrate His-gC1q beyond 125µM without precipitation. However, as the His-gC1q concentration should be 10-20 times the cell concentration, a CFH concentration of 12.5µM would give an s value of 62.5. This is low but within the acceptable range of 20-1000. ITC was carried out using these protein concentrations at 25°C and 42 injections of 4.81µl. Again, no interaction was observed (Figure 5.28).

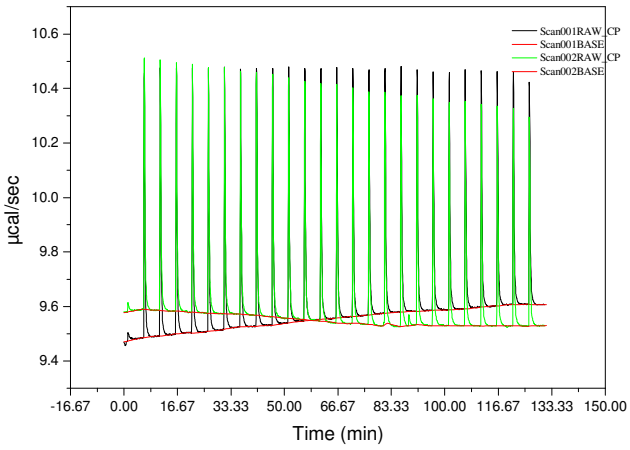

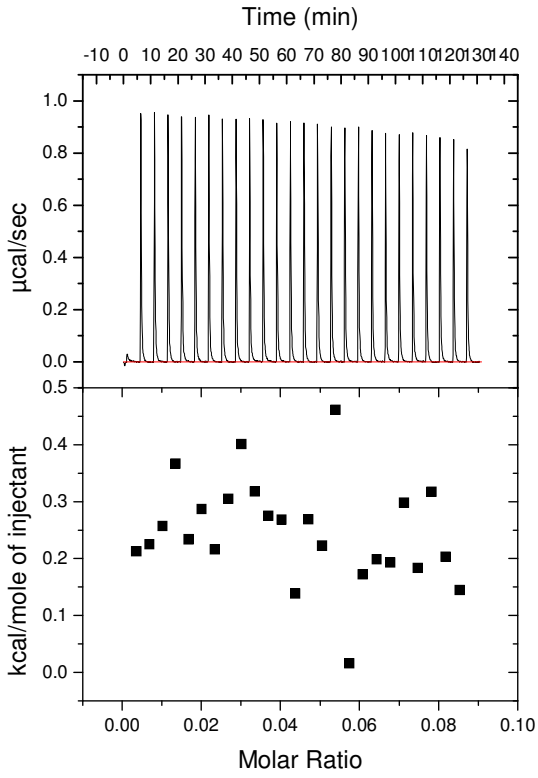

Figure 5.27: ITC was carried out investigating an interaction between CFH and His-gC1q.

Experimental concentrations of both proteins were calculated based upon a nM affinity (kD) of CFH for His-gC1q. The experiment was carried out at 25℃ with 25 injections of 4.81µl. No interaction was observed.

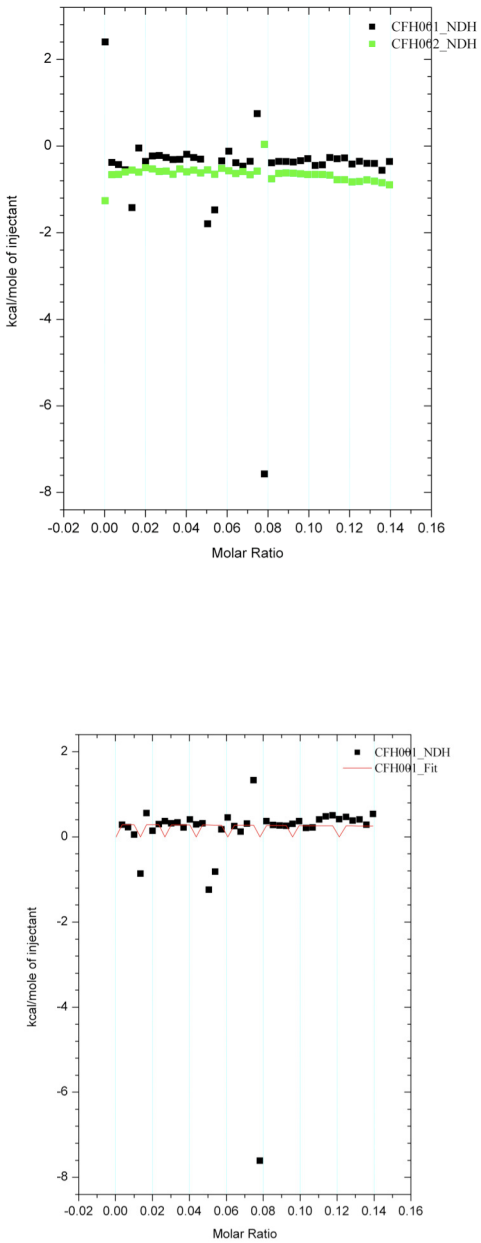

Figure 5.28: ITC was carried out investigating an interaction between CFH and His-gC1q.

Experimental concentrations of both proteins were calculated based upon a μM affinity (kD) of CFH for His-gC1q. The experiment was carried out at 25℃ with 42 injections of 4.81μl. No interaction was observed.

5.6 Investigating the effects of His-C1QTNF5 on CFH co-factor activity

One of the functions of CFH is to act as a co-factor for Factor I-mediated cleavage of C3b. This activity has been mapped to CFH SCRs 1-4, 12-14 and 20 (Kuhn *et al.,* 1995, Jokiranta *et al.,* 2000, Sharma *et al.,* 2003, Oppermann *et al.,* 2006). It has been shown in Sections 5.3 and 5.4 that His-C1QTNF5 interacts with CFH and that this interaction involves at least SCR7-8 and SCR19-20. It was therefore investigated whether His-C1QTNF5 (wild-type or mutant) had any effect on CFH co-factor activity, either in solution or when CFH was in complex with surface-bound His-C1QTNF5.

5.6.1 The effects of His-C1QTNF5 on CFH co-factor activity in solution

It has previously been shown that when CFH acts as a co-factor for Factor I-mediated C3b cleavage in solution, and the reaction mixture is analysed by SDS-PAGE, C3b degradation products at 68, 46 and 43kDa can be observed (Sim *et al.,* 1981, Alsenz *et al.,* 1984). This method was adapted to investigate any effects of His-C1QTNF5 on CFH co-factor activity, with wild-type His-C1QTNF5 either added to the reaction or replacing Factor I (FI). Following incubation at 37°C for 1 hour, the reaction mixture was analysed by reducing SDS-PAGE. As can be seen from Figure 5.29, CFH showed co-factor activity with FI resulting in C3b cleavage (lane A: note 68, 46 and 43kDa cleavage products). This was not affected by the addition of wild-type His-C1QTNF5 (lane B). When CFH was replaced with wild-type His-C1QTNF5 no degradation occurred (lane C), indicating C1QTNF5 is not capable of degrading C3b.

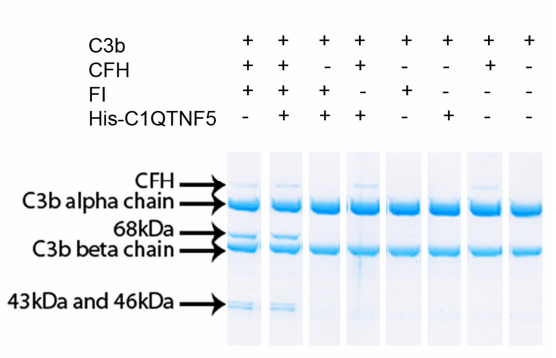

Figure 5.29: Wild-type His-C1QTNF5 has no effect on CFH co-factor activity in solution.

Different combinations of reactants were incubated at 37℃ for 1 hour and then analysed by reducing SDS-PAGE.
C3b degradation is indicated by the presence of degradation products at 68kDa, 43kDa and 46kDa.

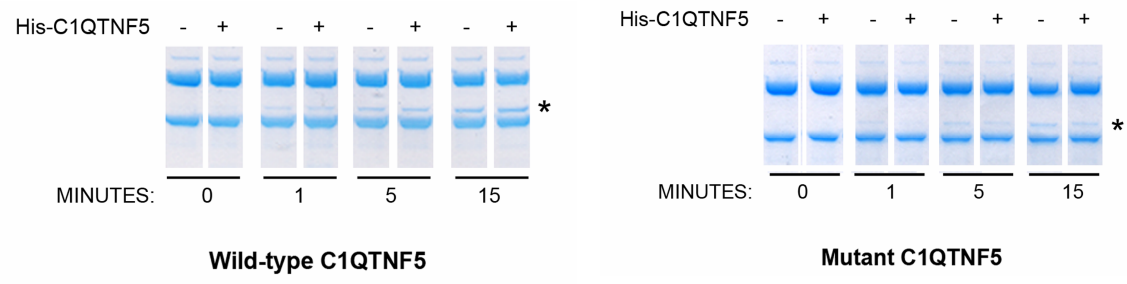

Figure 5.30: Wild-type and mutant His-C1QTNF5 have no effect on the rate of CFH co-factor activity in solution.

Reaction mixtures containing either C3b, CFH and FI or C3b, CFH, FI and His-C1QTNF5 were incubated at 37℃, with samples taken for analysis by reducing SDS-PAGE after 0, 1, 5 and 15 minutes.
C3b degradation is indicated by the presence of degradation products at 68kDa, 43kDa and 46kDa.
No differences were observed either with or without His-C1QTNF5, or between wild-type and mutant His-C1QTNF5-containing samples.

The previous assay investigated the effects of His-C1QTNF5 on co-factor activity after incubation for 1 hour at 37°C, with no effects observed. However, it is possible that His-C1QTNF5 could affect the rate of C3b degradation, and the effects of this may not be observable after times as long as 1 hour. Therefore, the assay was repeated with samples taken for analysis by reducing SDS-PAGE after incubating at 37°C for 0, 1, 5 and 15 minutes. The assay was carried out with or without additional His-C1QTNF5 and both wild-type and mutant proteins were used. As can be seen from Figure 5.30, no effects were observed on the rate of C3b degradation for either wild-type or mutant His-C1QTNF5.

5.6.2 The effects on CFH co-factor activity when bound to C1QTNF5

The previous section investigated the effects of His-C1QTNF5 on CFH co-factor activity in solution. However, it was not possible to show any interaction between His-C1QTNF5 and CFH in solution when carrying out ITC (see Section 5.5). Whilst an interaction may occur and this may not affect CFH co-factor activity, it is also possible no effect was observed in Section 5.6.1 due to a lack of interaction between CFH and His-C1QTNF5. It has been shown by plate binding assay that CFH will bind to immobilised His-C1QTNF5. Therefore it was investigated whether CFH bound to immobilised His-C1QTNF5 still maintained co-factor activity. Following the plate binding assay method, wild-type or mutant His-C1QTNF5 was immobilised to microtitre plates and CFH was added at 0, 0.5 and 2.0µg/ml. Following incubation and adequate washing, the C3b co-factor assay reagents were added to the wells and the plates incubated at 37°C. Samples were taken after 30, 60 and 120 minutes and analysed by reducing SDS-PAGE for the presence of C3b cleavage products at 68, 46 and 43kDa. As can be seen from Figure 5.31, faint bands corresponding to cleavage products at 68kDa were observed for both wild-type and mutant His-C1QTNF5-coated plates after 120 minutes incubation, and this was greatest when 2.0µg/ml CFH was used. No cleavage products were observed when plates were not coated with His-C1QTNF5.

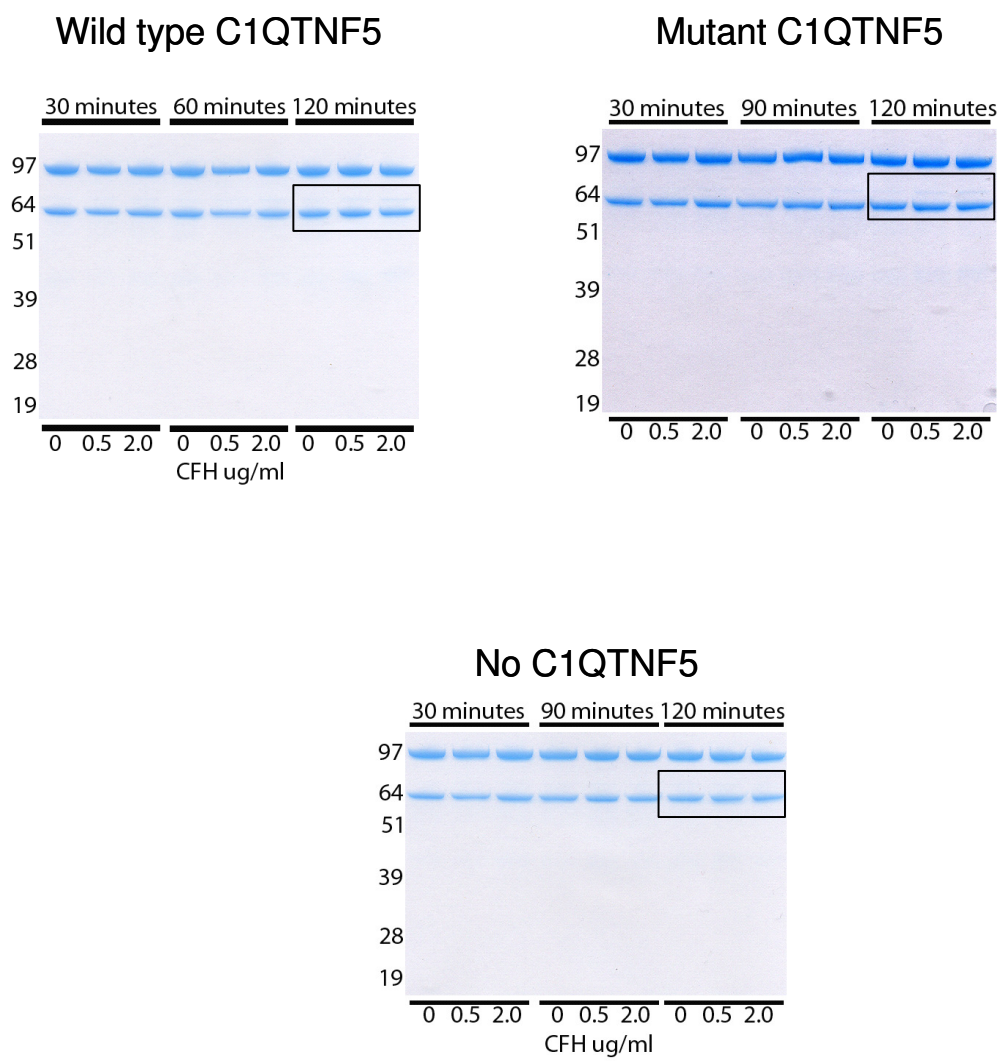

Figure 5.31: CFH which has interacted with immobilised His-C1QTNF5 (wild-type and mutant) retains co-factor activity.

Following the plate binding assay method, wild-type or mutant His-C1QTNF5 was immobilised to microtitre plates and CFH was added at 0, 0.5 and 2.0µg/ml. C3b co-factor assay reagents were added to the wells and the plates incubated at 37°C. Samples were taken after 30, 60 and 120 minutes and analysed by reducing SDS-PAGE for the presence of C3b cleavage products at 68, 46 and 43kDa. Faint bands corresponding to cleavage products at 68kDa were observed for both wild-type and mutant His-C1QTNF5-coated plates after 120 minutes incubation, and this was greatest when 2.0µg/ml CFH was used. No cleavage products were observed when plates were not coated with His-C1QTNF5. 68kDa cleavage products can be seen as faint bands above the darker C3bα bands present at 64kDa (see within boxes).

5.7 Discussion

It has been shown that CFH interacts with His-C1QTNF5, supporting the observations reported previously by Dr X. Shu. The interaction was confirmed by plate binding assays and SPR, and shown to occur between His-C1QTNF5 (wild-type and mutant) and full-length CFH, as well as SCRs 7-8 and 19-20. Interactions with full-length CFH have been shown to involve at least the gC1q domain of His-C1QTNF5. No interactions could be observed between His-C1QTNF5 and either SCR3-4 or CRP.

As well as confirming an interaction, both SPR and plate binding assays suggested that CFH has a greater affinity for mutant His-C1QTNF5 compared with wild-type. Average affinities (kD) obtained by SPR showed this to be in the nM range and an approximately 17.5-fold increase in affinity was observed for the mutant protein. When the data was analysed using the kinetics/affinity software facility, the predicted model which best fitted the data was 'two-state binding with conformational change.' Whilst this model did indeed provide the best fit for the data obtained, it cannot be concluded that this actually describes what occurs when CFH interacts with His-C1QTNF5. This is in part due to the limited number of available models with which to fit the data when carrying out kinetic analysis. It is also due to the limited amount of information SPR analysis provides. Very little is known about how the ligand is attached to the dextran matrix, for instance via which residues this occurs. Also, in the case of mutant His-C1QTNF5, the multimeric state of the protein has yet to be determined (see Chapter 4). Therefore, the predicted binding model should instead be taken as an indication that the reaction kinetics do not fit a simple 1:1 binding model and it is likely that some sort of conformational rearrangement is occurring, possibly involving multiple binding domains. Comparisons can be made between analyte affinities for wild-type and mutant proteins within each experiment, however further analysis would need to be carried out to determine if the scale of the affinites bears relation to the *in vivo* situation.

SCR7-8Y and SCR7-8H showed similar affinities (kD) for both wild-type and mutant His-C1QTNF5, although these were slightly higher for the mutant. SCR19-20, however, showed a 95-fold greater affinity for mutant His-C1QTNF5 compared with the wild-type. This can be explained by the 173-fold decrease in dissociation rate seen when SCR19-20 interacts with the mutant. When analysing the data for both SCR7-8 and SCR19-20 using the kinetics/affinity software facility, the predicted model offering the best fit in all cases was the '1:1 binding model', although, as discussed above, this prediction comes with limitations.

It has been proposed that when CFH interacts with polyanions it undergoes a conformational change allowing multiple subunits to bind. CFH is predicted to form a coiled omega structure when in solution (Oppermann *et al.,* 2006). It is proposed that initial polyanion binding occurs via the C-terminal SCR20 domain, which is exposed when the protein is in the coiled structure. The protein then undergoes a conformational change exposing other residues, such as SCR7, which are then able to interact with their appropriate ligands (Jokiranta *et al.,* 2005, Oppermann *et al.,* 2006, Prosser *et al.,* 2007). The data obtained by SPR also supports such a conformational change occurring when CFH interacts with C1QTNF5. It has been shown in this study that SCR19-20 interacts with His-C1QTNF5, as does SCR7-8. However the data obtained by SPR for these interactions conforms to a simple 1:1 binding model, unlike that for full length CFH. The dissociation rates for the SCR domains are much more rapid than for full length CFH, with this averaging to an approximately 75-fold difference for wild-type His-C1QTNF5. This would imply that, after initial association, multiple domains bind and 'solidify' the interaction. If CFH in solution is indeed in an omega structure, then the most accessible domains would be the C-terminal ones such as SCR19-20, which could undergo initial binding. SCR19-20 shows a 95-fold greater affinity for mutant His-C1QTNF5 compared with the wild-type, which could account for at least some of the increased affinity observed with full length CFH. It is also possible other domains are involved, providing scope for further investigation.

Further support for a conformational change comes from the plate binding assays. For both His-C1QTNF5- and His-gC1q-coated plates, CFH specific binding appears to increase up to a maximum CFH concentration (0.5µg/ml CFH for His-gC1q and 0.15µg/ml for His-C1QTNF5), after which a decrease in specific binding is observed. This observation could be explained if CFH undergoes a conformational change when it interacts with His-gC1q or His-C1QTNF5, so reducing the accessibility of the OX23 epitope. As increasing amounts of CFH bind, so the accessibility is reduced further still and the apparent specific binding decreases. OX23 is a monoclonal antibody whose epitope lies in SCR1-7. As discussed above, this region is predicted to be involved in a conformational change when CFH binds other ligands such as polyanions, so it is possible this is also the case when interacting with C1QTNF5. It was not possible to detect by plate binding assay any interaction between CFH and His-C1QTNF5 when CFH is in the solid phase. This observation could be a result of CFH attaching to the plate, preventing it from changing conformation upon His-C1QTNF5 binding, possibly via SCR19-20. Due to the rapid dissociation rate shown by SPR for interactions with this domain, and the lengthy stages involved in the plate binding assay, any bound His-C1QTNF5 would dissociate before it could be detected.

When carrying out the plate binding assays, CFH was diluted in 10mM MES pH6.5. This was shown to reduce background binding of CFH to the microtitre plate, when compared with PBS pH7.2, but not to reduce specific binding of CFH to His-C1QTNF5 or His-gC1q. Whilst physiological pH is usually around 7.4, at sites of inflammation this can be reduced slightly to around 6.5 (Lardner, 2001). The observation that this reduction in pH does not adversely affect the CFH-C1QTNF5 interaction is interesting, particularly with reference to the diseased eye. Inflammation plays a major role in AMD (Donoso *et al.,* 2006), and most likely in L-ORMD, which would imply the *in vivo* pH of a diseased retina may be nearer to 6.5 than 7.2. The evidence in this study would suggest that if this were the case, a slight reduction in pH would not adversely affect the interaction between CFH and His-C1QTNF5. SPR interactions were carried out at pH7.4, and for both SPR and plate

binding assays CFH showed a greater affinity for mutant His-C1QTNF5, which means that, within the range pH6.5 to pH7.4, this preference is not affected.

No interactions were observed between His-C1QTNF5 or His-gC1q and CRP by either SPR or plate binding assay. CFH has been shown to interact with CRP and this interaction is affected by the Y402H polymorphism in SCR7 (Blackmore *et al.,* 1996, Jarva *et al.,* 1999, Giannakis *et al.,* 2003). His-C1QTNF5 has been shown to bind CFH via this domain too. It is therefore possible, although no direct interaction with CRP was observed, that C1QTNF5 could affect its binding to CFH. This could be via steric hinderance, when C1QTNF5 is bound to CFH, or by competing with CRP for CFH binding. Instead of alterations in CRP binding to CFH due to the Y402H polymorphism contributing to the AMD phenotype, it is possible the altered affinity of CFH for C1QTNF5 due to the Ser163Arg mutation affects the CFH-CRP interaction and this could contribute to the disease mechanisms in L-ORMD.

The previously reported interaction between C1QTNF5 and polyanions was not investigated further in this study. However, CFH binding to polyanions also occurs via SCR7, so again it is possible that C1QTNF5 could cause steric hinderance or compete with polyanions for CFH binding, or vice versa. Mutation in C1QTNF5 affects its interaction with CFH, so it is possible that this could disrupt an equilibrium between C1QTNF5, CFH, CRP and/or polyanions, and this too could have possible implications for CFH function and disease mechanisms in retinal degeneration.

One of the functions of CFH is to act as a co-factor for Factor I-mediated cleavage of C3b (Whaley *et al.,* 1976, Pangburn *et al.,* 1977). It was investigated whether CFH interacting with His-C1QTNF5 could affect this function. Firstly, it was investigated whether any effects of His-C1QTNF5 could be observed on CFH co-factor activity whilst in solution. Adapting a previously described method (Sim *et al.,* 1981, Alsenz *et al.,* 1984), no effects were observed by either adding His-C1QTNF5 (wild-type and mutant) to the reaction mixture, or by replacing CFH with His-C1QTNF5. Therefore, fluid phase His-C1QTNF5 does not appear to have any effect on CFH co-

factor activity. However, *in vivo* C1QTNF5 has been shown to be associated with the RPE plasma membrane (Mandal *et al.,* 2006c), and also to interact with the membrane protein MFRP (Shu *et al.* 2006b, Mandal *et al.* 2006b). It is therefore unlikely that fluid-phase C1QTNF5 is in abundance in the retina, but rather that it is membrane associated, possibly in complex with other proteins. The plate binding assay was adapted to investigate whether any effects on co-factor activity could be observed when CFH was bound to immobilised His-C1QTNF5. It was shown that, for both wild-type and mutant His-C1QTNF5-coated plates, C3b degradation products were produced. Unfortunately, it is not possible to say whether these were the result of CFH which was interacting with His-C1QTNF5 or CFH which had dissociated from the complex. However, the assay did lend support to the theory that CFH undergoes a conformational change when it attaches to C1QTNF5. CFH was added to the wells at concentrations of 0, 0.5 and 2.0µg/ml. The greatest amount of C3b degradation products were observed when 2.0µg/ml CFH was used, implying that more CFH was present when added to the wells at the higher concentration. No degradation products were observed in the control wells without a His-C1QTNF5 coat. The plate binding assays appeared to show maximum CFH binding at 0.15µg/ml, and at 2.0µg/ml it appeared that there was no CFH bound. The C3b solid phase assay shows this was not the case, indicating that, when carrying out the plate binding assay, the OX23 antibody was unable to detect bound CFH above a maximum amount of bound protein.

As discussed above, it is possible there may not be abundant fluid-phase C1QTNF5 *in vivo.* No effects of fluid-phase His-C1QTNF5 were observed on CFH co-factor activity. This may be because CFH does not interact with fluid-phase C1QTNF5 and, as discussed above, it is likely that *in vivo* C1QTNF5 is membrane-associated and/or in complex with other proteins. This could affect its ability to interact with CFH, either due to accessibility of C1QTNF5 domains or because CFH may require a matrix to assist in undergoing a conformational change and forming a strong association with C1QTNF5. Indeed, this situation would be supported by the previous observation that C1QTNF5 interacts with GAGs. To test these hypotheses, ITC was carried out looking for an interaction between His-gC1q and CFH in

solution, both in the nM and the μM range of affinities. No interaction could be observed in either case. This may well be because the two proteins do not interact in solution. However, it cannot be ruled out that the lack of observed interaction was due to flaws in the experimental protocol. CFH is predicted to form a coiled omega structure in solution, with only the C-terminal domains accessible. His-C1QTNF5 has been shown by SPR to interact with SCR19-20, so it would still be predicted that an interaction could be observed between the C-terminal domains and His-gC1q, with rapid association and dissociation rates, even if the tertiary structure of CFH prevented a strong association involving multiple subunits. This was not the case. The proteins used in ITC were at near-maximum concentrations, just below those at which precipitation occurred, and the ITC process also involves continuous stirring of the reaction solution in the sample cell. It is possible that at such high concentrations and when undergoing vigorous stirring the proteins became misfolded and/or aggregated and were unable to interact. Analysis of the solutions by gel filtration before and after carrying out the experiment could confirm if any misfolding and/or aggregation had occurred.

Further analysis by gel filtration would also help answer some other questions regarding the CFH-C1QTNF5 interaction. It could provide clarification of whether full length CFH interacts with C1QTNF5 in solution. Incubating the two proteins together and then carrying out gel filtration analysis would result in a different pattern of elution if the two proteins were in complex compared with the elution patterns obtained for the individual proteins. This would, however, require the nM affinities obtained by SPR of CFH for His-C1QTNF5 to be correct. With affinities in this range it could be expected that the proteins would remain in complex whilst running through the column. If the affinities are actually in the μM range then it is likely dissociation would occur before the proteins were eluted from the column. For this reason, again assuming the SPR affinities are correct, it would not be possible to detect any interaction between C1QTNF5 and the recombinant SCR domains.

In addition to gel filtration, other experiments could also provide insight into the CFH-C1QTNF5 interaction. Using SPR, more in depth analysis of which particular

SCR domains are involved in the interaction could be carried out. This would involve using a wider range and combination of individual domains to determine those that are essential for the interaction. Focusing on a function for the interaction, it could be investigated whether His-C1QTNF5 has any effect on CFH decay accelerating activity. It could also be investigated whether there is any competition between CFH and His-C1QTNF5 for binding to polyanions, and whether this is affected by the His-C1QTNF5 mutation. Whilst it is possible that C1QTNF5 may have a role in regulating CFH activity, it is also possible this is not the case. It may be found that there is no effect, but rather that C1QTNF5 helps to localise CFH within the retina. Either way, it needs to be determined which is the case as this could have important implications for disease mechanisms.

6 CHAPTER 6

:

INVESTIGATING A ROLE FOR C1QTNF5 IN PHAGOCYTOSIS

6.1 Introduction

One of the major roles of the RPE is the daily phagocytosis of shed ROS (Young & Bok, 1969). This follows a circadian rhythm, with disc shedding promoted by the onset of light (La Vail, 1976). Phagocytosis of ROS involves two stages; binding and internalisation. Binding occurs via the integrin receptor, αvβ5. This is the only integrin receptor expressed by the RPE, which plays a role in retinal adhesion and maintenance of the ROS-RPE microvilli interdigitation, as well as in phagocytosis (Nandrot *et al.,* 2006). ROS binding to αvβ5 occurs through the ligand MFG-E8, which recognises exposed PS residues on the shed outer segments (Nandrot *et al.,* 2007). The tetraspanin, CD81, facilitates αvβ5 attachment to the ROS, probably by regulating the processing and/or turnover of the integrin receptor (Chang *et al.,* 2007). Internalisation of ROS has been shown to occur by two pathways. Firstly, the αvβ5 receptor stimulates phagocytosis by the FAK/MerTK signalling pathways, which was shown to occur independently of CD81 (Finnemann *et al.,* 2003, Finnemann *et al.,* 2006b, Chang *et al.,* 2007). Secondly, in a completely separate process, CD36 recognises oxidised phospholipids on the ROS membrane, promoting their phagocytosis. It is suggested that these phospholipids arise due to light-induced oxidative damage, which is predicted to occur frequently in the highly exposed retinal region (Sun *et al.,* 2006).

C1QTNF5 has been shown to localise to the RPE apical processes (Mandal *et al.,* 2005), with individuals having L-ORMD showing abnormalities in rod adaptation kinetics, sub-retinal deposits and retinal degeneration (Jacobson *et al.,* 2001, Kuntz *et al.,* 1996, Miliam *et al.,* 2000). Analysis of a diseased eye revealed shortened ROS with disorganised disc membranes (Duval *et al.,* 1986). The *rd6* mouse, which has a mutation in *MFRP*, has a reduced number of apical microvilli, decreased photoreceptor function, deficiencies in ROS phagocytosis and also undergoes retinal degeneration (Won *et al.,* 2008). *C1QTNF5* is expressed as a bicistronic transcript with *MFRP* (Hayward *et al.* 2003), and C1QTNF5 has been shown to interact with MFRP CUB domains (Shu *et al.,* 2006b). This would suggest common functional pathways between the two proteins. Since both proteins have been shown to localise

to the ROS-RPE apical boundary (Mandal *et al.,* 2006b, Mandal *et al.,* 2006c), where ROS phagocytosis occurs, it was investigated whether a role could be found for C1QTNF5 in RPE phagocytosis of ROS.

6.2 Investigating a role for C1QTNF5 in RPE phagocytosis of rod outer segments

Comparisons were made between the different transfected ARPE-19 cell lines to see if any effects of wild-type or mutant His-C1QTNF5 over-expression could be observed on phagocytosis of bovine ROS. The same transfected cell lines as used in Chapter 3 were used here, and have already been shown to have similar His-C1QTNF5 secretion levels, with no differences observed in levels of apoptosis, cell adhesion or cellular trafficking of His-C1QTNF5.

6.2.1 Preparing and labelling ROS

ROS were isolated from bovine retinas and labelled with FITC following previously described methods (Papermaster *et al.,* 1974, McLaren *et al.,* 1993). Briefly, following removal from the eye and separation from the RPE, retinas were stored at -80°C prior to use. After thawing on ice and resuspending in homogenising medium, ROS were removed by gentle shaking-induced shearing and collected by centrifugation. Washed ROS were then labelled over night with 10μg/ml FITC in 0.1mM sodium bicarbonate and washed twice with PBS prior to use.

6.2.2 Investigating phagocytosis by flow cytometry

Flow cytometry identifies cells based upon size, granularity and fluorescence. Using these parameters is it possible to distinguish between different types of cells within a heterogeneous population. Analysis by flow cytometry has been used previously to measure levels of FITC-ROS phagocytosis by cultured RPE cells (Miceli *et al.,* 1994, Kennedy *et al.,* 1996), and these methods were adapted for use in this study. Briefly, cells were grown to confluence in 10% serum, after which they were cultured in serum-free media for 3 days. This was to promote differentiation (Karl *et al.,* 2007).

Following any specified treatments (e.g. addition of CFH or anti-gC1q), FITC-ROS were added to the culture media and the cells incubated for the specified time periods. Cells were detached from the culture flasks by digestion with trypsin and analysed by flow cytometry. Trypsin digestion removes externally bound ROS (Miceli *et al.,* 1994), so analysis by flow cytometry measures levels of internalisation only. It has been shown previously that labelling of cultured RPE with FITC is negligible (Kennedy *et al.,* 1996), so this was not considered to be an issue here.

Following incubation with FITC-ROS, it was possible firstly to identify the ARPE-19 cell lines based upon size and granularity and then secondly to determine the degree of phagocytosis based upon the mean fluorescence of the cell population. Figure 6.1 shows the plots obtained when a) measuring cell size and granularity, allowing for identification of the ARPE-19 population, and b) size and fluorescence within the identified ARPE-19 population. These different parameters allow for identification of ARPE-19 or ARPE-19 plus FITC-ROS, with specified levels of phagocytosis based upon the mean fluorescence of the identified population.

6.2.2.1 Investigating levels of phagocytosis in the ARPE-19 transfected cell lines

It was investigated whether any differences in levels of phagocytosis could be observed when comparing the transfected cell lines over-expressing wild-type or mutant His-C1QTNF5, or untransfected ARPE-19. The assay was carried out as described above, with levels of phagocytosis determined after 0, 1.5, 3, 7, 24 and 48 hours. Levels of phagocytosis were calculated by deducting the mean fluorescence of the cell population from the mean fluorescence of the cell population plus FITC-ROS, as described previously (Kennedy *et al.,* 1996). This was calculated separately for each cell line, with final levels of phagocytosis expressed as the fold-difference compared with untransfected ARPE-19 after 48 hours incubation. The assay was repeated three times and the data pooled. Cells over-expressing wild-type His-C1QTNF5 showed increased levels of phagocytosis up to 48 hours compared with the other cell lines. Cells expressing mutant His-C1QTNF5 showed approximately the same levels of phagocytosis as untransfected ARPE-19 (see Figure 6.2).

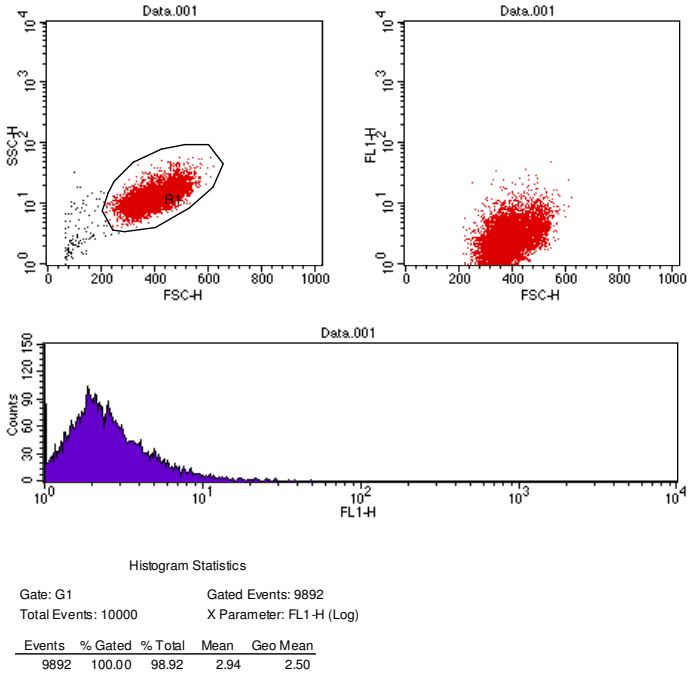

Histogram Statistics

Gate: G1 Gated Events: 9892
Total Events: 10000 X Parameter: FL1-H (Log)

Events	% Gated	% Total	Mean	Geo Mean
9892	100.00	98.92	2.94	2.50

(A)

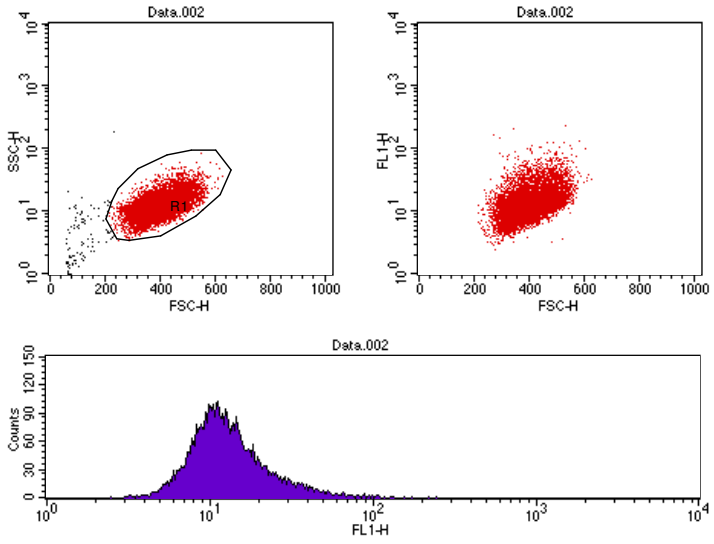

Histogram Statistics

Gate: G1 Gated Events: 9896
Total Events: 10000 X Parameter: FL1-H (Log)

Events	% Gated	% Total	Mean	Geo Mean
9896	100.00	98.96	14.99	12.88

(B)

Figure 6.1: Flow cytometry plots showing ARPE-19 (A) and ARPE-19 incubated with FITC-ROS (B).
ARPE-19 are identified by size (FSC-H) and granularity (SSC-H) and highlighted by the gate, R1. The fluorescence (FHL-1) of the gated cells is then determined. Cells incubated with FITC-ROS show a greater geometric mean fluorescence (12.98) than ARPE-19 alone (2.50) indicating they have pahgocytosed the FITC-ROS.

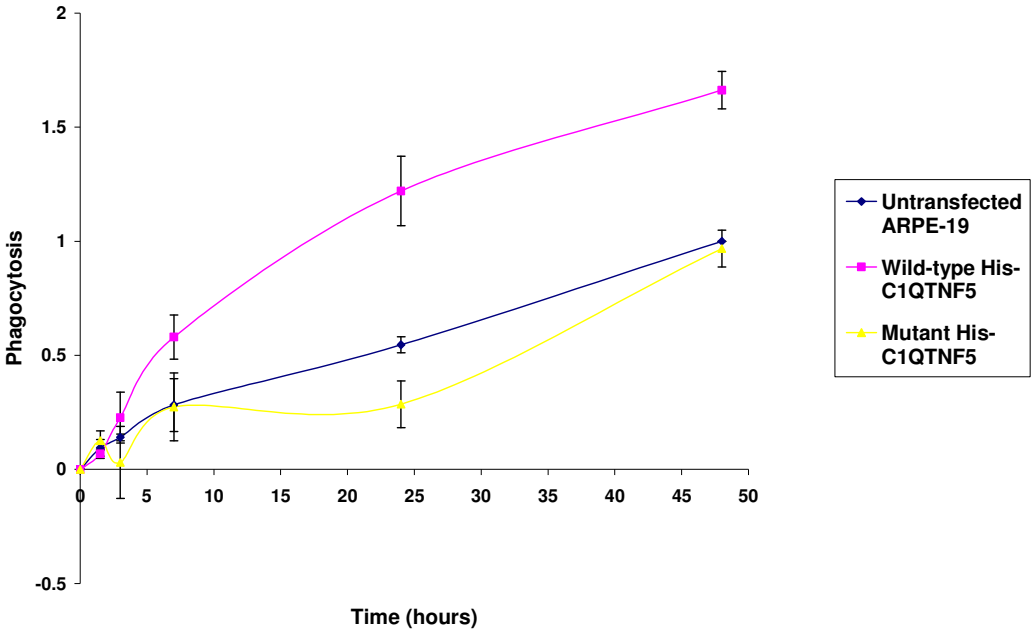

Figure 6.2: ARPE-19 over-expressing wild-type His-C1QTNF5 show greater levels of FITC-ROS phagocytosis compared with cells over-expressing mutant His-C1QTNF5 and untransfected ARPE-19, which show similar phagocytosis levels.

Cells were incubated with FITC-ROS for increasing time periods up to 48 hours and analysed by flow cytometry. Levels of phagocytosis were calculated as the fold difference in fluorescence compared with untransfected ARPE-19 after 48 hours. The assay was repeated 3 times. Error bars indicate standard errors.

6.2.2.2 Investigating the effects of additional His-C1QTNF5

Using untransfected ARPE-19, wild-type or mutant His-C1QTNF5 was added to the culture medium at concentrations of 0, 0.25 and 10μg/ml. Following incubation for 1 hour, the FITC-ROS were also added and the cells incubated for 30 hours. Levels of phagocytosis were measured as before. No effects of additional His-C1QTNF5 were observed (see Figure 6.3). The assay was not repeated.

6.2.2.3 Investigating the effects of an anti-gC1q antibody

The results from Section 6.2.2.1 show that over-expression of wild-type His-C1QTNF5 in ARPE-19 results in increased levels of FITC-ROS phagocytosis. It was investigated whether adding an antibody raised against C1QTNF5 could affect this observation. It has been shown in previous studies that adding antibodies raised against the mannose receptor or CD36 can alter levels of ROS phagocytosis by cultured RPE cells (Boyle *et al.,* 1991, Finnemann *et al.,* 2001). In the case of the mannose receptor, the antibody inhibited phagocytosis suggesting that it had a blocking effect. However, in the case of CD36, addition of the antibody actually increased the level of phagoytosis. It was suggested that the antibody caused dimerisation of the CD36 which had knock-on signalling effects, altering the rate of ROS internalisation.

6.2.2.3.1 Confirming the antibody interacts with His-C1QTNF5

A monoclonal antibody raised against an *E. coli*-produced recombinant gC1q domain had been produced previously by Dr X. Shu. The gC1q domain is at the C-terminal of C1QTNF5, and His-C1QTNF5 contains a C-terminal poly-His tag. It was therefore investigated whether the antibody would also recognise His-C1QTNF5. Recombinant wild-type and mutant His-C1QTNF5 (see Chapter 4) were analysed by Western blot, probing with the anti-gC1q antibody. As can be seen from Figure 5.5, the antibody recognised the protein (Figure 6.4).

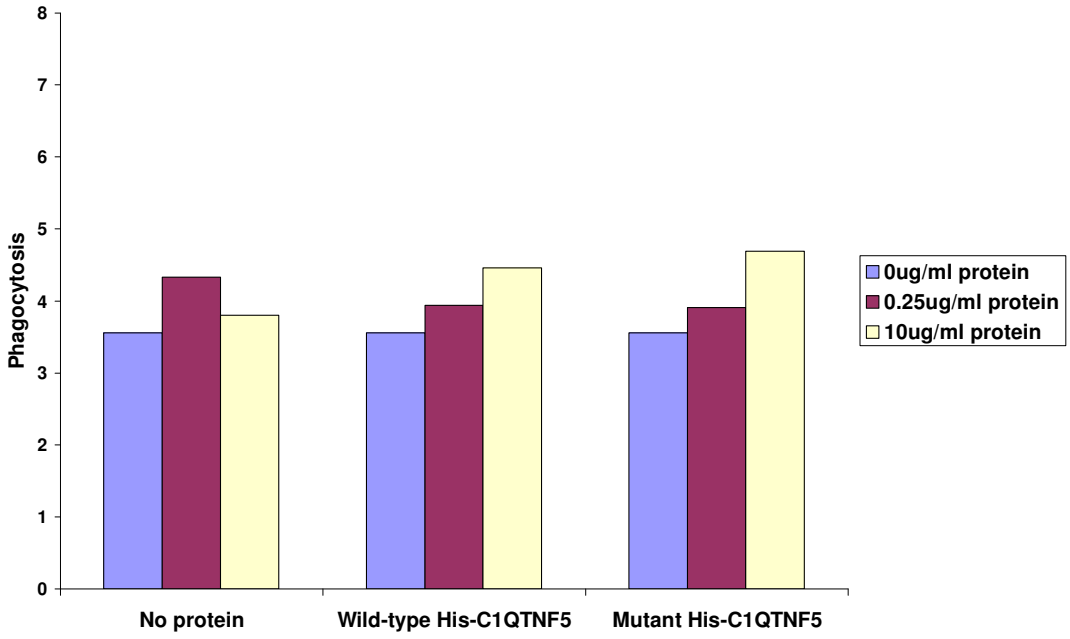

Figure 6.3: Adding wild-type or mutant His-C1QTNF5 to the culture media of untransfected ARPE-19 had no effect on levels of FITC-ROS phagocytosis.

The protein was added at concentrations of 0, 0.25 or 10µg/ml for 1 hour prior to addition of the FITC-ROS, and levels of phagocytosis determined by flow cytometry.

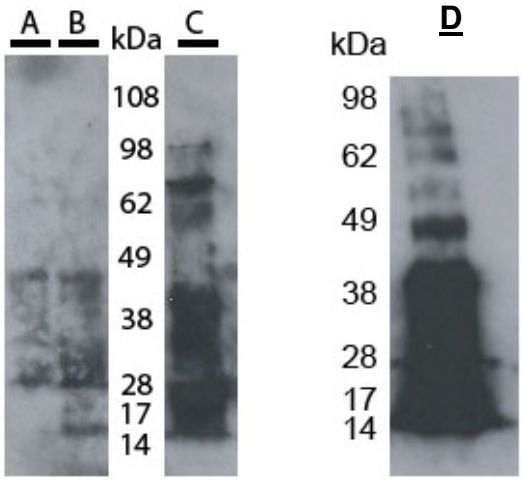

Figure 6.4: Western blot showing the anti-gC1q antibody recognises wild-type and mutant His-C1QTNF5.

A – Wild-type His-C1QTNF5, and B – Mutant His-C1QTNF5, detected with anti-gC1q.
C – Wild-type His-C1QTNF5, detected with anti-His.
D – His-gC1q, detected with anti-gC1q
kDa: relative molecular mass

6.2.2.3.2 The effects of adding anti-gC1q antibody

Following culture for 3 days post-confluence in serum-free media, cells were incubated with antibody diluted 1:60 from stock in serum-free media for 1 hour. FITC-ROS were then added to the wells and the cells incubated for 30 hours. This incubation time was shown in Figure 6.2 to be adequate to easily observe differences in levels of FITC-ROS phagocytosis between the cell lines. As can be seen from Figure 6.5, when no antibody was added wild-type His-C1QTNF5-expressing cells showed an approximately 1.5-fold significant increase (two-sample $t(4) = -2.735$, $p = 0.05$) in levels of phagocytosis compared with untransfected cells. No difference was observed between untransfected and mutant His-C1QTNF5-expressing cells. Upon addition of the antibody, levels of phagocytosis increased to 2.5-fold greater than untransfected ARPE-19 in the wild-type His-C1QTNF5-expressing cells (two-sample $t(4) = -5.311$, $p = 0.006$), but no differences were observed for the other two cell lines. The assay was repeated three times.

6.2.2.4 Investigating the effects of CFH treatment

It was shown in Chapter 5 that His-C1QTNF5 interacts with CFH, and this interaction involves the gC1q domain. To determine whether CFH interacting with His-C1QTNF5 had any effects on levels of phagocytosis, CFH was added to the assay at concentrations of 0, 1, 5, 10 and 50μg/ml and the cells incubated for 1 hour prior to the addition of FITC-ROS. The cells were then incubated for 30 hours and levels of phagocytosis determined by flow cytometry as the fold-increase when compared to ARPE-19 with no additional CFH, with the assay repeated two times. No effects on levels of phagocytosis were observed upon addition of CFH (Figure 6.6).

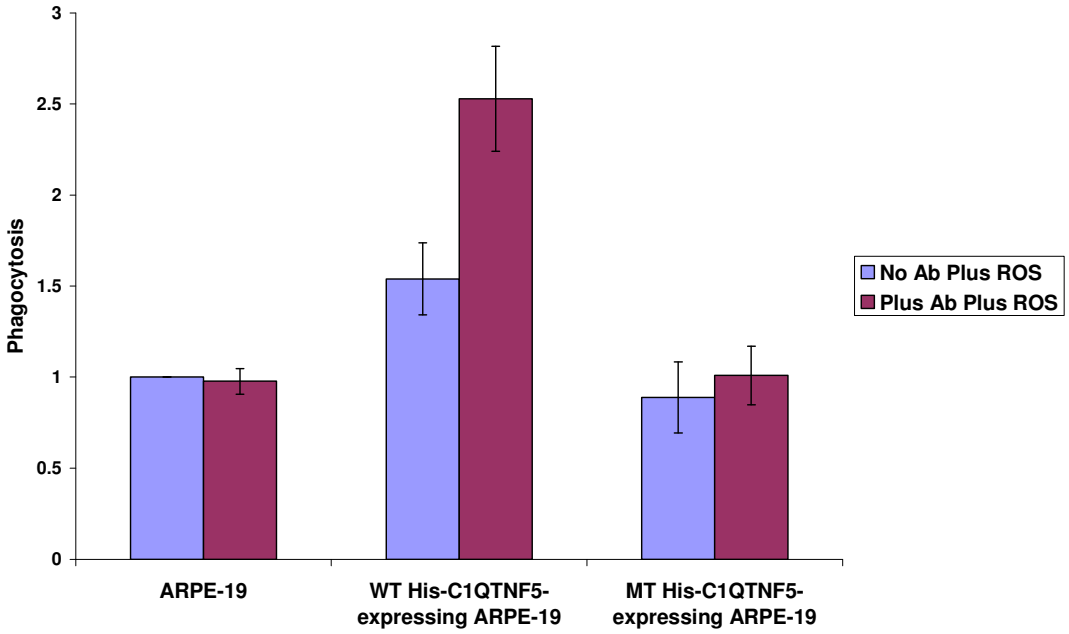

Figure 6.5: ARPE-19 stably over-expressing wild-type His-C1QTNF5 show increased levels of phagoytosis of FITC-ROS compared with ARPE-19 stably over-expressing mutant His-C1QTNF5 or untransfected ARPE-19. Adding anti-gC1q antibody (Ab) increases levels of phagocytosis in the wild-type His-C1QTNF5 cells further still, but has no effect on the other two cell lines. The assay was repeated 3 times, with the error bars indicating standard errors.

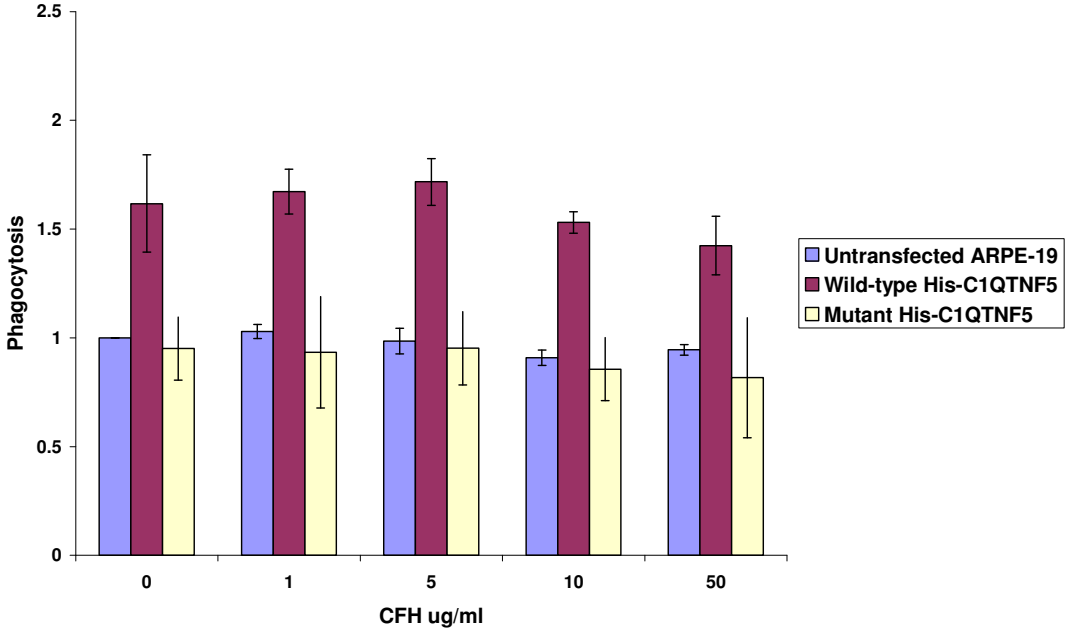

Figure 6.6: Adding CFH to the culture media of ARPE-19 or APRE-19 stably over-expressing wild-type or mutant His-C1QTNF5 has no effect on levels of FITC-ROS phagocytosis. Cells were incubated with CFH for 1 hour prior to the addition of FITC-ROS. The assay was repeated 3 times, with the error bars indicating standard errors.

6.3 The effects of C1QTNF5 on macrophage phagocytosis

Macrophages have also been suggested to play a role in AMD, possibly in the clearance of sub-RPE deposits (Forrester, 2003). Macrophages are present in the human diseased retina and CCL-2 knockout mice exhibit a phenotype very similar to AMD (Ambati *et al.,* 2003). It was therefore investigated whether His-C1QTNF5 had any effect on macrophage phagocytosis of apoptotic neutrophils, working with and adapting methods optimised by Aisleen McColl (MRC Centre for Inflamation Research). Monocytes were purified from whole blood and matured into macrophages by incubation at 37°C for 5 days. The mature macrophages were then added to 6-well plates, either coated with the various proteins under investigation or with the protein added to the media. Annexin-V-labelled apoptotic neutrophils were then added and, following incubation, levels of phagocytosis determined by flow cytometry. Some macrophages were stimulated with dexamethasone prior to carrying out the assay as it has been shown that dexamethasone enhances nonphlogistic phagocytosis of apoptotic leukocytes by macrophages (Liu *et al.,* 1999). The assay was carried out with or without autologous serum as it had previously been shown by A. McColl that autologous serum contained a substance which promoted phagocytosis of apoptotic cells.

6.3.1 Detecting macrophages by flow cytometry

Figure 6.7 shows the dot plots obtained when analysing the phagocytic macrophages by flow cytometry. It is possible to distinguish between macrophages, neutrophils and lymphocytes (as it is impossible to remove all of these), as can be seen from graph 1. It is also possible to distinguish which macrophages have phagocytosed annexin V-labelled neutrophils, as can be seen from graph 2.

6.3.2 Macrophage phagocytosis with autologous serum

To investigate whether wild-type His-gC1q, wild-type His-C1QTNF5 or CFH had any effect on macrophage phagocytosis of apoptotic neutrophils, the macrophages were plated onto 6-well plates coated with these proteins. The phagocytosis assay was then carried out with autologous serum present, and macrophages were either pre-treated or not pre-treated with dexamethasone. As can be seen from Figure 6.8,

there were no differences in levels of phagocytosis between the treatments, either with or without dexamethasone. As has been shown previously (Liu *et al.,* 1999), dexamethasone did increase levels of phagocytosis.

6.3.3 Macrophage phagocytosis without autologous serum

Following on from the observation by A. McColl that autologous serum contains a substance which promotes macrophage phagocytosis of apoptotic cells, the phagocytosis assay was carried out without autologous serum. Each of the treatments (wild-type His-C1QTNF5, mutant His-C1QTNF5 and CFH) was added to the culture media in replace of the serum to see if they could restore this property. As can be seen from Figure 6.9, there were no differences in levels of phagocytosis between the treatments, either with or without dexamethasone. Adding autologous serum did however increase levels of phagocytosis in both dexamethasone treated and untreated cells, with levels above those observed for any of the treatments.

(Graph 1) **(Graph 2)**

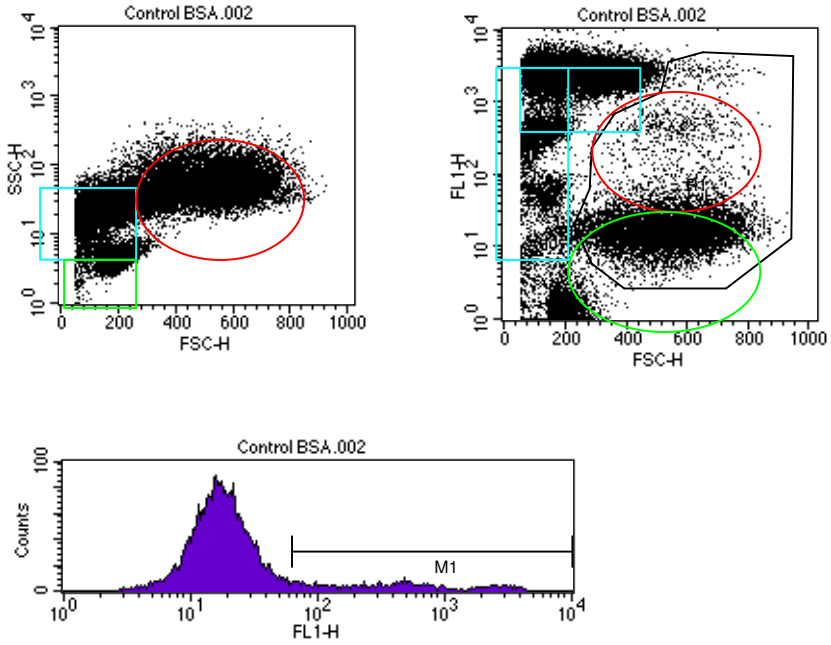

File: Control BSA.002 Acquisition Date: 08-Nov-06
Gate: G1 Gated Events: 9722
Total Events: 51850

Marker	Left, Right	Events	% Gated	% Total
All	1, 9910	9722	100.00	18.75
M1	63, 9910	824	8.48	1.59

Figure 6.7: Dot plots obtained when analysing phagocytic macrophages by flow cytometry.

Graph 1: The red circle indicates macrophages, the blue rectangle indicates neutrophils and the green rectangle indicates lymphocytes.
Graph 2: The blue rectangles indicate Annexin V-labelled neutrophils, the green circle indicates non-phagocytic macrophages and the red circle indicates phagocytic macrophages which have taken up labelled neutrophils.
The histogram shows macrophages contained within the black gate in graph 2. M1 indicates phagocytic macrophages.
FSC-H: cell size, SSC-H: cell granularity, FHL-1: fluorescence

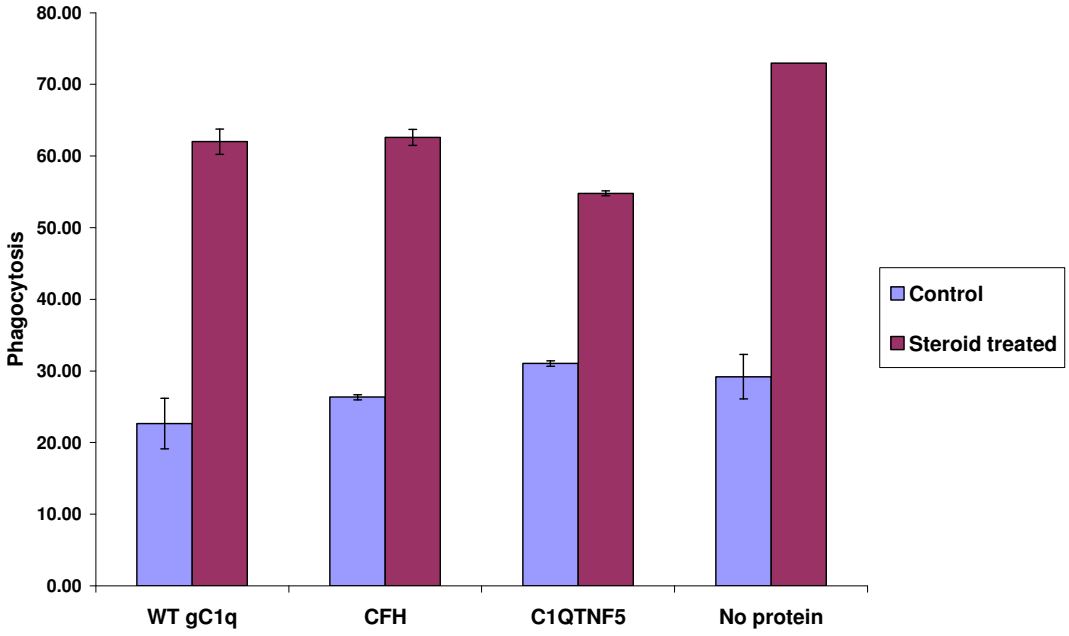

Figure 6.8: C1QTNF5, CFH and gC1q have no effect on levels of macrophage phagocytosis of apoptotic neutrophils in the presence of autologous serum.
Pre-treating cells with dexamethasone increased levels of phagocytosis in all cases, but no effect of C1QTNF5, CFH or gC1q was observed. THe assay was repeated twice with error bars showing standard errors.

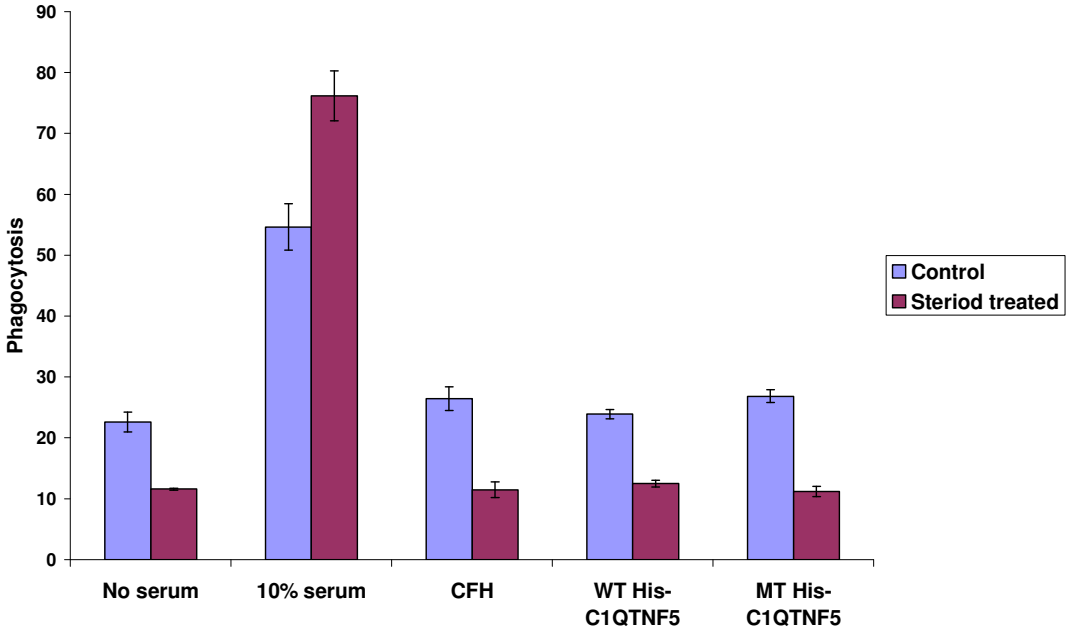

Figure 6.9: Wild-type His-C1QTNF5, mutant His-C1QTNF5 and have no effect on levels of macrophage phagocytosis of apoptotic neutrophils in the absence of autologous serum.
Pre-treating cells with dexamethasone increased levels of phagocytosis in all cases, but no effect of C1QTNF5, CFH or gC1q was observed. The assay was repeated twice with error bars showing standard errors.

6.4 Discussion

An assay has been developed for determining levels of FITC-labelled ROS phagocytosis by cultured ARPE-19 cells. Levels of internalisation only and not binding are measured, as the technique involves trypsinising the adherent cells prior to analysis by flow cytometry. It was shown using this assay that the levels of internalised FITC-ROS increase for up to 48 hours in all cell lines. The levels were compared between untransfected ARPE-19 and ARPE-19 over-expressing wild-type or mutant His-C1QTNF5, and were greater in the cells over-expressing the wild-type protein compared with the other two cell lines. Levels of phagocytosis were measured after 30 hours and found to be approximately 1.5-fold greater in this cell line, but again there was no difference in levels of phagocytosis between the untransfected or mutant His-C1QTNF5-expressing cell lines. It was shown in Chapter 3 that the transfected ARPE-19 cell lines used showed similar levels of His-C1QTNF5 secretion, so the differences observed between the two cell lines are unlikely to be due to differences in extracellular His-C1QTNF5. These results would suggest that C1QTNF5 plays a role in RPE phagocytosis of ROS and that the 163Arg mutant protein is unable to function fully in this role. Some levels of phagocytosis were observed in the mutant cell line, and these levels were the same as the untransfected cells. Endogenous C1QTNF5 expression was not knocked out in the transfected cell lines so it is possible that this enabled some phagocytosis to occur at endogenous levels.

However, it has been shown by Shu *et al.* (2006a) that wild-type and mutant C1QTNF5 interact. This could mean that over-expression of mutant protein would result in sequestering of the endogenous wild-type protein, and imply that the phagocytosis observed in the mutant cell line is occurring independently of C1QTNF5. It is not currently possible to say which situation is occurring.

Previous studies into receptors and ligands involved in ROS phagocytosis have shown some molecules to be involved in ROS binding to the RPE and some molecules to be involved in internalisation. For instance, the αvβ5 integrin receptor is involved in ROS binding but not internalisation (Finnemann *et al.,* 1997).

However, ROS attachment to this receptor stimulates proteins and signalling pathways which are responsible for internalising the ROS, such as FAK and MerTK (Finnemann *et al.,* 2003, Finnemann *et al.,* 2006b). CD81, for instance, is not involved directly involved in ROS attachment to the RPE. Rather, it is thought to regulate the processing and/or turnover of the intergrin receptor which indirectly affects both rate of binding and internalisation. The assays used in this study only measured levels of internalisation, not binding. However, although levels of internalisation were greater in the wild-type His-C1QTNF5-expressing cells, this could be due to increased binding and subsequent up-regulating of internalisation pathways. Previous assays have used antibodies to investigate whether particular molecules are directly involved in ROS binding, for instance, when investigating the mannose receptor, anti-mannose receptor antibodies blocked ROS binding (Boyle *et al.,* 1991), or whether the molecules are involved in signalling pathways, for instance anti-CD36 antibodies upregulated levels of internalisation, probably via dimerisation of the molecule (Finnemann *et al.,* 2001). When an antibody to the gC1q domain of C1QTNF5 was added to the phagocytosis assay, levels of FITC-ROS phagocyotsis increased in the wild-type His-C1QTNF5-expressing cell. No differences were observed for the other two cell lines. This not provides evidence that it is C1QTNF5 which is responsible for the increased levels of phagocytosis seen when no antibody was present, but it would also suggest that the molecule is not directly involved in ROS binding otherwise this would have been blocked by the antibody. Repeating the assay with a non-specific IgG antibody would confirm whether that this was the result of a specific interaction of the anti-gC1q antibody with gC1q. C1QTNF5 is known to multimerise via its gC1q domain, so it is possible that addition of the antibody caused clustering of the molecules. C1QTNF5, although secreted, has been shown to be membrane associated (Mandal *et al.,* 2006c), and to interact with the membrane protein MFRP (Shu *et al.,* 2006b, Mandal *et al.,* 2006b). It could therefore be predicted that C1QTNF5 plays a signalling role in phagocytosis, transmitting signals intracellularly via interactions with membrane-associated proteins.

Whilst the assay results would certainly suggest a role for C1QTNF5 in ROS phagocytosis, there are several further experiments which could help to confirm this. Perhaps the most obvious is to add recombinant C1QTNF5 to untransfected ARPE-19 and see if this has any effect. This was carried out using the recombinant His-C1QTNF5 (wild-type and mutant) produced previously, however no effects were observed. This observation may have arisen for several reasons. It is possible that the recombinant protein was not added at sufficiently high levels. It is also possible that the cells were not incubated with the protein for long enough prior to addition of the FITC-ROS. C1QTNF5 over-expression may regulate the expression or localisation of other proteins necessary for ROS phagocytosis and this did not occur after only 1 hour incubation. It is also possible that the recombinant protein did not interact with whichever proteins endogenous C1QTNF5 interacts with, and that for interactions to occur the protein needs to be expressed within the cell and subsequently secreted. Therefore, although the result was negative for this assay, this does not categorically rule out any involvement of C1QTNF5. Another way of confirming the involvement of C1QTNF5 would be by using small interfering ribonucleic acid (siRNA) to knockout *C1QTNF5* expression. If this reduced levels of phagocytosis in any of the cell lines it would confirm an involvement of C1QTNF5. In order to ascertain whether C1QTNF5 is involved in binding or internalisation of the ROS, fluorescence microscopy could be carried out. Several studies have looked at levels of ROS binding to cultured RPE cells (Nandrot *et al.,* 2005, Sun *et al.,* 2006), using fluorescently-labelled ROS and determining the number of bound ROS per cell. These methods could be adapted for the ARPE-19 cell lines used in this study.

Further evidence for an involvement of C1QTNF5 in RPE phagocytosis comes from studies into the *rd6* mouse. This mouse has a mutation in MFRP affecting its ability to phagocytose ROS (Won *et al.,* 2008). C1QTNF5 interacts with MFRP *in vitro* (Shu *et al.,* 2006b, Mandal *et al.,* 2006b), and the two proteins are expressed as a bicistronic transcript, which would imply they are functionally related (Hayward *et al.,* 2003). They have also been shown to co-localise in cultured MDCK cells (Mandal *et al.,* 2006). With the exception of CFH, this study has not shown what

other proteins C1QTNF5 interacts with. Adding anti-gC1q antibody to the phagocytosis assay has indicated that C1QTNF5 likely plays a signalling role, maybe involving clustering of the molecule. C1QTNF5 is a secreted protein, so is required to interact with membrane proteins in order for this signal transduction to occur. It is therefore highly likely that one such protein is MFRP. Further analysis is needed to confirm this, again, for instance, using siRNA or anti-MFRP antibodies. Other proteins shown to be involved in ROS phagocytosis include CD81, CD36 and the αvβ5 integrin. It would be interesting to investigate whether C1QTNF5 interacts with any of these proteins and so is involved in these known pathways, or if it is involved in a totally separate, novel pathway.

It was shown in Chapter 5 that C1QTNF5 interacts with CFH. Therefore, CFH was added to the phagocytosis assay to see if it had any effects on levels of phagocytosis. None was observed. It is possible that this is because CFH interactions with C1QTNF5 are not involved in the phagocytosis process. For instance, the purpose of the interaction with C1QTNF5 may be to localise CFH to a specific area, preventing complement activation. However, it is also possible that CFH may be involved in phagocytosis but this was not detected by the assay. As with adding C1QTNF5 to the assay, it is possible that a longer incubation time may be required. It is also possible that the added CFH was not interacting with C1QTNF5 at the cell surface. This may be because CFH will only interact with C1QTNF5 under certain conditions, as was found in Chapter 5. Maybe CFH interacts with ligands on the ROS surface, and so pre-incubating the ROS with CFH may have an effect on phagocytosis levels instead. There are other ways in which the assay could be adapted to determine if CFH is involved. Anti-CFH antibodies could be added, as was carried out for gC1q, or siRNA against *CFH* and so prevention of CFH production may also affect the levels of ROS phagocytosis. Therefore, it is not at present possible to rule out any effect of CFH on ROS phagocytosis by the RPE.

It is suggested that AMD disease mechanisms involve ineffective clearance of sub-retinal debris, with some of this clearance being carried out by macrophages, and that defective macrophage recruitment leads to an accumulation of debris. C1QTNF5 has

been shown to be involved in RPE apical phagocytosis, so it was hypothesised it may be able to promote phagocytosis by macrophages too. C1q is a collagen homologous to C1QTNF5 which has been shown to do just that (Ogden *et al.,* 2001). No evidence was found in this study that C1QTNF5 has an effect on macrophage phagocytosis of apoptotic neutrophils. This was not investigated in depth, with only preliminary experiments carried out. Whilst it is possible that C1QTNF5 has no effect on macrophages, it is equally likely that the assay needs to be developed further before any effects can be seen. Such developments could include pre-incubating the apoptotic cells with C1QTNF5 or maturing the macrophages on plates coated with C1QTNF5. These experiments however go beyond what it was possible to achieve within this study.

It has been shown that C1QTNF5 is involved in the RPE phagocytosis of ROS. As C1QTNF5 is mutated in L-ORMD, it is likely that deficits in this function are a major contributing factor towards disease progression, particularly as the mutant protein appears unable to carry out this role. One of the major symptoms of L-ORMD is extensive sub-RPE deposits. It is possible these arise as a result of aberrant ROS phagocytosis. For instance, Amin *et al.* (2004) showed that the composition of basal deposits secreted by RPE cells is dependant upon what they are phagocytosing apically. L-ORMD patients are heterozygous for the Ser163Arg mutation, meaning that they also have wild-type protein present. Therefore it would be expected that their phagocytosis mechanisms, although functioning to some degree, are compromised. Over time this could lead to accumulation of sub-RPE deposits. Lipofuscin, for instance, is thought to be the result of incomplete digestion of phagocytosed material (Reinboth *et al.,* 1997). The sub-RPE deposits seen in L-ORMD resemble the BlamD seen in AMD. These have been suggested to arise due to excess basal secretions by stressed RPE cells (van der Schaft *et al.,* 1994). If the RPE cells are not effectively phagocytosing shed ROS then this may in turn lead to RPE stress and subsequent BlamD deposition by the same mechanisms proposed to occur in AMD.

Dark adaptation difficulties are an early phenotypic marker for L-ORMD. This would suggest that rod photoreceptor function is compromised. It is possible that slight deficiencies in the ability to phagocytose shed ROS over several years would lead to photoreceptor dysfunction. As part of the visual cycle, all-*trans*-retinal is trafficked between the ROS and RPE, where it is recycled back into 11-*cis*-retinal to be used again in the visual cycle (Strauss, 2005). Although dark adaptation difficulties would therefore suggest problems with retinoid recycling rather than phagocytosis, accumulated phagocytosis deficiencies could have knock-on effects on other pathways occurring in the same tissue vicinity, or cause low levels of ROS debris to accumulate between the RPE and ROS, providing a physical barrier to retinoid trafficking between the two cell layers. One of the major problems with slow, progressive late-onset diseases is determining which symptoms are cause and effect, particularly when in depth examination of the affected tissue can only occur after the individual has died. Therefore, it remains unanswered whether sub-RPE debris leads to apical RPE and photoreceptor dysfunction, or vice versa.

7 CHAPTER 7 : DISCUSSION

7.1 Introduction

Age-related macular degeneration is a disease with serious implications, not only for the affected individual but also for society as a whole. The population is ageing and prevalence of AMD increasing, which will inevitably increase the burden on healthcare systems (Evans *et al.,* 1996). Understanding the processes involved in AMD is therefore very important. However, AMD is a complex disease with many contributing factors, both genetic and environmental (Hawkins *et al.,* 1999, Mares-Perlman *et al.,* 1995, Smith *et al.,* 2001, Hammond *et al.,* 2002, Vojnikovic *et al.,* 2007). This makes understanding disease mechanisms difficult. Inherited diseases which show symptoms related to those in AMD can be very helpful in determining molecular pathways that may be involved. One such disease is L-ORMD. L-ORMD patients initially present with dark adaptation abnormalities, indicating photoreceptor dysfunction, and in later stages extensive sub-RPE deposits similar to those seen in AMD, leading to retinal degeneration (Duval *et al.,* 1986, Brosnahan *et al.,* 1994, Kuntz *et al.,* 1996, Milam *et al.,* 2000, Jacobson *et al.,* 2001). L-ORMD is an autosomal dominant disease caused by a Ser163Arg mutation in C1QTNF5 (Hayward *et al.,* 2003). C1QTNF5 is a short-chain collagen, homologous to the C1q and TNF superfamily of proteins. It is secreted and known to form multimeric species, and although studies have shown that it is secreted by the RPE and interacts with the membrane protein MFRP (with which it is thought to be co-expressed as a bicistronic transcript) (Shu *et al.,* 2006b, Mandal *et al.,* 2006c), no conclusive evidence has yet been published in relation to its function. This study aimed to investigate a role for C1QTNF5 and the effects of the Ser163Arg mutation, both by creating and studying a stably transfected, physiologically relevant, mammalian cellular model, and by producing recombinant protein for use in assays. Specifically, the study aimed to investigate in greater detail reports that the protein may be involved in adhesion of the RPE to Bruch's membrane (Shu *et al.,* 2006b), that the mutant protein aggregates and is not secreted (Shu *et al.,* 2006b, Mandal *et al.,* 2006c), that the protein appears to interact with CFH (implicated in increased risk of developing AMD) and to determine if C1QTNF5 plays a role in RPE phagocytosis of ROS, as has been suggested for MFRP (Won *et al.,* 2008).

7.2 The main findings of the study

Stably transfected cell lines were created and used to investigate further previous reports that C1QTNF5 may have a role in cell adhesion, with mutation in C1QTNF5 causing it to aggregate and be retained within the cell. Recombinant proteins were produced and assays developed to gain further insights into the interaction between C1QTNF5 and CFH. Also, the stably transfected cell lines were used to show that C1QTNF5 has a role in RPE phagocytosis of shed ROS.

7.2.1 C1QTNF5 and extracellular matrix interactions

Contrary to previous reports (Shu *et al.,* 2006b), no evidence was found to support a role for C1QTNF5 in RPE cell adhesion to ECM surfaces such as Bruch's membrane. It was investigated whether ARPE-19 cells were able to adhere to C1QTNF5-coated plates, or whether any differences in levels of adhesion to laminin- or fibronectin-coated plates could be found between ARPE-19 over-expressing either wild-type or mutant C1QTNF5. However in each case no differences were observed. As discussed in Chapter 3, the previously reported results regarding cell adhesion may have been the result of using a non-physiologically relevant cell line. Cells are known to interact with laminin via integrin receptors, of which the RPE expresses only one – the αvβ5 integrin receptor (Nandrot *et al.,* 2006). Over-expression of C1QTNF5 in EBNA293 cells may have promoted cell-extracellular matrix interactions involving proteins not expressed by ARPE-19. Stably transfected ARPE-19 over-expressing wild-type His-C1QTNF5 did however show increased spreading on laminin- and fibronectin-coated plates. This would suggest that C1QTNF5 may be involved in cell-ECM interactions and cytoskeletal rearrangements, possibly involving the αvβ5 integrin.

This study has shown that C1QTNF5 plays a role in RPE phagocytosis of shed ROS. Apically, the RPE-ROS boundary consists of RPE microvilli interdigitating with the ROS, and basally the RPE has infoldings. C1QTNF5 has been shown to localise to both of these locations (Mandal *et al.,* 2006a, Mandal *et al.,* 2006b). It was shown in

Chapter 6 that C1QTNF5 over-expression results in increased levels of ROS phagocytosis, and that this result probably involves clustering of C1QTNF5 and perhaps interacting proteins. The results also suggested that C1QTNF5 was not directly involved in ROS binding, as anti-gC1q antibodies did not inhibit but rather up-regulated phagocytosis. Combining this result with the observation of increased spreading would point towards a C1QTNF5 function involving cytoskeletal rearrangements, possible facilitating phagocytosis. Obviously the current results only allow speculation that this is the case. However, it is conceivable that C1QTNF5 may be involved in maintenance of the RPE-ROS interdigitation by co-ordinating cytoskeletal rearrangements. Mutations in MFRP, with which C1QTNF5 interacts, result in reduced apical microvilli and reduced phagoytosis, again raising the possibility that the two proteins share a functional pathway.

7.2.2 The effects of mutation in C1QTNF5 on secretion and protein function

Again contrary to previous reports (Shu *et al.,* 2006b, Mandal *et al.,* 2006c), mutant His-C1QTNF5 was not found to aggregate or to be retained within the ER. Both the wild-type and mutant proteins were secreted, in both stably transfected ARPE-19 and EBNA293 cell lines. This result implies that disease mechanisms in L-ORMD are probably not due to ER stress as a result of retained and aggregated protein, or haploinsufficiency due to lack of secreted protein. It has, however, previously been shown that the wild-type and mutant proteins interact (Shu *et al.,* 2006a), so it is possible that this may result in a reduction in the effective amount of secreted wild-type protein. Indeed, as results have shown that cells over-expressing mutant His-C1QTNF5 do not show an increase in cell spreading or phagocytosis of ROS, this would imply that the mutant protein is unable to function correctly. Therefore secreted mutant protein interacting with secreted wild-type protein may well prevent the wild-type protein from performing properly.

7.2.3 C1QTNF5 interactions with CFH

It has been shown that C1QTNF5 interacts with CFH, with this interaction involving at least SCR19-20 and SCR7-8. CFH is known to undergo a conformational change

when it interacts with other ligands (Opperman *et al.,* 2006, Prosser *et al.,* 2007), and evidence in this study suggested that this was also the case when interacting with C1QTNF5. When in solution, CFH is predicted to be in a folded back (omega) structure with an exposed C-terminus. It binds ligands initially via its C-terminal domains and then undergoes a conformational change, facilitating interactions involving other domains. The evidence obtained in this study indicates that this may also be the case in binding to C1QTNF5.

The purpose of CFH interacting with C1QTNF5 has not yet been determined. It is possible that C1QTNF5 is acting to localise CFH to a particular site within the retina, possibly acting in combination with GAGs. Due to the high levels of ROS shedding and phagocytosis, it may be necessary to have a higher local concentration of CFH at this site to ensure there is no complement activation. This would imply that C1QTNF5 is a multifunctional protein, acting to localise CFH as well as being involved in phagocytosis. It is also possible that the CFH-C1QTNF5 interaction provides a novel function for CFH. It may be involved in regulating C1QTNF5 activity. Adding anti-gC1q antibody to the phagocytosis assay suggested that clustering of C1QTNF5 may be involved in up-regulating ROS phagocytosis, so it is possible that this occurs when CFH binds. Although no evidence was found for an effect of CFH on the phagocytosis assay, as discussed in Chapter 6, this does not rule out such an involvement.

CFH showed a 17.5-fold higher affinity for mutant compared with wild-type His-C1QTNF5, with SCR19-20 showing a 95-fold increase for the mutant. It is possible that this altered affinity contributes to disease mechanisms in L-ORMD. Whether C1QTNF5 is involved in localising CFH or as part of a signalling pathway, too high an affinity could have adverse effects. It could prevent CFH interacting with other proteins, for instance in regulation of complement, or it could decrease dissociation or increase association rates which may alter a fine-tuned signalling pathway. This might lead to a gain of function leading to the dominant inheritance pattern.

7.2.4 C1QTNF5 and RPE phagocytosis of ROS

C1QTNF5 has been shown in this study to be involved in RPE phagocytosis of shed ROS. Over-expression of the wild-type protein in ARPE-19 cells results in increased levels of phagocytosis, whilst cells over-expressing the mutant protein showed the same levels as in untransfected cells. Further analysis using anti-gC1q antibody suggests that clustering of the protein may be involved, for instance in a signalling pathway, as this up-regulates phagocytosis, as observed for CD36 (Finnemann *et al.,* 2001). In the mutant no effect on phagocytosis was observed. It is perhaps unsurprising that C1QTNF5 is involved in phagocytosis. It interacts with MFRP, and mutations in this protein are associated with RPE-ROS abnormaliltes and reduced phagocytosis.

7.3 A role for C1QTNF5

In order to understand how C1QTNF5 mutation contributes towards retinal degeneration, it is necessary to understand its role in the healthy retina. This study has shed light on certain aspects of this role, for instance its interaction with CFH and role in phagocytosis. However, specific details of these functions have not yet been determined. For instance, what proteins interact with C1QTNF5, what is the relevance of the CFH interaction and how does the interaction with MFRP affect its function? By combining the data from this study with published results from other studies it is possible to speculate as to what may be occurring. These models can explain the various pieces of evidence regarding a role for C1QTNF5, and can provide hypotheses for future studies to investigate. C1QTNF5 is expressed in both the adult and developing eye. It is likely that its roles differ at these different stages of the life cycle, not least because embryonic eyes do not undergo ROS shedding and subsequent phagocytosis. The results from this study will be discussed with reference to a role in the adult eye, although it is also possible that developmental abnormalities may also contribute towards L-ORMD disease mechanisms.

7.3.1 C1QTNF5 in the healthy retina

Previous studies have shown that C1QTNF5 is localised to the apical and basal plasma membranes of the RPE, as well as ganglion cells, ciliary body apical membranes and the plasma membrane of the lens epithelial cells (Mandal *et al.,* 2006c). This study has investigated a role for C1QTNF5 in the RPE, so discussion will focus on this tissue only. The results from this study showed that C1QTNF5 was involved in cell spreading, which involves cell-ECM interactions and changes in cytoskeletal structure (Hynes, 1999). With C1QTNF5 secreted and localised to the RPE plasma membrane it is likely to be involved in regulating *in vivo* cytoskeletal structure too, either directly or indirectly. One of the most obvious structural features of the RPE is the apical microvilli, which increase RPE surface area and so facilitate phagocytosis of ROS. It was shown in this study that C1QTNF5 is involved in ROS phagocyotsis, probably via a signalling pathway rather than direct ROS binding. Previous studies have shown C1QTNF5 to interact with MFRP, although this protein was found to be located only at the base of the microvilli (Mandal *et al.,* 2006b). It was shown here that another C1QTNF5 interacting protein is CFH, which is localised throughout the entire length of the microvilli (Mandal *et al.,* 2006c), and Dr X. Shu showed that C1QTNF5 interacts with heparin-like GAGs. Figure 7.1 shows a hypothetical model of the RPE-ROS boundary, and how these various molecules and their interactions may be arranged. Concentrating on the apical microvillar base, MFRP is localised here where it probably interacts with C1QTNF5. This interaction may involve clustering of both the C1QTNF5 and attached MFRP, possibly via additional interacting proteins. Clustering of C1QTNF5 is predicted to upregulate phagocytosis, a process MFRP is known to be involved in, so if this were to occur in this region it could promote signalling pathways and subsequent phagocytosis of the shed ROS tips. Alternatively, if C1QTNF5 is involved in forming and maintaining the microvilli by interactions with the ECM, then local MFRP interactions could prevent certain cytoskeletal rearrangements and thus define the basal boundaries of each microvillus. Adding MFRP to the cell spreading assays may help to confirm or refute this.

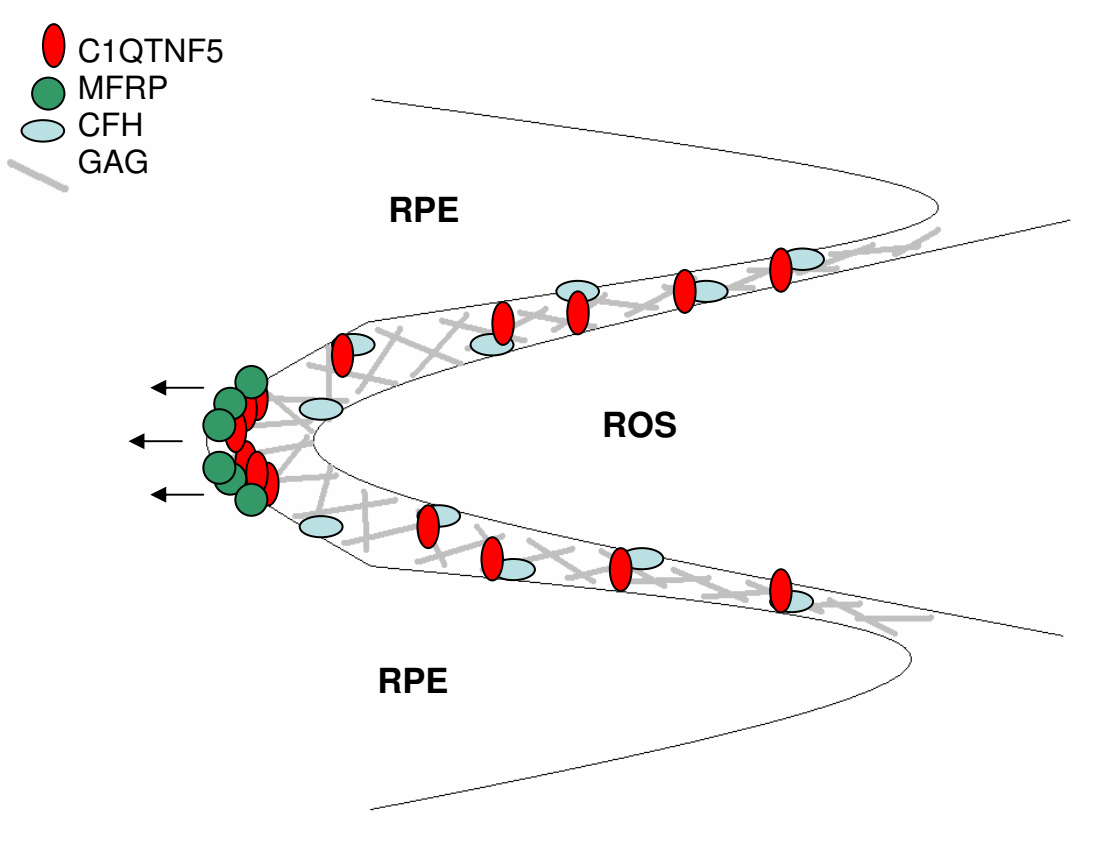

Figure 7.1: C1QTNF5 clustering may help to promote RPE phagocyotsis of shed ROS tips.

C1QTNF5 interacts with CFH and MFRP. CFH is located throughout the length of the microvilli, whilst MFRP is only located at the base. It is possible that CFH, possibly in conjunction with a GAG framework, helps to prevent C1QTNF5 clustering. This may also have effects on the cytoskeleton, helping to maintain the microvilli structure. However, at the microvilli base C1QTNF5 interacts with MFRP, causing clustering of the two molecules and possibly cytosketal rearrangements, resulting in phagocytosis of the shed ROS tips.

As well as being attached to cell surfaces, GAGs can form part of the ECM. CFH is localised to the RPE microvilli and so plausibly could interact with these ECM-associated GAGs throughout the whole of this boundary. One possibility is that by interacting with CFH and a framework of GAGs, C1QTNF5 is prevented from clustering. Alternatively, interacting with GAGs alone may provide the framework whilst C1QTNF5 interacts with CFH merely to localise additional CFH protein to the area. CFH may also have a new function, interacting with C1QTNF5 to help maintain the microvillar structure, as a counter balance to the MRFP interactions basally or with a signalling role in phagocytosis. Unfortunately, it is not possible to predict what may or may not be the case until further analyses are carried out.

7.3.1.1 Potential C1QTNF5 interacting proteins

It is highly likely that MFRP and CFH are not the only proteins that C1QTNF5 interacts with, although this has yet to be determined. Figure 1.4 (Section 1.1.6.1) highlighted the main proteins and pathways involved in ROS phagocytosis, so it is possible that C1QTNF5 interacts with one or more of these, as well as yet-unidentified proteins. The αvβ5 integrin is known to be involved in phagocytosis as well as cell-ECM interactions and, as discussed in section 7.1.1, it would not be implausible for C1QTNF5 to have an effect on interactions involving this protein, possibly through the membrane protein MFRP, as both proteins share overlapping functions (as summarised in Figure 7.2).

Another plausible interacting protein would be CD81. CD81 is a tetraspanin, and tetraspanins form membrane-associated webs involving many proteins (Berditchevski *et al.,* 2001, Hemler *et al.,* 2005, Levy *et al.,* 2005). CD81 is not involved directly in ROS phagocytosis, but has an indirect role in the processing of the αvβ5 integrin (Chang *et al.,* 2007). CD81 requires regulation, and it has been shown in this study that C1QTNF5 has a regulatory or signalling role in ROS phagocytosis, rather than direct ROS binding. C1QTNF5 may therefore interact with CD81, either directly or via MFRP. CD81 is also known to interact with EBP50, which in turn interacts with ezrin and CRALBP. Interestingly, C1QTNF5 and ezrin have been shown to localise to the RPE apical processes (Mandal *et al.,* 2006c,

Bonilha *et al.,* 1999) and ezrin knockout mice present with a retinal phenotype very similar to that of the MFRP knockout mouse with reductions in apical microvilli and retarded photoreceptor development (Bonilha *et al.,* 2005). Also, if the mutation in C1QTNF5 were to affect how it interacts with other proteins, this could have knock-on effects on downstream molecular pathways. CRALBP, for instance, is involved in retinoid processing and indirectly interacts with CD81 (Strauss *et al.,* 2005) so it is plausible that if C1QTNF5 interacts with CD81 this could indirectly disrupt finely-tuned pathways such as retinoid processing in the visual cycle. This would certainly explain the dark adaptation abnormalities seen in L-ORMD patients (discussed in more detail in Section 7.3.2). Figure 7.3 summarises CD81 interactions and how they could be related to C1QTNF5.

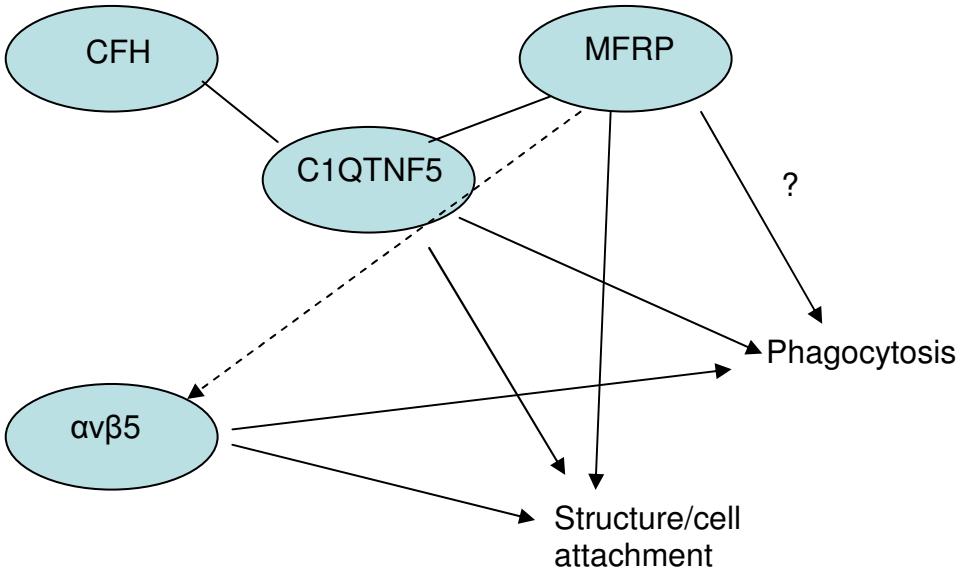

Figure 7.2: C1QTNF5 and MFRP share overlapping functions with the αvβ5 integrin, namey in phagocytosis of shed ROS and in organising cell structure.

It is possible, due to these overlapping functions that C1QTNF5 and MFRP interact or share interacting proteins and functional pathways. C1QTNF5 interacts with CFH, although a function for this interaction has yet to be determined.

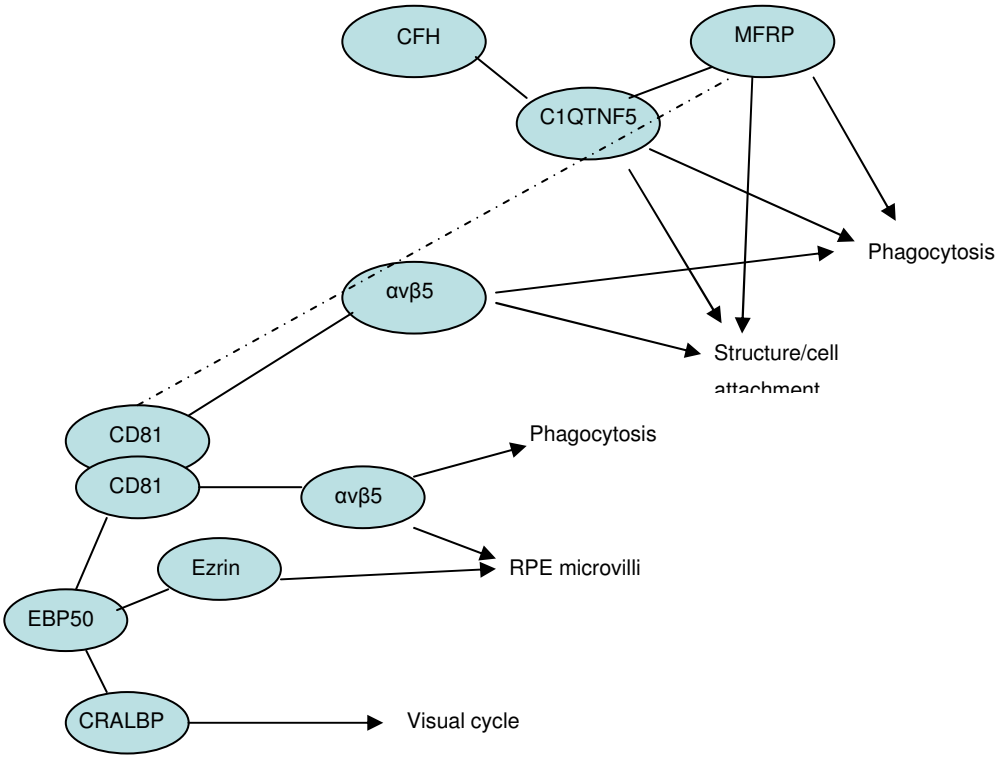

Figure 7.3: CD81 may interact with both MFRP and the αvβ5 integrin.

CD81 is a tetraspanin and is known to interact with EBP50 as well as the αvβ5 integrin. EBP50 interacts with ezrin, which is required for formation of the RPE apical microvilli, as well as CRALBP, which is involved in retinoid processing in the visual cycle. C1QTNF5 co-localises with ezrin, and patients with L-ORMD initially present with dark adaptation abnormalities, which could potentially be the result of mutant C1QTNF5 affecting CRALBP indirectly via interacting proteins such as MFRP, CD81 and EBP50. If MFRP were to interact with CD81 then this would connect C1QTNF5 with other proteins involved in this pathway.

7.3.2 C1QTNF5 in L-ORMD

Disease progression in L-ORMD starts with initial dark adaptation abnormalities, leading to sub-RPE deposits, photoreceptor degeneration, retinal atrophy and CNV (Duval *et al.,* 1986, Brosnahan *et al.,* 1994, Kuntz *et al.,* 1996, Milam *et al.,* 2000, Jacobson *et al.,* 2001). As with AMD, it is not easy to determine which symptoms are cause and which are effect, i.e. what processes does the Ser163Arg mutation actually affect, what are the results of this and what symptoms are secondary to them? Unlike AMD, L-ORMD is caused by a single point mutation in an identified protein and the disease has an early phenotypic marker – dark adaptation (Jacobson *et al.,* 2001). Dark adaptation in itself may be the result of sub-RPE deposits compromising the RPE and overlying photoreceptors. However, when patients were given vitamin A supplements this improved their dark adaptation slightly, implying that it could be caused by photoreceptor dysfunction at this initial stage of the disease. Duval *et al.* (1986) noted ROS were disorganised and shortened in a donated L-ORMD eye. This may indicate that photoreceptor dysfunction is a major factor in L-ORMD disease progression, or, as discussed above, because it is not easy to determine primary and secondary symptoms, this may not be the case.

The observation that over-expression of wild-type His-C1QTNF5 increases levels of phagocytosis of ROS in ARPE-19 cell cultures, whereas the mutant does not, supports the initial defects leading to L-ORMD occurring at the RPE apical boundary, rather than basally as has been suggested previously (Shu *et al.,* 2006b). Any additional basal disease mechanisms cannot be ruled out at this stage, especially as C1QTNF5 is expressed basally too, although results from this study support an apical abnormality. It is possible that dark adaptation difficulties are the result of an abnormality in the RPE-ROS boundary, possibly due to reduced apical microvilli, as seen in the *rd6* mouse (Won *et al.,* 2008). This could lead to photoreceptor dysfunction and a stressed RPE. Although in the *rd6* mouse it is MFRP which is mutated, and in L-ORMD patients it is C1QTNF5, these proteins probably interact *in vivo* (Shu *et al.,* 2006b, Mandal *et al.,* 2006b). Also, whilst the homozygous *rd6* mouse has a severe phenotype with fairly early onset and L-ORMD manifests later in

life, L-ORMD patients are heterozygous for the disease-causing mutation (Hayward *et al.,* 2003) so it can be assumed that some residual C1QTNF5 function remains.

It is also possible that the dark adaptation abnormalities observed in L-ORMD may be a result of ineffective ROS phagocytosis. The young retina may be able to cope with a system that is not functioning at 100% efficiency, however as the tissue ages it becomes less able to do so and symptoms appear. Dark adaptation abnormalities would perhaps suggest a deficit in retinoid recycling, rather than ROS phagocytosis. However, retinoid is required to be transported from the ROS to the RPE and back again, so it would not be implausible to suggest that stressing the photoreceptors or RPE by ineffective phagocytosis could have knock-on effects on other functions of these cells, particularly those involving molecular pathways occurring in the same vicinity. There is also the possibility that C1QTNF5 or one of its interacting proteins is involved in retinoid recycling, and mutation in C1QTNF5 has an effect by altering the homeostasis of carefully balanced molecular pathways. Determining C1QTNF5 interacting proteins (as discussed in Section 7.2.1) would help ascertain which, if any, of these possibilities is occurring.

Extensive sub-RPE deposits are another feature of L-ORMD. These deposits resemble the BlamD seen in AMD, which are thought to be secreted by a stressed RPE (van der Schaft *et al.,* 1994). Assuming the sub-RPE deposits seen in L-ORMD do not cause the dark adaptation difficulties, then it would be plausible to suggest that the deposits may be the result of a compromised RPE which is secreting extra basement membrane material. In addition, it has been shown by Amin *et al.,* (2004) that when cultured RPE are fed ROS it is possible to modulate the amount and type of basal deposits formed, further supporting the involvement of ROS phagocytosis in sub-RPE deposit formation. Cultured ARPE-19 cells were fed retinal homogenate, with the structure of sub-RPE deposits analysed by electron microscopy and compared to cells which had not received such treatment. Deposits were classified as fibrillar, condensed and banded, and thought to be similar to BlamD, or membranous, thought to be similar to BlinD. After feeding with retinal homogenate, the proportion of condensed and banded deposits formed was signifcantly increased

when compared with the control cultures. A recent study by Hollyfield *et al.* (2008) showed that immunising mice against CEP could provoke inflammatory responses resulting in a pathology similar to that seen in AMD. In addition, treated mice showed an increase in sub-RPE BlamD deposits. CEP forms when oxidised DHA fragments interact with tissue proteins. It is conceivable that reduced levels of ROS phagocytosis could cause accumulation of oxidised DHA either within the RPE or between the photoreceptors and RPE, resulting in increased CEP production. This could then contribute towards the accumulation of basal laminar deposits and inflammatory response observed in L-ORMD (Milam *et al.,* 2000).

7.3.3 C1QTNF5 in AMD

AMD is characterised by drusen, sub-RPE deposits, CNV and loss of central vision (Tezel, 2004). Determining the underlying causes of these symptoms is difficult, although several genomic loci have been identified and molecular pathways suggested which may play a role in disease progression. Drusen are thought to arise from initial nucleation events, possibly due to basal blebs from compromised RPE cells, which are not effectively removed and subsequently increase in size due to deposition of additional material and autoimmune responses. Polymorphisms in CFH have been associated with increased risk of developing AMD (Edwards *et al.,* 2005, Haines *et al.,* 2005, Klein *et al.,* 2005), with extensive studies focusing on how the Y402H polymorphism affects the protein's ability to interact with known ligands such as GAGs and CRP (Clark *et al.,* 2006, Herbert *et al.,* 2007, Prosser *et al.,* 2007). Variations in CFH interacting proteins such as C3 have also been implicated (Yates *et al*., 2007, Spencer *et al.,* 2008). Also, it has been suggested that deficiencies in extracellular deposit clearance by phagocytes such as macrophages contribute to their build-up in the sub-RPE space (Ambati *et al.,* 2003). The current theory with regards to AMD disease progression would therefore appear to be that the ageing RPE becomes compromised, as do the mechanisms which are in place to deal with this, initially leading to localised sub-RPE deposits. These are not effectively cleared and an inflammatory response ensues. This progresses, like a chain reaction, and leads to increased deposit formation, further compromising of the RPE and subsequent photoreceptor dysfunction and CNV. Variations in proteins such as CFH

can affect how the eye is able to cope with these processes, increasing or decreasing the risk of developing symptoms.

So how does C1QTNF5 fit into this picture? It has been shown in this study that mutation in C1QTNF5 compromised the ability of the RPE to phagocytose ROS and possibly to organise its cytoskeleton. This probably stresses the RPE causing fine-tuned systems to be compromised and extracellular deposits to form. With this model of RPE cell dysfunction in L-ORMD, it is assumed that apical C1QTNF5 interactions are the primary site initiating the disease. It has also been shown in this study that C1QTNF5 interacts with CFH. However, the suggested model for how CFH polymorphism affects AMD disease progression assumes that its effects are primarily basal. It is possible that there are two CFH-related events going on within the retina. Apically, CFH (secreted by the RPE) may interact with C1QTNF5, affecting phagocytosis. Slight differences in binding specificity between the two Y402H polymorphisms and C1QTNF5 may be enough to disrupt fine-tuned balances in molecular interactions. This could have slow but significant effects on C1QTNF5 and associated proteins functions, resulting in a slightly elevated level of sub-RPE deosits. As the retina ages, these are enough to cause the initiation events predicted to result in drusen formation. Once drusen have formed then CFH could play a part in regulating complement activation and so disease progression at this new basal location. Therefore it is possible there are two different functions for CFH in AMD – one initiating the disease and one contributing towards its progression.

7.4 Future work

This study has highlighted several possible avenues for future investigation. It has been shown that C1QTNF5 has involvement in ROS phagocytosis, contributing towards disease mechanisms in L-ORMD. Further investigation of how C1QTNF5 integrates into pathways involved in phagocytosis needs to be carried out. As discussed in Section 7.3.1.1, it is possible C1QTNF5 is acting through CD81. This possibility could be investigated by siRNA, targeting CD81 or its known interacting proteins and comparing subsequent levels of phagocytosis in the stably transfected

ARPE-19 cell lines. To identify further molecular pathways involving C1QTNF5 during phagocytosis, microarray analysis could be carried out. This could be done using the stably transfected cell lines, before and after exposure to ROS. It could also be investigated, using the protocol described by Amin *et al.* (2004), whether any differences in deposit formation are observed between cells over-expressing either wild-type or mutant C1QTNF5, with or without exposure to ROS. It could be predicted that increased deposits would be observed in cells over-expressing wild-type C1QTNF5 due to increased levels of phagocytosis. However, if it is predicted that cellular stress contributes towards increased basal secretions in L-ORMD, it is possible that this method may not result in sufficient cellular stress to cause increased deposit formation in cells over-expressing mutant C1QTNF5. Investigating levels of deposit formation when the cells are exposed to oxidised ROS could help to test this.

In addition to using a cellular system, transgenic mice would help answer questions raised in this study. For instance, it would be possible to look at the retinal structure and determine if loss or mutation of C1QTNF5 results in any abnormalities of the apical microvilli. It would also be possible, assuming the same disease phenotype is observed as occurs in humans, to determine the composition of the sub-RPE deposits. This is an important question which it has not yet been possible to answer. Determining deposit composition shed light on their origin, and so on the initiating factors in disease progression.

The ultimate aim of this study is to understand how C1QTNF5 contributes towards disease mechanisms in L-ORMD. This knowledge can then be applied to developing therapies for affected individuals. One of the most important questions regarding such potential therapies is whether mutation in C1QTNF5 results in a loss or gain of function. Disease mechanisms involving a loss of function have the potential to be targeted by gene therapy. Wild-type and mutant C1QTNF5 interact, so it is likely formation of heterotrimers can have a dominant negative effect. Localised over-expression of wild-type C1QTNF5 may help to overcome this issue. Prior to carrying out this study, it appeared that there was a gain of function in L-ORMD pathogenesis, caused by aggregation of mutant C1QTNF5 and retention within the

cell. This study has not been able to support these findings. If the Ser163Arg mutation results in loss of function alone, particularly in relation to ROS phagocytosis, then this greatly increase the likelyhood of gene therapy becoming a realistic approach for treating L-ORMD.

References

Abecasis, G. R., B. M. Yashar, et al. (2004). "Age-related macular degeneration: a high-resolution genome scan for susceptibility loci in a population enriched for late-stage disease." *Am J Hum Genet* **74**(3): 482-94.

Abrera-Abeleda, M. A., C. Nishimura, et al. (2006). "Variations in the complement regulatory genes factor H (CFH) and factor H related 5 (CFHR5) are associated with membranoproliferative glomerulonephritis type II (dense deposit disease)." *J Med Genet* **43**(7): 582-9.

Adler, P. N. (1992). "The genetic control of tissue polarity in Drosophila." *Bioessays* **14**(11): 735-41.

Alberts, J., Lewis, Raff, Roberts, Walter (2002). *Molecular Biology of the Cell.* New York, Garland Science. pp1463

Alexander, J. P., J. M. Bradley, et al. (1990). "Expression of matrix metalloproteinases and inhibitor by human retinal pigment epithelium." *Invest Ophthalmol Vis Sci* **31**(12): 2520-8.

Algvere, P. V., J. Marshall, et al. (2006). "Age-related maculopathy and the impact of blue light hazard." *Acta Ophthalmol Scand* **84**(1): 4-15.

Allikmets, R. (2000). "Further evidence for an association of ABCR alleles with age-related macular degeneration. The International ABCR Screening Consortium." Am J Hum Genet **67**(2): 487-91.

Allikmets, R. and M. Dean (2008). "Bringing age-related macular degeneration into focus." *Nat Genet* **40**(7): 820-1.

Allikmets, R., N. F. Shroyer, et al. (1997). "Mutation of the Stargardt disease gene (ABCR) in age-related macular degeneration." *Science* **277**(5333): 1805-7.

Alm, A. and A. Bill (1973). "Ocular and optic nerve blood flow at normal and increased intraocular pressures in monkeys (*Macaca irus*): a study with radioactively labelled microspheres including flow determinations in brain and some other tissues." *Exp Eye Res* **15**(1): 15-29.

Alsenz, J., J. D. Lambris, et al. (1984). "Localization of the complement-component-C3b-binding site and the cofactor activity for factor I in the 38kDa tryptic fragment of factor H." *Biochem J* **224**(2): 389-98.

Ambati, J., A. Anand, et al. (2003). "An animal model of age-related macular degeneration in senescent Ccl-2- or Ccr-2-deficient mice." *Nat Med* **9**(11): 1390-7.

Amin, S., N. H. Chong, et al. (2004). "Modulation of Sub-RPE deposits in vitro: a potential model for age-related macular degeneration." *Invest Ophthalmol Vis Sci* **45**(5): 1281-8.

Anderson, D. H., R. F. Mullins, et al. (2002). "A role for local inflammation in the formation of drusen in the aging eye." *Am J Ophthalmol* **134**(3): 411-31.

Anderson, R. E. and M. B. Maude (1970). "Phospholipids of bovine outer segments." *Biochemistry* **9**(18): 3624-8.

Arris, C. E., D. J. Bevitt, et al. (2003). "Expression of mutant and wild-type TIMP3 in primary gingival fibroblasts from Sorsby's fundus dystrophy patients." *Biochim Biophys Acta* **1638**(1): 20-8.

Ayala-Ramirez, R., F. Graue-Wiechers, et al. (2006). "A new autosomal recessive syndrome consisting of posterior microphthalmos, retinitis pigmentosa, foveoschisis, and optic disc drusen is caused by a MFRP gene mutation." *Mol Vis* **12**: 1483-9.

Ayyagari, R., M. N. Mandal, et al. (2005). "Late-onset macular degeneration and long anterior lens zonules result from a CTRP5 gene mutation." *Invest Ophthalmol Vis Sci* **46**(9): 3363-71.

Baumann, H. and J. Gauldie (1994). "The acute phase response." *Immunol Today* **15**(2): 74-80.

Bax, D. V., S. E. Bernard, et al. (2003). "Cell adhesion to fibrillin-1 molecules and microfibrils is mediated by alpha 5 beta 1 and alpha v beta 3 integrins." *J Biol Chem* **278**(36): 34605-16.

Baylor, D. (1996). "How photons start vision." *Proc Natl Acad Sci U S A* **93**(2): 560-5.

Baylor, D. A. and M. E. Burns (1998). "Control of rhodopsin activity in vision." Eye **12 (Pt 3b)**: 521-5.

Beatty, S., H. Koh, et al. (2000). "The role of oxidative stress in the pathogenesis of age-related macular degeneration." *Surv Ophthalmol* **45**(2): 115-34.

Berditchevski, F. (2001). "Complexes of tetraspanins with integrins: more than meets the eye." *J Cell Sci* **114**(Pt 23): 4143-51.

Bird, A. C. (2003). "The Bowman lecture. Towards an understanding of age-related macular disease." *Eye* **17**(4): 457-66.

Biro, A., Z. Rovo, et al. (2007). "Studies on the interactions between C-reactive protein and complement proteins." *Immunology* **121**(1): 40-50.

Blackmore, T. K., J. Hellwage, et al. (1998). "Identification of the second heparin-binding domain in human complement factor H." *J Immunol* **160**(7): 3342-8.

Blackmore, T. K., T. A. Sadlon, et al. (1996). "Identification of a heparin binding domain in the seventh short consensus repeat of complement factor H." *J Immunol* **157**(12): 5422-7.

Bogin, O., M. Kvansakul, et al. (2002). "Insight into Schmid metaphyseal chondrodysplasia from the crystal structure of the collagen X NC1 domain trimer." *Structure* **10**(2): 165-73.

Bok, D. (2005). "Evidence for an inflammatory process in age-related macular degeneration gains new support." *Proc Natl Acad Sci U S A* **102**(20): 7053-4.

Bok, D. and M. O. Hall (1971). "The role of the pigment epithelium in the etiology of inherited retinal dystrophy in the rat." *J Cell Biol* **49**(3): 664-82.

Bonilha, V. L., S. C. Finnemann, et al. (1999). "Ezrin promotes morphogenesis of apical microvilli and basal infoldings in retinal pigment epithelium." *J Cell Biol* **147**(7): 1533-48.

Bonilha, V. L., M. E. Rayborn, et al. (2006). "Microvilli defects in retinas of ezrin knockout mice." *Exp Eye Res* **82**(4): 720-9.

Bortner, C. D., N. B. Oldenburg, et al. (1995). "The role of DNA fragmentation in apoptosis." *Trends Cell Biol* **5**(1): 21-6.

Boyle, D., L. F. Tien, et al. (1991). "A mannose receptor is involved in retinal phagocytosis." *Invest Ophthalmol Vis Sci* **32**(5): 1464-70.

Brass, A., K. E. Kadler, et al. (1992). "The fibrillar collagens, collagen VIII, collagen X and the C1q complement proteins share a similar domain in their C-terminal non-collagenous regions." *FEBS Lett* **303**(2-3): 126-8.

Brosnahan, D. M., S. M. Kennedy, et al. (1994). "Pathology of hereditary retinal degeneration associated with hypobetalipoproteinemia." *Ophthalmology* **101**(1): 38-45.

Caicedo, A., D. G. Espinosa-Heidmann, et al. (2005). "Blood-derived macrophages infiltrate the retina and activate Muller glial cells under experimental choroidal neovascularization." *Exp Eye Res* **81**(1): 38-47.

Chan, D., S. Freddi, et al. (1999). "Interaction of collagen alpha1(X) containing engineered NC1 mutations with normal alpha1(X) in vitro. Implications for the molecular basis of schmid metaphyseal chondrodysplasia." *J Biol Chem* **274**(19): 13091-7.

Chang, Y. and S. C. Finnemann (2007). "Tetraspanin CD81 is required for the alpha v beta5-integrin-dependent particle-binding step of RPE phagocytosis." *J Cell Sci* **120**(Pt 17): 3053-63.

Chen, L., P. Yang, et al. (2002). "Distribution, markers, and functions of retinal microglia." *Ocul Immunol Inflamm* **10**(1): 27-39.

Chen, M., J. V. Forrester, et al. (2007). "Synthesis of complement factor H by retinal pigment epithelial cells is down-regulated by oxidized photoreceptor outer segments." *Exp Eye Res* **84**(4): 635-45.

Clark, S. J., V. A. Higman, et al. (2006). "His-384 allotypic variant of factor H associated with age-related macular degeneration has different heparin binding properties from the non-disease-associated form." *J Biol Chem* **281**(34): 24713-20.

Coffey, P. J., C. Gias, et al. (2007). "Complement factor H deficiency in aged mice causes retinal abnormalities and visual dysfunction." *Proc Natl Acad Sci U S A* **104**(42): 16651-6.

Conrad, D. H., J. R. Carlo, et al. (1978). "Interaction of beta1H globulin with cell-bound C3b: quantitative analysis of binding and influence of alternative pathway components on binding." *J Exp Med* **147**(6): 1792-1805.

Crabb, J. W., M. Miyagi, et al. (2002). "Drusen proteome analysis: an approach to the etiology of age-related macular degeneration." *Proc Natl Acad Sci U S A* **99**(23): 14682-7.

Crespi, J., J. A. Buil, et al. (2008). "A novel mutation confirms MFRP as the gene causing the syndrome of nanophthalmos-renititis pigmentosa-foveoschisis-optic disk drusen." *Am J Ophthalmol* **146**(2): 323-328.

Curcio, C. A. and C. L. Millican (1999). "Basal linear deposit and large drusen are specific for early age-related maculopathy." *Arch Ophthalmol* **117**(3): 329-39.

D'Cruz, P. M., D. Yasumura, et al. (2000). "Mutation of the receptor tyrosine kinase gene Mertk in the retinal dystrophic RCS rat." *Hum Mol Genet* **9**(4): 645-51.

Despriet, D. D., A. A. Bergen, et al. (2008). "Comprehensive analysis of the candidate genes CCL2, CCR2, and TLR4 in age-related macular degeneration." *Invest Ophthalmol Vis Sci* **49**(1): 364-71.

Dewan, A., M. Liu, et al. (2006). "HTRA1 promoter polymorphism in wet age-related macular degeneration." *Science* **314**(5801): 989-92.

Donoso, L. A., D. Kim, et al. (2006). "The role of inflammation in the pathogenesis of age-related macular degeneration." *Surv Ophthalmol* **51**(2): 137-52.

Dowling, J. E. and R. L. Sidman (1962). "Inherited retinal dystrophy in the rat." *J Cell Biol* **14**: 73-109.

Dunn, K. C., A. D. Marmorstein, et al. (1998). "Use of the ARPE-19 cell line as a model of RPE polarity: basolateral secretion of FGF5." *Invest Ophthalmol Vis Sci* **39**(13): 2744-9.

Duvall, J., N. M. McKechnie, et al. (1986). "Extensive subretinal pigment epithelial deposit in two brothers suffering from dominant retinitis pigmentosa. A histopathological study." *Graefes Arch Clin Exp Ophthalmol* **224**(3): 299-309.

Edwards, A. O., R. Ritter, 3rd, et al. (2005). "Complement factor H polymorphism and age-related macular degeneration." *Science* **308**(5720): 421-4.

Eibl, K. H., D. Kook, et al. (2006). "Inhibition of human retinal pigment epithelial cell attachment, spreading, and migration by alkylphosphocholines." *Invest Ophthalmol Vis Sci* **47**(1): 364-70.

Ellgaard, L. and A. Helenius (2003). "Quality control in the endoplasmic reticulum." *Nat Rev Mol Cell Biol* **4**(3): 181-91.

Evans, J. and R. Wormald (1996). "Is the incidence of registrable age-related macular degeneration increasing?" *Br J Ophthalmol* **80**(1): 9-14.

Evans, J. R., A. E. Fletcher, et al. (2004). "Age-related macular degeneration causing visual impairment in people 75 years or older in Britain: an add-on study to the Medical Research Council Trial of Assessment and Management of Older People in the Community." *Ophthalmology* **111**(3): 513-7.

Fearon, D. T. and K. F. Austen (1977). "Activation of the alternative complement pathway with rabbit erythrocytes by circumvention of the regulatory action of endogenous control proteins." *J Exp Med* **146**(1): 22-33.

Feeney-Burns, L., E. S. Hilderbrand, et al. (1984). "Aging human RPE: morphometric analysis of macular, equatorial, and peripheral cells." *Invest Ophthalmol Vis Sci* **25**(2): 195-200.

Fernando, A. N., P. B. Furtado, et al. (2007). "Associative and structural properties of the region of complement factor H encompassing the Tyr402His disease-related polymorphism and its interactions with heparin." *J Mol Biol* **368**(2): 564-81.

Ferreira, V. P., A. P. Herbert, et al. (2006). "Critical role of the C-terminal domains of factor H in regulating complement activation at cell surfaces." *J Immunol* **177**(9): 6308-16.

Fine, S. L., J. W. Berger, et al. (2000). "Age-related macular degeneration." *N Engl J Med* **342**(7): 483-92.

Finnemann, S. C. (2003). "Focal adhesion kinase signaling promotes phagocytosis of integrin-bound photoreceptors." *Embo J* **22**(16): 4143-54.

Finnemann, S. C., V. L. Bonilha, et al. (1997). "Phagocytosis of rod outer segments by retinal pigment epithelial cells requires alpha(v)beta5 integrin for binding but not for internalization." *Proc Natl Acad Sci U S A* **94**(24): 12932-7.

Finnemann, S. C. and E. F. Nandrot (2006). "MerTK activation during RPE phagocytosis in vivo requires alphaVbeta5 integrin." *Adv Exp Med Biol* **572**: 499-503.

Finnemann, S. C. and R. L. Silverstein (2001). "Differential roles of CD36 and alphavbeta5 integrin in photoreceptor phagocytosis by the retinal pigment epithelium." *J Exp Med* **194**(9): 1289-98.

Fisher, S. A., G. R. Abecasis, et al. (2005). "Meta-analysis of genome scans of age-related macular degeneration." *Hum Mol Genet* **14**(15): 2257-64.

Forrester, J. V. (2003). "Macrophages eyed in macular degeneration." *Nat Med* **9**(11): 1350-1.

Frank, R. N., R. H. Amin, et al. (1999). "Antioxidant enzymes in the macular retinal pigment epithelium of eyes with neovascular age-related macular degeneration." *Am J Ophthalmol* **127**(6): 694-709.

Fritsche, L. G., T. Loenhardt, et al. (2008). "Age-related macular degeneration is associated with an unstable ARMS2 (LOC387715) mRNA." *Nat Genet* **40**(7): 892-6.

Gal, A., Y. Li, et al. (2000). "Mutations in MERTK, the human orthologue of the RCS rat retinal dystrophy gene, cause retinitis pigmentosa." *Nat Genet* **26**(3): 270-1.

Gallagher, S. R. (2000). "One-dimensional electrophoresis using non-denaturing conditions." *Curr. Protoc. cell Biol.* (5): 6.5.1-6.5.11

Gershov, D., S. Kim, et al. (2000). "C-Reactive protein binds to apoptotic cells, protects the cells from assembly of the terminal complement components, and sustains an antiinflammatory innate immune response: implications for systemic autoimmunity." *J Exp Med* **192**(9): 1353-64.

Giannakis, E., T. S. Jokiranta, et al. (2003). "A common site within factor H SCR 7 responsible for binding heparin, C-reactive protein and streptococcal M protein." *Eur J Immunol* **33**(4): 962-9.

Gregory, C. Y. and M. O. Hall (1992). "The phagocytosis of ROS by RPE cells is inhibited by an antiserum to rat RPE cell plasma membranes." *Exp Eye Res* **54**(6): 843-51.

Gros, P., F. J. Milder, et al. (2008). "Complement driven by conformational changes." *Nat Rev Immunol* **8**(1): 48-58.

Hageman, G. S., D. H. Anderson, et al. (2005). "A common haplotype in the complement regulatory gene factor H (HF1/CFH) predisposes individuals to age-related macular degeneration." *Proc Natl Acad Sci U S A* **102**(20): 7227-32.

Hageman, G. S., L. S. Hancox, et al. (2006). "Extended haplotypes in the complement factor H (CFH) and CFH-related (CFHR) family of genes protect against age-related macular degeneration: characterization, ethnic distribution and evolutionary implications." *Ann Med* **38**(8): 592-604.

Hageman, G. S., P. J. Luthert, et al. (2001). "An integrated hypothesis that considers drusen as biomarkers of immune-mediated processes at the RPE-Bruch's membrane interface in aging and age-related macular degeneration." *Prog Retin Eye Res* **20**(6): 705-32.

Hageman, G. S. and R. F. Mullins (1999). "Molecular composition of drusen as related to substructural phenotype." *Mol Vis* **5**: 28.

Haines, J. L., M. A. Hauser, et al. (2005). "Complement factor H variant increases the risk of age-related macular degeneration." *Science* **308**(5720): 419-21.

Hakobyan, S., C. L. Harris, et al. (2008). "Complement factor H binds to denatured rather than to native pentameric C-reactive protein." *J Biol Chem* **283**(45): 30451-60.

Hall, M. O., B. L. Burgess, et al. (1990). "The effect of inhibitors of glycoprotein synthesis and processing on the phagocytosis of rod outer segments by cultured retinal pigment epithelial cells." *Glycobiology* **1**(1): 51-61.

Hammond, C. J., A. R. Webster, et al. (2002). "Genetic influence on early age-related maculopathy: a twin study." *Ophthalmology* **109**(4): 730-6.

Hargrave, P. A. (2001). "Rhodopsin structure, function, and topography the Friedenwald lecture." *Invest Ophthalmol Vis Sci* **42**(1): 3-9.

Hart, S. P., K. M. Alexander, et al. (2005). "C-reactive protein does not opsonize early apoptotic human neutrophils, but binds only membrane-permeable late apoptotic cells and has no effect on their phagocytosis by macrophages." *J Inflamm (Lond)* **2**: 5.

Hawkins, B. S., A. Bird, et al. (1999). "Epidemiology of age-related macular degeneration." *Mol Vis* **5**: 26.

Hayward, C., X. Shu, et al. (2003). "Mutation in a short-chain collagen gene, CTRP5, results in extracellular deposit formation in late-onset retinal degeneration: a genetic model for age-related macular degeneration." *Hum Mol Genet* **12**(20): 2657-67.

Hellwage, J., T. S. Jokiranta, et al. (1999). "Functional properties of complement factor H-related proteins FHR-3 and FHR-4: binding to the C3d region of C3b and differential regulation by heparin." *FEBS Lett* **462**(3): 345-52.

Hellwage, J., S. Kuhn, et al. (1997). "The human complement regulatory factor-H-like protein 1, which represents a truncated form of factor H, displays cell-attachment activity." *Biochem J* **326 (Pt 2)**: 321-7.

Hemler, M. E. (2005). "Tetraspanin functions and associated microdomains." *Nat Rev Mol Cell Biol* **6**(10): 801-11.

Herbert, A. P., J. A. Deakin, et al. (2007). "Structure shows that a glycosaminoglycan and protein recognition site in factor H is perturbed by age-related macular degeneration-linked single nucleotide polymorphism." *J Biol Chem* **282**(26): 18960-8.

Herbert, A. P., D. C. Soares, et al. (2006). "Disease-associated sequence variations in factor H: a structural biology approach." *Adv Exp Med Biol* **586**: 313-27.

Hildebrand M, G. G. (2001). Analysis of Vertebrate Structure. New York, John Wiley & Sons Inc. pp635

Holers, V. M., T. Kinoshita, et al. (1992). "The evolution of mouse and human complement C3-binding proteins: divergence of form but conservation of function." *Immunol Today* **13**(6): 231-6.

Hollyfield J. G., V. L. Bonilha, et al. (2008). "Oxidative damage-induced inflammation initiates age-related macular degeneration." *Nat. Med.* **14**(2):194-8.

Hopf, M., W. Gohring, et al. (2001). "Crystal structure and mutational analysis of a perlecan-binding fragment of nidogen-1." *Nat Struct Biol* **8**(7): 634-40.

Hortin, G. L. (2006). "The MALDI-TOF mass spectrometric view of the plasma proteome and peptidome." *Clin Chem* **52**(7): 1223-37.

Hughes, A. E., N. Orr, et al. (2006). "A common CFH haplotype, with deletion of CFHR1 and CFHR3, is associated with lower risk of age-related macular degeneration." *Nat Genet* **38**(10): 1173-7.

Humphries, M. J. (2001). "Cell adhesion assays." *Mol Biotechnol* **18**(1): 57-61.

Hynes, R. O. (1999). "Cell adhesion: old and new questions." *Trends Cell Biol* **9**(12): M33-7.

Iyengar, S. K., D. Song, et al. (2004). "Dissection of genomewide-scan data in extended families reveals a major locus and oligogenic susceptibility for age-related macular degeneration." *Am J Hum Genet* **74**(1): 20-39.

Jacobson, S. G., A. V. Cideciyan, et al. (2001). "Phenotypic marker for early disease detection in dominant late-onset retinal degeneration." *Invest Ophthalmol Vis Sci* **42**(8): 1882-90.

Jarva, H., T. S. Jokiranta, et al. (1999). "Regulation of complement activation by C-reactive protein: targeting the complement inhibitory activity of factor H by an interaction with short consensus repeat domains 7 and 8-11." *J Immunol* **163**(7): 3957-62.

Jin, G. F., J. S. Hurst, et al. (2001). "Rod outer segments mediate mitochondrial DNA damage and apoptosis in human retinal pigment epithelium." *Curr Eye Res* **23**(1): 11-9.

Johnson, L. V., S. Ozaki, et al. (2000). "A potential role for immune complex pathogenesis in drusen formation." *Exp Eye Res* **70**(4): 441-9.

Johnson, P. T., K. E. Betts, et al. (2006). "Individuals homozygous for the age-related macular degeneration risk-conferring variant of complement factor H have elevated levels of CRP in the choroid." *Proc Natl Acad Sci U S A* **103**(46): 17456-61.

Jokiranta, T. S., Z. Z. Cheng, et al. (2005). "Binding of complement factor H to endothelial cells is mediated by the carboxy-terminal glycosaminoglycan binding site." *Am J Pathol* **167**(4): 1173-81.

Jokiranta, T. S., J. Hellwage, et al. (2000). "Each of the three binding sites on complement factor H interacts with a distinct site on C3b." *J Biol Chem* **275**(36): 27657-62.

Jozsi, M. and P. F. Zipfel (2008). "Factor H family proteins and human diseases." *Trends Immunol* **29**(8): 380-7.

Kameya, S., N. L. Hawes, et al. (2002). "Mfrp, a gene encoding a frizzled related protein, is mutated in the mouse retinal degeneration 6." *Hum Mol Genet* **11**(16): 1879-86.

Kanda, A., W. Chen, et al. (2007). "A variant of mitochondrial protein LOC387715/ARMS2, not HTRA1, is strongly associated with age-related macular degeneration." *Proc Natl Acad Sci U S A* **104**(41): 16227-32.

Karas, M. and F. Hillenkamp (1988). "Laser desorption ionization of proteins with molecular masses exceeding 10,000 daltons." *Anal Chem* **60**(20): 2299-301.

Kennedy, C. J., P. E. Rakoczy, et al. (1996). "A simple flow cytometric technique to quantify rod outer segment phagocytosis in cultured retinal pigment epithelial cells." *Curr Eye Res* **15**(9): 998-1003.

Killingsworth, M. C., J. P. Sarks, et al. (1990). "Macrophages related to Bruch's membrane in age-related macular degeneration." *Eye* **4 (Pt 4)**: 613-21.

Kim, D. D. and W. C. Song (2006). "Membrane complement regulatory proteins." *Clin Immunol* **118**(2-3): 127-36.

Kishore, U., C. Gaboriaud, et al. (2004). "C1q and tumor necrosis factor superfamily: modularity and versatility." *Trends Immunol* **25**(10): 551-61.

Kishore, U., R. Ghai, et al. (2004). "Structural and functional anatomy of the globular domain of complement protein C1q." *Immunol Lett* **95**(2): 113-28.

Klein, M. L., D. W. Schultz, et al. (1998). "Age-related macular degeneration. Clinical features in a large family and linkage to chromosome 1q." *Arch Ophthalmol* **116**(8): 1082-8.

Klein, R. J., C. Zeiss, et al. (2005). "Complement factor H polymorphism in age-related macular degeneration." *Science* **308**(5720): 385-9.

Kuhn, S., C. Skerka, et al. (1995). "Mapping of the complement regulatory domains in the human factor H-like protein 1 and in factor H1." *J Immunol* **155**(12): 5663-70.

Kuhn, S. and P. F. Zipfel (1996). "Mapping of the domains required for decay acceleration activity of the human factor H-like protein 1 and factor H." *Eur J Immunol* **26**(10): 2383-7.

Kuntz, C. A., S. G. Jacobson, et al. (1996). "Sub-retinal pigment epithelial deposits in a dominant late-onset retinal degeneration." *Invest Ophthalmol Vis Sci* **37**(9): 1772-82.

Kwan, A. P., C. E. Cummings, et al. (1991). "Macromolecular organization of chicken type X collagen in vitro." *J Cell Biol* **114**(3): 597-604.

Laine, M., H. Jarva, et al. (2007). "Y402H polymorphism of complement factor H affects binding affinity to C-reactive protein." *J Immunol* **178**(6): 3831-6.

Lardner, A. (2001). "The effects of extracellular pH on immune function." *J Leukoc Biol* **69**(4): 522-30.

LaVail, M. M. (1976). "Rod outer segment disc shedding in relation to cyclic lighting." *Exp Eye Res* **23**(2): 277-80.

Lee, Y. H., S. Nair, et al. (2005). "Microarray profiling of isolated abdominal subcutaneous adipocytes from obese vs non-obese Pima Indians: increased expression of inflammation-related genes." *Diabetologia* **48**(9): 1776-83.

Lengyel, I., J. M. Flinn, et al. (2007). "High concentration of zinc in sub-retinal pigment epithelial deposits." *Exp Eye Res* **84**(4): 772-80.

Levy, S. and T. Shoham (2005). "Protein-protein interactions in the tetraspanin web." *Physiology (Bethesda)* **20**: 218-24.

Li, M., P. Atmaca-Sonmez, et al. (2006). "CFH haplotypes without the Y402H coding variant show strong association with susceptibility to age-related macular degeneration." *Nat Genet* **38**(9): 1049-54.

Lin, R. J., M. S. Blumenkranz, et al. (2006). "A novel His158Arg mutation in TIMP3 causes a late-onset form of Sorsby fundus dystrophy." *Am J Ophthalmol* **142**(5): 839-48.

Luckman, S. P., E. Rees, et al. (2003). "Partial characterization of cell-type X collagen interactions." *Biochem J* **372**(Pt 2): 485-93.

Lutz, D. A., Y. Guo, et al. (1995). "Natural, high-mannose glycoproteins inhibit ROS binding and ingestion by RPE cell cultures." *Exp Eye Res* **61**(4): 487-93.

Majewski, J., D. W. Schultz, et al. (2003). "Age-related macular degeneration--a genome scan in extended families." *Am J Hum Genet* **73**(3): 540-50.

Maller, J., S. George, et al. (2006). "Common variation in three genes, including a noncoding variant in CFH, strongly influences risk of age-related macular degeneration." *Nat Genet* **38**(9): 1055-9.

Mandal, M. N. and R. Ayyagari (2006). "Complement factor H: spatial and temporal expression and localization in the eye." *Invest Ophthalmol Vis Sci* **47**(9): 4091-7.

Mandal, M. N., V. Vasireddy, et al. (2006). "Spatial and temporal expression of MFRP and its interaction with CTRP5." *Invest Ophthalmol Vis Sci* **47**(12): 5514-21.

Mandal, M. N., V. Vasireddy, et al. (2006). "CTRP5 is a membrane-associated and secretory protein in the RPE and ciliary body and the S163R mutation of CTRP5 impairs its secretion." *Invest Ophthalmol Vis Sci* **47**(12): 5505-13.

Mares-Perlman, J. A., W. E. Brady, et al. (1995). "Dietary fat and age-related maculopathy." *Arch Ophthalmol* **113**(6): 743-8.

Marmor M, W. T. (1998). The Retinal Pigment Epithelium. New York, Oxford University Press. pp745

Marshall, G. E., A. G. Konstas, et al. (1993). "Collagens in ocular tissues." *Br J Ophthalmol* **77**(8): 515-24.

Marshall, G. E., A. G. Konstas, et al. (1992). "Type IV collagen and laminin in Bruch's membrane and basal linear deposit in the human macula." *Br J Ophthalmol* **76**(10): 607-14.

Mayerson, P. L. and M. O. Hall (1986). "Rat retinal pigment epithelial cells show specificity of phagocytosis in vitro." *J Cell Biol* **103**(1): 299-308.

McDonnell, J. M. (2001). "Surface plasmon resonance: towards an understanding of the mechanisms of biological molecular recognition." *Curr Opin Chem Biol* **5**(5): 572-7.

McRae, J. L., T. G. Duthy, et al. (2005). "Human factor H-related protein 5 has cofactor activity, inhibits C3 convertase activity, binds heparin and C-reactive protein, and associates with lipoprotein." *J Immunol* **174**(10): 6250-6.

Meri, S. and M. K. Pangburn (1990). "Discrimination between activators and nonactivators of the alternative pathway of complement: regulation via a sialic acid/polyanion binding site on factor H." *Proc Natl Acad Sci U S A* **87**(10): 3982-6.

Miceli, M. V. and D. A. Newsome (1994). "Insulin stimulation of retinal outer segment uptake by cultured human retinal pigment epithelial cells determined by a flow cytometric method." *Exp Eye Res* **59**(3): 271-80.

Milam, A. H., C. A. Curcio, et al. (2000). "Dominant late-onset retinal degeneration with regional variation of sub-retinal pigment epithelium deposits, retinal function, and photoreceptor degeneration." *Ophthalmology* **107**(12): 2256-66.

Miner, J. H. (2008). "Laminins and their roles in mammals." *Microsc Res Tech* **71**(5): 349-56.

Montes, T., E. Goicoechea de Jorge, et al. (2008). "Genetic deficiency of complement factor H in a patient with age-related macular degeneration and membranoproliferative glomerulonephritis." *Mol Immunol* **45**(10): 2897-904.

Moore, D. J. and G. M. Clover (2001). "The effect of age on the macromolecular permeability of human Bruch's membrane." *Invest Ophthalmol Vis Sci* **42**(12): 2970-5.

Mullins, R. F., N. Aptsiauri, et al. (2001). "Structure and composition of drusen associated with glomerulonephritis: implications for the role of complement activation in drusen biogenesis." *Eye* **15**(Pt 3): 390-5.

Nagaki, K., K. Iida, et al. (1978). "Reaction mechanisms of beta1H globulin." *Int Arch Allergy Appl Immunol* **57**(3): 221-32.

Nandrot, E. F., M. Anand, et al. (2007). "Essential role for MFG-E8 as ligand for alphavbeta5 integrin in diurnal retinal phagocytosis." *Proc Natl Acad Sci U S A* **104**(29): 12005-10.

Nandrot, E. F., M. Anand, et al. (2006). "Novel role for alphavbeta5-integrin in retinal adhesion and its diurnal peak." *Am J Physiol Cell Physiol* **290**(4): C1256-62.

Nandrot, E. F., Y. Kim, et al. (2004). "Loss of synchronized retinal phagocytosis and age-related blindness in mice lacking alphavbeta5 integrin." *J Exp Med* **200**(12): 1539-45.

Ogden, C. A., A. deCathelineau, et al. (2001). "C1q and mannose binding lectin engagement of cell surface calreticulin and CD91 initiates macropinocytosis and uptake of apoptotic cells." *J Exp Med* **194**(6): 781-95.

Okada, T., O. P. Ernst, et al. (2001). "Activation of rhodopsin: new insights from structural and biochemical studies." *Trends Biochem Sci* **26**(5): 318-24.

Okhrimenko, O. and I. Jelesarov (2008). "A survey of the year 2006 literature on applications of isothermal titration calorimetry." *J Mol Recognit* **21**(1): 1-19.

Oppermann, M., T. Manuelian, et al. (2006). "The C-terminus of complement regulator Factor H mediates target recognition: evidence for a compact conformation of the native protein." *Clin Exp Immunol* **144**(2): 342-52.

Pangburn, M. K., D. C. Morrison, et al. (1980). "Activation of the alternative complement pathway: recognition of surface structures on activators by bound C3b." *J Immunol* **124**(2): 977-82.

Pangburn, M. K. and H. J. Muller-Eberhard (1978). "Complement C3 convertase: cell surface restriction of beta1H control and generation of restriction on neuraminidase-treated cells." *Proc Natl Acad Sci U S A* **75**(5): 2416-20.

Pangburn, M. K., R. D. Schreiber, et al. (1977). "Human complement C3b inactivator: isolation, characterization, and demonstration of an absolute requirement for the serum protein beta1H for cleavage of C3b and C4b in solution." *J Exp Med* **146**(1): 257-70.

Pierce, M. M., C. S. Raman, et al. (1999). "Isothermal titration calorimetry of protein-protein interactions." *Methods* **19**(2): 213-21.

Pino, R. M. and E. Essner (1981). "Permeability of rat choriocapillaris to hemeproteins. Restriction of tracers by a fenestrated endothelium." *J Histochem Cytochem* **29**(2): 281-90.

Prosser, B. E., S. Johnson, et al. (2007). "Structural basis for complement factor H linked age-related macular degeneration." *J Exp Med* **204**(10): 2277-83.

Qi, J. H., Q. Ebrahem, et al. (2002). "Expression of Sorsby's fundus dystrophy mutations in human retinal pigment epithelial cells reduces matrix metalloproteinase inhibition and may promote angiogenesis." *J Biol Chem* **277**(16): 13394-400.

Reinboth, J. J., K. Gautschi, et al. (1997). "Lipofuscin in the retina: quantitative assay for an unprecedented autofluorescent compound (pyridinium bis-retinoid, A2-E) of ocular age pigment." *Exp Eye Res* **65**(5): 639-43.

Riley-Vargas, R. C., D. B. Gill, et al. (2004). "CD46: expanding beyond complement regulation." *Trends Immunol* **25**(9): 496-503.

Ripoche, J., A. J. Day, et al. (1988). "The complete amino acid sequence of human complement factor H." *Biochem J* **249**(2): 593-602.

Ryeom, S. W., R. L. Silverstein, et al. (1996). "Binding of anionic phospholipids to retinal pigment epithelium may be mediated by the scavenger receptor CD36." *J Biol Chem* **271**(34): 20536-9.

Ryeom, S. W., J. R. Sparrow, et al. (1996). "CD36 participates in the phagocytosis of rod outer segments by retinal pigment epithelium." *J Cell Sci* **109 (Pt 2)**: 387-95.

Sarks, S., S. Cherepanoff, et al. (2007). "Relationship of Basal laminar deposit and membranous debris to the clinical presentation of early age-related macular degeneration." *Invest Ophthalmol Vis Sci* **48**(3): 968-77.

Schick, J. H., S. K. Iyengar, et al. (2003). "A whole-genome screen of a quantitative trait of age-related maculopathy in sibships from the Beaver Dam Eye Study." *Am J Hum Genet* **72**(6): 1412-24.

Schmidt S, E. A. Postel E. A et al. (2003). "Detailed analysis of allelic variation in the ABCA4 gene in age-related maculopathy." *Invest Ophthalmol Vis Sci* **44**(7): 2868-75.

Scholl, H. P., M. Fleckenstein, et al. (2007). "An update on the genetics of age-related macular degeneration." *Mol Vis* **13**: 196-205.

Seddon, J. M., S. L. Santangelo, et al. (2003). "A genomewide scan for age-related macular degeneration provides evidence for linkage to several chromosomal regions." *Am J Hum Genet* **73**(4): 780-90.

Shapiro, L. and P. E. Scherer (1998). "The crystal structure of a complement-1q family protein suggests an evolutionary link to tumor necrosis factor." *Curr Biol* **8**(6): 335-8.

Sharma, A. K. and M. K. Pangburn (1996). "Identification of three physically and functionally distinct binding sites for C3b in human complement factor H by deletion mutagenesis." *Proc Natl Acad Sci U S A* **93**(20): 10996-1001.

Sheraidah, G., R. Steinmetz, et al. (1993). "Correlation between lipids extracted from Bruch's membrane and age." *Ophthalmology* **100**(1): 47-51.

Shu, X., B. Tulloch, et al. (2006). "Biochemical characterisation of the C1QTNF5 gene associated with late-onset retinal degeneration. A genetic model of age-related macular degeneration." *Adv Exp Med Biol* **572**: 41-8.

Shu, X., B. Tulloch, et al. (2006). "Disease mechanisms in late-onset retinal macular degeneration associated with mutation in C1QTNF5." *Hum Mol Genet* **15**(10): 1680-9.

Silverstein, R. L. and M. Febbraio (2000). "CD36 and atherosclerosis." *Curr Opin Lipidol* **11**(5): 483-91.

Sim, E., A. B. Wood, et al. (1981). "Pattern of degradation of human complement fragment, C3b." *FEBS Lett* **132**(1): 55-60.

Sim, R. B., A. J. Day, et al. (1993). "Complement factor I and cofactors in control of complement system convertase enzymes." *Methods Enzymol* **223**: 13-35.

Sjoberg, A. P., L. A. Trouw, et al. (2007). "The factor H variant associated with age-related macular degeneration (His-384) and the non-disease-associated form bind differentially to C-reactive protein, fibromodulin, DNA, and necrotic cells." *J Biol Chem* **282**(15): 10894-900.

Skerka, C., N. Lauer, et al. (2007). "Defective complement control of factor H (Y402H) and FHL-1 in age-related macular degeneration." *Mol Immunol* **44**(13): 3398-406.

Smith, W., J. Assink, et al. (2001). "Risk factors for age-related macular degeneration: Pooled findings from three continents." *Ophthalmology* **108**(4): 697-704.

Soames, C. J. and R. B. Sim (1997). "Interactions between human complement components factor H, factor I and C3b." *Biochem J* **326 (Pt 2)**: 553-61.

Spencer, K. L., M. A. Hauser, et al. (2007). "Haplotypes spanning the complement factor H gene are protective against age-related macular degeneration." *Invest Ophthalmol Vis Sci* **48**(9): 4277-83.

Spencer, K. L., L. M. Olson, et al. (2008). "C3 R102G polymorphism increases risk of age-related macular degeneration." *Hum Mol Genet* **17**(12): 1821-4.

Spessotto, P., M. Cervi, et al. (2003). "beta 1 Integrin-dependent cell adhesion to EMILIN-1 is mediated by the gC1q domain." *J Biol Chem* **278**(8): 6160-7.

Starita, C., A. A. Hussain, et al. (1995). "Decreasing hydraulic conductivity of Bruch's membrane: relevance to photoreceptor survival and lipofuscinoses." *Am J Med Genet* **57**(2): 235-7.

Stephan, S., M. J. Sherratt, et al. (2004). "Expression and supramolecular assembly of recombinant alpha1(viii) and alpha2(viii) collagen homotrimers." *J Biol Chem* **279**(20): 21469-77.

Stone, E. M., T. A. Braun, et al. (2004). "Missense variations in the fibulin 5 gene and age-related macular degeneration." *N Engl J Med* **351**(4): 346-53.

Stone, E. M., A. J. Lotery, et al. (1999). "A single EFEMP1 mutation associated with both Malattia Leventinese and Doyne honeycomb retinal dystrophy." *Nat Genet* **22**(2): 199-202.

Strauss, O. (2005). "The retinal pigment epithelium in visual function." *Physiol Rev* **85**(3): 845-81.

Sun, M., S. C. Finnemann, et al. (2006). "Light-induced oxidation of photoreceptor outer segment phospholipids generates ligands for CD36-mediated phagocytosis by retinal pigment epithelium: a potential mechanism for modulating outer segment phagocytosis under oxidant stress conditions." *J Biol Chem* **281**(7): 4222-30.

Sundin, O. H., G. S. Leppert, et al. (2005). "Extreme hyperopia is the result of null mutations in MFRP, which encodes a Frizzled-related protein." *Proc Natl Acad Sci U S A* **102**(27): 9553-8.

Tate, D. J., Jr., M. V. Miceli, et al. (1995). "Phagocytosis and H2O2 induce catalase and metallothionein gene expression in human retinal pigment epithelial cells." *Invest Ophthalmol Vis Sci* **36**(7): 1271-9.

Tezel, T. H., N. S. Bora, et al. (2004). "Pathogenesis of age-related macular degeneration." *Trends Mol Med* **10**(9): 417-20.

Tong, J. P. and Y. F. Yao (2006). "Contribution of VEGF and PEDF to choroidal angiogenesis: a need for balanced expressions." *Clin Biochem* **39**(3): 267-76.

van der Schaft, T. L., W. C. de Bruijn, et al. (1993). "Basal laminar deposit in the aging peripheral human retina." *Graefes Arch Clin Exp Ophthalmol* **231**(8): 470-5.

van der Schaft, T. L., W. C. de Bruijn, et al. (1992). "Element analysis of the early stages of age-related macular degeneration." *Arch Ophthalmol* **110**(3): 389-94.

van Lookeren Campagne, M., C. Wiesmann, et al. (2007). "Macrophage complement receptors and pathogen clearance." *Cell Microbiol* **9**(9): 2095-102.

Venables, J. P., L. Strain, et al. (2006). "Atypical haemolytic uraemic syndrome associated with a hybrid complement gene." *PLoS Med* **3**(10): e431.

Vojnikovic, B., S. Njiric, et al. (2007). "Ultraviolet sun radiation and incidence of age-related macular degeneration on Croatian Island Rab." *Coll Antropol* **31 Suppl 1**: 43-4.

Volanakis, J. E. and M. H. Kaplan (1974). "Interaction of C-reactive protein complexes with the complement system. II. Consumption of guinea pig complement by CRP complexes: requirement for human C1q." *J Immunol* **113**(1): 9-17.

Walport, M. J. (2001). "Complement. First of two parts." *N Engl J Med* **344**(14): 1058-66.

Walport, M. J. (2001). "Complement. Second of two parts." *N Engl J Med* **344**(15): 1140-4.

Wear, M. A. and M. D. Walkinshaw (2006). "Thermodynamics of the cyclophilin-A/cyclosporin-A interaction: a direct comparison of parameters determined by surface plasmon resonance using Biacore T100 and isothermal titration calorimetry." *Anal Biochem* **359**(2): 285-7.

Weeks, D. E., Y. P. Conley, et al. (2004). "Age-related maculopathy: a genomewide scan with continued evidence of susceptibility loci within the 1q31, 10q26, and 17q25 regions." *Am J Hum Genet* **75**(2): 174-89.

Weiter, J. J., F. C. Delori, et al. (1986). "Retinal pigment epithelial lipofuscin and melanin and choroidal melanin in human eyes." *Invest Ophthalmol Vis Sci* **27**(2): 145-52.

Whaley, K. and S. Ruddy (1976). "Modulation of the alternative complement pathways by beta 1 H globulin." *J Exp Med* **144**(5): 1147-63.

Wiesmann, C., K. J. Katschke, et al. (2006). "Structure of C3b in complex with CRIg gives insights into regulation of complement activation." *Nature* **444**(7116): 217-20.

Won, J., R. S. Smith, et al. (2008). "Membrane frizzled-related protein is necessary for the normal development and maintenance of photoreceptor outer segments." *Vis Neurosci* **25**(4): 563-74.

Wu, Z., T. W. Lauer, et al. (2007). "Oxidative stress modulates complement factor H expression in retinal pigmented epithelial cells by acetylation of FOXO3." *J Biol Chem* **282**(31): 22414-25.

Yamada, Y., S. Ichihara, et al. (2008). "Genetic risk for metabolic syndrome: examination of candidate gene polymorphisms related to lipid metabolism in Japanese people." *J Med Genet* **45**(1): 22-8.

Yang, Z., N. J. Camp, et al. (2006). "A variant of the HTRA1 gene increases susceptibility to age-related macular degeneration." *Science* **314**(5801): 992-3.

Yates, J. R., T. Sepp, et al. (2007). "Complement C3 variant and the risk of age-related macular degeneration." *N Engl J Med* **357**(6): 553-61.

Young, R. W. and D. Bok (1969). "Participation of the retinal pigment epithelium in the rod outer segment renewal process." *J Cell Biol* **42**(2): 392-403.

Yurchenco, P. D. and G. C. Ruben (1987). "Basement membrane structure in situ: evidence for lateral associations in the type IV collagen network." *J Cell Biol* **105**(6 Pt 1): 2559-68.

Zaluzec, E. J., D. A. Gage, et al. (1995). "Matrix-assisted laser desorption ionization mass spectrometry: applications in peptide and protein characterization." *Protein Expr Purif* **6**(2): 109-23.

Zipfel, P. F., M. Edey, et al. (2007). "Deletion of complement factor H-related genes CFHR1 and CFHR3 is associated with atypical hemolytic uremic syndrome." *PLoS Genet* **3**(3): e41.

Zipfel, P. F., S. Heinen, et al. (2006). "Complement and diseases: defective alternative pathway control results in kidney and eye diseases." *Mol Immunol* **43**(1-2): 97-106.

Zipfel, P. F. and C. Skerka (1994). "Complement factor H and related proteins: an expanding family of complement-regulatory proteins?" *Immunol Today* **15**(3): 121-6.

Zipfel, P. F. and C. Skerka (1999). "FHL-1/reconectin: a human complement and immune regulator with cell-adhesive function." *Immunol Today* **20**(3): 135-40.